[redacted]

Rensselaer Polytechnic Institute

[redacted]

R.P.I. Technical Report MP-44

A Progress Report for
July 1, 1973 to June 30, 1974

ANALYSIS AND DESIGN OF A CAPSULE LANDING SYSTEM AND SURFACE VEHICLE CONTROL SYSTEM FOR MARS EXPLORATION

National Aeronautics and Space Administration

Grant NGL 33-018-091

Submitted by the Special Projects Committee

D.K. Frederick
P.K. Lashmet
W.R. Moyer
G.N. Sandor
C.N. Shen
E.J. Smith
S.W. Yerazunis

School of Engineering
Rensselaer Polytechnic Institute

ABSTRACT

A number of problems related to the design, construction and evaluation of an autonomous roving planetary vehicle and its control and operating systems intended for an unmanned exploration of Mars have been under study. Broad problem areas receiving attention include: vehicle configuration, dynamics, control, systems and propulsion; systems analysis; terrain sensing and modeling and path selection; and chemical analysis of samples.

The following tasks have been under active study: design, construction and testing of a 0.5 scale dynamic vehicle, mathematical modeling of vehicle dynamics, experimental 0.4 scale vehicle dynamics measurements and interpretation, propulsion and deployment systems, electromechanical control systems, remote control systems, collapsibility and deployment concepts and hardware, design, construction and evaluation of a wheel with increased lateral stiffness, systems design optimization, design of an on-board computer, design and construction of a laser rangefinder, measurement of reflectivity of sands and other surfaces, obstacle perception by edge detection, terrain modeling based on gradients, obstacle classification, path selection system simulation and evaluation of a mid-range and a short-range system, gas chromatograph systems design concepts, experimental chromatograph separation measurements, and chromatograph model improvement and evaluation.

These tasks are defined in detail and the progress which has been achieved during the period July 1, 1973 to June 30, 1974 is summarized.

TABLE OF CONTENTS

Analysis and Design of a Capsule Landing System and Surface Vehicle Control System for Mars Exploration

I. Introduction

Current national goals in space exploration include a detailed study and examination of the planet Mars. The effectiveness of Mars exploration missions would be enhanced according to the extent to which the investigative devices which are landed are mobile, to the range of their mobility, and to the ability to control their motion. In order to achieve basic mission objectives, and beyond that, to maximize the return on the commitment of resources to the mission, formidable technical problems must be resolved. The major factor contributing to these problems is the round trip communications time delay between martian and earth control stations which varies from a minimum of about 9 minutes to a maximum of 25 minutes. This time delay imposes stringent requirements on the vehicle, on its control and communication systems and on those systems included on board to make the scientific measurements, in terms of their ability to function autonomously. These systems must be able to operate with a high degree of reliability and must be capable of calling for earth control under appropriate circumstances.

A number of important problems originating with these factors and relating directly the basic mission objectives of an unmanned exploration of Mars have been and are currently being investigated by a faculty-student project team at Rensselaer Polytechnic Institute with the support of NASA Grant NGL-33-018-091.

In addition to the technical objectives, the project is intended to involve students in meaningful design and problem-solving activities and by so doing to enhance their formal education in the area of design.

This progress report describes the tasks which have been undertaken and documents the progress which has been achieved in the interval July 1, 1973 to June 30, 1974 in addition to appraising the educational implications of the project.

II. Overview of the Project

The tasks which have been undertaken and which are proposed to be pursued in the future have been selected on the basis of their relevance to an unmanned mission of exploration of Mars. This mission is conceived as involving an autonomous roving laboratory capable of a range of at least 1000 kilometers and a minimum operational life of one year. A performance exceeding these specifications would be desirable to gain a maximum return on the national investment. While the major purpose of the early mission is to establish whether or not life at any level exists or has existed on Mars, an understanding of chemical, mineral and geological nature of the planet is desired to provide the knowledge required in establishing the origin of the solar system. Beyond these objectives, a more thorough knowledge of the planet will provide a basis for appraising Mars as a resource of critical materials for earth in the very long run.

In achieving these goals, a roving laboratory which is able to relocate itself autonomously on the planet surface under limited instructions from earth is essential if a thorough exploration is to be effected. Such a roving laboratory must be able to navigate to new positions as specified by instructions from earth with a minimum of "on-line" earth control. Indeed "on-line" control would involve an extremely slow process because of the round-trip delay time for information transfer.

Accordingly, one essential prerequisite to a successful mission is development of an effective path selection system which includes scanners and sensors capable of identifying obstacles or terrain features as being either passable or impassable for the vehicle as well as the software and on-board computers required to process the information. Such a system must be sensitive to potentially dangerous terrain features which the vehicle may not be able to resolve under which conditions a call for earth assistance must be made. Although early missions or at least a portion of a first mission would involve "safe" martian regions, a second major prerequisite is that the roving vehicle must have an acceptable obstacle and terrain negotiation capability. Sooner or later, the desire to explore "difficult" regions of the planet must be satisfied. High maneuverability and ability for the vehicle to extricate itself from difficult circumstances are essential characteristics.

The roving vehicle will be a means to an end rather than an end in itself in that it will house, protect, transport and allow to function a number of instruments and devices which will make the desired scientific observations. Equipped with TV camera, the vehicle will make available to earth observers detailed views of the planet surface. Devices such as arms, manipulators and scoops will gather desired samples and deliver them to the on-board laboratory for processing. Other instruments will measure temperature, winds, magnetic fields, gravitational fields, etc. directly. Still other instruments may be deployed at strategic locations for extended observations. The information, which may receive some preliminary processing on an on-board computer, will then be transmitted to earth. In turn, earth control will transmit additional instructions or may alter basic instructions on the basis of the knowledge gained.

Although the scientific instruments which will be required to achieve the fundamental mission knowledge goals are crucial components, the means of housing, protecting and transporting them safely over the martian surface is a prerequisite to a successful mission.

The major emphasis at Rensselaer has been directed to the roving vehicle and to the systems required for reliable and safe relocation of the vehicle to permit a full execution of mission objectives. Beyond tasks originating with this major emphasis, we have undertaken the study of one key component of a chemical analysis system, namely, the gas chromtograph.

A. Vehicle Configuration, Control, Dynamics, Systems and Propulsion
The objective of this task is the design of a roving vehicle for the exploration of Mars. This design includes the aspects of vehicle configuration, collapsibility for launch configuration, deployment, dynamics, motion and attitude control, obstacle negotiation capability, and performance evaluation. The efforts of this task are made within the context of the mission definition and delivery system constraints. The ultimate goal is the development of a vehicle capable of operating within the constraints of the Mars mission, but flexible in design, to insure reliability with respect to the unknowns of Mars, and to accommodate the alterations in the mission as a result of information gathered during the exploration.

B. General Systems Analysis. One major objective of this task is to develop a framework within which decisions in design involving conflicting requirements can be made rationally and in the context of the whole system and mission. Relationships between alternative mission profiles and specifications and weight, energy and space

allocation and management will be sought.

The second major objective is to develop the software and hardware design specifications for the on-board computer of a Mars roving vehicle and to provide computer support for the vehicle task.

C. Surface Navigation and Path Control. Once the capsule is landed and the roving vehicle is in an operational state, it is necessary that the vehicle can be directed to proceed under remote control from the landing site to specified positions on the martian surface. This task is concerned with the problems of terrain sensing, obstacle detection, terrain modeling, path selection and navigation between the initial and terminal sites when major terrain features precluding direct paths are to be anticipated. On board decision making capability must be designed to minimize earth control responsibility except in the most adverse circumstances.

D. Chemical Analysis of Specimens. A major objective of martian surface exploration will be to obtain chemical, biochemical or biological information. Many experiments proposed for the mission require a general duty, gas chromotgraph-mass spectrometer system for chemical analysis. The objective of this task is to generate fundamental data and concepts required to optimize this chemical analysis sytem.

III. Summary of Results

Task A. Vehicle Configuration, Control, Dynamics, Systems and Propulsion

This broad task has been subdivided into the following subtasks: experimental and analytical studies of vehicle dynamics; detailed design of structural components; design of deployment hardware; motor drive and mechanical transmission details; development of launch configuration and deployment procedure; wheel tester and grouser design; wheel analysis; detailed wheel design and construction; on-board controls for steering, motor drive for levelizing, deployment and emergency maneuvers; radio link for remote operation; and remote control station and transmitter design.

A.1. Vehicle Structure and Dynamics

A.1.a. Experimental and Analytical Studies of Vehicle Dynamics

Physical characteristics such as spring constants, damping constants and moments of inertia of the 0.4 scale vehicle model were measured experimentally. A three dimensional, three degree-of-freedom mathematical model was developed and its predictions were compared with the dynamic behavior of the model. Satisfactory agreement was observed indicating that the mathematical model can be used as a design tool to obtain desired dynamic characteristics. Extensions of the mathematical model have been identified. No further work is planned pending dynamic testing of the 0.5 scale roving vehicle.

A.1.b. Structural Components

All structural components for the 0.5 scale model including front

and rear struts, payload box, torsion bar assembly, front axle, front steering gear box, payload levelers, motor drive system and all other required components were designed, constructed and assembled in an operating roving vehicle.

A.1.c. Deployment Hardware

A concept for deploying the front and rear wheels was developed, designed, constructed and implemented on the 0.5 scale roving vehicle. One unique feature is that this deployment scheme makes use only of motors required for mission operations.

A.1.d. Motor Drive and Mechanical Transmission Details

The propulsion system including motors, gear train, feedback control of motor speed and supporting electronics to provide proper drive wheel speed in relation to steering, (see Task A.4.a.), was designed, constructed and implemented on the 0.5 scale roving vehicle. One unique feature of this system is that the feedback control makes brakes unnecessary.

A.2. Launch Configuration and Deployment Procedures

The previous launch configuration concept was modified in order to permit a simpler deployment procedure. The new configuration remains consistent with Viking capsule constraints and yields a satisfactory center of gravity location.

A.3. Wheel Design and Testing

A.3.a. Wheel Tester and Grouser Design

Three alternative grouser concepts were tested in depth. A knobly tread grouser was selected and implemented in the 0.5 scale roving vehicle.

A.3.b. Wheel Analysis

A modified wheel design was developed to increase the lateral stiffness of the wheel. The final design met specifications and was implemented on the 0.5 scale roving vehicle.

A.3.c. Detail Wheel Design and Construction

The improved wheel design develcped under Task A.3.b. was implemented on the 0.5 scale roving vehicle. Testing of the vehicle confirmed the effectiveness of the design.

A.4. Radio Control

A.4.a. On-Board Electrical Controls

A system for controlling the steering, propulsion, payload and strut motors with digital input has been conceived, constructed

and implemented. The system involves digital/analog converters and analog speed and position feedback.

A.4.b. Radio Link

Frequency shift key encoding is used with walkie-talkies to provide a 100 bit/sec radio link to the vehicle. The system has been designed, constructed and implemented on the 0.5 scale roving vehicle.

A.4.c. Remote Control Station and Transmitter Design

A remote control package interfacing with the vehicle via the radio link has been designed, constructed and implemented in conjunction with the 0.5 scale roving vehicle. This station permits manual, open-loop control of the vehicle.

Task B. General Systems Analysis

B.1. System-Modeling and Design Optimization

Optimal designs have been developed for three major alternative models, i.e. four-wheeled vehicle with either direct earth link or an orbiter-earth link and a six-wheeled vehicle with direct earth link. The method by which to obtain optimal design for these and other cases has been developed in general terms. Methods for determining the sensitivity of the optimal designs to perturbation of design parameters have also been developed. This task is now complete and a technical report was issued in June, 1974.

B.2. On-Board Computer Design

Previous work in this area involved the use of a statistical approach using queuing theory and random variables to study the average behavior of the computer-vehicle system. This study identified a higher level problem in design of an on-board computer, namely the need to define computer design specifications both in regard to software and hardware prior to the computer design process. The present task is aimed at defining the software and hardware specifications for an on-board computer. It is assumed that all control and scheduling decisions will be provided autonomously. The goal will be to synthesize a design that will meet the lowest realizable specification bound. Ultimately, volume, weight, cost, power requirements and heat generation will have to be optimized to meet mission requirements. Alternative hardware and software configurations will have to be considered and trade-offs evaluated.

Task C. Surface Navigation and Path Control

This task deals with problems of terrain sensing, terrain modeling, obstacle detection, path selection algorithms and evaluation of path selection systems. Active tasks are: design and construction of a laser range finder, measurement of bidirectional reflectance ratios, three dimensional obstacle recognition, terrain parameter estimation from gradient data, laser range finder scanning systems and path selection system evaluation.

C.1. Laser Range Finder

C.1.a. Construction of a Laser Range Finder

A laser pulse generator employing a laser diode for fast rise time and incorporating a coaxial symmetry to minimize circuit inductance was constructed and shown to have a 28 nanosecond current rise time. A photomultiplier tube was selected as a receiver and preliminary measurements indicate a light pulse 10-90% rise time of 15 nanoseconds. It is believed that with modification, even lower light pulse rise times will be obtained.

C.1.b. Surface Reflectivity and Laser Range Finder Power Requirements

The quantities which must be measured to provide meaningful data for purposes of defining minimum laser range finder power was determined and a test apparatus was constructed. Surface reflectivities for several sands and for copper were measured and are reported.

C.2. Obstacle Classification and Detection and Terrain Modeling

C.2.a. Obstacle Identification by Edge Detection

Two algorithms, one already existing in the literature and a second developed in this study, were used to obtain the outlines of obstacles from a range image. Both of these algorithms require a thresholding operation. A theoretical analysis shows how a proper value of the threshold may be chosen given the type of irregularity to be detected. The analysis also shows how large the statistics of measurement noise can be allowed without leading to false alarms. Computer simulations of these schemes have demonstrated their feasibility. The related problems of scanning scheme determination, the effect of reduced number of data points and bottom edge detection have been explored providing a basis for future investigation.

C.2.b. Parameter Estimation for Terrain Modeling from Gradient Data

A two step modeling procedure employing height, location and gradient data computed from sixteen raw data points was developed. The resulting terrain model is a third degree, two dimensional polynomial. The two step modeling process is used to give proper emphasis to the measured gradient as well as height. A complete error analysis has been developed which provides the standard deviations of height and gradient for simulated models. Finally, a computer program has been produced which simulates the scanning process, takes rangefinder readings, forms polynomial models, carries out the error analysis and compares the modeled results with the actual surface and gradient.

C.2.c. Obstacle and Terrain Classification

A classification of landforms by basic size and shape was developed on the assumption of no restrictions on the size or capabilities of the actual vehicle. The present classification organizes obstacles into some basic classes depending on the

magnitude of the height to width and/or depth of the obstacle. Some more complex parameters are suggested for further refinement. Other factors to be considered in defining slope obstacles are the shear strength and flotation properties of the surface soil.

Recommendations for refining the classification system are made. These will involve consideration of the vehicle's relationship to the terrain with such factors as the orientation of the obstacle with respect to the vehicle and the vehicle's inability to see the far side of the obstacle.

C.3. Path Selection System Development and Evaluation

A reliable but efficient procedure for evaluating proposed terrain sensing and path selection concepts has been further refined and applied. This procedure involves a series of tests which increase in complexity and sophistication from elementary single obstacle encounters to complex, multi-obstacle tests with and without sensor and vehicle motion noise. A proposed mid-range sensor system involving laser sweeps in the plane of the vehicle was investigated and found to have some significant but potentially curable defects. A short range system, ($\sim$ 3 meter), was proposed and a preliminary evaluation was obtained. The simulation was modified to accept a non-zero vehicle width. Plans were formulated for improving the program documentation and for implementing an existing computer monitoring program to increase execution efficiency.

Task D. Chemical Analysis of Specimens

D.1. Chromatograph System Characteristics

These studies were intended to provide chromatograph design techniques and guides using simulation models currently under development. Specific studies included 1) a quantitative definition of chromatograph performance under a given set of circumstances; and 2) a study of the effect of system parameters upon performance using simulation. Resolution as often used in the literature as an index of performance and based on moment analysis was shown to represent inadequately separations in multicomponent systems because the definition was insensitive to chemical composition. A definition based on each component's contribution to the area under a chromatograph peak was shown to represent realistically the performance of a chromatograph. System simulation showed trends of parameter effects, heretofore described qualitatively, could be easily predicted quantitatively.

D.2. Chromatograph Simulation Development

D.2.a. Multicomponent Chromatography

Modifications to the chromatographic test facility resulted in sharper input pulses for liquid samples and full scale chromatogram recordings which reduced relative reading errors by a factor of 3 or

4 in some cases. To supplement pentane-heptane data on the porous Chromosorb-102 column, which deviated appreciably from linear superposition predictions, additional experiments were conducted on two nonporous columns. A Carbowax-1500 column failed to separate the two chemicals because values of the thermodynamic parameter mR_0 were too similar. A DES column separated the two components and superposition of pure component data was an excellent representation of the binary data. Further experiments with ethylene and pentane-heptane on Chromosorb 102 showed that the observed nonlinear effects were composition dependent. Chromatograms were well represented if the compositions were low. A nonlinear adsorption isotherm was proposed to account for these observations.

D.2.b. Chromatograph Model Improvement

A recently released technical report documented a more complete chromatograph model which included intraparticle as well as interparticle transport effects and finite rates of adsorption. Mathematical complexity precluded analytical solutions, so numerical techniques were investigated. Orthogonal collocation was applied to two simplified versions of the model which had known analytic solutions. Comparison between the exact and numerical solutions was then possible. Space discretizations using 15 to 21 elements have represented responses for the simple models well. Preliminary investigation of the more complete model showed computation time was excessive, and practical implementation of orthogonal collocation as it was formulated in this study was impractical. Considering the results in Task D.2.a, it was proposed that this work be terminated and that the simple, nonlinear model receive major attention.

IV. Educational Implications

As noted earlier, one of the objectives of the project is to involve engineering students in meaningful design and problem-solving activities enhancing, therefore, their overall education. Over the past year, this project has been successful in attracting many students over and above those attracted by financial support. These students, who participate on the project in this fashion, not only gain academic credit but also share in the challenge and the stimulation offered by the program. This past year is no exception with a total of 26 students actively involved in the project, only 14 of whom received some financial support. Of this total, four were doctoral level, fourteen were master's level and seven were undergraduate level students. Three doctoral, fourteen masters and four undergraduate degree programs were completed.

The student's reactions regarding the educational value continue to be very positive as evidenced by the number of new students attracted each year. The faculty appraisal of value is also very high. The project provides a unique learning experience in an academic setting for a number of reasons.

First, all of the problems addressed by the students are relevant and significant. The student realizes that the problem must be solved within the constraints that apply and not within artificial constraints which would make the solution relatively straightforward. Faculty attitudes and guidance are very important in this regard as are those of the technical monitors from Jet Propulsion

Laboratory whose role is described below.

Second, the project is so organized and administered as to create a meaningful industrial climate. The students are aware of the short and long-term technical objectives and of their role in the project. The problem of interfacing their task with those tasks on which it impinges becomes painfully clear. They realize that interfacing with other tasks is just as crucial a constraint as are the direct technical objectives. The students are expected to plan their task, to formulate a milestone schedule and to achieve their stated objectives. Even though the students tend to be overly optimistic, they learn from this experience how to go about planning and executing their assignments. The students are required to make periodic progress reports and to prepare such progress and technical reports as are necessary. All in all, the students are experiencing the responsibilities of practicing engineers.

Third, progress review meetings involving the project technical monitors from JPL and invited guests are held at approximately ten week intervals. These review meetings are one of the most vital aspects of the project both from the technical and educational points of view. Students make presentations of progress to the group of monitors, guests, faculty and the other participating students. The progress is reviewed critically by all participants with appropriate comments and discussion. These meetings develop the student's ability to prepare his materials, including visual aids and demonstrations, to deliver his presentation and to react to questions and suggestions. The monitors and guests frequently provide additional information, knowledge and guidance which promotes the progress of the work. The progress review meetings are of considerable value in maintaining steady and coordinated progress.

In summary, the project has contributed substantially to the education of engineering students and the professional growth of faculty interested in advanced study in the area of design.

V. Detailed Summaries of Progress

Task A. Vehicle Configuration, Control, Dynamics, Systems and Propulsion

The objective of this task is to design and construct an operational half-size demonstration model of a Mars roving vehicle to verify proposed concepts for:

1. Collapsibility
2. Deployment
3. Controllability of propulsion and maneuvering
4. Obstacle negotiation capability
5. Payload carrying capability
6. Operation by radio control

Towards the accomplishment of this objective, the vehicle design task has been organized into several subtasks headquartered in the Engineering Design Laboratory of the Machines and Structures Division. While these subtasks are intimately related and there is a good deal of interaction between the team members working on them, each will be described separately in the following report, organized as follows:

Task A.1. Vehicle Structure

- A.1.a. Experimental and analytical studies of vehicle dynamics
- A.1.b. Structural components
- A.1.c. Deployment hardware
- A.1.d. Motor drive and mechanical transmission details

Task A.2. Launch Configuration and Deployment Procedure

Task A.3. Wheel Design and Testing

- A.3.a. Wheel tester and grouser design
- A.3.b. Wheel analysis
- A.3.c. Detail design and wheel construction

Task A.4. Radio Control

- A.4.a. On-board electrical/electronic controls for steering, motor drives for levelizing, deployment and emergency maneuvers
- A.4.b. Radio link for remote operation
- A.4.c. Remote control station and transmitter design

As a result of these tasks, two papers have been prepared, Ref. 1 and 2, one of which is scheduled for publication.

Task A.1. Vehicle Structure - P. Marino, F. Gorton, D. Kern, M. Miecznikowsik, C. Deno, G. Scapellati, C. Eame, B. Morin, B. Musig and G. Skevington

Faculty Advisor: Profs. G. N. Sandor, W. Moyer

A.1.a. Experimental and Analytical Studies of Vehicle Dynamics

Objective. To determine the dynamic response of the .4 size model and develop a mathematical tool for the dynamic optimization of the forthcoming half-size model and eventually the full-size prototype vehicle.

Progress Summary. Physical characteristics, such as spring constants, damping constants and moments of inertia of the .4 size vehicle model were measured experimentally. A three-dimensional three-degree-of-freedom mathematical model was developed, programmed for digital computation and its predictions compared with the dynamic behavior of the model. Satisfactory agreement was found indicating that the mathematical model can be used as a design tool. Further extensions of the mathematical model to include more degrees of freedom have been outlined. A technical report covering this work has been issued, Ref. 3.

Discussion. The dynamic analysis of the MRV was approached by two methods:

1. mathematical modeling
2. physical testing

Initially the equations of motic of a three-dimensional, three-degree-of-freedom (roll, pitch, vertical displacement) model was established. Then, the measure of the physical characteristics of the 0.4 MRV model and dynamic tests were conducted. Finally, a comparison of actual response with the mathematically predicted response was made. The result showed the mathematical model to be a basic design tool from which gross vehicle motions may be predicted. It also may be expanded upon to develop a more sophisticated mathematical model. Figure 1 shows the schematic model. The wheels have been replaced by springs and dashpots. This is the schematic from which the mathematical model was developed.

For simplicity, three degrees of freedom were considered. Vertical displacement was an obvious choice since the MRV bouncing across Martian terrain

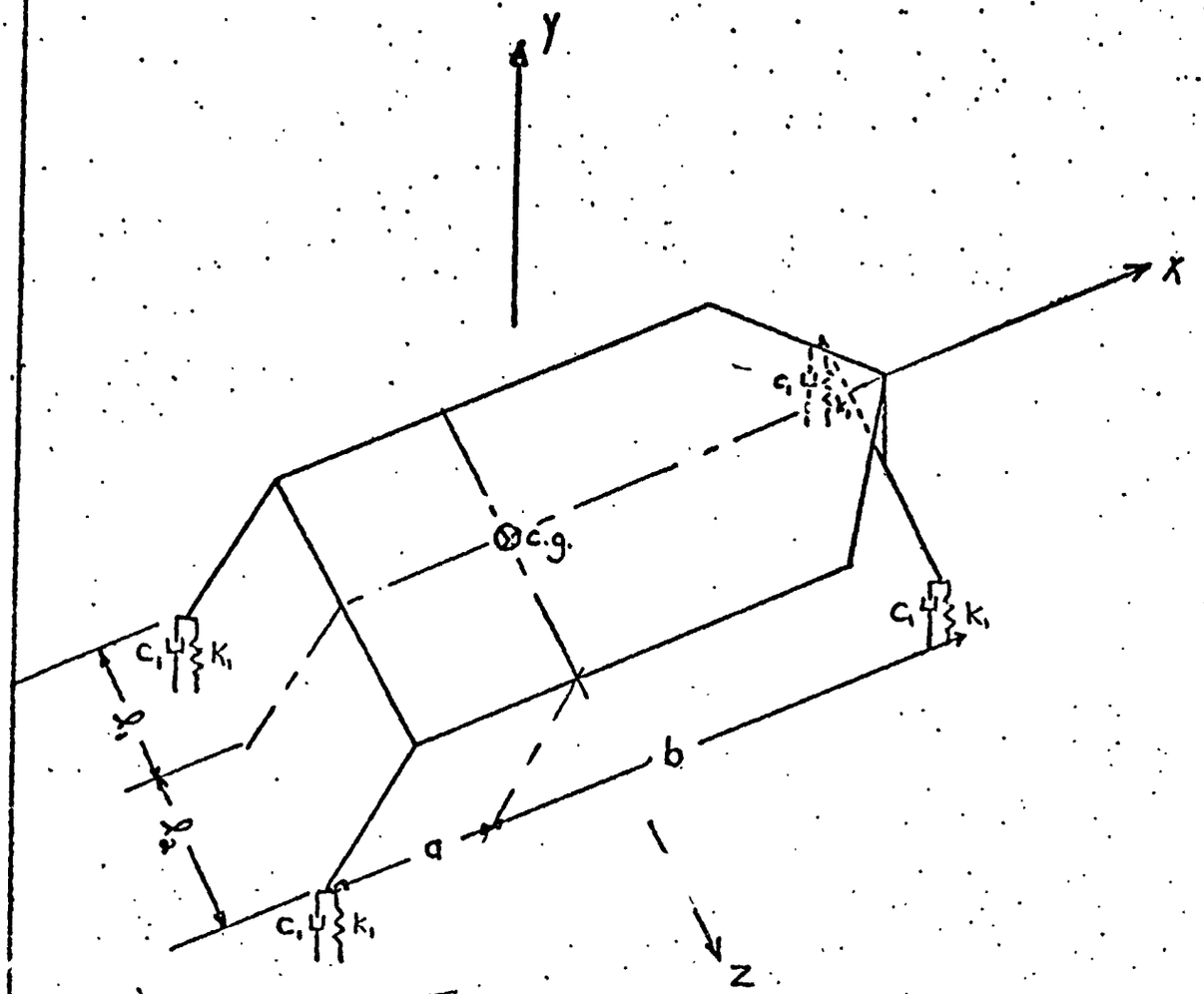

FIGURE 1

RPI-MRV Schematic Model

will be carrying a scientific payload. Because of the "dragster" design of the RPI-MRV, the vehicle center of gravity was located near the rear wheel base far from the center of suspension. A natural pitching motion was therefore introduced by the vehicle design. As a result, the mathematical model also includes pitch motion. Finally, the movement of the MRV over rocks and potholes easily introduced a rolling motion. Therefore, with the three degrees of freedom chosen to be vertical displacement, roll, and pitch rotation, the development of the equations of motion proceeded.

Simplifying Assumptions. In order to greatly simplify the equations of motion, the MRV was considered to be a two-mass system: a rolling (spring) mass, and a non-rolling (unsprung) or fixed mass. Additionally, if a moving coordinate system, x'y'z' fixed to the vehicle was adopted, the inertial terms in the equations of motion would become much easier to determine. Therefore, the coordinate system of Figure 2 was used. The xyz axis system was fixed to the unsprung portion of the vehicle.

To determine the external forces and moments, the vehicle model assumed two sets of virtual displacements:

1. roll with vertical displacement, Fig. 3.
2. pitch with vertical displacement, Fig. 4.

The resulting equations are a set of second-order linear differential equations to be solved simultaneously. A digital computer program titled, DYNAMO (from DYNAmic MOdels) was used to solve these equations.

Various terrain conditions may be simulated on the mathematical model. A step input to the vehicle c.g. was simulated by assuming an initial condition on the vertical displacement. An initial condition on pitch displacement simulates a step either to the front or rear wheel pair as would be encountered by the vehicle's front wheels hitting a sudden difference in elevation. Similarly an initial condition on roll displacement simulates a step to either the right or left side wheel pair. A washboard terrain effect can be modeled by equating the left side of the first equation of motion to a sinusoidal forcing function of desired frequency and amplitude. The c.g. response to various terrains may be simulated by equating the left side of the corresponding equation of motion t the appropriate function.

This mathametical model may be easily extended to:

1. include a spring and damper to be located in the connection of the frame to the front axle, or

2. to consider wheels of different elastic properties.

It is planned to determine the dynamics of the 0.5 scale model experimentally and to verify or modify this analytical model to assist in obtaining the desired dynamic characteristics.

A.1.b. Structural Components

Objective. Design and construction of the individual parts of the model were to be completed early enough for assembly and testing of the vehicle by early May, 1974.

Progress. The full scale vehicle dimensions, and thus the half-scale model dimensions, were firmly established. Designs and construction have

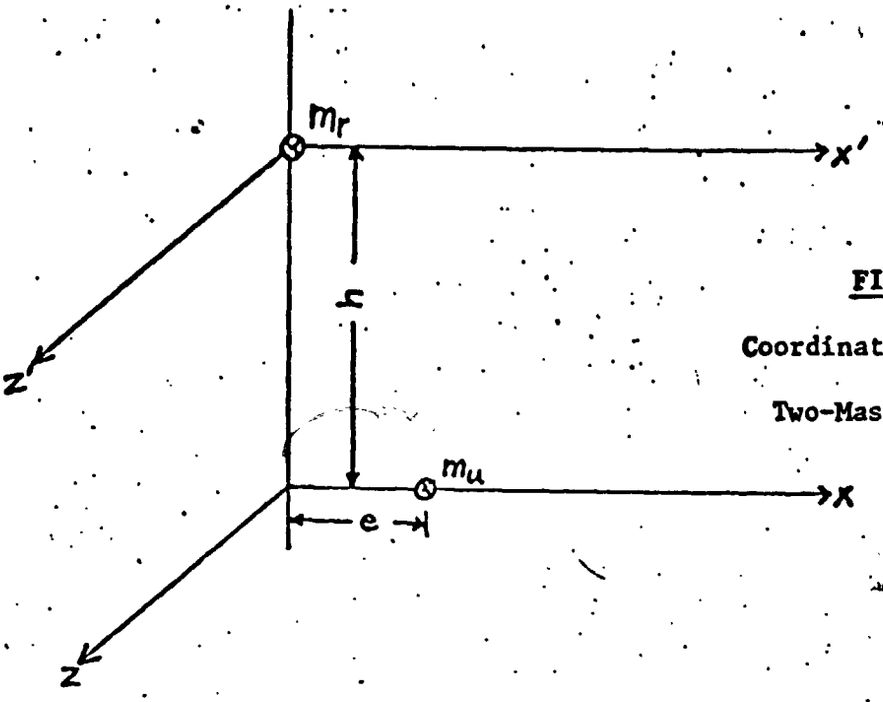

FIGURE 2

Coordinate System of

Two-Mass Vehicle

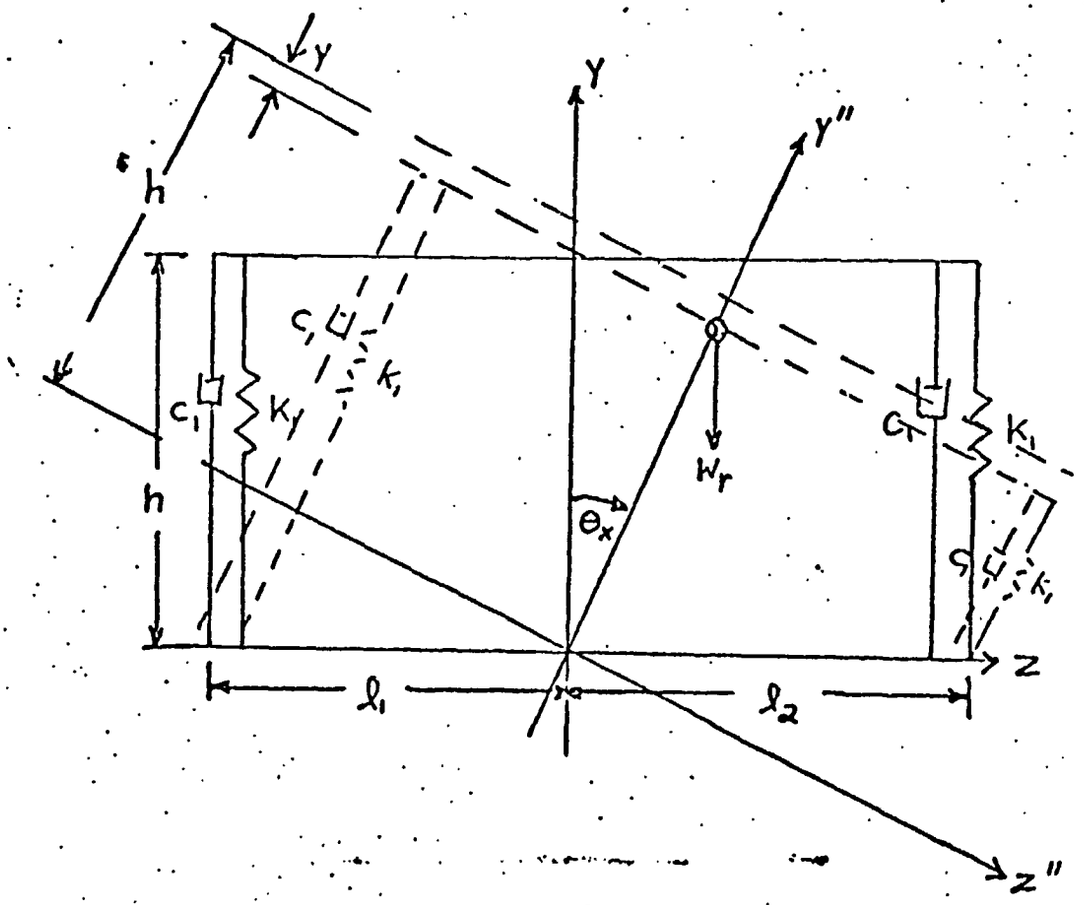

FIGURE 3

Roll (θ_x) with Vertical Displacement (y)

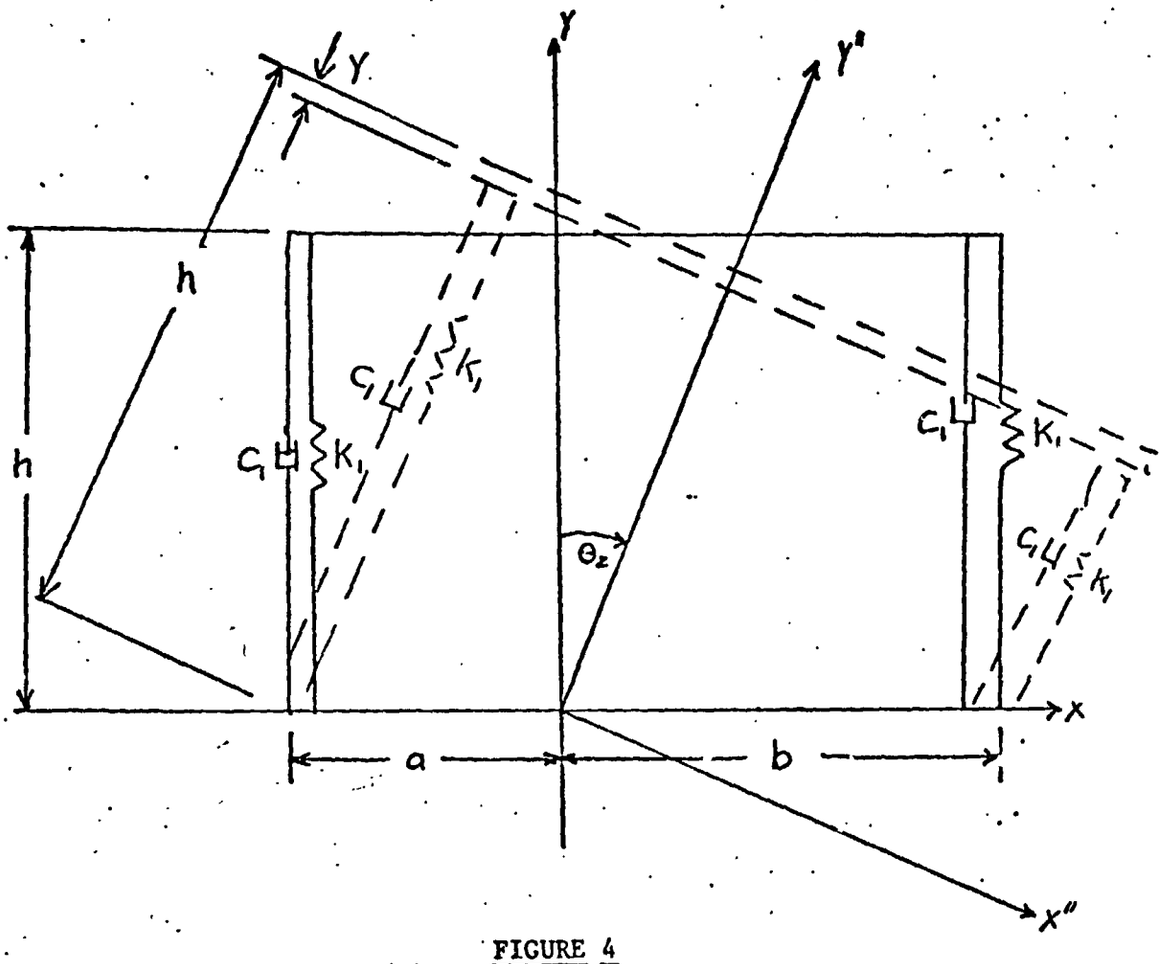

FIGURE 4

Pitch (θ_z) with Vertical Displacement (y)

been completed on the front steering gear box, the payload box, and the front axle. Design and construction is also complete on the back and front struts, the torsion bar assembly, and motor drive system.

Front steering gear box. This component shown in Fig. 5a and 5b must turn the front axle through the proper steering angles and, in the emergency maneuver (flip over of the vehicle), pivots the front axle 180° about the front struts. These two functions are accomplished by two self-locking worm gear pairs at right angles to each other. One worm gear pair governs the steering angle and the other controls the angle between the front axle pivot and the vehicle's front struts. Being self-locking, this design requires no brakes or other locking devices, and at the same time provides large gear reductions across each gear set.

Payload box. This component, Fig. 6, holds the scientific package, torsion bar assembly, batteries, etc. It is also a main structural member of the vehicle frame. It consists of an aluminum angle box frame with a 1/8" thick plexiglass skin. This construction allows visual inspection of contents and mechanisms inside the payload box while the vehicle is being demonstrated.

A.1.c. Deployment Hardware

Objective. To finalize the design of hardware components which enable the 0.5 scale model vehicle to deploy. The design of these components is based on the results of Task A.2., "Development of Launch Configuration and Deployment Procedure."

Progress Summary. The design and construction of deployment devices is complete. Finalized detail design and bench testing of hardware was completed and fully implemented on the 0.5 scale model.

Discussion. The deployment system consists of four subassemblies. These are:

- the front axle flip-over mechanism, Fig. 5a and 5b,
- the torsion bar assembly, Fig. 7, 10 and 11,
- the front strut hinge and locking mechanisms, Fig. 8 and
- the rear strut unfolding and locking mechanisms, Fig. 9.

The front axle flip-over mechanism has been finalized, Fig. 5a and 5b. It consists of a motor driving the front axle vis a worm-gear pair. The torsion bar assembly, Fig. 6 and 7, which controls vehicle height and payload attitude, and also takes part in deployment, is complete. Motors and gears have been selected, purchased and installed.

The basic design of the front hinge and locking device is shown in Fig. 9. This mechanism was constructed and bench-tested before it was incorporated into the overall design.

Testing has shown the front end to be subject to unexpectedly high shock loadings. Modifications are underway to sustain these loads without malfunction.

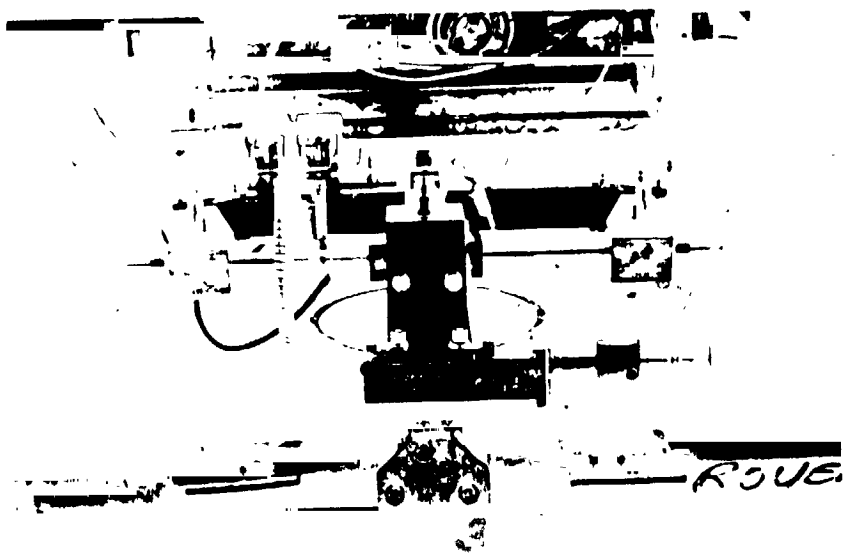

Fig. 5a. Front View of Steering and Front-Axle Flip-Over Mechanisms

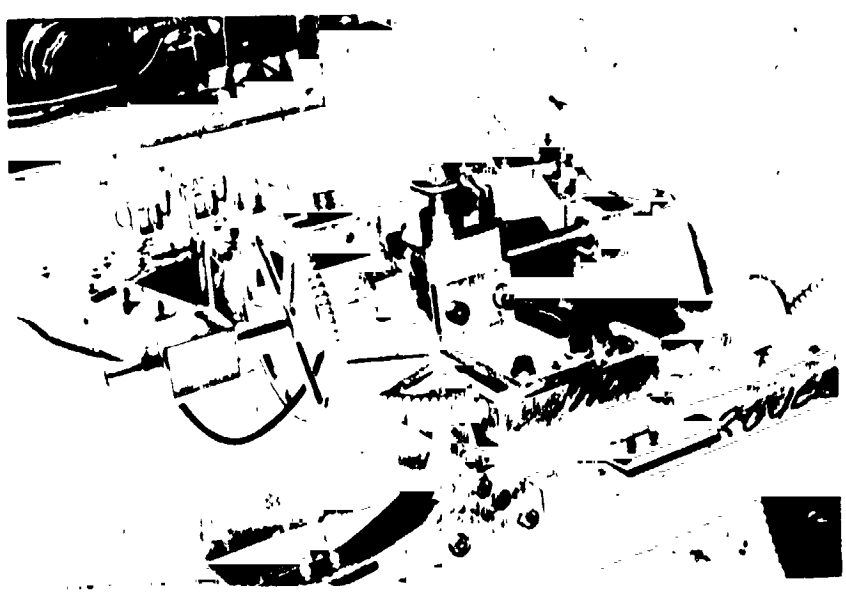

Fig. 5b. Front-Quarter View of Steering and Front-Axle Flip-Over Mechanisms

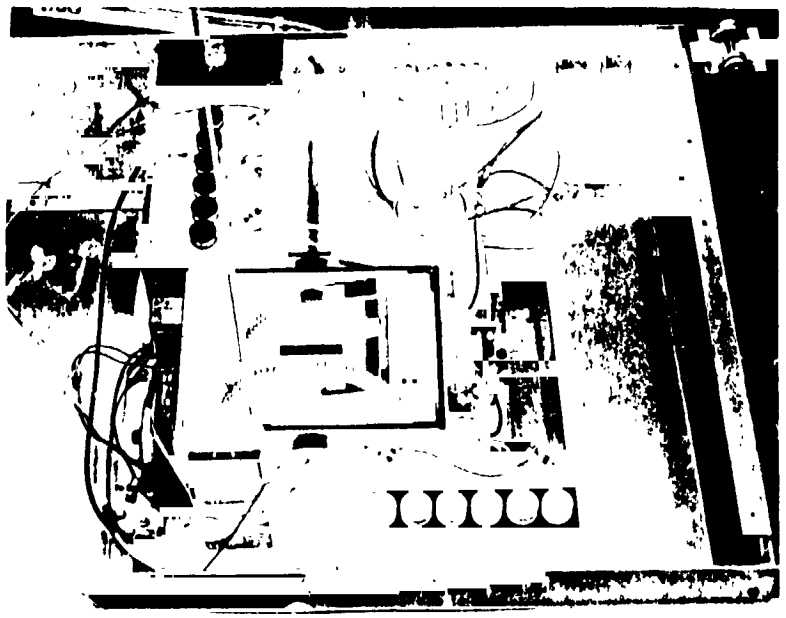

Fig. 6.Payload box contains batteries, communication and control equipment, front & rear-strut rotator and torsion-bar mechanisms.

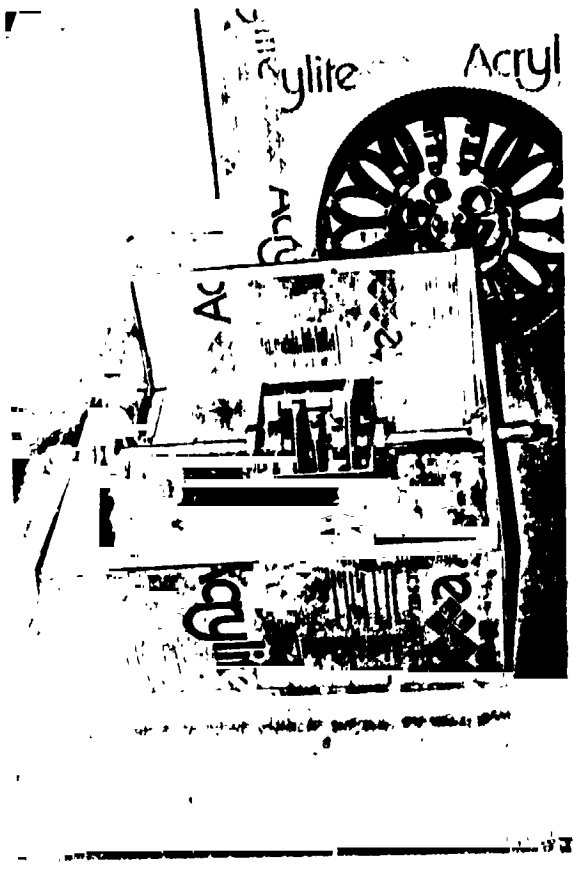

Fig. 7. Torsion-bar assembly for rear struts

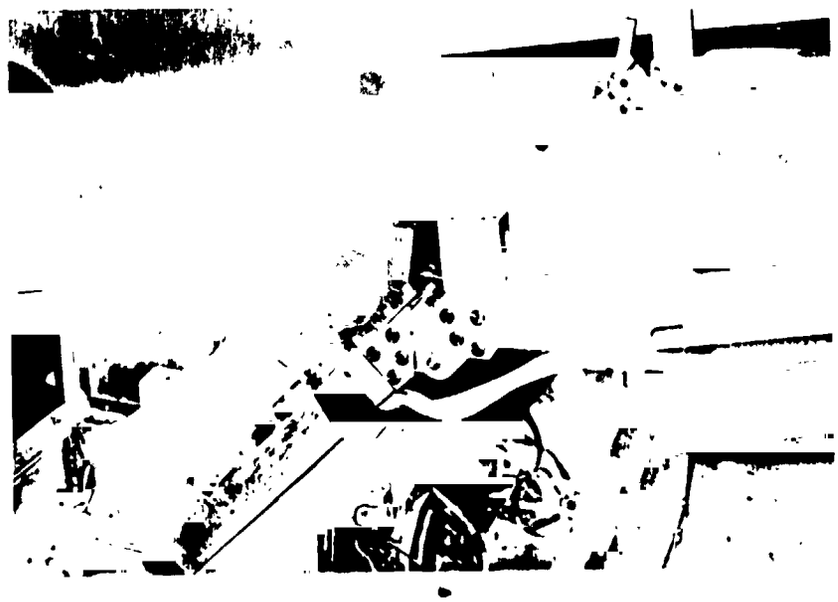

Fig. 8. Front-strut hinge and locking mechanism being deployed.

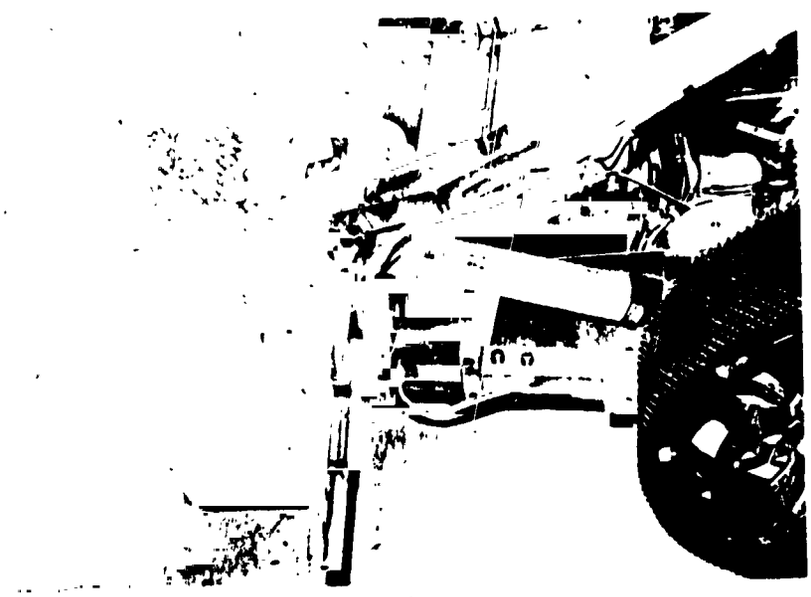

Fig. 9. Rear-strut folding and locking mechanisms

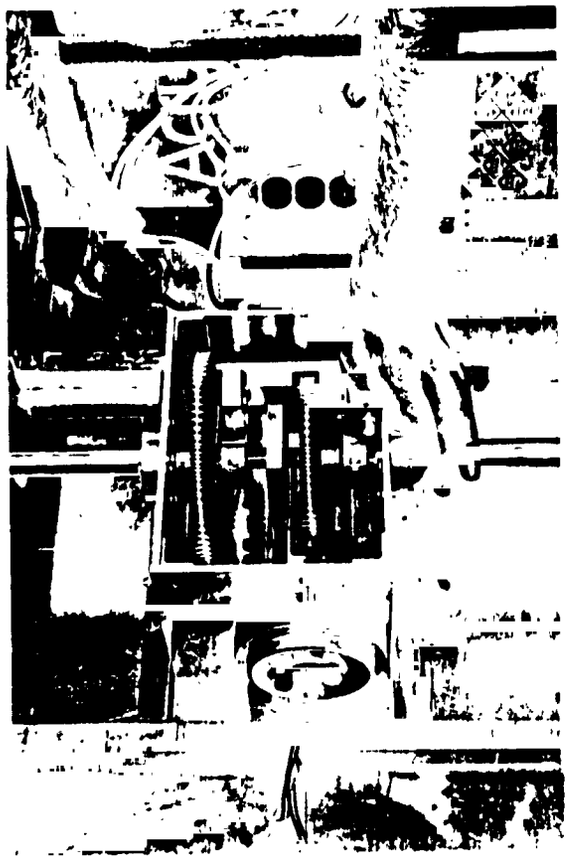

Fig. 10. Torsion bar assembly and its motor drive forward strut attitude motor is on far side of gear box, on the outside, near the demonstrator's right hand.

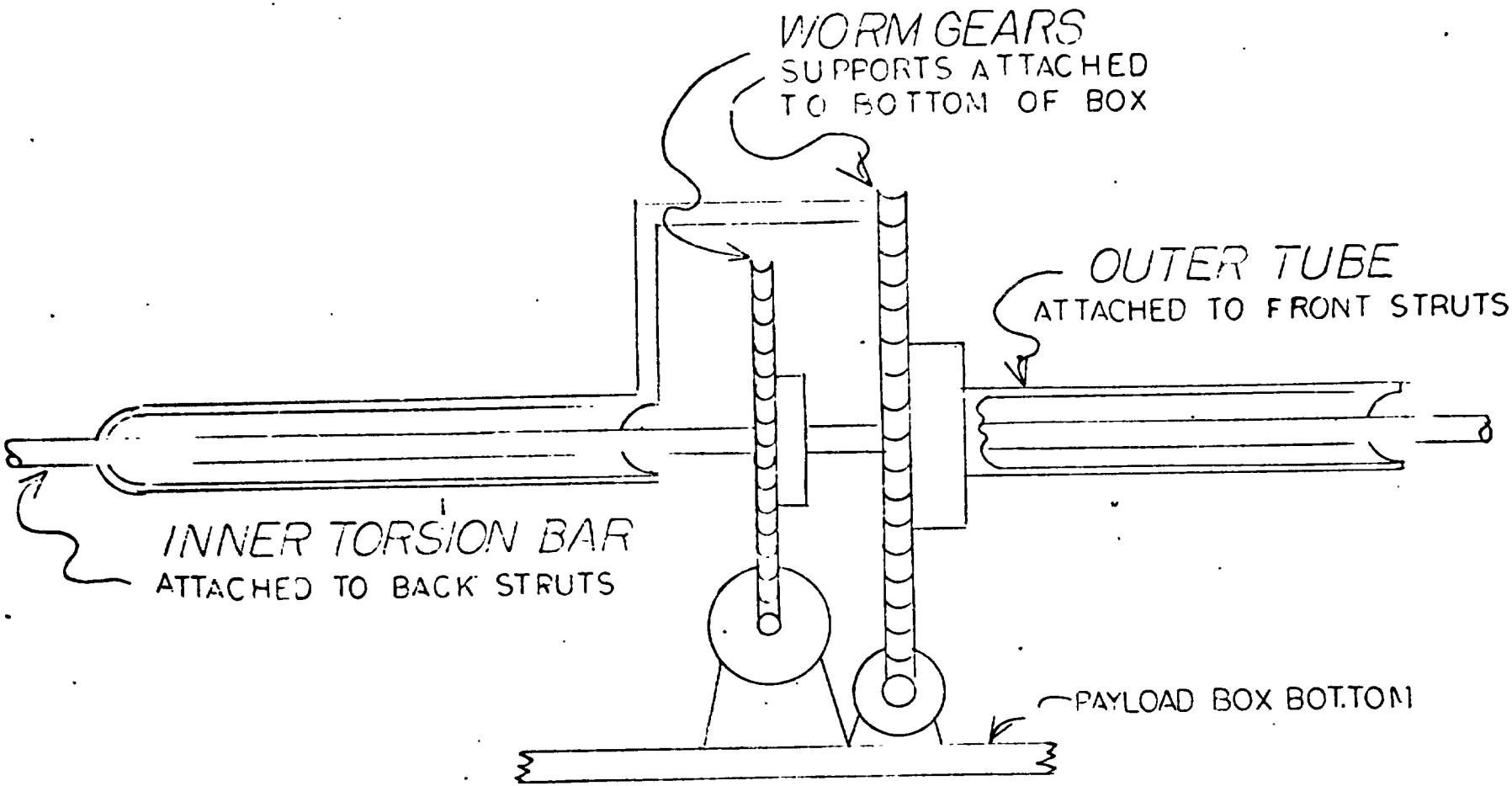

Fig. 11. TORSION BAR SCHEMATIC
(SEE ALSO FIG 10)

Schedule. Detailed design of all parts had to be completed by mid-February with fabrication of all parts completed some time in early May. This was accomplished.

A.1.d. Motor Drive and Mechanical Transmission Details

Objective. To design the most advantageous main drive motor and gear system for the half-scale model considering both physical and economic constraints.

Progress. Motors have been selected and procured. Design of the gear train, Fig. 12, 13, and 14,has been completed, tested, and installed.

Discussion. Based on tests and analysis of the previous 0.4 scale model, power and torque requirements were established for the half-scale model. With a selected design speed of approximately 1 mph the power required from each back wheel drive motor was set at 1/8 hp.

The market place was then searched for available motors. It was quickly established that torque motor types could not be used because of both their cost and their relatively high weight. It was also found that most other motors that would meet specifications would have to be made to order. This meant high price and long delivery delays.

A solution was found in some government surplus aircraft control motors. These motors could be obtained in a reasonable time and for a reasonable price. They served our purpose with only slight modification. Because the speed of the motors is 7500 rpm and the speed of the wheel at 1 mph is approximately 20 rpm, a gear train is necessary with a ratio of between 300 and 400.

The desired gear ratio is obtained from two sets of gears, a primary set of spur gears and a secondary set of worm and wheel. The design and analysis of the gear assembly is complete and has been implemented. There were no major problems in this area. The actual performance meets or exceeds design goals.

A.2. Launch Configuration and Deployment Procedure - P. Marino
Faculty Advisor: Prof. G. N. Sandor

Objective. To devise a launch configuration consistent with Viking Aeroshell limitations which would allow simple and reliable deployment.

Progress Summary. The basic launch configuration has been changed since last year's design so as to simplify the deployment procedure. This configuration is consistent with Viking capsule constraints and yields a satisfactory center of gravity location, Fig. 15 and 16.

Discussion. Last year's launch configuration required some type of device to lift the front section of the vehicle in order to put the Rover into its operational mode. Investigation showed this to be a source of difficulty, due to the large torques required and because of strict space and weight restrictions. With this in mind, a new launch configuration was devised which enabled the motors and gearing associated with the torsion-bar assembly in the

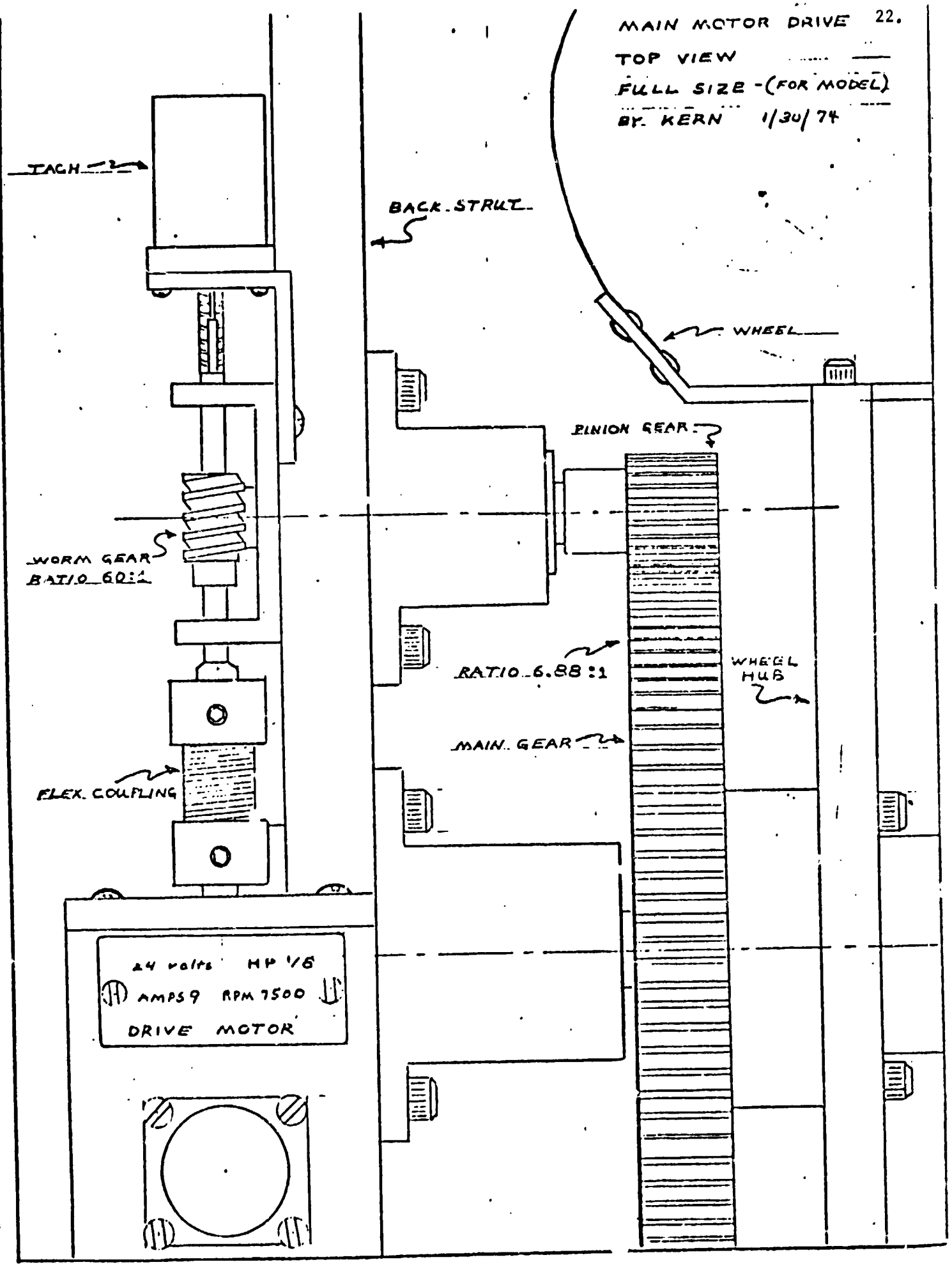

Fig. 1

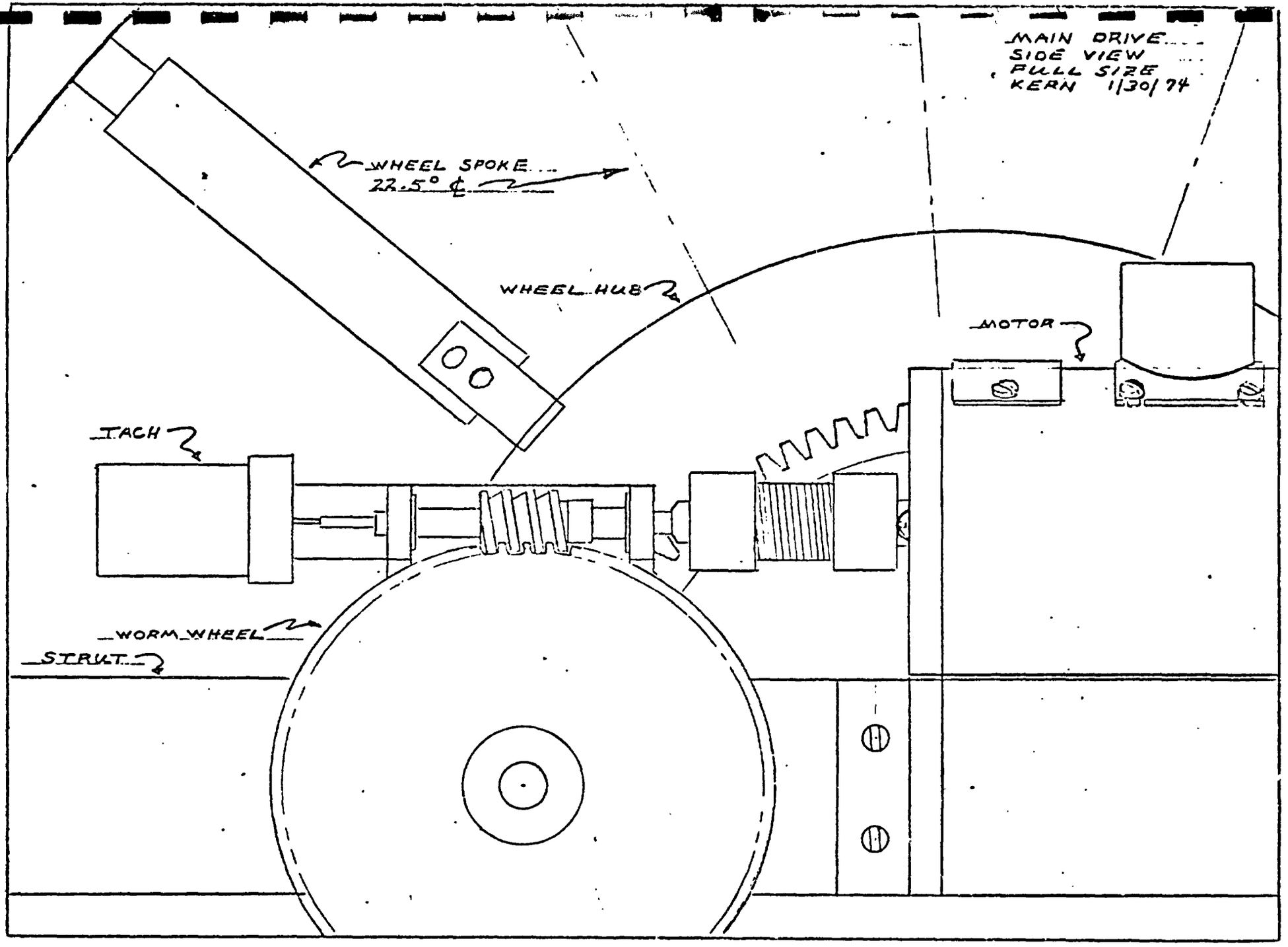

FIG 13 MAIN DRIVE MOTOR & GEAR TRAIN

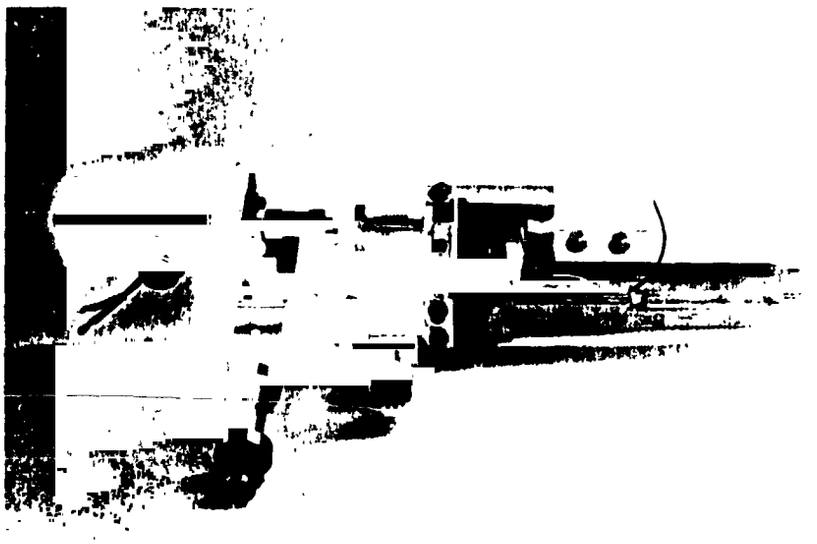

Fig. 14. Rear motor drive mechanism without rear wheel mounted

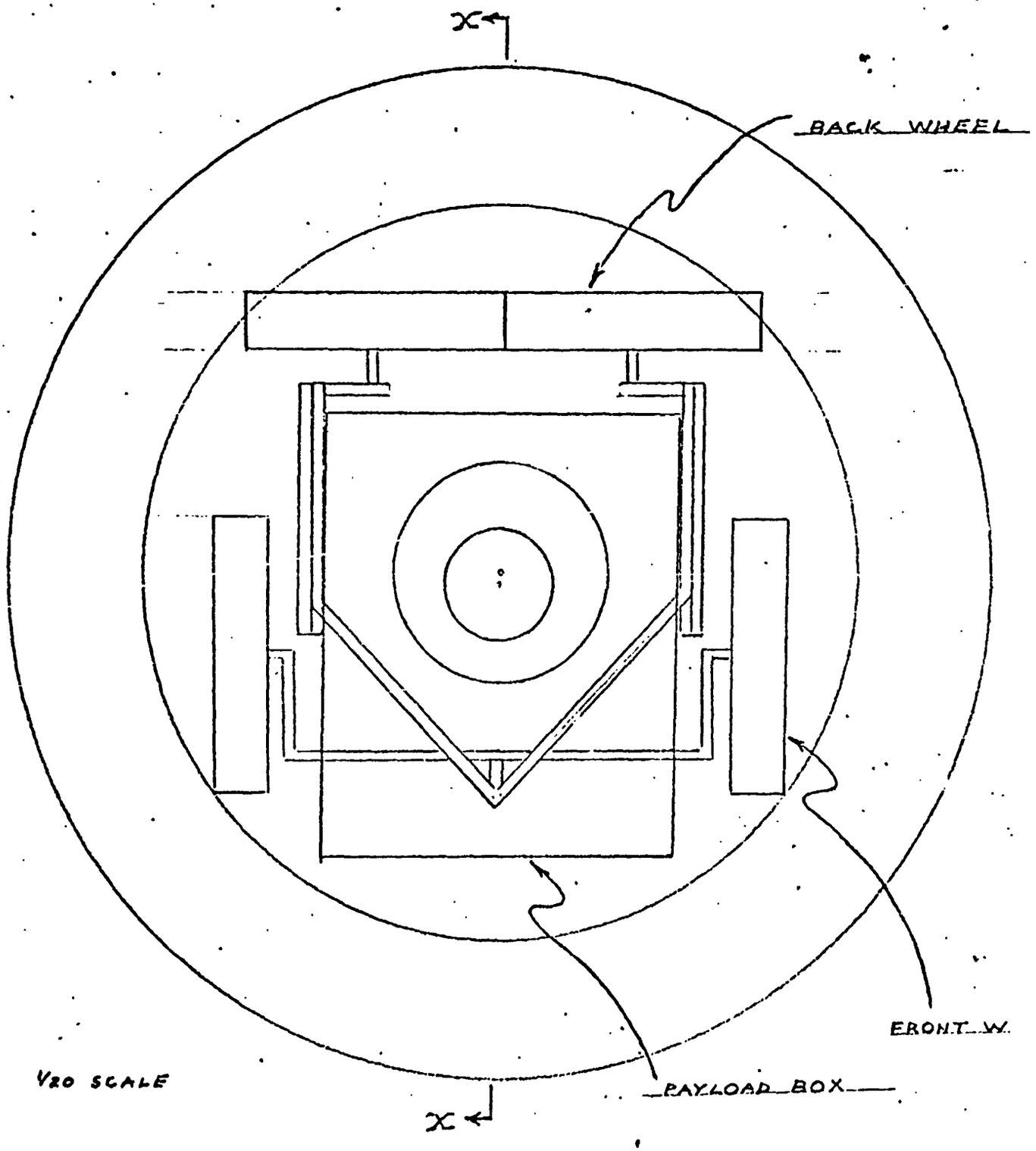

Fig. 15. FOLDED VEHICLE IN Viking Capsule
TOP VIEW

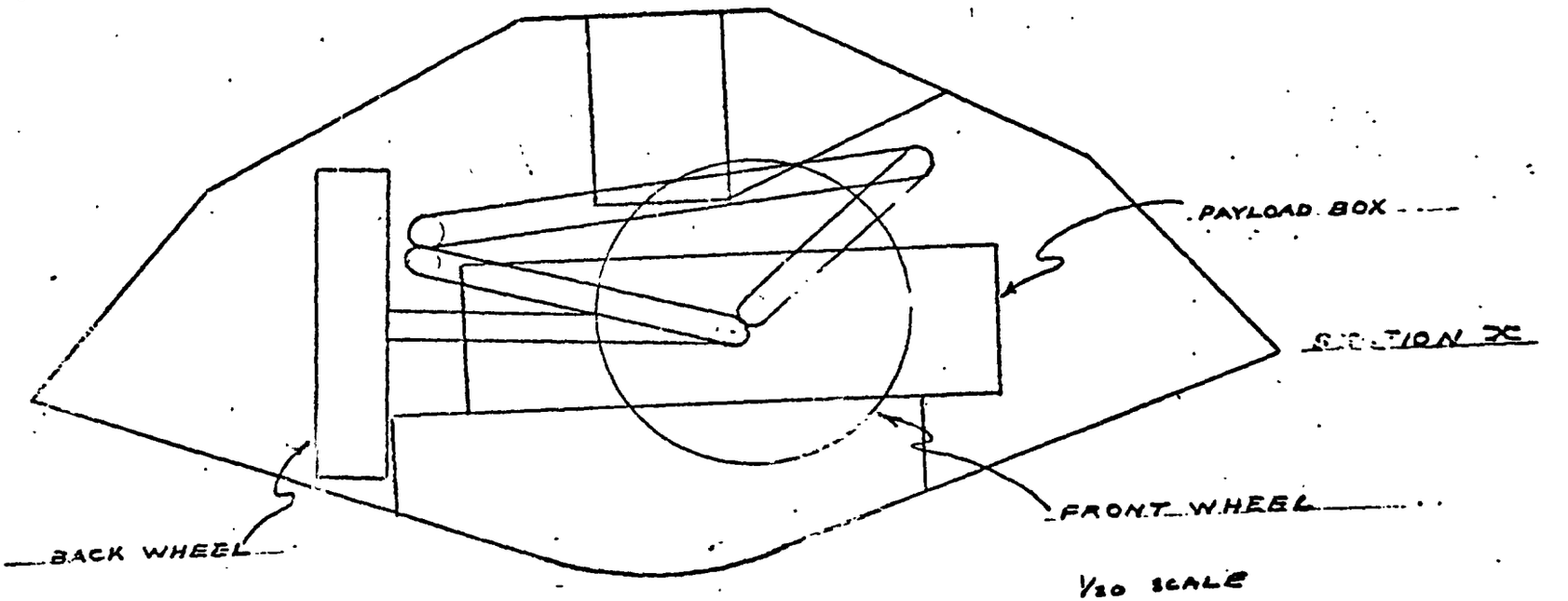

Fig. 16. FOLDED VEHICLE IN VIKING CAPSULE

payload to double as the source of power for deploying the front section of the vehicle. This turned out to be an excellent solution to what appeared as a potential problem.

To deploy from the launch-land configuration, Fig. 17, the front axle flipping motor changes the angle between the front struts and the axle to its normal attitude, moving the steering axle into a vertical position.

The forward strut attitude motor, Fig. 10, is then utilized to drive the rear section of the forward strut ahead while the front wheels roll forward on the ground, Fig. 18 and 19. This straightens the front struts to a position where the automatic latching devices, Fig. 20 and 21, lock the articulation in the deployed position, Fig. 22. To deploy the rear wheels, the strut-mounted individual rear-wheel propulsion drive motors are activated in the forward direction. As the rear wheels roll on the ground, they straighten out the articulated rear struts, Fig. 23 and 24, while the payload box still rests on the ground. Once straightened out, the rear strut articulation hinges are locked in the extended position, Fig. 24.

By driving both front and rear struts downward, the payload is now raised off the ground and the vehicle becomes fully operational, Fig. 25 and 26.

A.3. Wheel Testing and Design - D. Kern, J. Harrison, C. Deno and G. Scapellati
Faculty Advisor: Prof. G. N. Sandor

A.3.a. Wheel Tester and Grouser Design

Objective. To determine the optimum grouser design for use on the RPI MRV.

Progress Summary. Several grouser designs have been tested on the wheel testing machine. One design was shown to be superior to the others and has been used on the half-size design.

Discussion. Studies showed that the proportions of the old .2 scale wheels were close to the desired proportions of the wheels for the .5 scale model. These .2 scale wheels were used to conduct run-offs between several grouser designs with respect to pulling power and also distance/time performance with identical restraining loads. With the aid of EDL's wheel testing equipment, Fig. 27, three alternative grouser designs, Fig. 28, were tested in detail. As a result of this program, the knobby tread was selected for implementation.

A.3.b. Wheel Analysis

Objective. To analyze the various possible wheel hoop configurations and select the optimum design for the RPI MRV.

Progress Summary. A wheel design has been chosen, constructed and tested, and proved to be superior to last year's wheel.

Discussion. Last year's circular hoop-spoke design proved to lack sufficient lateral stiffness. During the 1973 summer, several hoop designs were constructed and analyzed. The best design with respect to lateral stiffness was chosen and was used on the wheel in 1973-74, Fig. 29.

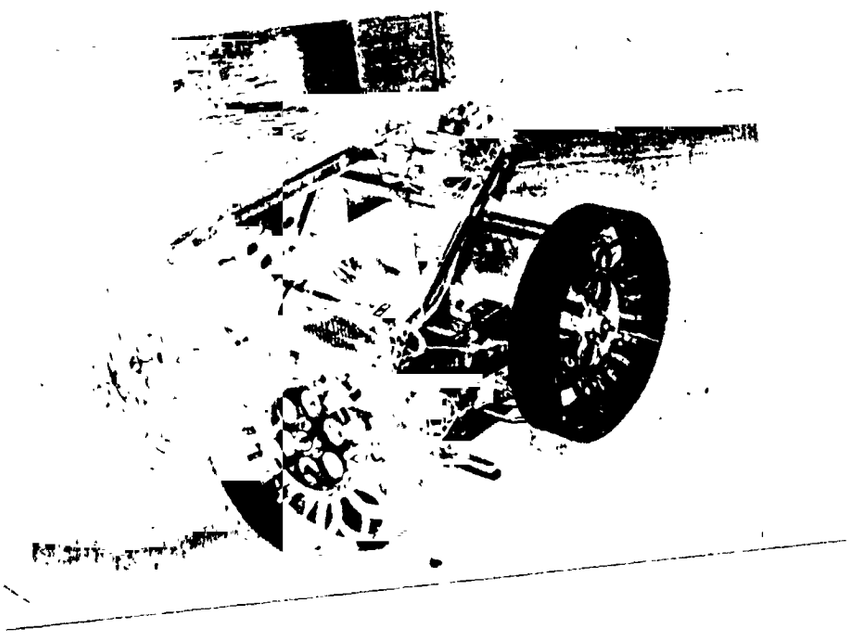

Fig. 17. Folded launch-land configuration

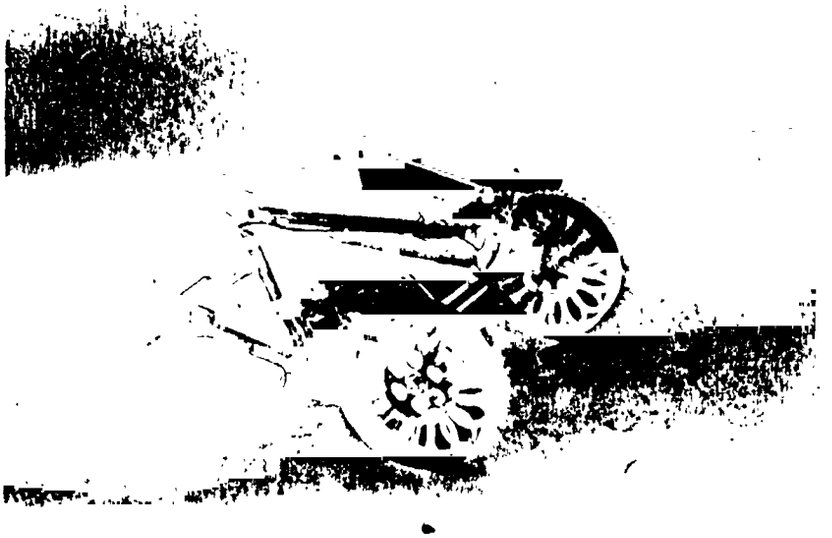

Fig. 18. Deployment Sequence #1: Front Struts are rotated clockwise rolling the front wheels on the ground.

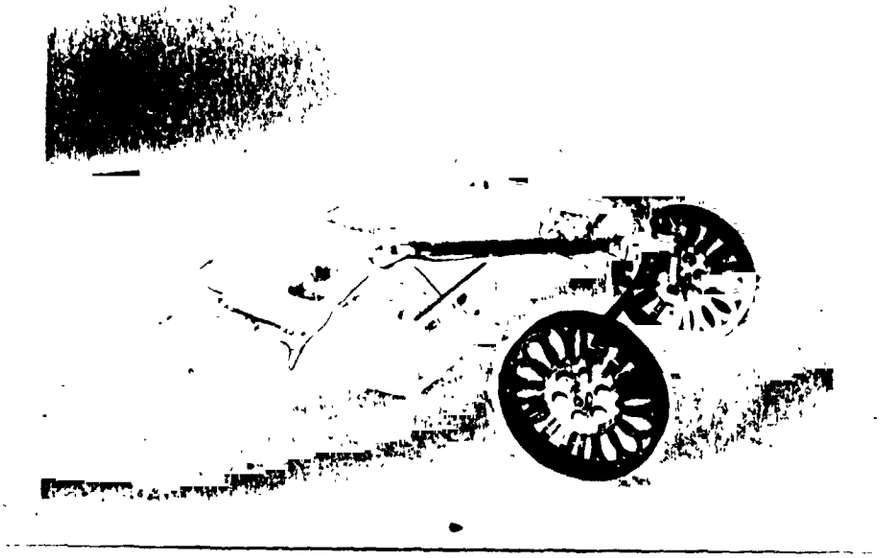

Fig. 19. Deployment Sequence #2: Front strut articulation begins to straighten while front wheels roll forward

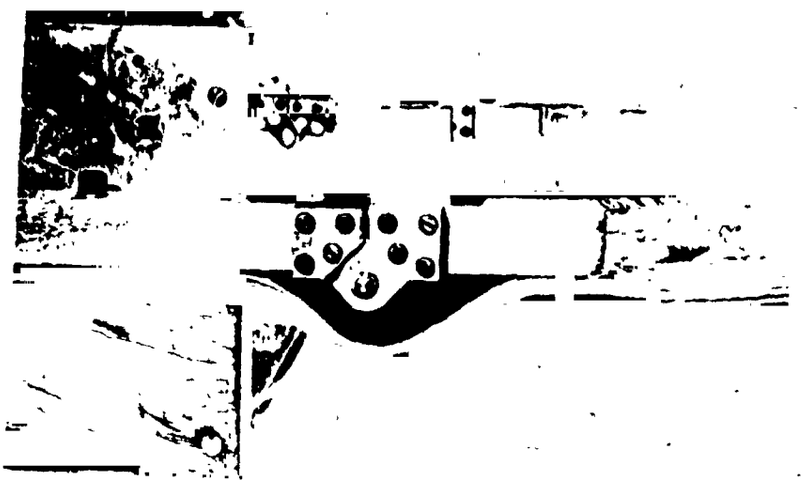

Fig. 20. Front strut latching device in deployed, locked position

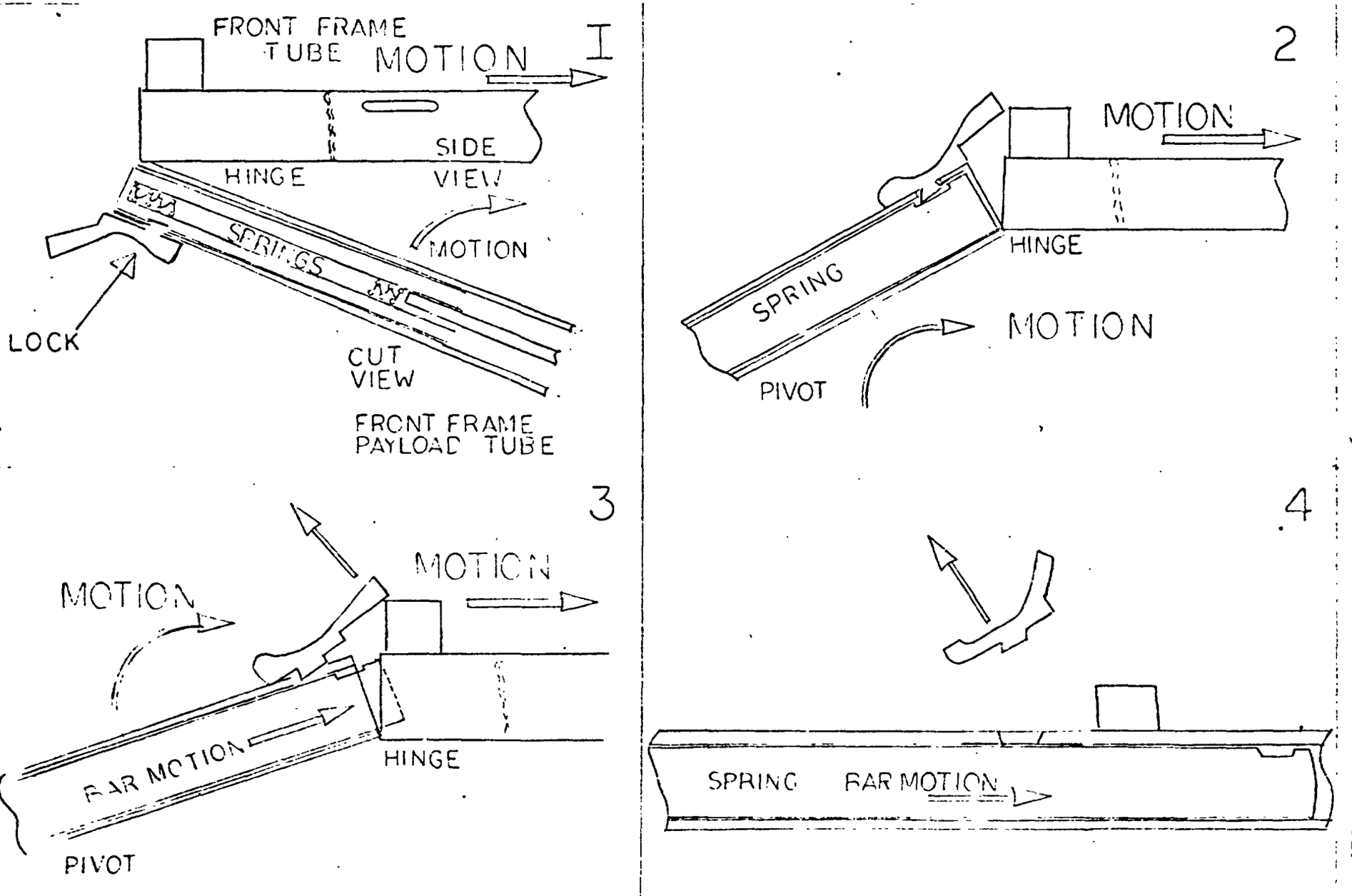

FIG.21. RPI MRV FRONT HINGING MECHANISM

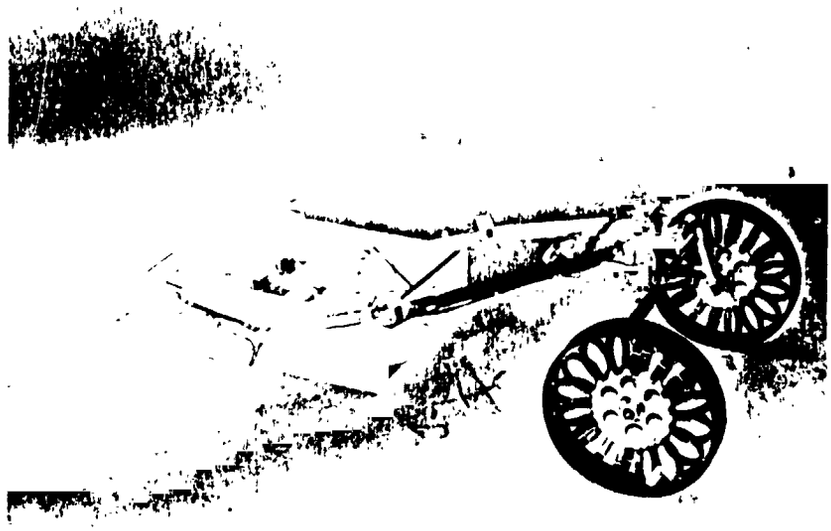

Fig. 22. Deployment Sequence #3: Front struts straight and locked, payload still on the ground.

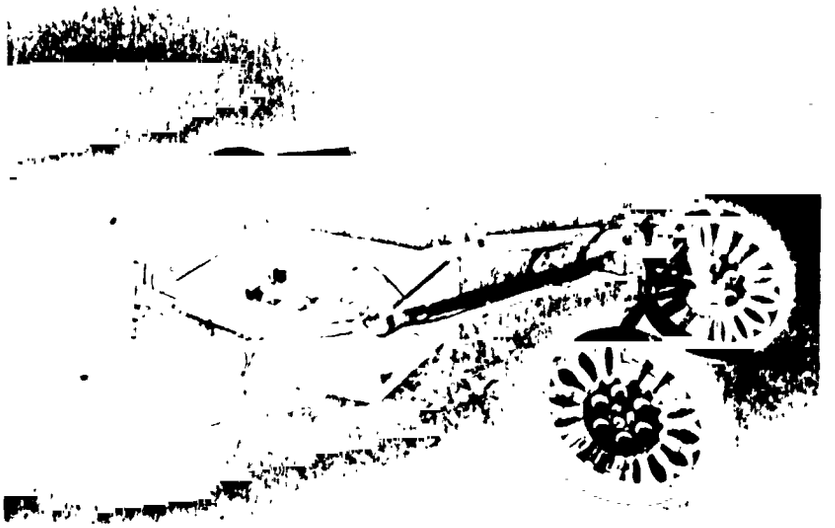

Fig. 23. Deployment Sequence #4: Rear Wheels begin to rotate forward, rolling on the ground and straightening out the folded rear struts.

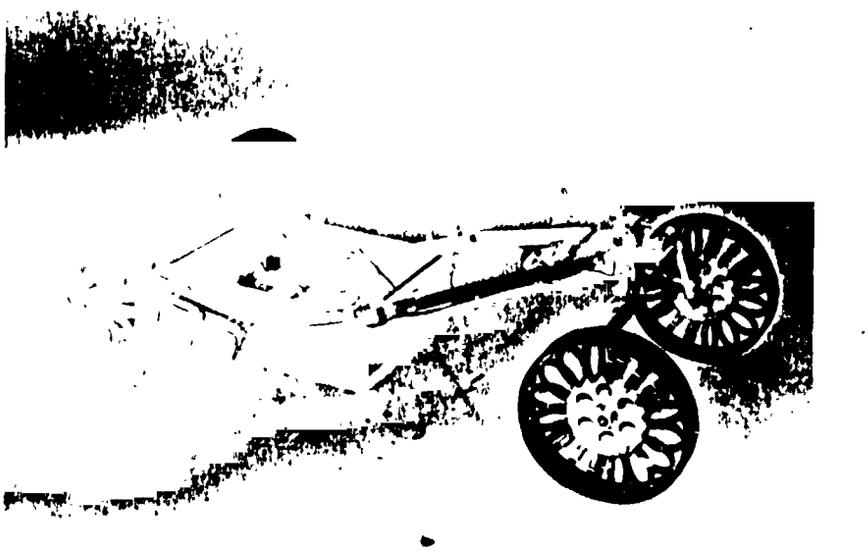

Fig. 24. Deployment Sequence #5: Rear Struts also straight and locked, payload still on the ground.

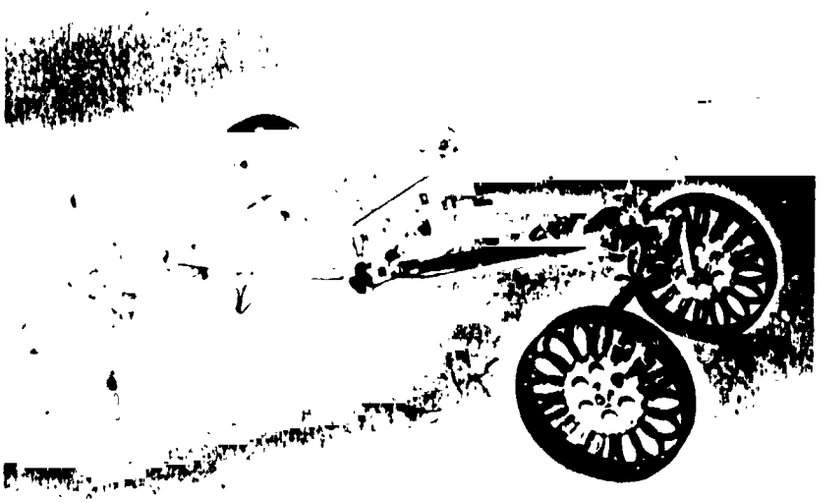

Fig. 25. Deployment Sequence #6: Front end of payload box begins to lift off the ground.

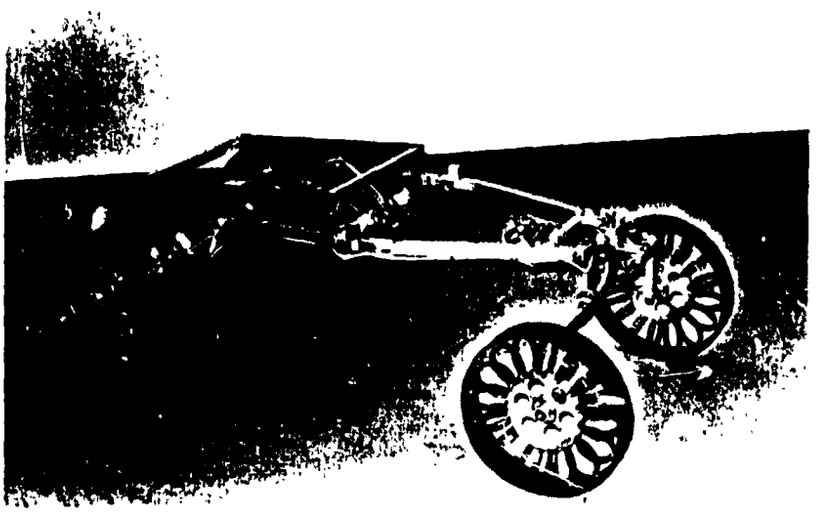

Fig. 26. Deployment Sequence #7: Ready to Rove!

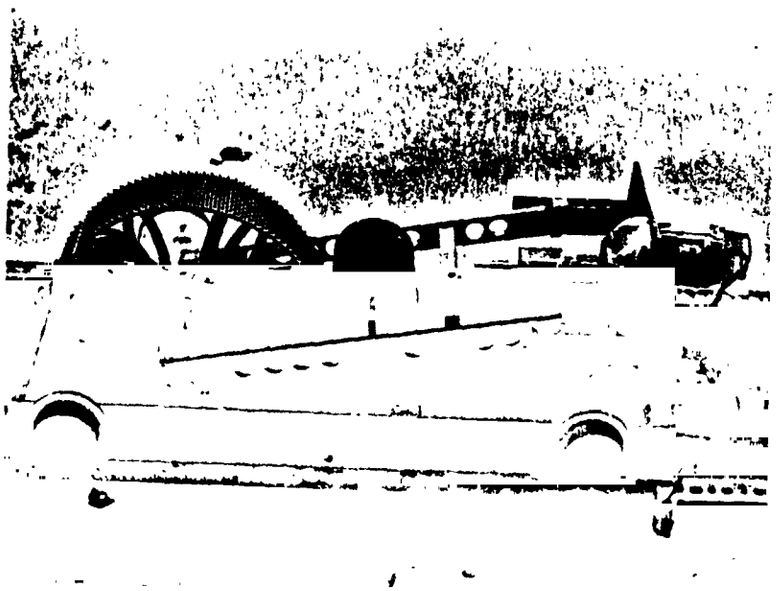

Fig. 27. The NASA-RPI Scaled-down Wheel tester facility.

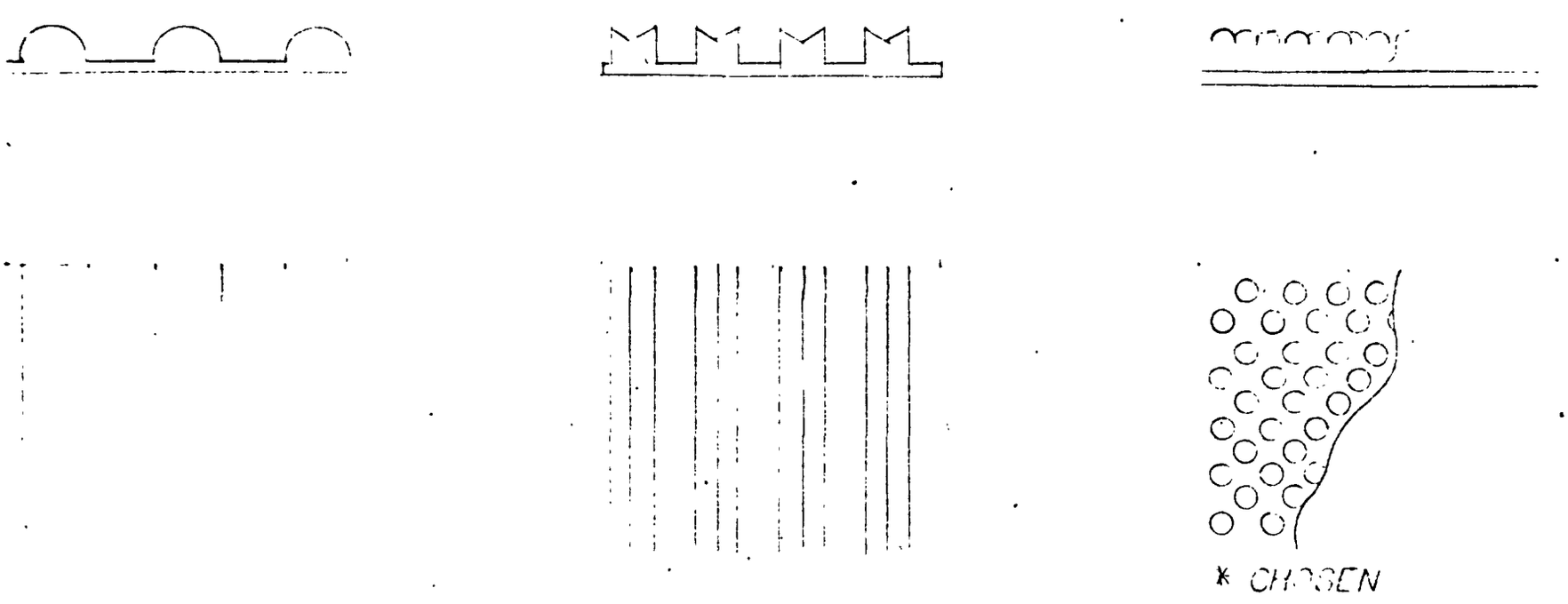

Fig. 28. TESTED GROUSER DESIGNS

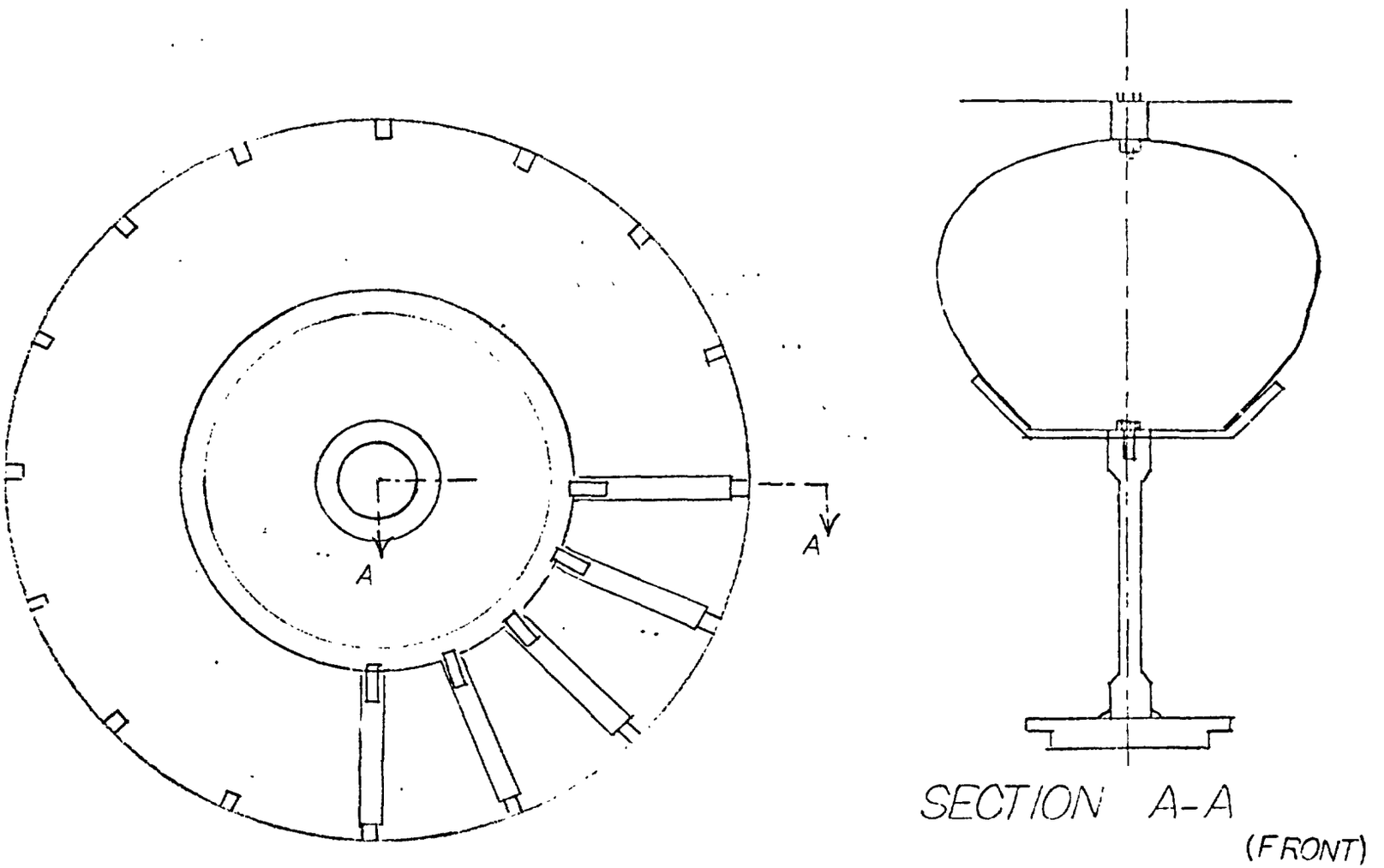

Fig. 29. RPI'S TOROIDAL WHEEL

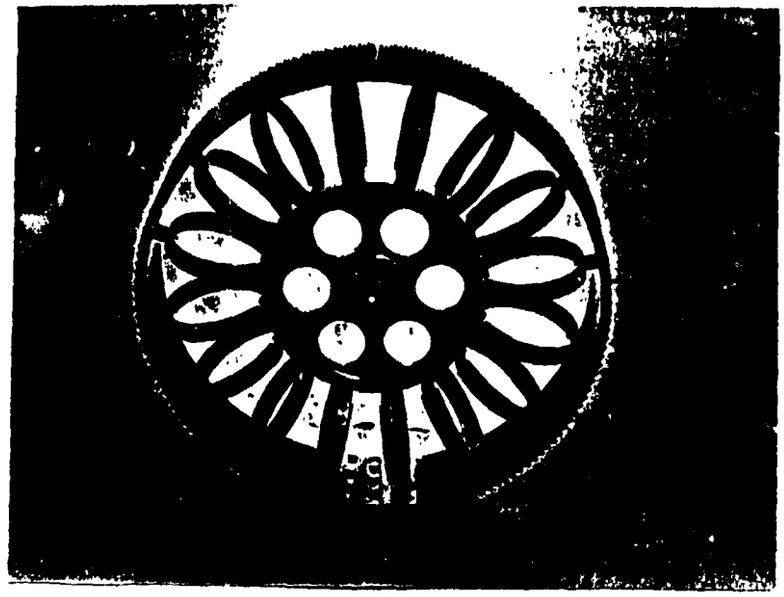

Fig. 30. RPI's toroidal metal-elastic wheel with improved lateral stiffness.

A.3.c. Detailed Wheel Design and Construction

Objective. Wheels of the new improved design were constructed for the half-scale model, Fig. 30.

Summary Progress. An improved design is complete, four wheels have been constructed and installed on the 1/2 scale model.

Discussion. The previous design for the MRV wheels had a problem in lateral stability: the old wheels could not resist side loads of any great magnitude. To solve this problem, the hoop-spokes were stiffened near the hub and their shape altered from the former circular configuration to a pear-shaped curve, Fig. 29.

The detailed mechanical configuration of hub and bearings has been established. A method of construction of the wheel hubs was found to save aluminum and weight; heliarc-welded bearing sleeves in the wheel web saved many hours of machining. In addition to these points, it was decided to make the rear wheels stiffer than the front wheels by increasing the thickness of both the hoops and the rim, rather than to change the configuration or the number of spokes. Rubber mounts were selected and procured to serve as hinges between spokes and outer rim, assuring larger footprint.

A.4. Radio Control - J. Cooley, D. Perly, L. Heyl, L. Bradshaw, T. Geis, K. Fell
Faculty Advisors: Prof. G. N. Sandor, W. Moyer

A.4.a. On-board Electrical Controls

Objectives. Control of on-board motors for steering, speed, payload raising and leveling, and emergency maneuver.

Progress Summary. A scheme for controlling the motors with digital information has been developed, Fig. 31. It involves digital/analog (D/A) converters and analog speed and position feedback at the motors. This system is complete, has been constructed, tested and is operational.

Discussion. The vehicle functions are divided into four subsystems as follows:

Subsystem A - steering

Subsystem B - speed

Subsystem C - payload

Subsystem D - miscellaneous

A. The steering commands are stored in an analog Read Only Memory (ROM), consisting of an operational amplifier and a resistor ladder. The commands are addressed by a 4-bit digital word, and take the form of a reference voltage. This voltage is fed into a position control feedback network which controls the steering motor. The analog ROM has been built and tested for steering angles of 0^{o}, $\pm 5^{o}$, $\pm 20^{o}$, $\pm 30^{o}$,

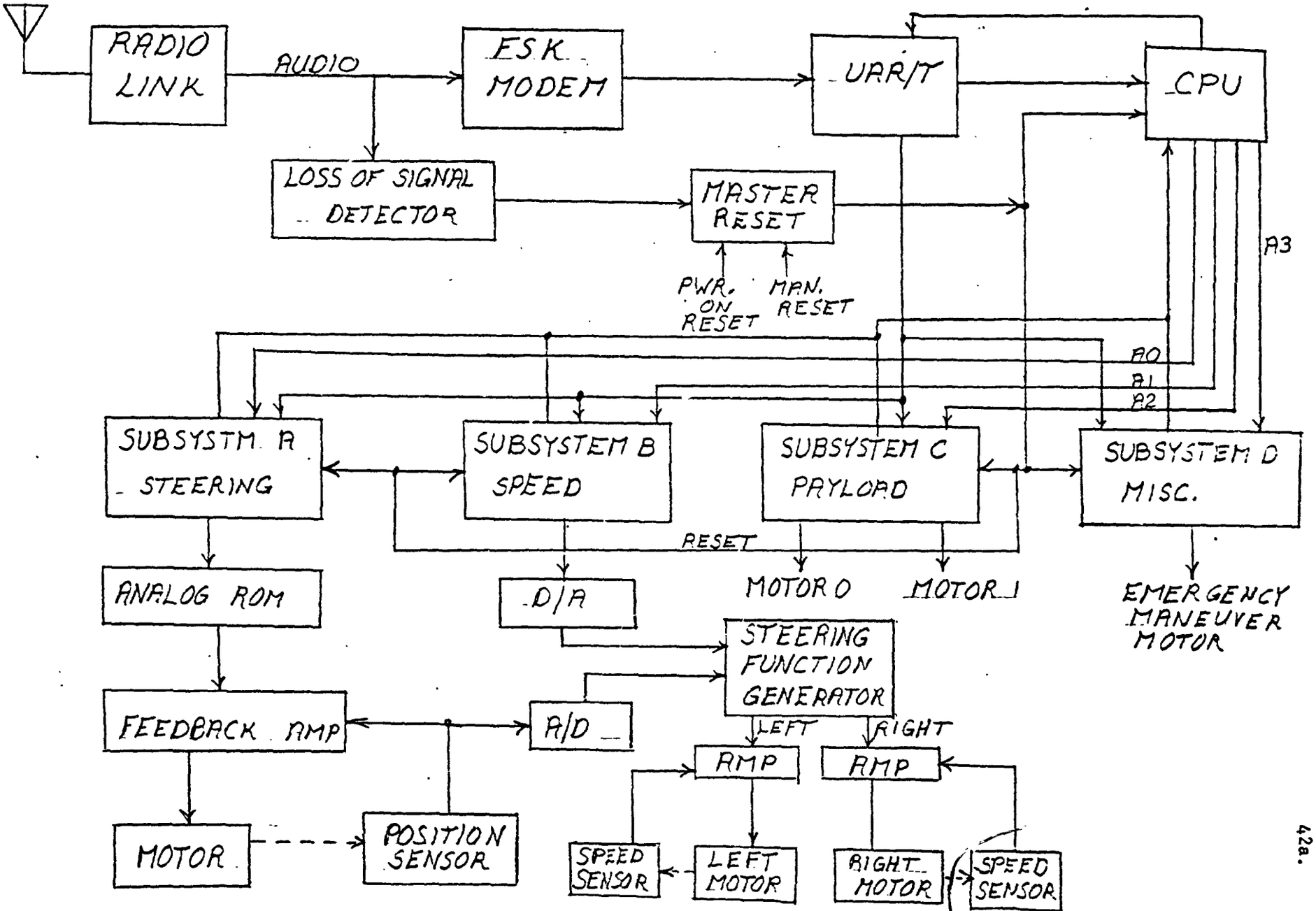

Fig. 3 1. Receiver Logic

$\pm 45^{\circ}$, $\pm 60^{\circ}$, and $\pm 90^{\circ}$. The motor control is a lead-compensation control system, with a relay driver for the motor. This system is currently operational.

B. The speed voltage reference selected by the operator, is generated in a 2-bit plus sign-bit D/A converter. This signal is fed into an electronic differential which uses a signal from the steering subsystem to generate the required differential action in the rear wheels to avcid skidding in a turn. The rear wheel motors are controlled from there by a tachometer feedback scheme. This system is also in operation.

C. The two payload motors raise and lower front and rear struts, levelize the payload and activate the deployment sequence. They are controlled in a forward-backward-stop mode by relay drivers.

D. The remaining subsystem controls only the emergency maneuver motor in the forward-backward-stop mode. This motor causes the steering post to rotate with respect to the front struts about a transverse horizontal axis. The status of this and the last subsystem is the same as the previous one: all are operational.

The major problem encountered was motor noise interference with the control system. The judicious use of shunt capacitors, grounding and similar noise-reduction techniques helped overcome this problem.

A.4.b. Radio Link

Objectives. Radio communication with the vehicle and routing of commands to proper subsystem.

Progress Summary. Frequency shift key (FSK), encoding is used with walkie-talkies to provide the necessary link. The entire system is in operation.

Discussion. The serial output of a Universal Asyncronous Receiver/Transmitter (UAR/T) is fed into an FSK modem (modulator/demodulator) which uses a Voltage Controlled Oscillator to generate two audio tones corresponding to the two binary logic values. These tones are transmitted via the walkie-talkies to the vehicle. They are decoded to voltage levels via a Phase Lock Loop and Comparator. The signal then goes to another UAR/T for decoding. Control Logic then checks the validity of the signal and routes the signal to the proper subsystem.

This entire system has been run on the bench, repackaged for installation in the remote control box, Fig. 32a, and on the vehicle and is in operation.

A.4.c. Remote Control Station and Transmitter Design

Objectives. Manual interface for remote control of the vehicle.

Progress Summary. An interface permitting manual open-loop remote control of the vehicle was designed, constructed and implemented on the 0.5 scale model rover.

Discussion. There is a rotary switch to select one of the four subsystems and an array of sixteen pushbuttons to select the command desired for each subsystem, Fig. 32c. Once the command is loaded in with the pushbuttons, it is transmitted by pushing the "send" button. This is to avoid inadvertently sending the wrong command.

In transmitting, the command is loaded into the UAR/T mentioned earlier. The UAR/T then provides a serial signal for the FSK modem and walkie-talkie. The physical system is shown in Figure 32b.

Task B. General Systems Analysis

B.1. System Modeling and Design Optimization - C. Pavarini
Faculty Advisor - Prof. E. J. Smith

Optimal designs have been developed for three major alternative models, i.e. four-wheeled vehicle with either direct earth link or an orbiter-earth link and a six-wheeled vehicle with a direct earth link. The method by which to obtain optimal design for these and other cases has been developed in general terms. Methods for determining the sensitivity of the optimal designs to perturbation of design parameters have also been developed. This task was completed during the fall of 1973 and a technical report, Ref. 4, was issued in June, 1974.

B.2. On-Board Computer Design - B. Fishman*
Faculty Advisor: Prof. E. J. Smith

The objective of this task is to develop the software and hardware design specifications for the on-board computer. In addition, support will be provided for the remote control of the 0.5 scale vehicle.

During the 1972-1974 period the on-board computer design was investigated by a statistical approach using queuing theory and random variables to study the average behavior of the computer-vehicle system. The computer-vehicle system interaction was modeled by assuming the computer could be viewed as a queue server, servicing "customers" on two queues, a fixed queue and an interrupt queue. The results of this initial study brought into focus the more important problem of the overall computer design. It was apparent that the computer design specifications, both in regard to software and hardware, was necessary before a logical design process could be initiated. To determine these specifications, it is assumed that all of the control and scheduling decisions will be provided autonomously by the computer. The goal will be to synthesize a design that will meet the lowest realizable specification bound. Since changes in one part of the design can affect other areas, the design process has been initially divided into several steps.

The first step is the identification of what would determine an optimal design. Volume, weight, and cost are the physical restrictions on the computer. Power consumption and heat generation also affect the usefulness of a design. In the process of optimization one can compare the amount of hardware necessary for various approaches to a part of the

* Work was temporarily discontinued in this subtask as of February 1, 1974. This section summarizes the status as of that date.

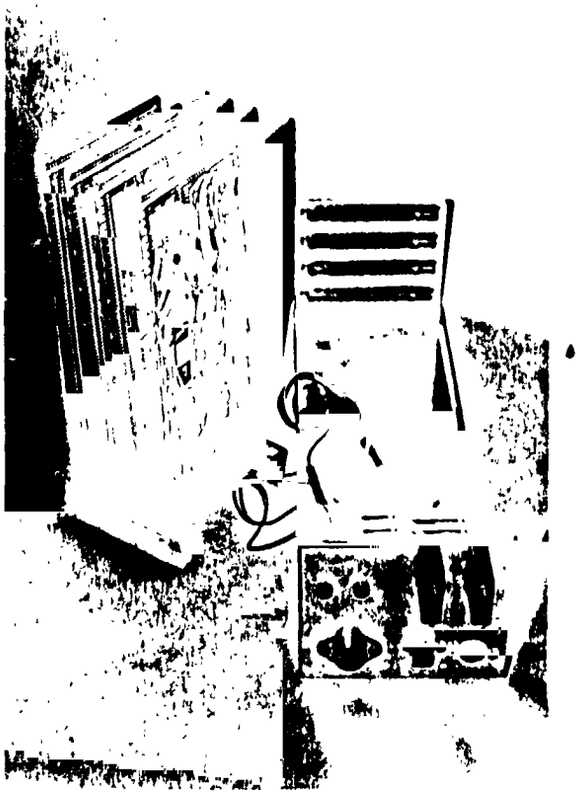

Fig. 32a. Vehicle (receiver) electronics

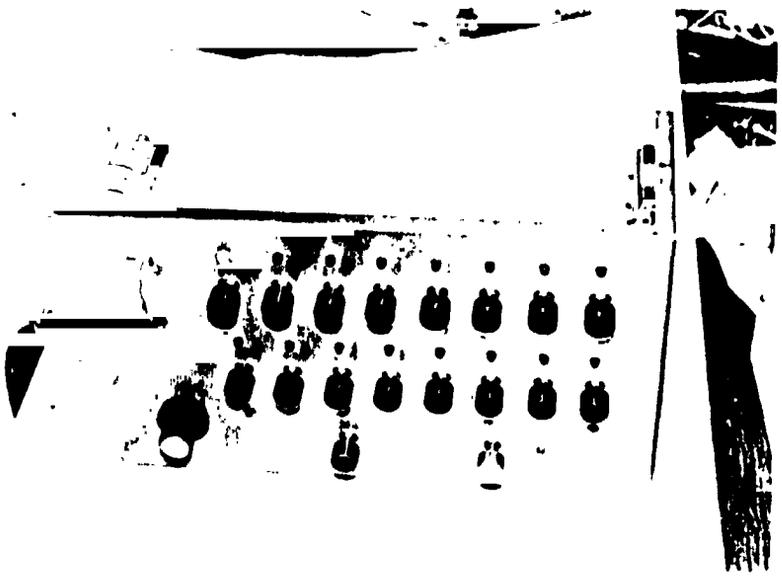

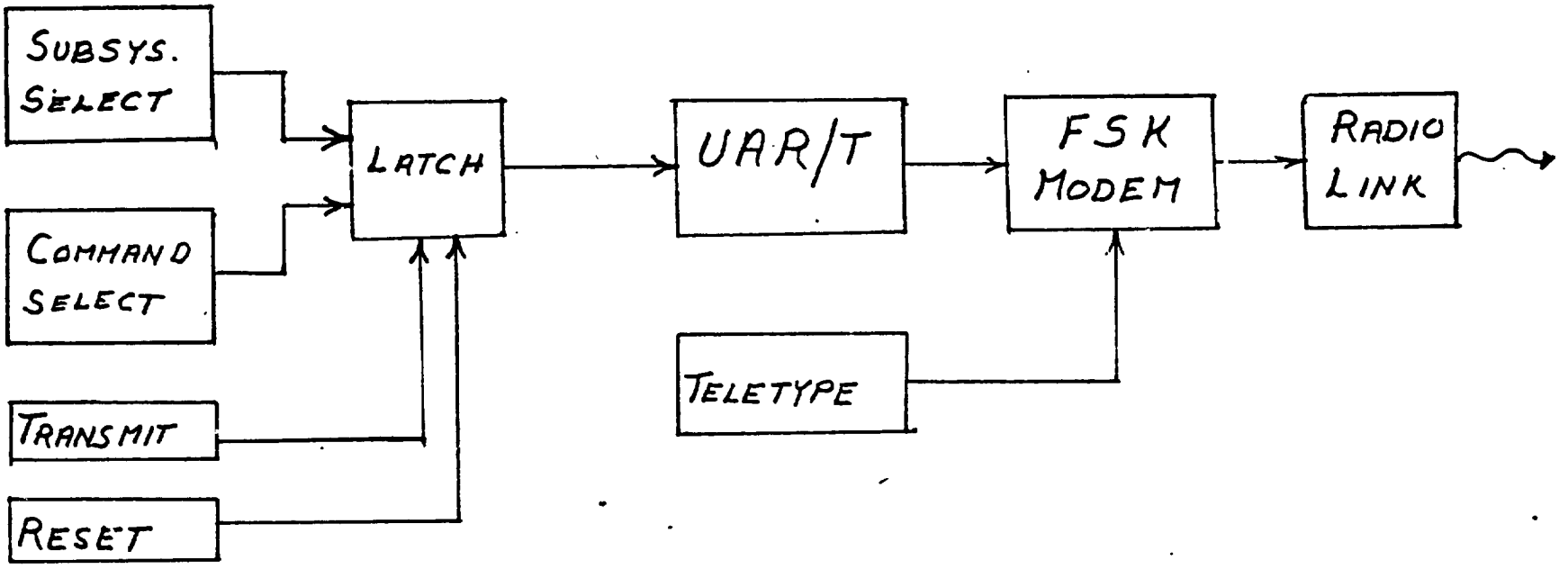

Fig. 32c. WITH ROVER DEMONSTRATION MODEL

design. In terms of primary storage, switching networks, and operation features which are fabricated by means of integrated circuit chips the above restrictions are monotonically related so that changes in one of them such as weight gives predeterminable and closely related changes in the others.

Therefore except for changes in input-output devices and possible use of secondary storage the above "costs" can be looked at in one measure, complexity.

The other restriction on the design of the on-board computer is the ability to perform the functions required of it. These functions can be looked at in the general sense as the reading of sensors, making of decisions which may involve further reading of sensors, and operation until finally a result is stored for later use and/or commands generated for the purpose of control. This could further be reduced to requirements of storage and the amounts of various types of operations performed. Due to the presence of decisions and therefore multiple logical paths the storage and operation requirements may be random variables. The requirements produced by these functions would be how often they need to be done, and the response quickness required.

At this point the initial hardware decisions can be made. Assuming the sequencing method uses little time or storage, the word size or sizes can be chosen in regard to the accuracy needed in calculations and information content of logical variables. The decision of what types of operations should be hardware wired, and how, can be made. The number and types of operations are known. Since the time an operation takes can be balanced against the hardware required, the value of shortening of time vs gain in hardware is not precisely known at this point. However, an estimate should be reasonable knowing that the computer time required cannot be reduced without changing the handling of the functions.

Some of the software decisions can be made at this point. Due to considerations outside the computer, many functions cannot take place simultaneously. This could be due to battery drain as well as physical incompatibility of some functions. The vehicle would not rove and be expected to charge the batteries at the same time. The decisions of the types of modes can be made now since consideration of response times will have been made. This would not significantly effect hardware since even if an operation is used more frequently in a particular mode, its average use remains the same. Changes in mode would be by interrupt, i.e. low battery, or simple completion of mode purpose.

The design so far will have tried to keep the complexity of the software to a minimum. At this stage the amount of hardware needed could be excessive. To reduce the amount of primary storage, paging for each mode could be done using a highly dense (logically) secondary storage. To reduce storage further, paging could be extended to a more frequent basis or even some sort of dynamic primary storage allocation might be considered.

The time required to perform some of the functions might be reduced by the use of queues and interrupts within modes. So far the times

of reading measuring devices and control actions were considered fixed or at least predictable enough to be interwoven into a predetermined flow of events and modified only by change of mode or earth initiated procedure. If the initiations of contro procedures are queued by the existence of a detected situation, control procedures could be eliminated from periods when values of measuring devices are not changing significantly. This would reduce time spent on the function, but would require a more complex software and hardware.

The control procedures may be more complex in nature due to the fact that they are not initiated at fixed intervals. Also a scheduler would be needed for the modes affected having possibly more than one level of priority. This scheduler would need the hardware to monitor the status of the several sensors and to detect critical situations independently of what the computer is doing at the moment (within a given mode). It would have the ability to time a particular procedure accurately if need be. Also changes in function programs length would not be as harmful to the system timing.

The independence of the scheduler would result in some problems. It would be difficult to detect malfunctions in the additional hardware required to monitor the status of activities to be controlled. Also the activity of the computer over a given period of time would be hard to predict, increasing the difficulty of locating malfunctions in the computer itself. A compromise could be made by having the CPU time used to do the scheduling via the normal input-output devices. This would consume time but not require as much new hardware. In effect this would be redefining the function procedures and with the inclusion of a scheduling function the design procedures used so far would hold.

The computer must have the ability to handle breakdowns in functions of the rover including parts of its own hardware. Important parts of the rover might have alternate procedures which could be brought into play if a component breaks down. Also critical input-output devices, storage blocks, operations and switching networks may be replicated according to their expected lifetime. The function programs could be written in terms of "virtual" operation codes and addresses whose interpretation would be determined by setting of special storage areas. The locating of breakdowns could be done partly from the interpretation of information sent to earth. During rover time or when directed from earth, test programs could be run to locate and bypass problems. Areas where problems are difficult to detect or of importance in detecting problems, such as the direct operation of the computer from earth, might require alternative paths to be used simultaneously and the results compared. These considerations would have to be included at the time decisions relating to the complexity of the hardware are made early in the computer design.

In summary, this task is aimed at developing a framework within which software and hardware specifications can be determined systematically according to the mission requirements.

Task C. Surface Navigation and Path Control

This task is subdivided as follows: design and construction of a laser range finder; surface reflectivity and laser power requirements; three dimensional obstacle recognition; terrain parameter estimate from gradient data; obstacle and terrain classification and path selection system evaluation.

C.1. Terrain and Obstacle Sensors

C.1.a. Construction of a Laser Range Finder - E. E. Svendsen
Faculty Advisors: Profs. C. N. Shen, W. Moyer

Objective. The objective of this task is to construct a laser transmitter and a receiver as part of a rangefinding and obstacle detection system. Range data eventually obtained with this device can be used as measurements for the software tasks such as the Terrain Modeling and Obstacle Detection. The present rangefinding system after proper future refinements is expected to be installed on the 0.5 scale roving vehicle for testing of alternative path selection systems.

Progress Summary. The project began by collecting data and concepts for a laser transmitter which was constructed and tested. Next, work was performed in the area of a receiver where a photomultiplier tube was chosen. This subsystem was designed and constructed and is currently in operation. Furthermore, investigation into optics for the rangefinder was undertaken and some of the concepts were implemented.

Discussion. Due to the accuracy requirements of the rangefinding system, many state-of-the-art techniques were employed in the transmitter. A laser diode was chosen as the light pulse generator because of its fast rise time and low power requirements. This implies that the time of flight of a light pulse will be the basis of this rangefinder.

The circuit used for pulsing the laser diode with current is shown in Fig. 33. In operation the capacitors charge up from voltage V_s through resistor R while the SCR's are off. When the SCR's are triggered, the stored charge is quickly dumped through the laser diode resulting in a short and fast rise time pulse. The back-biased diode protects the laser diode from current backlash and reverse voltages. A Tektronix CT-2 current monitor is used to observe the current pulse.

A sketch of the constructed transmitter is shown in Fig. 34. Note that an overall coaxial symmetry is used to lower the overall circuit inductance. This is one reason why five small capacitors are used instead of one lumped one. Three SCR's are employed in order to pump more current through the laser diode more quickly. Copper sheeting is used on the return ground path because flat conductors are less inductive than round ones.

The characteristics of the laser transmitter are shown in Figs. 35 through 40. Fig. 35 shows the general shape of the current pulse through the laser diode. Pulse width measured at zero current is about 100 nanoseconds and pulse height is 25 amperes (adjustable by changing V_s). Fig. 36 is an enlargement of the time scale showing a rise time of 28 nanoseconds. Fig. 37 displays the trailing edge of the current pulse which shows that the protective diode is not entirely ideal and there is some current undershoot.

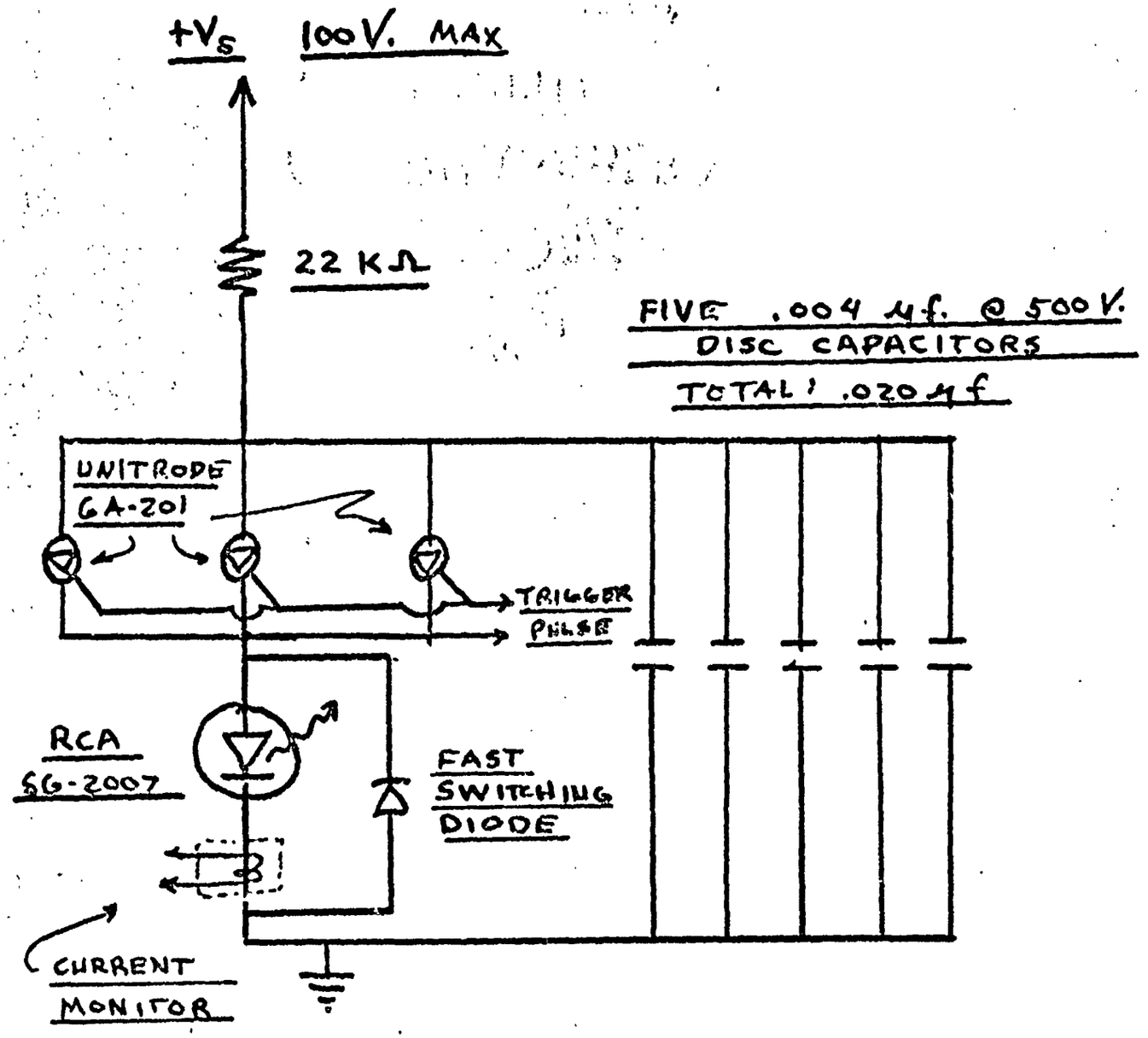

Fig. 33. Laser Pulser Circuit Diagram

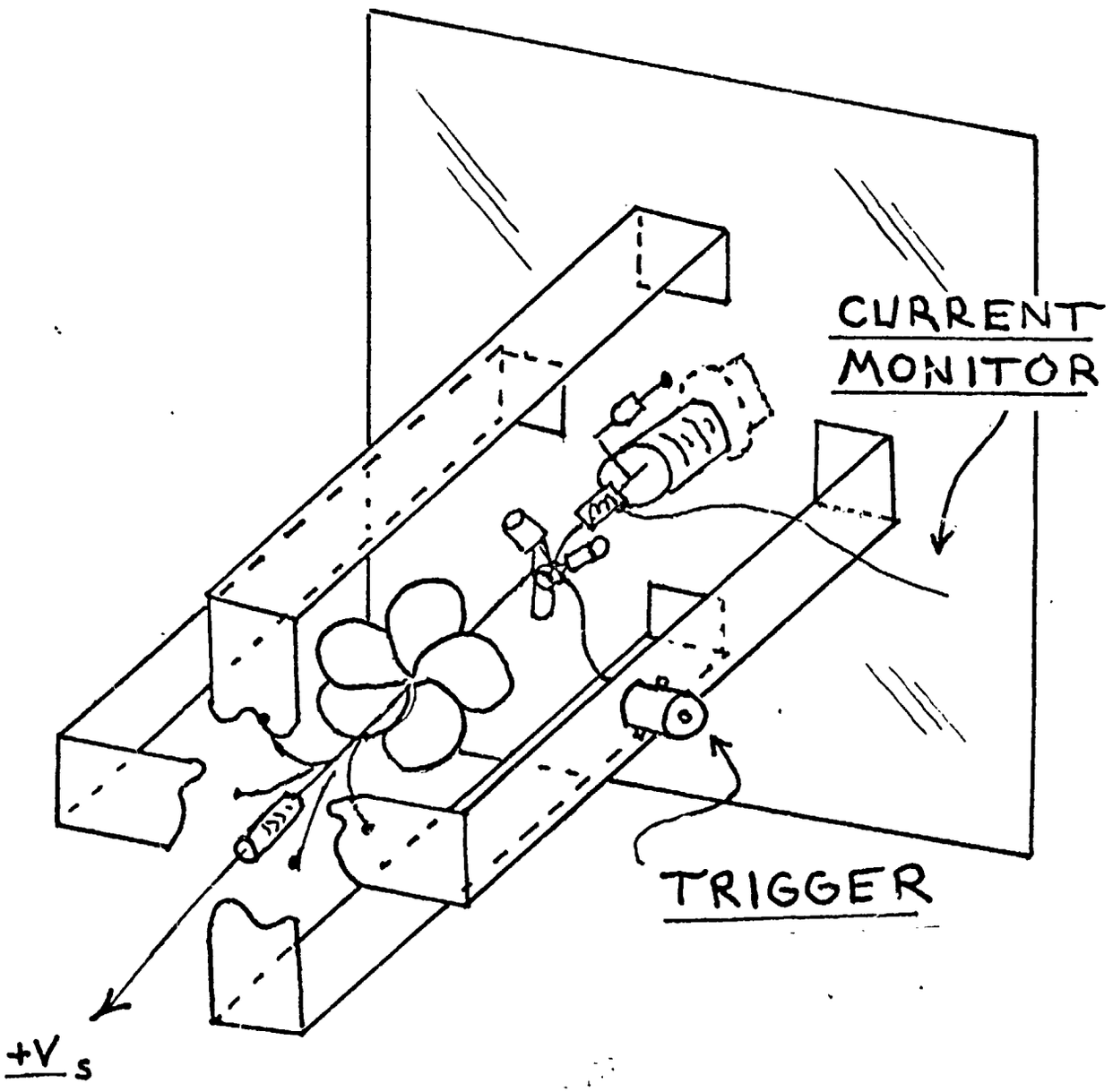

Fig. 34. Sketch of Transmitter

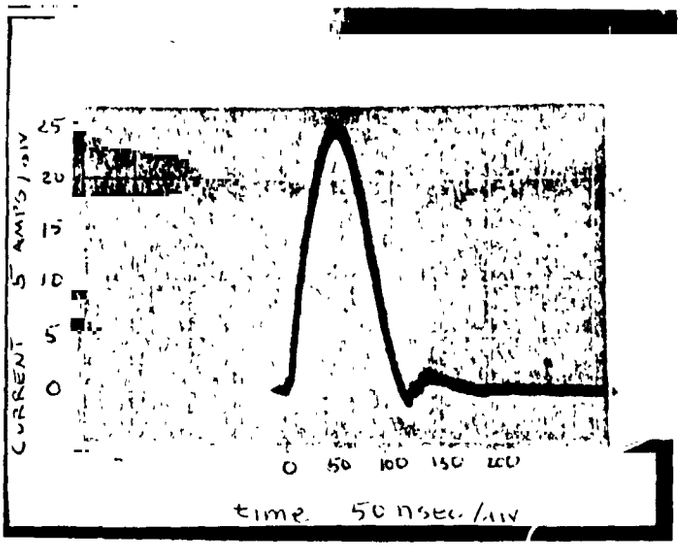

Fig. 35. Current Through Laser Diode

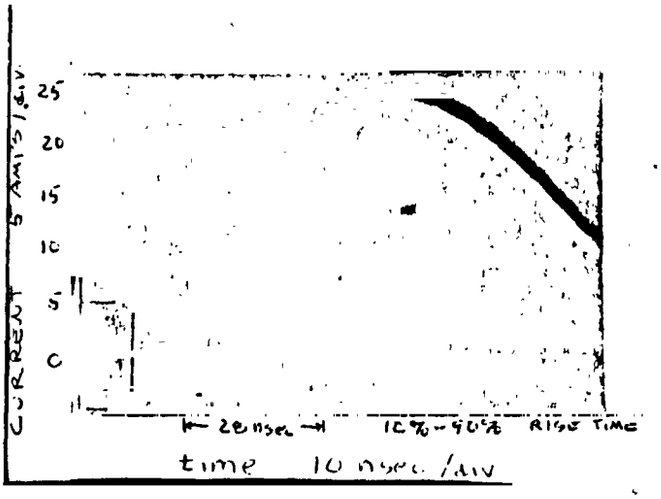

Fig. 36. Pulse of Figure 35 stretched in time showing current rise time of 28

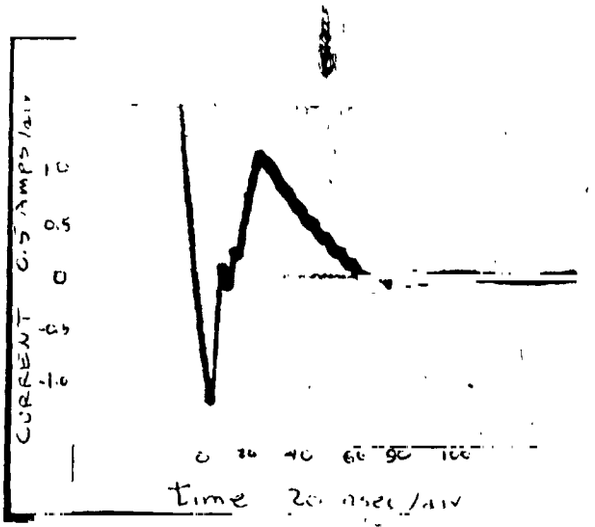

Fig. 37. Enlargement of tail of current pulse

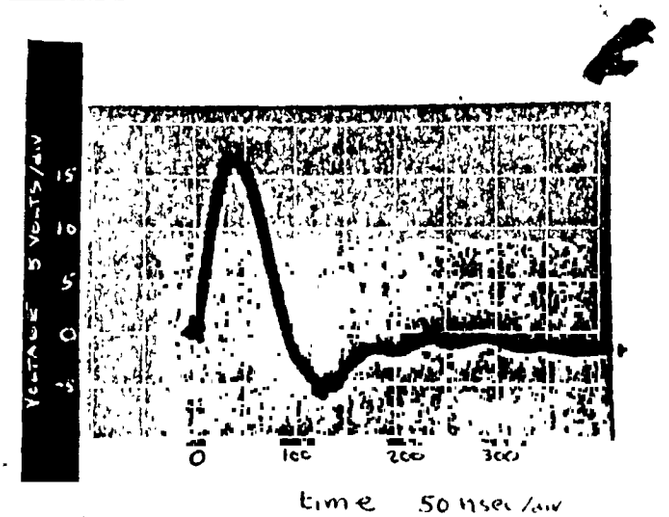

Fig. 38. Voltage across laser diode

The current then goes above zero again but the laser diode will not refire because the threshold of 7 amperes is not exceeded. Fig. 36 shows the voltage across the laser diode. Note that the voltage undershoots by about 5 volts but the laser diode is not harmed since the duration is so short. Fig. 38 shows the current and voltage traces on the same time scale.

In general, test results from the transmitter were good. It only remains to determine whether or not the actual light output pulse of the laser diode has a faster rise time than the current pulse. In order to detect this however, a receiver had to be built.

A photomultiplier tube was chosen as the best overall receiver. The selected tube, an RCA #C70042K, has good sensitivity and built-in amplification, doing away with the necessity of an external amplifer. This tube is a developmental type designed for use with gallium arsenide laser diodes. The receiver design incorporated a self protecting voltage divider. The specifications of the tube state that the maximum average anode current cannot exceed 0.5 mA. However, if the divider string does not exceed this value, the tube can be protected. Assuming that the highest voltage to be applied to the string is 2000 volts, a total string resistance of 4 Megohms is used. Twice as much voltage is dropped across the cathode to first stage to improve overall sensitivity. The final circuit is shown in Fig. 41.

Results of using the receiver with the laser diode are summarized in Figs. 42 and 43. Fig. 42 shows the laser diode current pulse and the detected light output as represented by a pulse in the anode current. The light pulse occurs after the current pulse of the laser for three reasons. The laser does not actually lase until a certain delay time after the threshold current is reached. The optical path between the laser and photomultiplier tube causes more delay. Also the transit time of the tube causes even further delay. Fig. 43 shows the light pulse shifted along the time axis to demonstrate the different in rise time between current pulse and light output. The 10 to 90% rise time of the light pulse is measured from Fig. 43 and is about 15 nanoseconds. In Figs. 42 and 43 the photomultiplier tube is operated at 2000 volts. The response time of the tube is dependent on applied voltage and lower applied voltages yield slower rise times.

Results of the photomultiplier tube were very good. The photographs of oscilloscope traces prove that the rise time of the light pulse is much faster than the current pulse through the laser diode as was hoped.

The proposed design for optics is shown in Fig. 44. Three lenses on the transmitter focus the light into a columnated beam. The lens at the receiver collects a large amount of the reflected beam and focuses it on the photomultiplier tube. The optical filter allows only light at the wavelength of the laser diode to pass through. This filter has already been incorporated on the receiver and was used with the tube in obtaining the photographs in Fig. 42 and 43.

At this point, the capability of generating and detecting the laser pulses has been developed. In the future, it is planned to investigate alternative methods for measuring the time of flight, (which is necessary for range

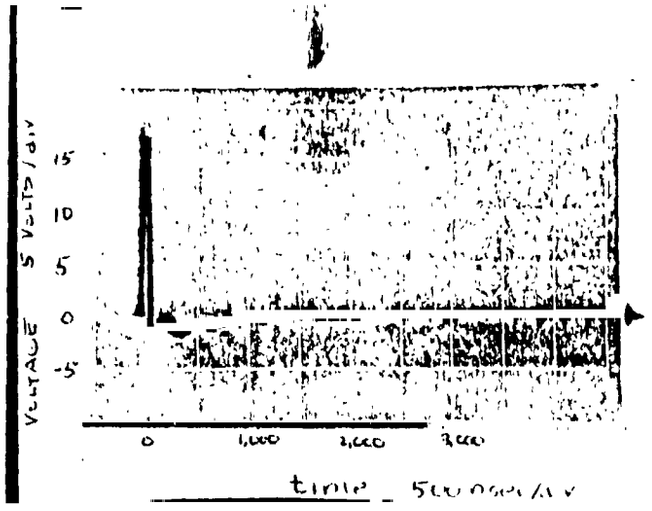

Fig. 39. Voltage pulse on longer time scale showing die-out time.

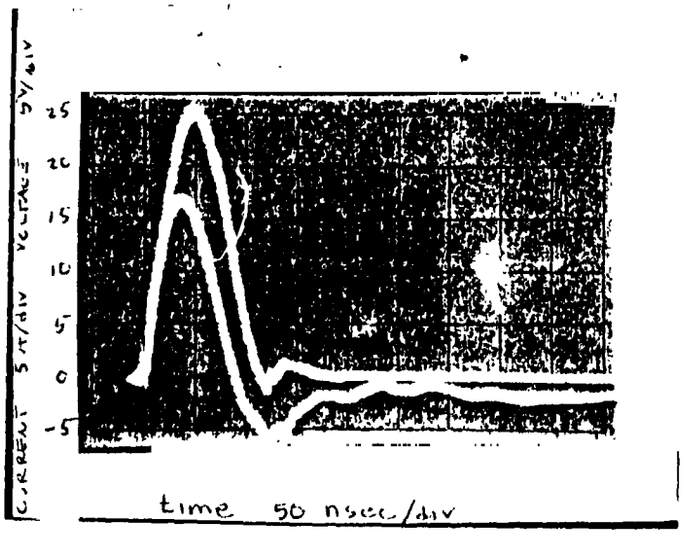

Fig. 40. Current and voltage pulses on same time scale

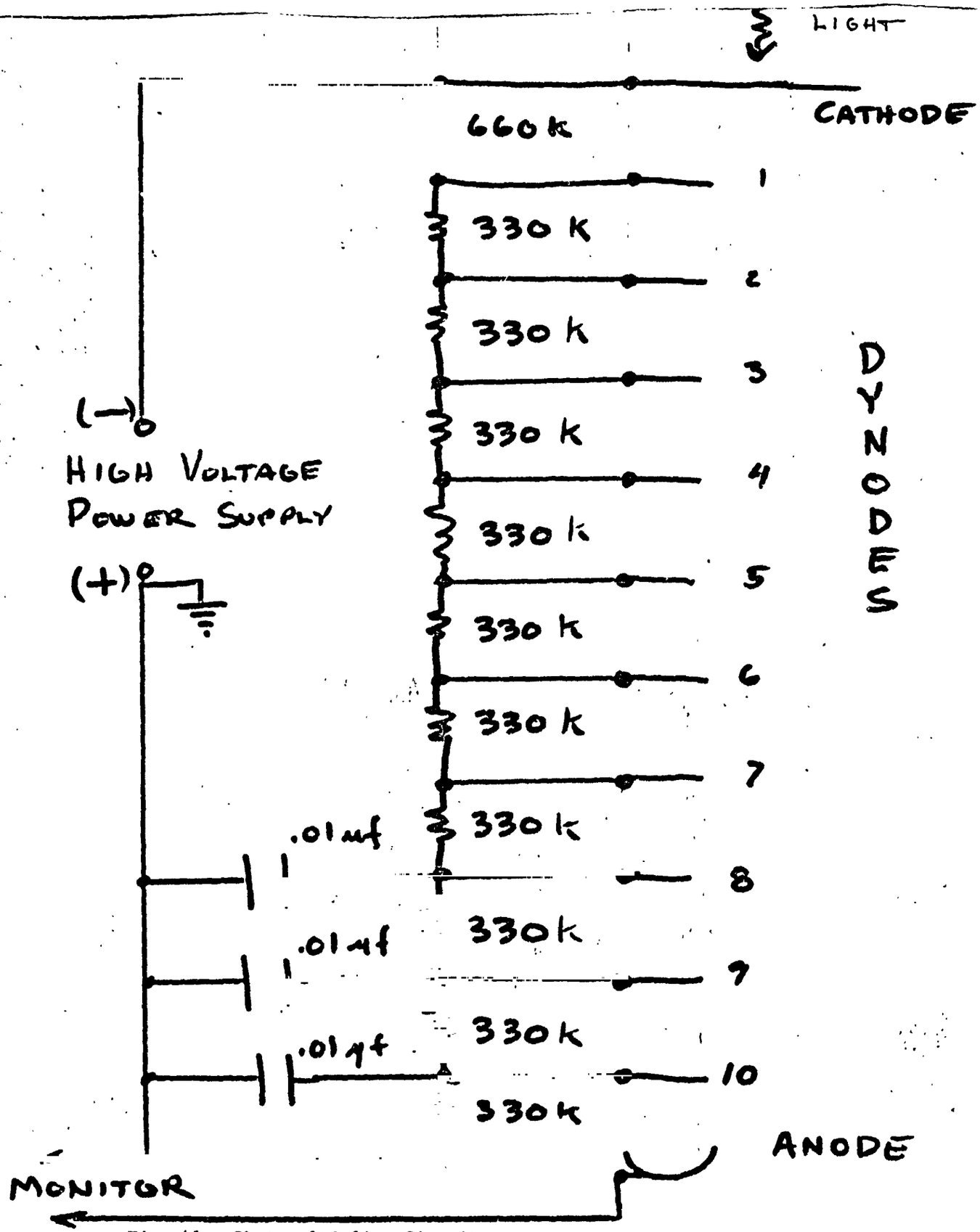

Fig. 41. Photomultiplier Circuit

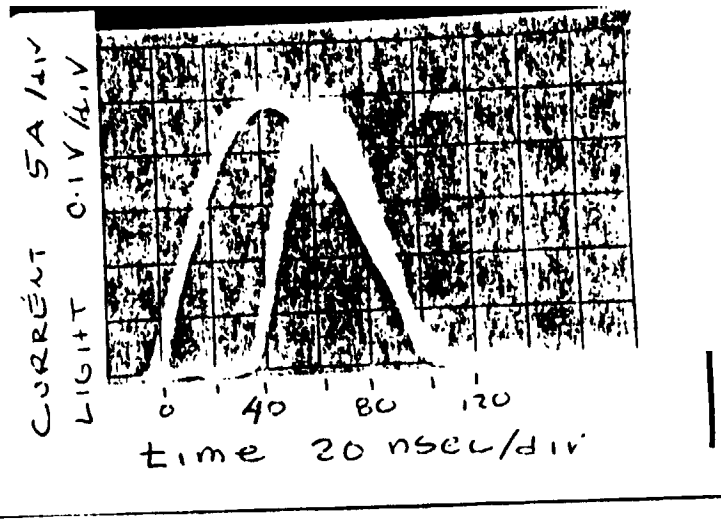

Fig. 42. Laser diode current pulse and detected light pulse

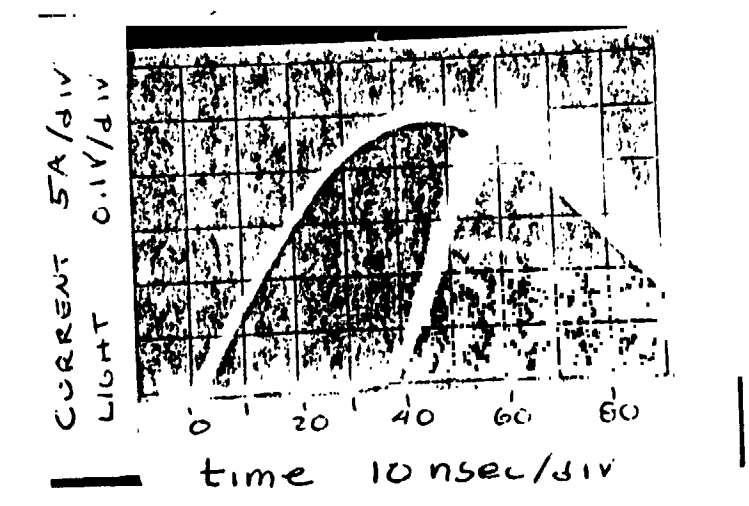

Fig. 43. Current and light pulse expanded on time scale to measure rise time.

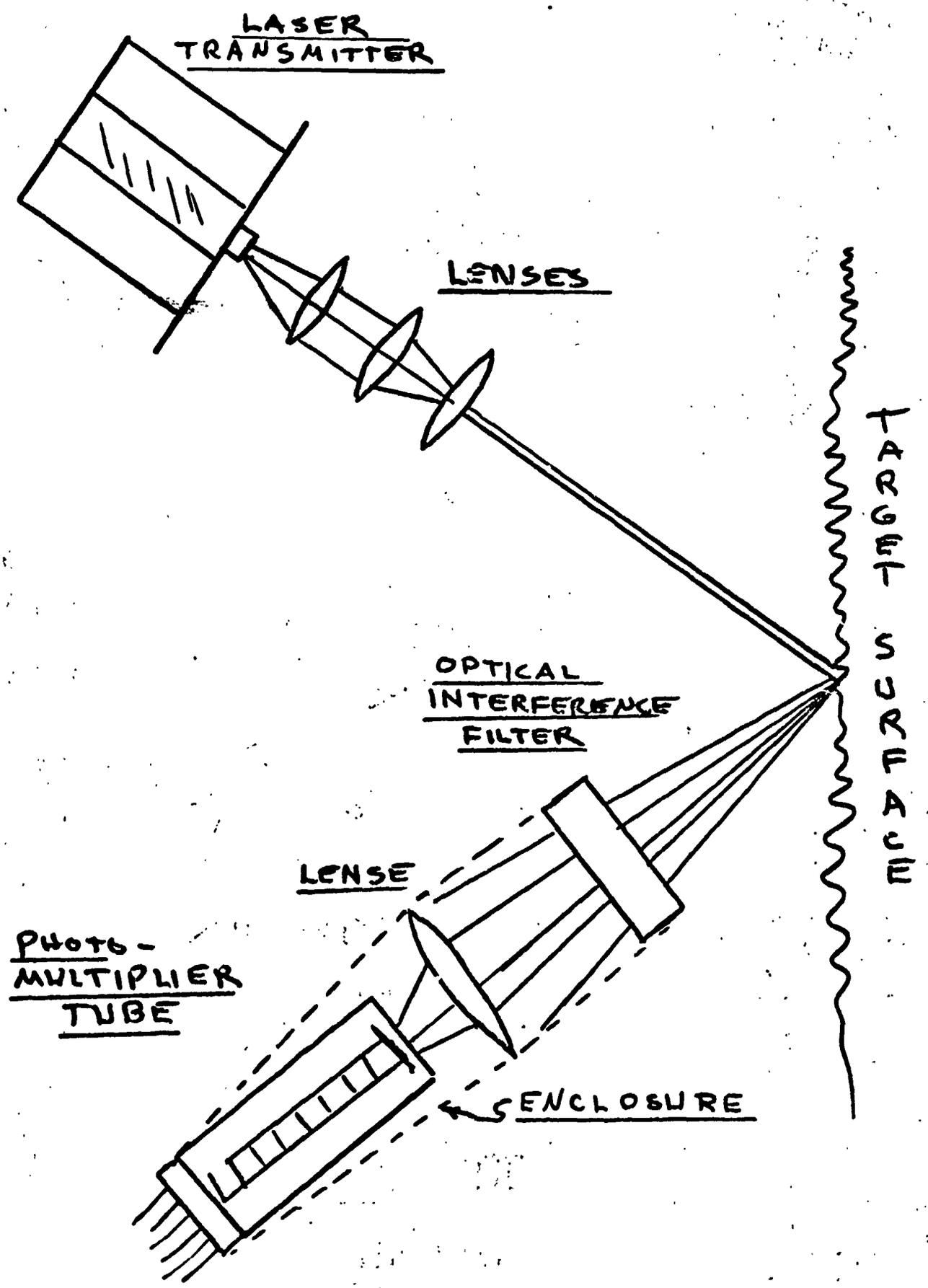

Fig. 44. Proposed Optical Set-up

measurement), to assess experimentally the rangefinding capabilities of the system.

C.1.b. Surface Reflectivity and Laser Rangefinder Power Requirements - W. Dull
Faculty Advisors: Profs. C. N. Shen and W. R. Moyer

Objective. The major objective of this subtask was to determine the reflectance of laser light from diffuse reflectors similar to those that might be found on the Martian surface. A second objective was to obtain a preliminary indication of rangefinder transmitter and receiver specifications as determined by the dynamic range of the reflected laser light.

Progress Summary. Progress to date has been in the determination of what quantities must be experimentally measured to accomplish the stated objective, construction of a test apparatus to perform the measurements, and in the actual measurement of the reflectivity of several diffuse reflectors.

Discussion. The basic problem to be faced in using a laser rangefinder on Mars is the uncertainty regarding the reflected signal levels to be expected for ranges varying from three to thirty meters. As can be seen from Fig. 45, the expected range of incident angles measured with respect to the local surface normal that the rangefinder might encounter can vary anywhere from 0 degrees to 90 degrees. It is thus desired to be able to measure some physical parameter of a given diffuse reflector that will give the received signal level for a given transmitter and receiver as a function of the position of the laser transmitter and receiver with respect to the reflecting surface.

A parameter which can be used to characterize reflections from a diffuse reflector is the bidirectional reflectance ratio. It was decided that the bidirectional reflectance ratio should be measured experimentally rather than calculated analytically for two reasons. First, models for diffuse reflectors from which analytical calculations of the bidirectional reflectance ratio can be made have been developed only recently. As a result, there are not a large number of comparisons between analytically determined and experimentally determined bidirectional reflectance ratios for a wide range of reflector types, Ref. 5 and 6. Secondly, the actual analytical calculation of the bidirectional reflectance ratio can be rather involved requiring detailed knowledge of the characteristics of the diffuse reflector, Ref. 7.

Fig. 46 shows the coordinate system used to measure the bidirectional reflectance ratio. The bidirectional reflectance ratio is defined as

$$\rho(\psi;\theta,\alpha) = \frac{N_r(\psi;\theta,\alpha)}{d\Phi_i(\psi)/dA} \qquad (1)$$

where $N_r(\psi;\theta,\alpha)$ is the reflected radiance in the direction θ, α due to the incident beam at angle ψ, dA is the area of the reflector that is illuminated, and $d\Phi_i(\psi)$ is the radiant flux from the laser source that is incident upon the reflecting surface.

Making use of the bidirectional reflectance ratio as defined in equation (1) from Ref. 5, the reflectance at any receiver position can be studied.

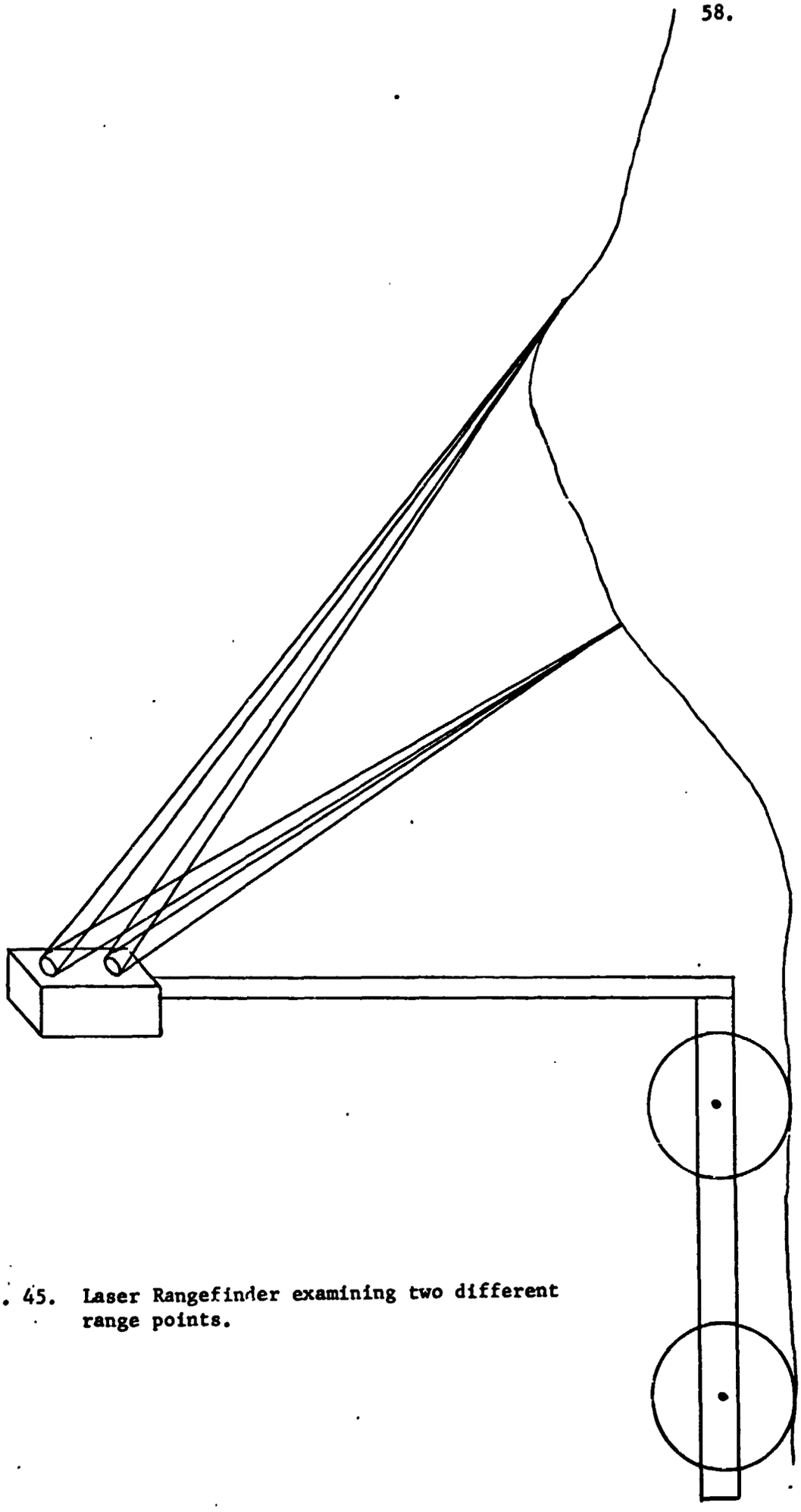

Fig. 45. Laser Rangefinder examining two different range points.

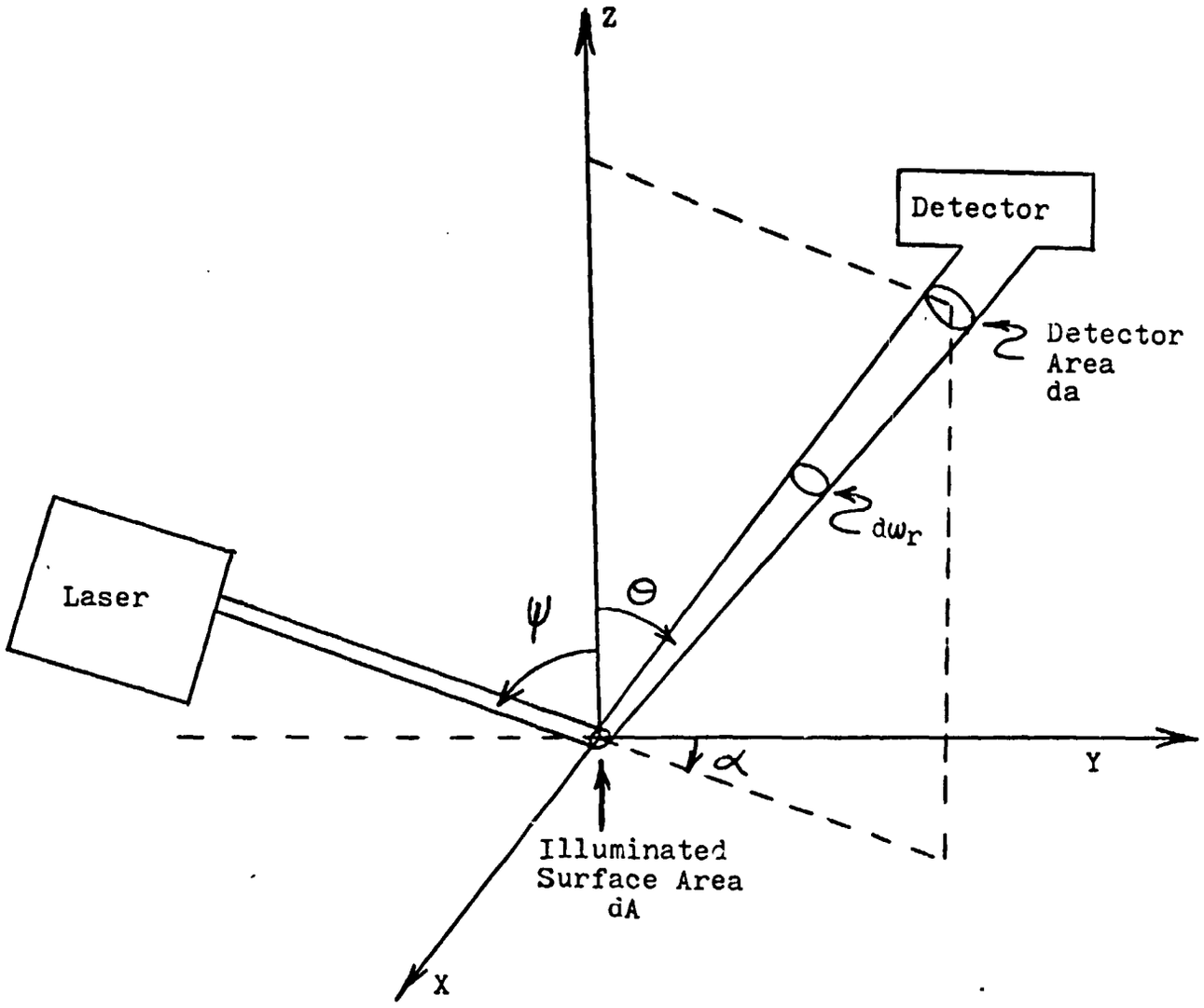

1) The reflecting surface is in the XY plane

2) The incident beam is in the ZY plane

Fig. 46. Bidirectional reflectance ratio coordinate system

The receiver position of interest to this subtask is one at which the receiver is located in close proximity to the transmitter. Therefore, from examination of Fig. 46, it can be seen that the bidirectional reflectance ratio should be evaluated at approximately the angular position $(\psi; -\psi, 180^\circ)$.

It was decided to use a photodiode in a first attempt to measure the bidirectional reflectance ratio. To use the photodiode to measure bidirectional reflectance ratios, the device must be biased so as to operate in a nonsaturated mode. In making reflectance measurements, the diode operating characteristic used is that the back bias current flow of the diode is proportional to the amount of light striking the photo diode light sensitive area. Fig. 47 shows how the photo diode might be used to make reflectivity measurements.

Fig. 48 shows the overall block diagram of the test apparatus used to measure the bidirectional reflectance ratio. The light source used in the reflectance measurements was a 2 mw. HeNe continuous laser. The laser output is chopped mechanically at a frequency of about 200 hz. The output of the chopper is aimed at the reflecting surface under test. The photo diode detector is positioned at the point above the reflecting surface at which the bidirectional reflectance is to be measured. The current pulses produced by the photo diode detector are fed into a high pass filter which converts the current pulses to voltage pulses at the input of the A.C. amp. The high pass filter also separates the current pulses produced by the reflected laser light from the D.C. current flow produced by the ambient light present in the room. The A.C. amplifier produces output voltage pulses whose amplitude are in proportion to the size of the reflected signal detected by the photo diode.

The next problem was to express the quantities used to define the bidirectional reflectance ratio in terms of measurable angles, distances, and back bias current flow in the photo dioe. Because the incident laser beam is of much greater intensity than the light reflected from the diffuse reflector, an optical attenuator had to be placed between the laser source and the photo diode when measuring the incident laser beam. The final expression arrived at was

$$\rho(\psi; -\psi, 180^\circ) = \frac{r\, I_r(\psi; -\psi, 180^\circ)\, da}{I_i(\psi)\, dA_1\, (d\omega_r) \cos(\psi)} \qquad (2)$$

where r =attenuation of the optical attenuator used to measure the incident beam, $I_r(\psi; -\psi, 180^\circ)$, = the back bias current flow in the photo diode when used to measure reflectance at the angular position $(\psi; -\psi, 180^\circ)$, da = light sensitive area of the receiver, $I_i(\psi)$ = diode back bias current flow when used to measure the incident beam, dA_1 = laser beam cross-sectional area, and dw_r is the solid angle of the illuminated surface area of the reflector as viewed from the receiver.

A drawing of the actual test apparatus used to make the reflectance measurements is shown in Fig. 49. Plate 'A' is used to hold the diffuse reflector under test. Structure 'B' holds the photo diode detector, high pass filter, and A.C. amp. Structure 'C' holds the mechanical chopper while the component

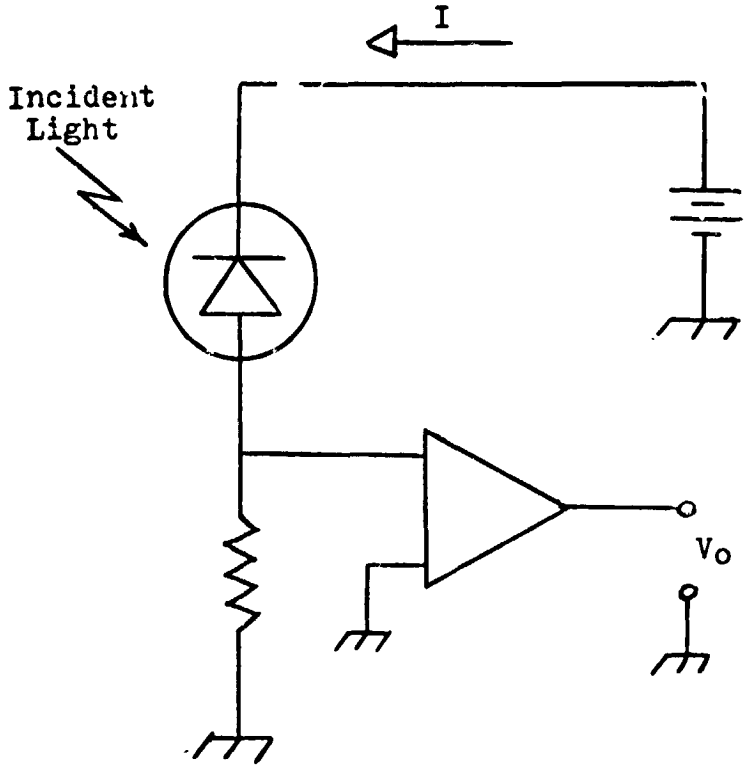

1) I = Back bias diode current flow

2) V_o = Amplifier output voltage proportional to I

Fig. 47. Use of the photo diode to make reflectivity measurements.

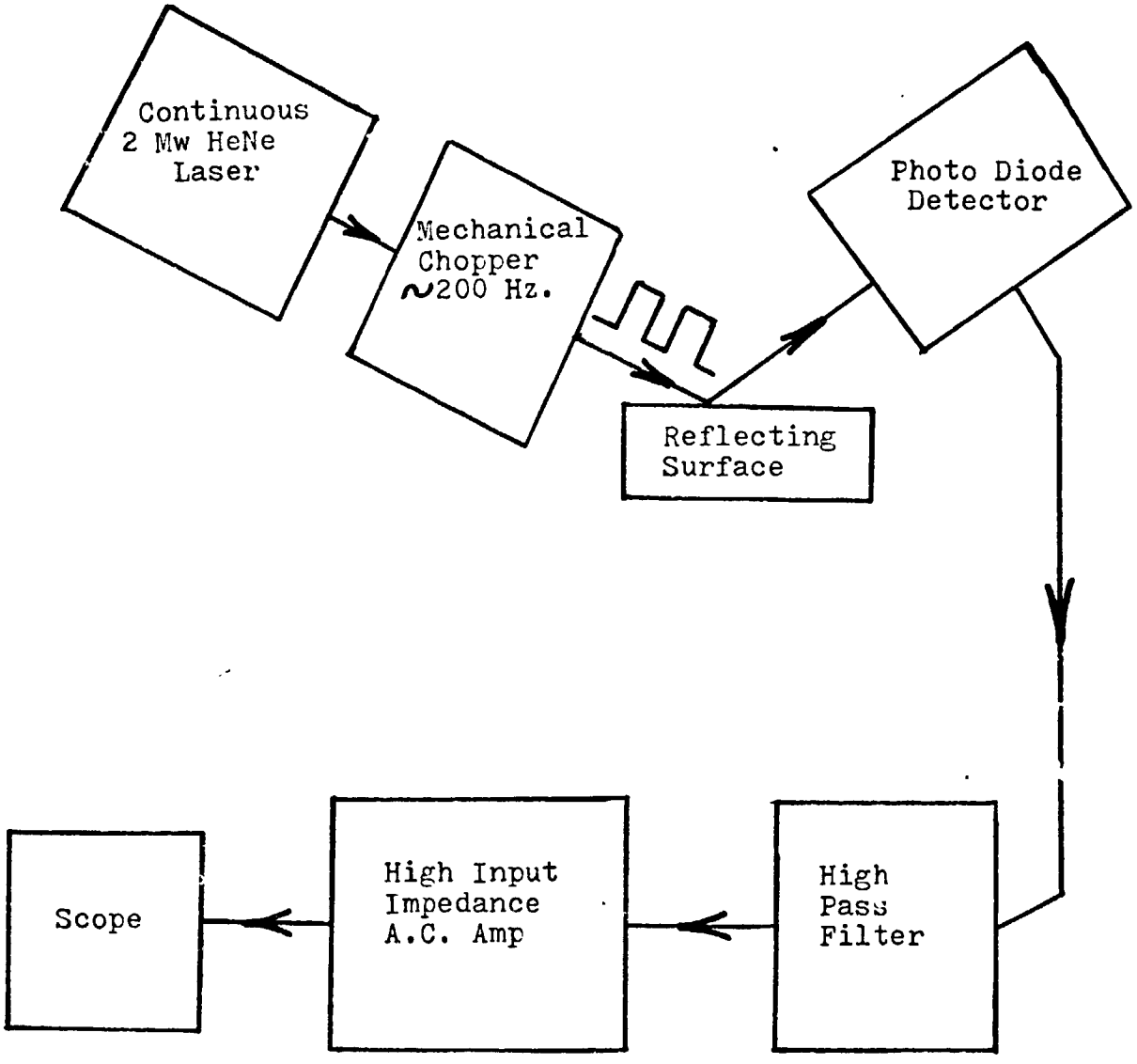

Fig. 48. Bidirectional Reflectance Ratio Measurement Scheme

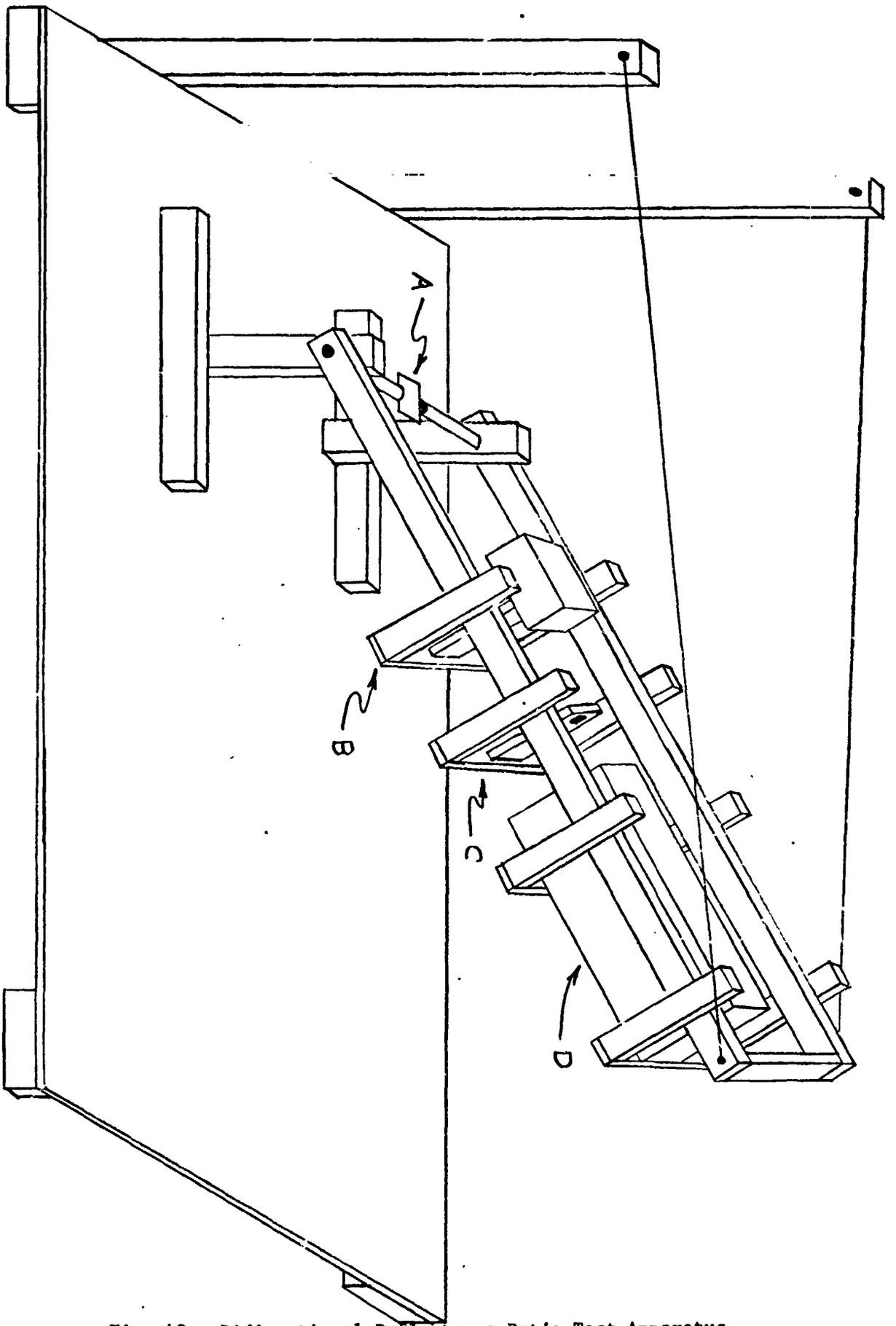

Fig. 49. Bidirectional Reflectance Ratio Test Apparatus

labeled 'D' is the HeNe laser. The angle ψ is changed by rotating the two arms about the bar to which plate 'A' is attached. It was decided to rotate the transmitter and receiver about the sample rather than rotate the sample itself because some of the diffuse reflectors examined were granular.

The next major step was to determine the specifications of the high pass filter and A.C. amplifier. Given that the reflected signal of interest is a pulse train, the first requirement on the high pass filter is that its current to voltage transfer function should have a lower 6 db. frequency which is much less than the 200 hz. frequency of the mechanical chopper. This is to ensure that the fundamental frequency component of the reflected signal be transmitted to the input of the A.C. amplifier largely unattenuated.

Since the sensitivity of the photo diode is directly proportional to the size of the impedance it sees, the impedanceof the high pass filter should be made large. It was arbitrarily decided to make the impedance of the high pass filter about 500 kΩ. Fig. 50 shows the high pass filter used. With R_1 = 1 Meg.Ω, R_2 = 1 Meg.Ω, and C_1 = 0.08 μf, the high pass filter has a lower cutoff frequency of about 1 hz. and an input impedance of about 500 kΩwhich is nearly a pure resistance.

The first requirement of the A.C. amplifier is that it have a very high input impedance. This requirement is important so that the amplifier will not load the high pass filter and thus reduce the sensitivity of the photo diode.

The second amplifier requirement is that it have sufficient gain and bandwidth to amplify the voltage pulses at its input with a minimum of distortion and also to produce output voltage pulses of sufficient amplitude to be observable on the oscilloscope. It was decided that the first stage of amplification should be flat from several hz. to about 5 khz. and have a voltage gain of about 20 db. in order to satisfy the above two requirements. Fig. 51 is the circuit diagram of the laser receiver front end. Amplifier A_1 is a 741C operational amplifier used in the non-inverting mode. For a voltage gain of 20 db, $R_3 \approx 1$ kΩ and $R_4 \approx 10$ kΩ. The resulting bandwith is about 100 khz. with an input impedance of about 280 MegΩ Ref. 9. D_i is the photo diode while R_1, R_2, and C_1 comprise the high pass filter. R_6 is used to null out any D.C. offset at the output of the amplifier.

Fig. 52 is a plot of the relative reflectivity of two different surfaces. These curves were obtained by dividing the detector response at each angular position by the maximum detector response that occurred. The curve for the copper reflectance has a sharp peak because it approximates a mirror surface much better than does the sand.

An impression of the different reflected signal levels that might be expected for different types of reflectors can be obtained from Table I in which are tabulated the actual detector output voltages for the reflectors of Fig. 52 for several different values of ψ. As can be seen from examination of the table, the size of the reflected signal from the copper surface at $\psi = 1^o$ is about 42 times the size of the reflected signal from the sand surface. At $\psi = 29^o$, however, the size of the reflected signals become roughly the same order of magnitude. The size of the reflected signal at $\psi = 1^o$ shows one of the more hostile operating conditions the receiver may be facing.

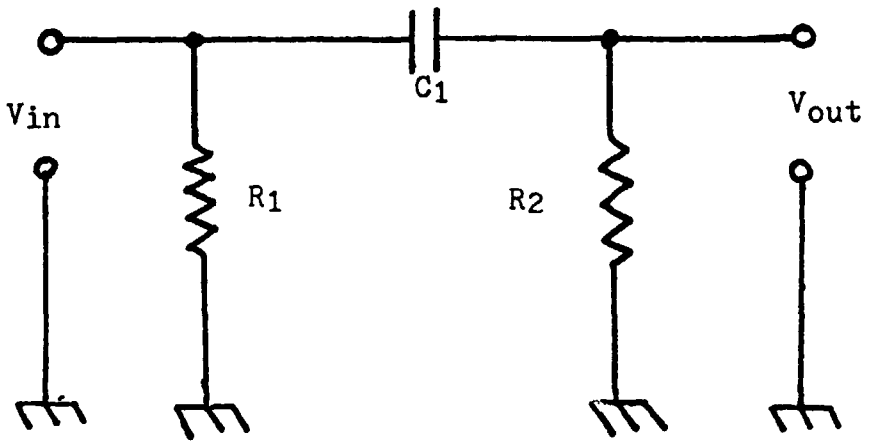

Fig. 50. High Pass Filter

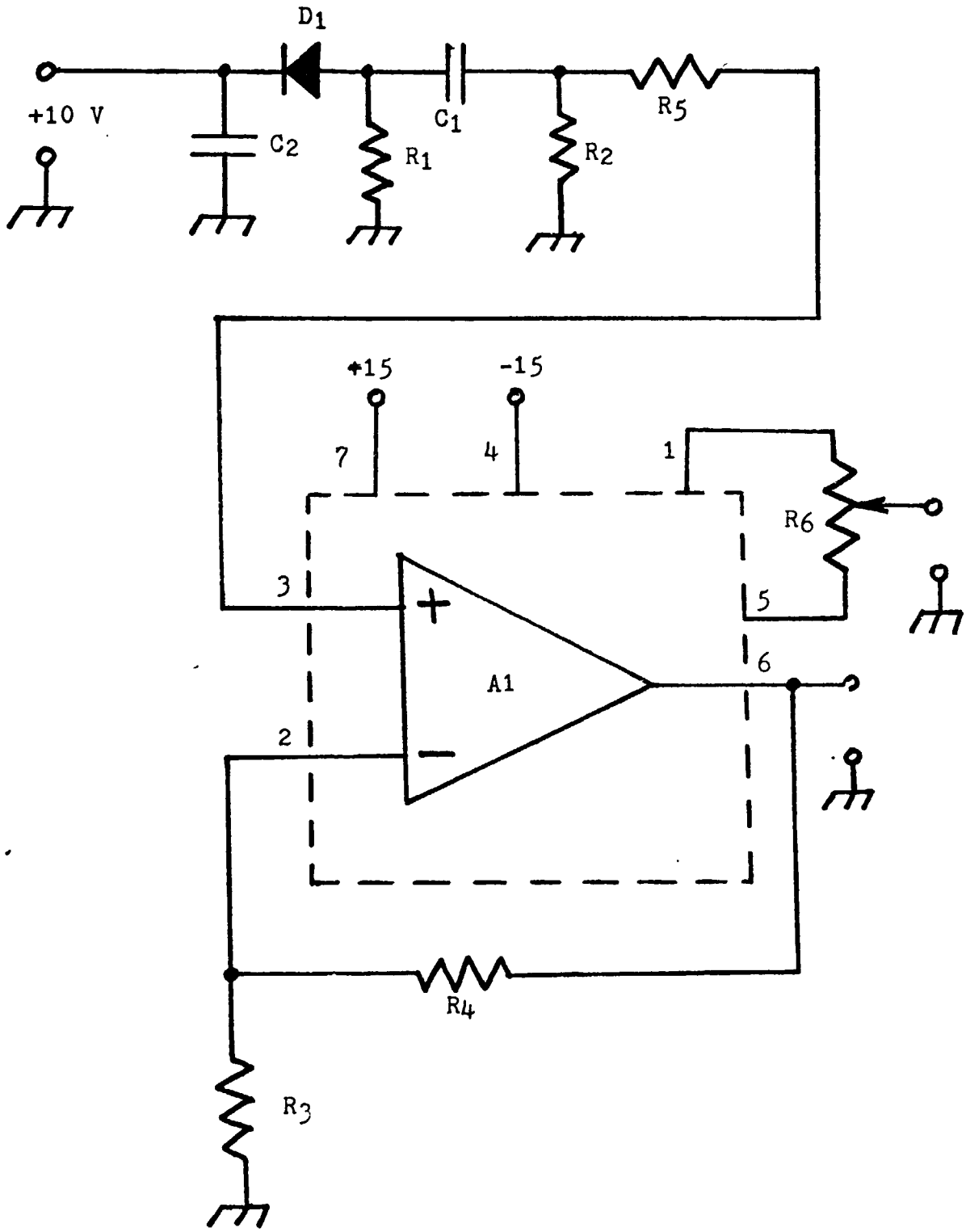

Fig. 51. Receive Front End

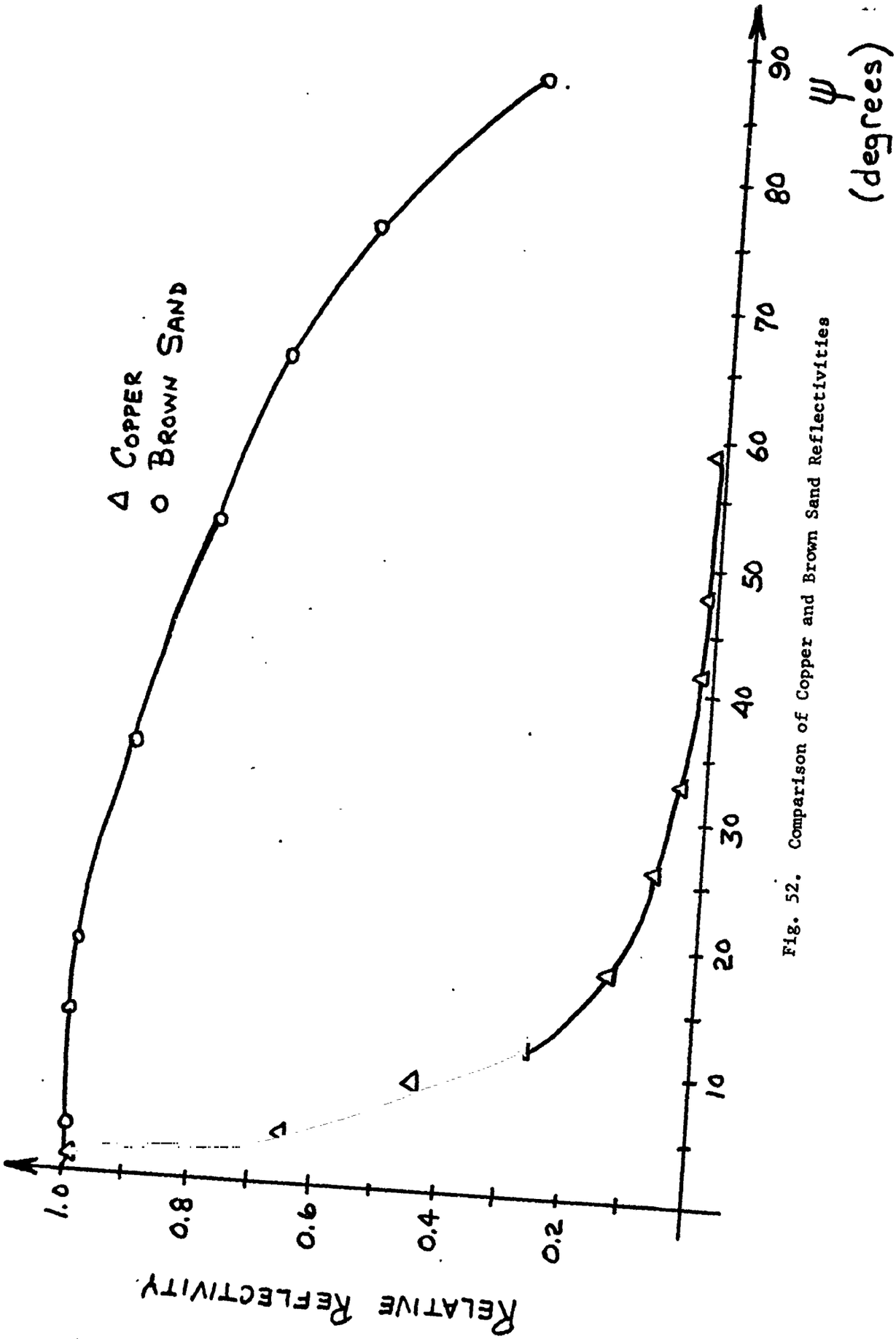

Fig. 52. Comparison of Copper and Brown Sand Reflectivities

TABLE I

Detector Response for Copper and Brown Sand

Ψ (degrees)	Detector Output Voltage (volts)	
	Copper	Brown Sand
1	10.0	0.24
17	1.6	0.24
29	0.6	0.22
42	0.32	0.20
49	0.17	0.20
58	0.14	0.18

If the laser rangefinder were examining the Martian terrain and encountered a reflector like the copper at one data point and then encountered a reflector like the sand at an immediately adjacent data point, the receiver and data processor would have to be able to accommodate this large change in signal level without suffering severe degradation of performance.

Fig. 53 is a plot of the relative reflectivity of two different sands. These curves were also obtained in the same manner as the curves in Fig. 52.

Table II is a tabulation of the actual detector output voltage for the reflectors of Fig. 53 for several different values of ψ.

Possible future activities include expanding the present scope of the measurements to include a larger number of reflectors. If reflectance measurements were performed for a suitable variety of reflectors, a detector could be chosen and a processor designed that would be able to function for the entire range of reflectances measured.

C.2.a. Obstacle Identification by Edge Detection - Martin Reed
Faculty Advisor: Prof. C. N. Shen

Objective. In order to navigate autonomously on the Martian surface, the proposed Mars roving vehicle, Ref. 10, must be able to distinguish between passable and impassable terrain by means of a laser rangefinder which scans in a field approximately 3 to 30 meters ahead of the Rover. Data obtained by this means will be used to determine a sufficiently accurate 'range image' of the terrain in order for the Rover to choose the safest path of travel.

This task is concerned specifically with the objectives of obstacle detection. This section summarizes work on an obstacle detection system for this purpose, which is intended to process the information obtained by the laser rangefinder to provide a basis for a path selection decision making.

Progress Summary. Two algorithms, one already existing in the literature and one developed under this project, were used to obtain the outlines of obstacles from the 'range image'. Both of these algorithms end with a thresholding operation. A theoretical analysis shows how a proper value of the threshold may be chosen, given the type of irregularity of the terrain to be detected. The analysis also shows how large the statistics of measurement noise can be allowed without leading to false alarms, Ref. 11 and 12. Computer simulations of the schemes have proven their feasibility, and some typical results have been included. In addition, the related questions of scanning scheme determination and bottom edge detection have been explored, providing a basis for future investigations.

Discussion.

The Scan. The laser is assumed to be mounted on a mast at a height of 3 meters from ground level. The on-board computer controls the direction of the beam. By varying the elevation angle β and the azimuth angle θ, the laser can scan a desired area, Fig. 54.

The range data obtained in this fashion, denoted by $z_{i,j}$, can be stored in a matrix form with the elements ordered according to the values of β and θ. This matrix Z, called the measurement matrix, forms a 'range image' of the scene ahead.

TABLE II

Detector Response for White Sand and Brown Sand

ψ (degrees)	Detector output voltage (volts)	
	White Sand	Brown Sand
1	0.70	0.24
33	0.65	0.22
58	0.45	0.18
79	0.24	0.14

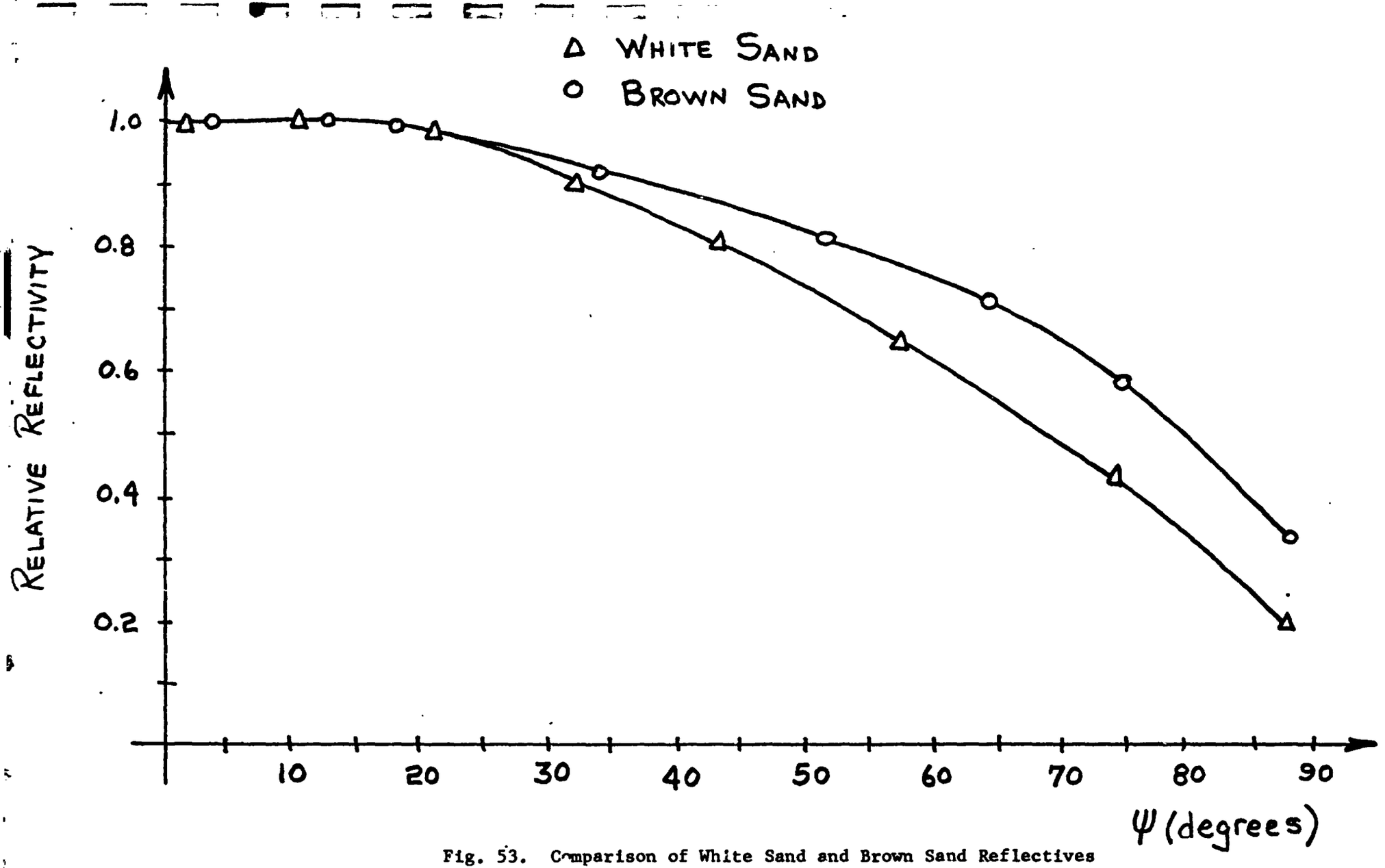

Fig. 53. Comparison of White Sand and Brown Sand Reflectives

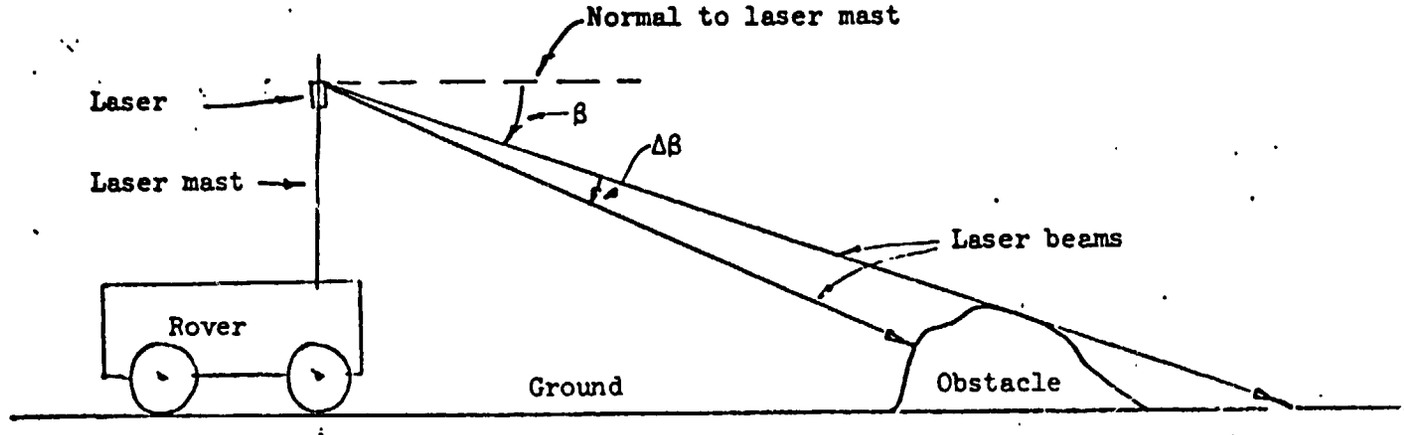

(a) Side view

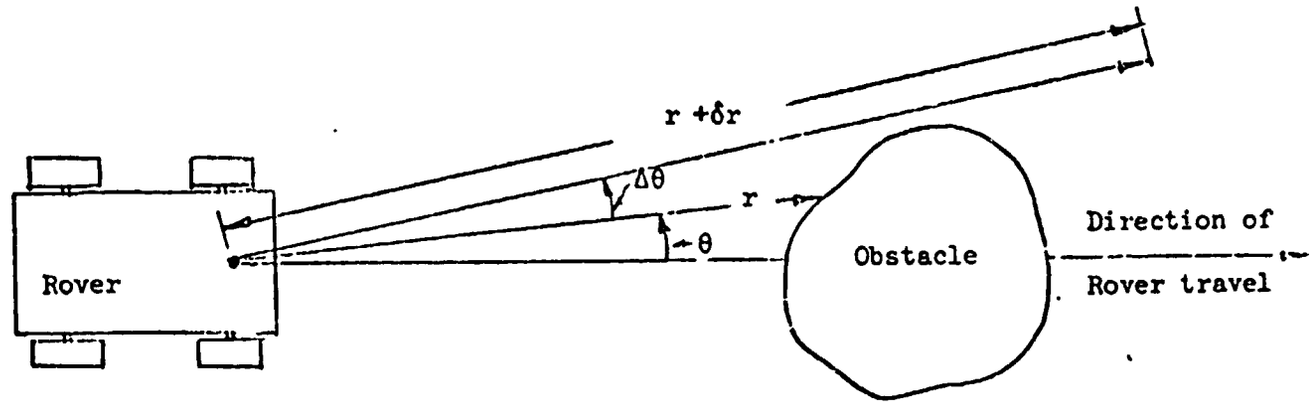

(b) Top view

Fig. 54. The Laser Rangefinder

$$Z = \begin{vmatrix} z_{11} & z_{12} & \cdots & z_{1n} \\ & & z_{i-1,j} & \\ & z_{i,j-1} & z_{i,j} & z_{i,j+1} \\ & & z_{i+1,j} & \\ z_{m1} & z_{m2} & \cdots & z_{mn} \end{vmatrix} \qquad (1)$$

The Algorithms. The presence of sharp changes in the range values on the Z matrix indicates the presence of obstacles. Algorithms used to show up these sharp changes end with a thresholding operation, and the success of the algorithm depends on the relative ease with which a proper threshold can be chosen. Both algorithms tried appear to be quite successful.

1. Normalized Laplacian, Ref. 13:

   A new matrix Q can be obtained by the following operation:

$$q_{ij} = \frac{z_{i-1,j} + z_{i+1,j} + z_{i,j-1} + z_{i,j+1} - 4z_{ij}}{z_{i-1,j} + z_{i+1,j} + z_{i,j-1} + z_{i,j+1}} \qquad (2)$$

2. Four Directional Ratio:

   A new matrix S is obtained by the operation given below:

$$S_{ij} = \frac{1}{4}\left[\left(\frac{z_{i-1,j}}{z_{ij}}\right)^n + \left(\frac{z_{i+1,j}}{z_{ij}}\right)^n + \left(\frac{z_{i,j-1}}{z_{ij}}\right)^n + \left(\frac{z_{i,j+1}}{z_{ij}}\right)^n\right] \qquad (3)$$

The Normalized Laplacian is from the existing literature, while the four Directional Ratio was developed specifically for this application. Analysis and application of these algorithms is described in Ref. 14.

Analysis of the Algorithms

$$\text{Let } Z_{i,j} = r_{i,j} + V_{i,j} \qquad (4)$$

where $r_{i,j}$ is the true range measurement and $V_{i,j}$ the additive noise in the measurement.

$$\text{Also let } r_{i-1,j} = (1 + \alpha_{i-1,j})\, r_{i,j} \qquad (5)$$

where $\alpha_{i-1,j}$ indicates the fractional change in range at point (i-1,j) with respect to point (i,j).

From eqs. (4) and (5) one can write,

$$Z_{i-1,j} = (1 + \alpha_{i-1,j})\, r_{i,j} + V_{i-1,j} \tag{6}$$

The measurements $Z_{i+1,j}$, $Z_{i,j-1}$, $Z_{i,j+1}$ can also be expressed in terms of $r_{i,j}$.

Using eqs. (2) and (6), expanding the resulting fractions in infinite series, and dropping higher order terms, for no noise, i.e. $V_{i,j} = 0$ for all i,j and for small

$$q^*_{i,j} = \left[\tfrac{1}{4}(\alpha_{i-1,j} + \alpha_{i+1,j} + \alpha_{i,j-1} + \alpha_{i,j+1})\right] \tag{7}$$

If somehow all $\alpha \approx 0$:

$$q^*_{i,j} \approx - \frac{V_{i,j}}{V_{i,j}} + \tfrac{1}{4}\left[\frac{V_{i-1,j}}{r_{i,j}} + \frac{V_{i+1,j}}{r_{i,j}} + \frac{V_{i,j-1}}{r_{i,j}} + \frac{V_{i,j+1}}{r_{i,j}}\right] \tag{8}$$

Assuming that the noise, V, with each measurement is independent, zero mean, and with the same standard deviation, σ, one can write from eq. (8)

$$\text{var}\,(q^*_{i,j}) \approx \frac{5\,\sigma^2}{4r^2_{i,j}} \tag{9}$$

In a similar manner for the four directional ratio, using eqs. (3) and (6):

If there is no noise:

$$S^*_{i,j} \quad 1 + \frac{n}{4}\,(\alpha_{i,-1,j} + \alpha_{i+1,j} + \alpha_{i,j-1} + \alpha_{i,j+1}) \tag{10}$$

If somehow all $\alpha \approx 0$:

$$S^*_{i,j} \approx 1 + \frac{n}{4}\left[\frac{V_{i-1,j}}{r_{i,j}} + \frac{V_{i+1,j}}{r_{i,j}} + \frac{V_{i,j-1}}{r_{i,j}} + \frac{V_{i,j+1}}{r_{,j}}\right] - n\,\frac{V_{i,j}}{r_{i,j}} \tag{11}$$

With the assumption of independent, zero mean noise with standard deviation σ, a first order approximation to the variance of $S^*_{i,j}$ can be shown to be:

$$\text{var}\,(S^*_{i,j}) \quad \frac{5n^2\sigma^2}{4r^2_{i,j}} \tag{12}$$

The foregoing analysis gives the means of choosing the proper threshold, given the values of α. For example, if two of the outerpoints (i-1,j) and (i,j-1) be outside the obstacle and the other three points, including the central point (i,j) be on the obstacle, then one may assume: $\alpha_{i-1,j}$,

$\alpha_{i,j-1} > 0$ and $\alpha_{i+1,j} \approx \alpha_{i,j+1} \approx 0$. Further let:

$$\alpha_{i-1,j} \approx \alpha_{i,j-1} \approx .04 \tag{13}$$

Then from eq. (7):

$$q^*_{i,j} \approx +\tfrac{1}{2}(.04 + 0 + .04 + 0) = .02 \tag{14}$$

Thus, the threshold may be set just below .02 if the point in consideration is to be detected, i.e.

$$T_q \approx .019 \tag{15}$$

If the central point is assumed to be just outside the obstacle with the other points as before, then one will have a negative threshold value, and this is used to detect points just outside the object.

If the Four Directional Ratio method is used, then from eq. (10):

$$S^*_{i,j} \approx 1 + \frac{n}{4}(0.04 + 0 + 0.04 + 0) = 1 + n(0.02) \tag{16a}$$

For n = 2: $$S^*_{i,j} \approx 1 + 2(0.02) = 1.04 \tag{16b}$$

Notice that by increasing n the apparent threshold value can be amplified.

The variances given in eqs. (9) and (12) provide an indication of how large a measurement noise may be tolerated by the algorithms. Suppose it is desired that the threshold lies outside the 1 σ limit of the variation in q. Then from eqs. (9) and (15):

$$\sqrt{\frac{50^2}{4r^2}_{i,j}} \leq .019$$

or: (17)

$$\sigma \leq .017\, r_{i,j}$$

Obviously at longer ranges, higher measurement noise may be allowed.

The values of α may be obtained from a physical model of obstacles and terrains.

Simulation Results

The boulder at 30m.

Fig. 55 illustrates the case study for positive obstacles (those which project above the surface of the terrain). The Rover is a perfectly flat terrain, with a hemispherical boulder of radius r directly in its path of travel, located 6 meters horizontally from the laser mast. A computer program was written to generate the range data points in the 'range image' given the elevation angles β and the azimuth angles θ as inputs. Fig. 56 illustrates the resultant 'range image' for a boulder at 30 m, both when the measurements are undistorted and when they are contaminated by zero mean, 5cm standard deviation, Gaussian noise. The reason for selection of σ_V = 5 cm was that this was one of the desired accuracies of the laser rangefinder stated under Task C.1 of the Mars Rover design.

Fig. 57 and 58 show the σ matrices for this case, which are used in the off-line determination of threshold values, as outlined in the previous section. As an example of the approximate thresholds to be expected, and to show agreement with the analysis given, a threshold of 1.02 was used in the Four Directional Ratio algorithm to pick out the inside edge, and a value of .96 for the outside edge.

Fig. 59a, 59b and 59c illustrate the resulting matrices after the algorithms (Four Directional Ratio with n= 1 and n = 2, and Normalized Laplacian) have been applied to the 'range image' The results are the same for both the noiseless and noisy cases; hence, only the noisy case is shown. The fact that they are the same should be expected, since from eq. (17), for $V_{i,j} = 30$, $\sigma_{allowable} = .017\, r_{i,j} = .51$, whereas the σ used is only .05. An error this small will obviously have little effect on the edge detection algorithms used.

Finally, in Figs. 60a and 60b we see the outlines of the boulder after the thresholding operation has been applied to the previous matrices. As seen, by proper choice of thresholds both pictures are the same, and are quite good reproductions of the true boulder's edge except for the obvious lack of a bottom edge.

The bottom edge

Due to the nature of the algorithms, the fact that the bottom edge is not detected is a characteristic outcome, and should be expected. In other words, since the detection scheme is based on the comparison of neighboring range values for sharp changes, there will be no indication of an edge if the adjacent range values are approximately the same (as they are for the points near the bottom edge). A different type of algorithm is therefore needed for this special case. The first attempt at a solution to this problem was based on the observation that range values measured to the bottom edge itself form a set of local maxima compared to the ranges just above and just below them in the range image. A printout of the outcome of this procedure is seen in Fig. 60. The picture is adequate; however, it was the noiseless range values which were compared in this case. When noise is added to the range values, and then are then compared, the result is as in Fig. 61a and 61b. The picture in this case is obviously unacceptable; the explanation is that the range values in the bottom edge only differ from their surrounding values by about .01 m, so that the standard deviation of noise of .05 m completely obscures this difference.

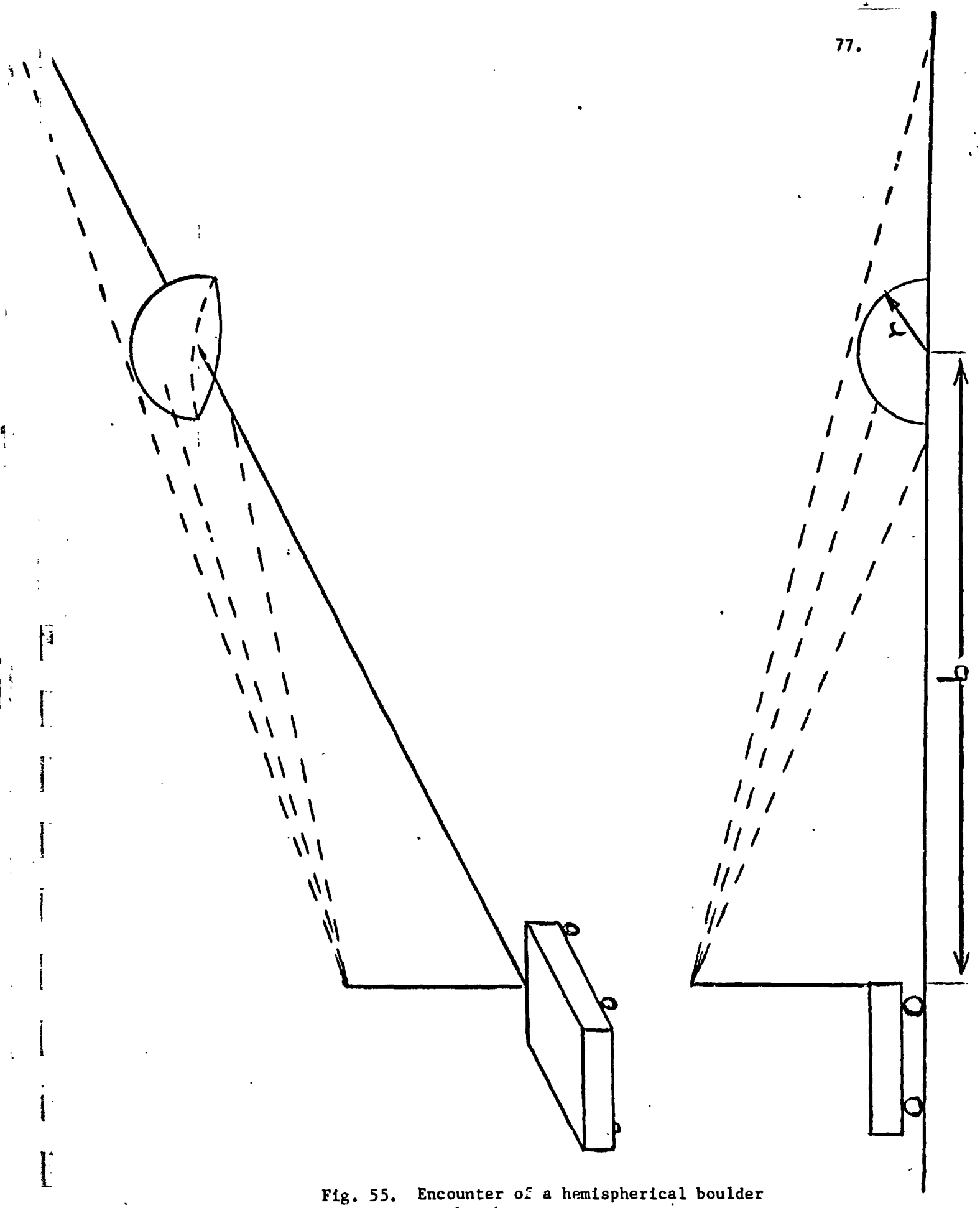

Fig. 55. Encounter of a hemispherical boulder by the Rover

CALCULATED RANGE DATA FOR A HEMISPHERICAL BOULDER (1.00 METER RADIUS) AT A DISTANCE OF 30.00 METERS FROM MARS ROVER

BETA MAX = 6.0 DEGREES   BETA MIN = 3.0 DEGREES   BETA INCREMENT = .15 DEGREES
THETA MAX = 3.0 DEGREES   THETA MIN = -3.0 DEGREES   THETA INCREMENT = .30 DEGREES

R(1,1)-----(BETA MIN, THETA MIN)   R(1,21)-----(BETA MIN, THETA MAX)
R(25,1)-----(BETA MAX, THETA MIN)   R(25,21)-----(BETA MAX, THETA MAX)

UNDISTORTED BY NOISE

50.00	50.00	50.00	50.00	50.00	50.00	50.00	50.00	50.00	50.00	50.00	50.00	50.00	50.00	50.00	50.00	50.00	50.00	50.00	50.00	50.00
50.00	50.00	50.00	50.00	50.00	50.00	50.00	50.00	50.00	50.00	50.00	50.00	50.00	50.00	50.00	50.00	50.00	50.00	50.00	50.00	50.00
50.00	50.00	50.00	50.00	50.00	50.00	50.00	50.00	50.00	50.00	50.00	50.00	50.00	50.00	50.00	50.00	50.00	50.00	50.00	50.00	50.00
49.88	49.88	49.88	49.88	49.88	49.88	49.88	49.88	49.88	49.88	49.88	49.88	49.88	49.88	49.88	49.88	49.88	49.88	49.88	49.88	49.88
47.75	47.75	47.75	47.75	47.75	47.75	47.75	47.75	47.75	47.75	47.75	47.75	47.75	47.75	47.75	47.75	47.75	47.75	47.75	47.75	47.75
45.88	45.88	45.88	45.88	45.88	45.88	45.88	45.88	45.88	45.88	45.88	45.88	45.88	45.88	45.88	45.88	45.88	45.88	45.88	45.88	45.88
44.13	44.13	44.13	44.13	44.13	44.13	44.13	44.13	44.13	[illegible]	[illegible]	[illegible]	44.13	44.13	44.13	44.13	44.13	44.13	44.13	44.13	44.13
42.50	42.50	42.50	42.50	42.50	42.50	42.50	42.50	[illegible]	29.67	29.65	29.67	29.77	42.53	42.50	42.50	42.50	42.50	42.50	42.50	42.50
40.94	40.94	40.94	40.94	40.94	40.94	40.94	[illegible]	29.63	29.55	29.53	29.55	29.63	[illegible]	40.94	40.94	40.94	40.94	40.94	40.94	40.94
39.50	39.50	39.50	39.50	39.50	39.50	[illegible]	29.53	29.52	29.46	29.44	29.40	29.57	29.63	[illegible]	39.50	39.50	39.50	39.50	39.50	39.50
38.25	38.25	38.25	38.25	38.25	38.25	29.67	29.53	29.44	29.37	29.38	29.37	29.44	29.53	29.64	38.25	38.25	38.25	38.25	38.25	38.25
37.06	37.06	37.06	37.06	37.06	[illegible]	29.59	29.46	29.33	29.33	29.31	29.33	29.38	29.46	29.59	[illegible]	37.06	37.06	37.06	37.06	37.06
35.88	35.88	35.88	35.88	35.88	29.75	29.52	29.40	29.32	29.28	29.27	29.28	29.32	29.40	29.52	29.75	35.88	35.88	35.88	35.88	35.88
34.75	34.75	34.75	34.75	34.75	29.65	29.46	29.35	29.29	29.24	29.23	29.24	29.29	29.35	29.45	29.66	34.75	34.75	34.75	34.75	34.75
33.75	33.75	33.75	33.75	33.75	29.61	29.43	29.32	29.25	29.22	29.20	29.21	29.25	29.32	29.43	29.51	33.75	33.75	33.75	33.75	33.75
32.75	32.75	32.75	32.75	[illegible]	29.57	29.40	29.30	29.23	29.19	29.19	29.19	29.23	29.30	29.40	29.57	[illegible]	32.75	32.75	32.75	32.75
31.88	31.88	31.88	31.88	29.84	29.54	29.38	29.28	29.21	29.14	29.16	29.16	29.21	29.28	29.38	29.54	29.84	31.88	31.88	31.88	31.88
31.06	31.06	31.06	31.06	29.61	29.53	29.37	29.27	29.20	29.17	29.15	29.17	29.20	29.27	29.37	29.53	29.61	31.06	31.06	31.06	31.06
30.25	30.25	30.25	30.25	[illegible]	[illegible]	29.36	29.26	29.20	29.16	29.15	29.16	29.20	29.26	29.36	29.52	[illegible]	30.25	30.25	30.25	30.25
29.44	29.44	29.44	29.44	29.44	[illegible]	[illegible]	29.27	29.20	29.17	29.15	29.17	29.20	29.27	29.37	29.44	29.44	29.44	29.44	29.44	29.44
28.69	28.69	28.69	28.69	28.69	28.67	[illegible]	28.67	28.67	28.57	28.67	28.69	[illegible]	[illegible]	[illegible]	28.69	28.67	28.69	28.69	28.69	28.69
28.03	28.03	28.03	28.03	28.03	28.03	28.03	28.03	28.03	28.03	28.03	28.03	28.03	28.03	28.03	28.03	28.03	28.03	28.03	28.03	28.03
27.38	27.38	27.38	27.38	27.38	27.38	27.38	27.38	27.38	27.38	27.38	27.38	27.38	27.38	27.38	27.38	27.38	27.38	27.38	27.38	27.38
26.69	26.69	26.69	26.69	26.69	26.69	26.69	26.69	26.69	26.69	26.69	26.69	26.69	26.69	26.69	26.69	26.69	26.69	26.69	26.69	26.69
26.13	26.13	26.13	26.13	26.13	26.13	26.13	26.13	26.13	26.13	26.13	26.13	26.13	26.13	26.13	26.13	26.13	26.13	26.13	26.13	26.13

CONTAMINATED BY ZERO MEAN, .05 METER STANDARD DEVIATION, GAUSSIAN NOISE

9.47	50.03	50.32	50.31	49.98	49.97	50.06	50.01	49.47	50.05	49.95	50.04	50.10	49.97	50.03	49.99	50.11	50.02	50.10	50.02	50.01
49.98	50.00	50.07	49.98	49.94	49.97	49.96	49.73	49.93	50.05	50.01	50.01	50.06	49.94	50.10	50.00	50.04	50.02	50.06	49.98	50.11
50.08	50.04	50.13	50.01	49.92	50.02	50.01	49.97	49.95	49.93	50.27	49.91	50.07	49.97	50.05	49.93	50.03	50.01	50.03	49.99	50.03
49.87	49.92	49.90	[illegible]	49.77	49.86	49.89	49.95	49.87	49.94	49.87	49.91	49.94	49.84	49.83	49.93	49.84	49.78	49.99	49.88	49.96
47.80	47.76	47.77	47.72	47.77	47.82	47.65	47.64	47.74	47.73	47.74	47.63	47.57	47.81	47.86	47.73	47.78	47.75	47.78	47.81	47.70
45.99	45.95	45.89	45.87	45.94	45.90	45.89	45.79	45.93	45.49	45.85	45.91	45.87	45.93	45.95	45.81	45.97	45.90	45.86	45.77	45.87
44.13	44.11	44.12	44.12	44.12	44.15	44.12	44.39	44.15	[illegible]	[illegible]	[illegible]	44.06	44.11	44.10	44.05	44.17	44.19	44.10	44.12	44.13
42.51	42.45	42.50	42.47	42.51	42.41	42.51	[illegible]	[illegible]	29.68	29.69	29.72	[illegible]	42.51	42.49	42.47	42.47	42.58	42.44	42.53	42.51
40.96	40.91	40.98	41.05	40.85	40.96	41.03	29.56	29.53	29.53	29.57	29.47	29.65	29.70	40.97	40.90	40.86	40.90	40.94	40.88	40.89
39.44	39.47	39.55	39.47	39.49	39.56	[illegible]	29.55	29.45	29.42	29.49	29.47	29.58	29.69	[illegible]	39.52	39.52	39.49	39.47	39.53	39.41
38.21	38.15	38.27	38.25	[illegible]	[illegible]	29.64	29.54	29.42	29.34	29.36	29.34	29.45	29.49	29.70	38.31	38.27	38.27	38.30	38.25	38.35
37.07	37.11	37.11	37.03	37.06	[illegible]	29.53	29.37	29.35	29.35	[illegible]	29.19	29.45	29.48	29.64	[illegible]	37.05	36.98	37.06	36.96	37.07
35.87	35.47	35.88	35.71	35.85	29.73	29.48	29.33	29.30	29.27	29.35	29.29	29.25	29.39	29.44	29.55	35.83	35.42	35.82	35.93	35.84
34.71	34.75	34.72	34.75	34.68	29.59	29.45	29.20	29.25	29.26	29.26	29.24	29.32	29.35	29.50	29.53	34.72	34.77	34.78	34.73	34.79
33.77	33.61	33.72	33.73	33.71	29.57	29.55	29.35	29.25	29.28	29.27	29.21	29.26	29.36	29.47	29.61	33.77	33.78	33.66	33.79	33.72
32.69	32.63	32.79	32.74	[illegible]	29.53	29.31	29.23	29.27	29.31	29.24	[illegible]	29.15	29.30	29.49	29.49	[illegible]	32.76	32.68	32.80	32.80
31.79	31.43	31.07	31.03	[illegible]	29.51	29.32	29.23	29.21	29.11	29.13	29.11	29.17	29.26	29.41	29.55	29.73	31.84	31.89	31.81	31.80
31.11	31.07	31.03	31.05	29.79	29.53	29.43	29.20	29.15	29.21	29.15	29.16	29.23	29.25	29.32	29.54	29.80	31.11	31.01	31.07	31.01
30.25	30.17	30.25	[illegible]	29.73	29.42	29.35	29.18	29.15	29.21	29.17	29.17	29.17	29.23	29.43	29.51	29.51	30.14	30.20	30.31	30.22
29.51	29.49	29.47	29.47	[illegible]	[illegible]	29.37	29.24	29.27	29.11	29.09	29.15	29.32	29.22	29.41	[illegible]	[illegible]	29.32	29.46	29.45	29.49
28.72	28.77	28.60	28.50	28.72	28.77	[illegible]	28.52	28.63	28.67	28.63	28.69	28.72	28.65	28.67	28.61	28.75	28.69	28.79	28.60	28.75
27.94	27.99	28.00	28.05	27.97	27.95	28.07	28.03	28.03	27.95	28.03	28.02	28.31	28.12	28.00	28.05	28.08	28.05	28.04	27.98	27.97
27.53	27.53	27.39	27.42	27.34	27.28	27.30	27.34	27.47	27.36	27.37	27.41	27.41	27.31	27.31	27.36	27.39	27.35	27.28	27.39	27.48
26.71	26.69	26.75	26.74	26.70	26.60	26.65	26.66	26.63	26.73	26.79	26.68	26.69	26.70	26.64	26.70	26.69	26.71	26.62	26.66	26.71
26.24	26.12	26.12	26.03	26.20	26.05	26.10	26.12	26.14	26.13	26.21	26.16	26.04	26.15	26.07	26.28	26.15	26.10	26.12	26.13	26.12

Fig. 56.   The Range Image

MATRIX OF ALPHA(I,J-1) VALUES

I = 1 TO 25 / J = 2 TO 21

MATRIX OF ALPHA(I,J+1) VALUES

I = 1 TO 25 / J = 1 TO 20

Fig. 57. Two Alpha Matrices

MATRIX OF ALPHA(I-1,J) VALUES

I = 2 TO 25 / J = 1 TO 21

0.0	0.0	0.0	0.0	0.0	0.0	0.0	0.0	0.0	0.0	0.0	0.0	0.0	0.0	0.0	0.0	0.0	0.0	0.0	0.0	0.0	0.0
0.0	0.0	0.0	0.0	0.0	0.0	0.0	0.0	0.0	0.0	0.0	0.0	0.0	0.0	0.0	0.0	0.0	0.0	0.0	0.0	0.0	0.0
0.003	0.003	0.003	0.003	0.003	0.003	0.003	0.003	0.003	0.003	0.003	0.003	0.003	0.003	0.003	0.003	0.003	0.003	0.003	0.003	0.003	0.003
0.045	0.045	0.045	0.045	0.045	0.045	0.045	0.045	0.045	0.045	0.045	0.045	0.045	0.045	0.045	0.045	0.045	0.045	0.045	0.045	0.045	0.045
0.041	0.041	0.041	0.041	0.041	0.041	0.041	0.041	0.041	0.041	0.041	0.041	0.041	0.041	0.041	0.041	0.041	0.041	0.041	0.041	0.041	0.041
0.040	0.040	0.040	0.040	0.040	0.040	0.040	0.040	0.040	0.040	0.040	0.040	0.040	0.040	0.040	0.040	0.040	0.040	0.040	0.040	0.040	0.040
0.038	0.038	0.038	0.038	0.038	0.038	0.038	0.038	0.038	0.038	0.038	0.038	0.038	0.038	0.038	0.038	0.038	0.038	0.038	0.038	0.038	0.038
0.038	0.038	0.038	0.038	0.038	0.038	0.038	0.038	0.038	0.038	0.038	0.038	0.038	0.038	0.038	0.038	0.038	0.038	0.038	0.038	0.038	0.038
0.036	0.036	0.036	0.036	0.036	0.036	0.036	0.036	0.036	0.036	0.036	0.036	0.036	0.036	0.036	0.036	0.036	0.036	0.036	0.036	0.036	0.036
0.033	0.033	0.033	0.033	0.033	0.033	0.033	0.033	0.033	0.033	0.033	0.033	0.033	0.033	0.033	0.033	0.033	0.033	0.033	0.033	0.033	0.033
0.032	0.032	0.032	0.032	0.032	0.032	0.032	0.032	0.032	0.032	0.032	0.032	0.032	0.032	0.032	0.032	0.032	0.032	0.032	0.032	0.032	0.032
0.033	0.033	0.033	0.033	0.033	0.033	0.033	0.033	0.033	0.033	0.033	0.033	0.033	0.033	0.033	0.033	0.033	0.033	0.033	0.033	0.033	0.033
0.032	0.032	0.032	0.032	0.032	0.002	0.002	0.002	0.002	0.002	0.002	0.002	0.002	0.002	0.002	0.002	0.002	0.002	0.002	0.032	0.032	0.032
0.030	0.030	0.030	0.030	0.030	0.002	0.001	0.001	0.001	0.001	0.001	0.001	0.001	0.001	0.001	0.001	0.001	0.002	0.030	0.030	0.030	0.030
0.031	0.031	0.031	0.031	0.124	0.031	0.001	0.001	0.001	0.001	0.001	0.001	0.001	0.001	0.001	0.001	0.001	0.124	0.031	0.031	0.031	0.031
0.027	0.027	0.027	0.027	0.002	0.001	0.001	0.001	0.001	0.001	0.001	0.001	0.001	0.001	0.001	0.001	0.001	0.002	0.027	0.027	0.027	0.027
0.026	0.026	0.026	0.026	0.001	0.001	0.000	0.000	0.000	0.000	0.000	0.000	0.000	0.000	0.000	0.000	0.001	0.001	0.026	0.026	0.026	0.026
0.027	0.027	0.027	0.027	[illegible]	[illegible]	[illegible]	[illegible]	[illegible]	[illegible]	[illegible]	[illegible]	[illegible]	[illegible]	[illegible]	[illegible]	[illegible]	[illegible]	0.027	0.027	0.027	0.027
0.028	0.028	0.028	0.028	[illegible]	[illegible]	[illegible]	[illegible]	[illegible]	[illegible]	[illegible]	[illegible]	[illegible]	[illegible]	[illegible]	[illegible]	[illegible]	[illegible]	0.028	0.028	0.028	0.028
0.026	0.026	0.026	0.026	0.026	0.026	0.026	0.026	0.026	0.026	0.026	0.026	0.026	0.026	0.026	0.026	0.026	0.026	0.026	0.026	0.026	0.026
0.023	0.023	0.023	0.023	0.023	0.023	0.023	0.023	0.023	0.023	0.023	0.023	0.023	0.023	0.023	0.023	0.023	0.023	0.023	0.023	0.023	0.023
0.024	0.024	0.024	0.024	0.024	0.024	0.024	0.024	0.024	0.024	0.024	0.024	0.024	0.024	0.024	0.024	0.024	0.024	0.024	0.024	0.024	0.024
0.026	0.026	0.026	0.026	0.026	0.026	0.026	0.026	0.026	0.026	0.026	0.026	0.026	0.026	0.026	0.026	0.026	0.026	0.026	0.026	0.026	0.026
0.022	0.022	0.022	0.022	0.022	0.022	0.022	0.022	0.022	0.022	0.022	0.022	0.022	0.022	0.022	0.022	0.022	0.022	0.022	0.022	0.022	0.022

MATRIX OF ALPHA(I+1,J) VALUES

I = 1 TO 24 / J = 1 TO 21

0.0	0.0	0.0	0.0	0.0	0.0	0.0	0.0	0.0	0.0	0.0	0.0	0.0	0.0	0.0	0.0	0.0	0.0	0.0	0.0	0.0	0.0
0.0	0.0	0.0	0.0	0.0	0.0	0.0	0.0	0.0	0.0	0.0	0.0	0.0	0.0	0.0	0.0	0.0	0.0	0.0	0.0	0.0	0.0
-0.003	-0.003	-0.003	-0.003	-0.003	-0.003	-0.003	-0.003	-0.003	-0.003	-0.003	-0.003	-0.003	-0.003	-0.003	-0.003	-0.003	-0.003	-0.003	-0.003	-0.003	-0.003
-0.043	-0.043	-0.043	-0.043	-0.043	-0.043	-0.043	-0.043	-0.043	-0.043	-0.043	-0.043	-0.043	-0.043	-0.043	-0.043	-0.043	-0.043	-0.043	-0.043	-0.043	-0.043
-0.039	-0.039	-0.039	-0.039	-0.039	-0.039	-0.039	-0.039	-0.039	-0.039	-0.039	-0.039	-0.039	-0.039	-0.039	-0.039	-0.039	-0.039	-0.039	-0.039	-0.039	-0.039
-0.038	-0.038	-0.038	-0.038	-0.038	-0.038	-0.038	-0.038	-0.038	-0.038	-0.038	-0.038	-0.038	-0.038	-0.038	-0.038	-0.038	-0.038	-0.038	-0.038	-0.038	-0.038
-0.037	-0.037	-0.037	-0.037	-0.037	-0.037	-0.037	-0.037	-0.037	-0.037	-0.037	-0.037	-0.037	-0.037	-0.037	-0.037	-0.037	-0.037	-0.037	-0.037	-0.037	-0.037
-0.037	-0.037	-0.037	-0.037	-0.037	-0.037	-0.037	-0.037	-0.037	-0.037	-0.037	-0.037	-0.037	-0.037	-0.037	-0.037	-0.037	-0.037	-0.037	-0.037	-0.037	-0.037
-0.035	-0.035	-0.035	-0.035	-0.035	-0.035	-0.035	-0.035	-0.035	-0.035	-0.035	-0.035	-0.035	-0.035	-0.035	-0.035	-0.035	-0.035	-0.035	-0.035	-0.035	-0.035
-0.032	-0.032	-0.032	-0.032	-0.032	-0.032	-0.003	-0.003	-0.003	-0.003	-0.003	-0.003	-0.003	-0.003	-0.003	-0.003	-0.003	-0.003	-0.032	-0.032	-0.032	-0.032
-0.031	-0.031	-0.031	-0.031	-0.219	-0.002	-0.002	-0.002	-0.002	-0.002	-0.002	-0.002	-0.002	-0.002	-0.002	-0.002	-0.002	-0.219	-0.031	-0.031	-0.031	-0.031
-0.032	-0.032	-0.032	-0.032	-0.032	-0.002	-0.002	-0.002	-0.002	-0.002	-0.002	-0.002	-0.002	-0.002	-0.002	-0.002	-0.002	-0.002	-0.032	-0.032	-0.032	-0.032
-0.031	-0.031	-0.031	-0.031	-0.031	-0.001	-0.001	-0.001	-0.001	-0.001	-0.001	-0.001	-0.001	-0.001	-0.001	-0.001	-0.001	-0.001	-0.031	-0.031	-0.031	-0.031
-0.029	-0.029	-0.029	-0.029	-0.029	-0.001	-0.001	-0.001	-0.001	-0.001	-0.001	-0.001	-0.001	-0.001	-0.001	-0.001	-0.001	-0.002	-0.029	-0.029	-0.029	-0.029
-0.030	-0.030	-0.030	-0.030	-0.030	-0.001	-0.001	-0.001	-0.001	-0.001	-0.001	-0.001	-0.001	-0.001	-0.001	-0.001	-0.001	-0.114	-0.030	-0.030	-0.030	-0.030
-0.027	-0.027	-0.027	-0.027	-0.027	-0.001	-0.001	-0.001	-0.001	-0.001	-0.001	-0.001	-0.001	-0.001	-0.001	-0.001	-0.001	-0.002	-0.027	-0.027	-0.027	-0.027
-0.025	-0.025	-0.025	-0.025	-0.001	-0.001	-0.001	-0.000	-0.000	-0.000	-0.000	-0.000	-0.000	-0.000	-0.000	-0.000	-0.001	-0.001	-0.025	-0.025	-0.025	-0.025
-0.026	-0.026	-0.026	-0.026	[illegible]	[illegible]	[illegible]	[illegible]	[illegible]	[illegible]	[illegible]	[illegible]	[illegible]	[illegible]	[illegible]	[illegible]	[illegible]	[illegible]	-0.026	-0.026	-0.026	-0.026
-0.027	-0.027	-0.027	-0.027	-0.002	[illegible]	[illegible]	[illegible]	[illegible]	[illegible]	[illegible]	[illegible]	[illegible]	[illegible]	[illegible]	[illegible]	[illegible]	[illegible]	-0.027	-0.027	-0.027	-0.027
-0.025	-0.025	-0.025	-0.025	-0.025	[illegible]	[illegible]	[illegible]	[illegible]	[illegible]	[illegible]	[illegible]	[illegible]	[illegible]	[illegible]	[illegible]	[illegible]	[illegible]	-0.025	-0.025	-0.025	-0.025
-0.023	-0.023	-0.023	-0.023	-0.023	-0.023	-0.023	-0.023	-0.023	-0.023	-0.023	-0.023	-0.023	-0.023	-0.023	-0.023	-0.023	-0.023	-0.023	-0.023	-0.023	-0.023
-0.023	-0.023	-0.023	-0.023	-0.023	-0.023	-0.023	-0.023	-0.023	-0.023	-0.023	-0.023	-0.023	-0.023	-0.023	-0.023	-0.023	-0.023	-0.023	-0.023	-0.023	-0.023
-0.025	-0.025	-0.025	-0.025	-0.025	-0.025	-0.025	-0.025	-0.025	-0.025	-0.025	-0.025	-0.025	-0.025	-0.025	-0.025	-0.025	-0.025	-0.025	-0.025	-0.025	-0.025
-0.021	-0.021	-0.021	-0.021	-0.021	-0.021	-0.021	-0.021	-0.021	-0.021	-0.021	-0.021	-0.021	-0.021	-0.021	-0.021	-0.021	-0.021	-0.021	-0.021	-0.021	-0.021

Fig. 58. Two Aloha Matrices

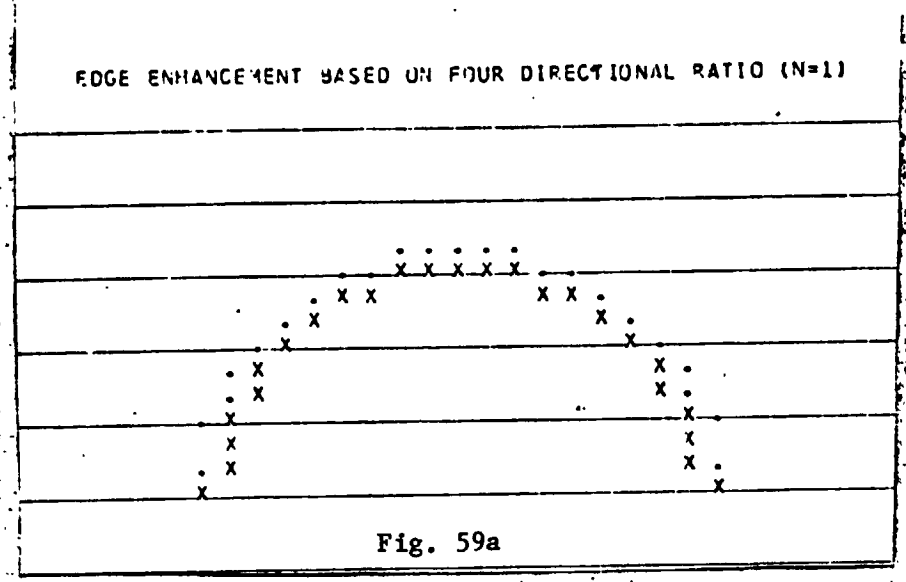

Fig. 59a

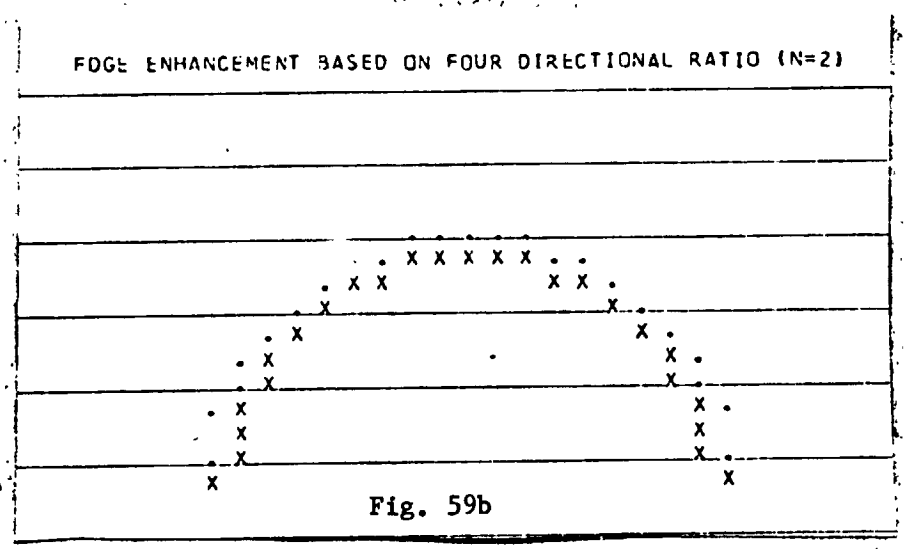

Fig. 59b

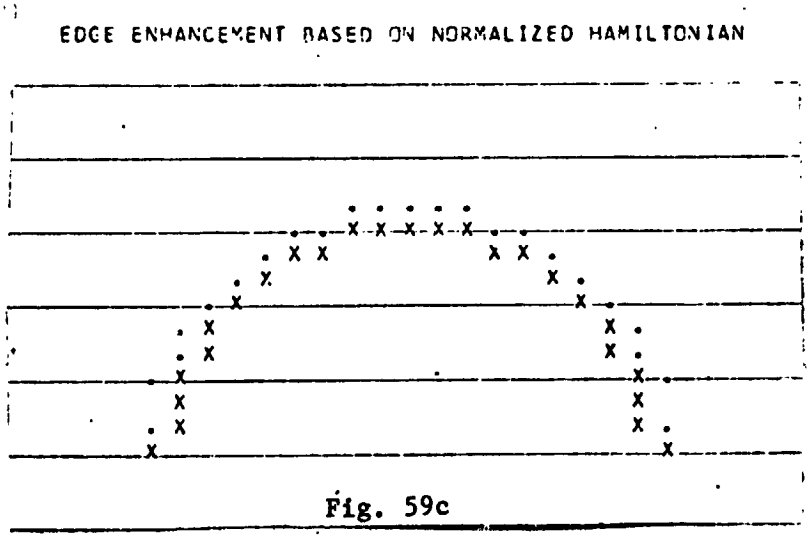

Fig. 59c

Fig. 59. Outcomes of the Edge Detection Scheme

EDGE ENHANCEMENT BASED ON FOUR DIRECTIONAL RATIO (N=2)

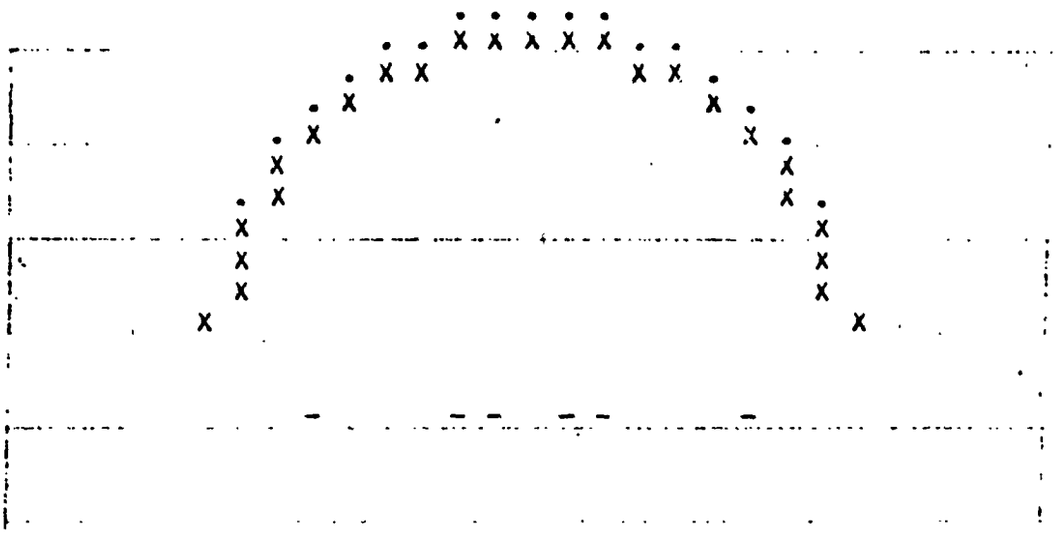

Fig. 60a

EDGE ENHANCEMENT BASED ON NORMALIZED HAMILTONIAN

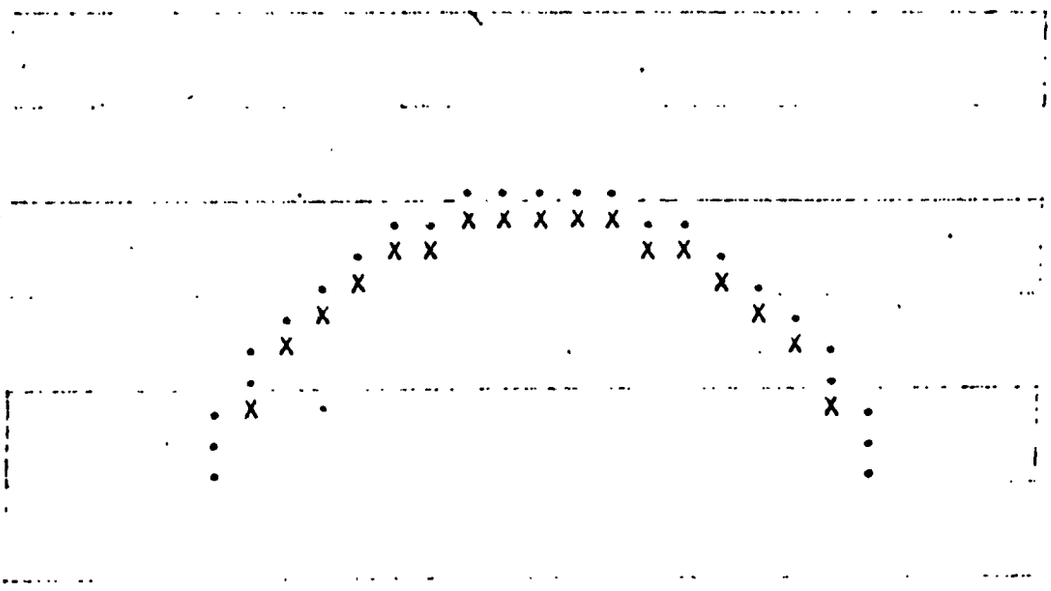

Fig. 60b

Fig. 60. First attempt at a bottom edge detection procedure

EDGE ENHANCEMENT BASED ON FOUR DIRECTIONAL RATIO (N=2)

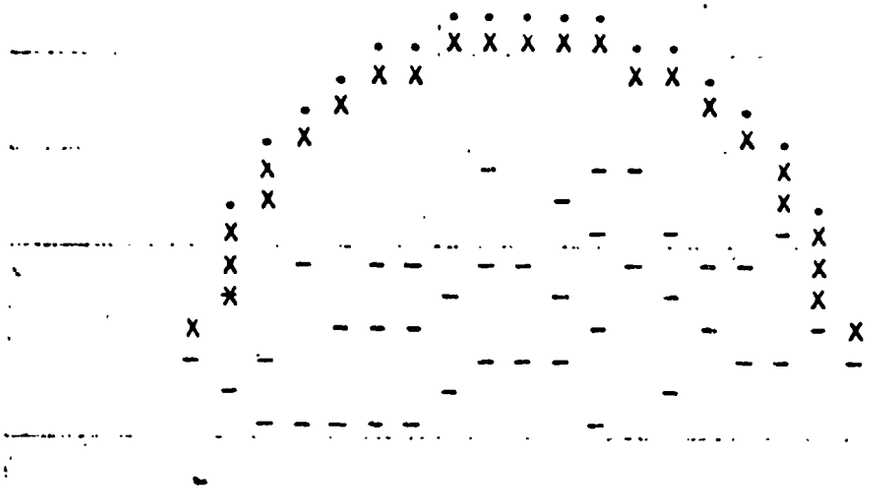

Fig. 61a

EDGE ENHANCEMENT BASED ON NORMALIZED HAMILTONIAN

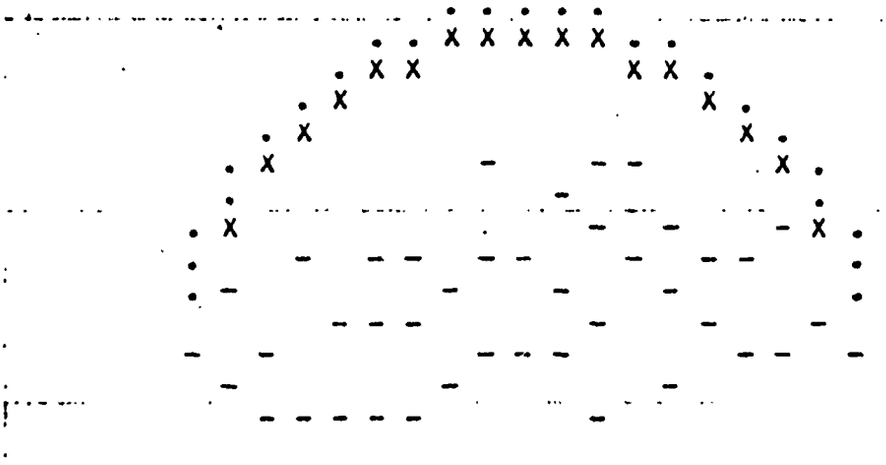

Fig. 61b

Fig. 61 Results when noisy range values are compared

In seeking a more useful method, the following procedure was developed. By examining each range value lying along the center of the 'range image' (which corresponds to an azimuth angle of zero, which is directly in front of the Rover) and comparing them to the range that would be obtained if the boulder were not present, the bottom edge can be detected if a given element is not "close" to the range without the boulder (given by the expression $r_{i,j} = 3/\sin\beta$) and the element just below this one is "close" to the range without the boulder. By "close" we are considering the effects of noise, so that the range without the boulder will be taken as $(3/\sin\beta) \pm 3\sigma_v$. By this process we may find a bottom edge point, and then interpolate to fill in the edge between this limit and the limits determined by the original edge detection scheme. As seen in Fig. 62a and 62b, this procedure yields a satisfactory result. But once again there is a problem, for if the terrain is not as smooth as assumed then a false indication is again a possibility. Therefore, it seems that the bottom edge will have to be determined by a completely different approach, possibly with the use of gradient methods, and this aspect of the edge detection scheme must be left to future research efforts.

Scanning scheme considerations

To this point the angle limits have been chosen with a priori knowledge of the boulder's size and location, so that the angle differences between the range points were as small as possible, in order to maximize the information received about the boulder and its immediate surroundings. In reality this information will obviously not be available. Therefore, in order to simulate the situation where the angle limits are fixed so as to include any 1 meter radius boulder between 10 and 40 meters from the vehicle, the geometry of Fig. 63 was defined. The pictures in Figs. 64 and 65 illustrate the effect of applying the edge detection scheme, using both these fixed limits (shown by the boulders on the left of the drawings) and the variable limits previously implemented, for comparison. As can be seen, for boulders beyond the 20 m range, the fixed scan technique is quite unacceptable for the edge detection scheme. Once again, this problem will require further investigation.

Other types of obstacles

Since it is expected that the Rover will encounter negative obstacles (those extending below surface level) as well, the edge detection scheme was tested for an obstacle of this type. A hemispherical crater of 1 meter radius, located 30 meters from the Rover, was placed on the terrain, and the same type of procedure was followed as for the boulder. The computer picture of the result appears in Fig. 66. Note that only the near edge of the crater is detected, and that the far edge is missed, just as the bottom edge of the boulder was missed, and for the same reason. Therefore, if the bottom edge problem of the boulder can be solved, then the far edge problem of the crater will also be solved, so that the edge detection scheme will indeed be useful for both types of obstacles.

Concluding remarks. The computer simulation program used in the development of the edge detection scheme is being documented, and will be available for the use of those continuing the research of this technique. It is expected that investigators working on the bottom edge problem, on the scanning scheme problem, and on the overall edge detection scheme implementation will find the program useful, and will enable them to obtain meaningful results with a minimum amount of time for problem familiarization.

EDGE ENHANCEMENT BASED ON FOUR DIRECTIONAL RATIO (N=2)

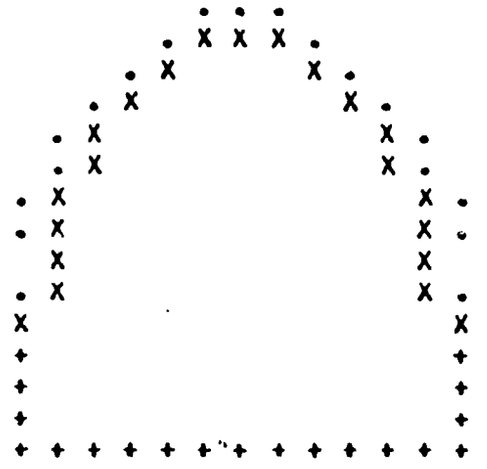

Fig. 62a

EDGE ENHANCEMENT BASED ON NORMALIZED HAMILTONIAN

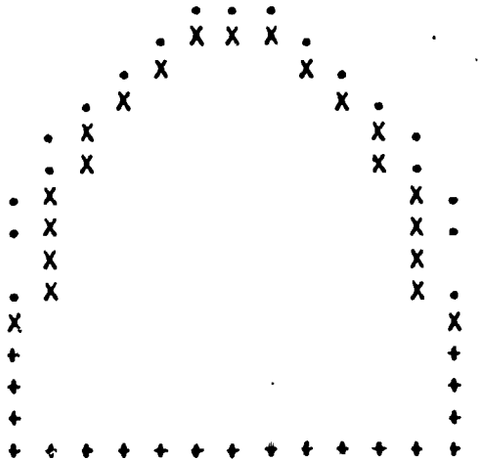

Fig. 62b

Fig. 62. Noise resistant, but terrain sensitive, bottom edge

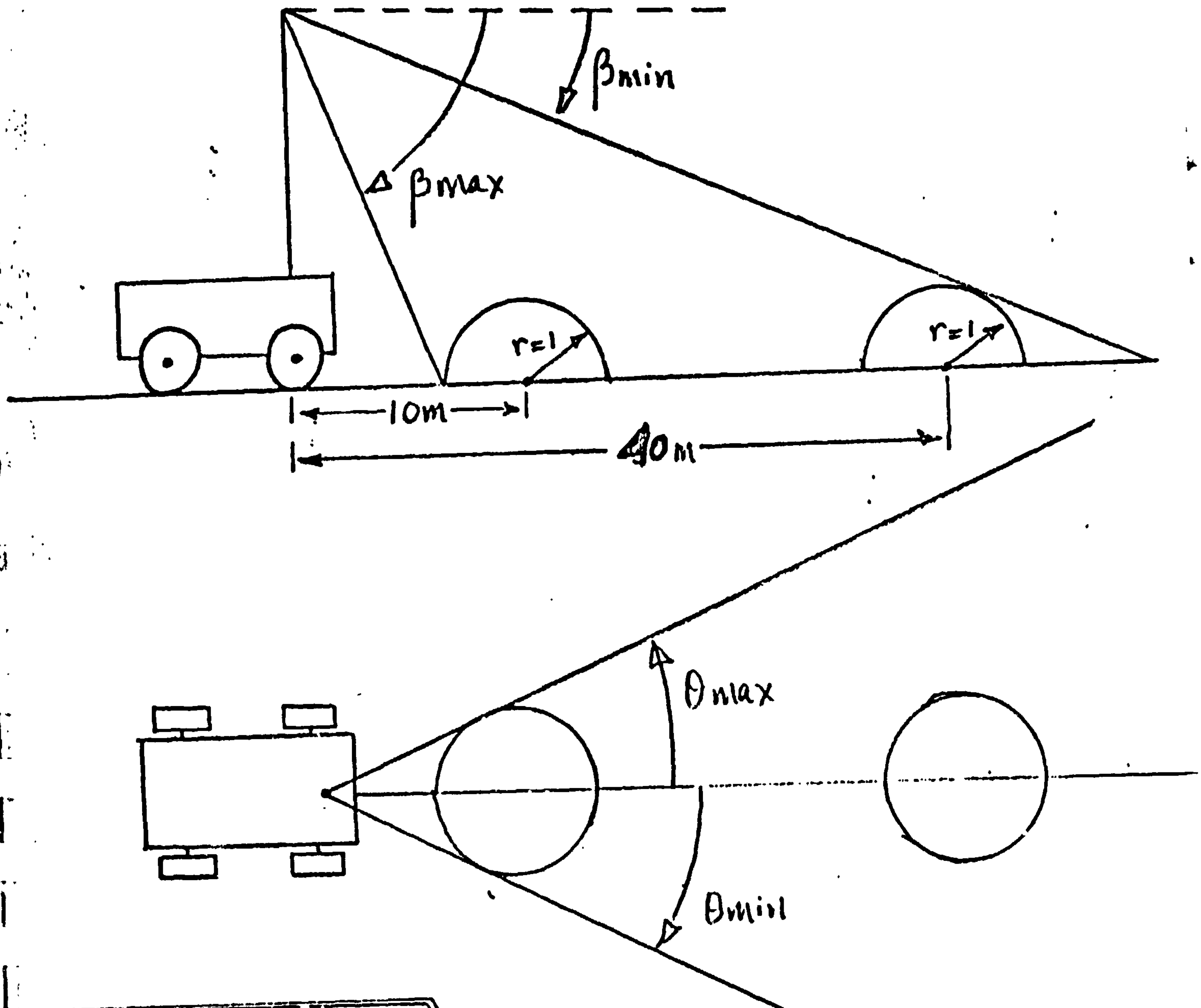

$$\beta_{increment} = \frac{\beta_{max} - \beta_{min}}{24}$$

$$\theta_{increment} = \frac{\theta_{max} - \theta_{min}}{20}$$

ANGLES <u>NOT</u> FUNCTIONS OF b.

Geometry of fixed scan

D = 10 m

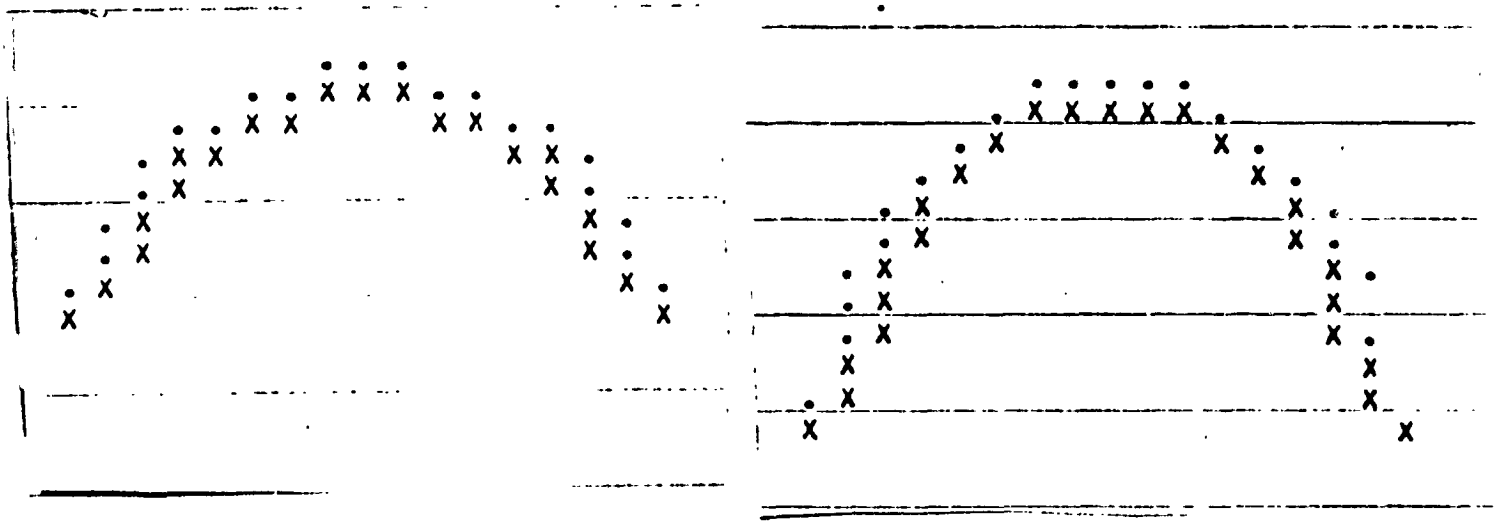

β, θ = const.

β, θ = f (b)

b = 20 m

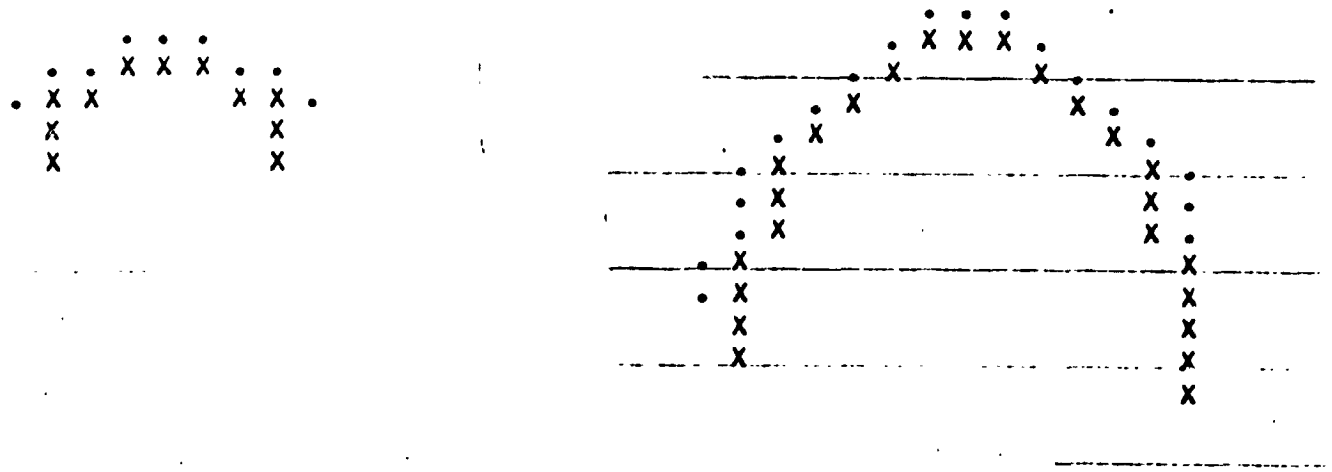

β, θ = const.

β, θ = f (b)

Fig. 64. Comparison between fixed and variable scan

$b = 30\ m$

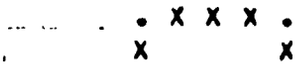

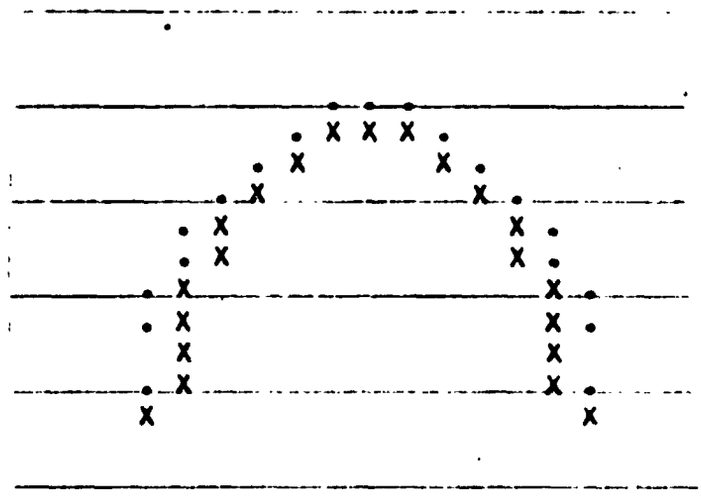

$\beta, \theta = const.$

$\beta, \theta = f(b)$

$b = 40\ m$

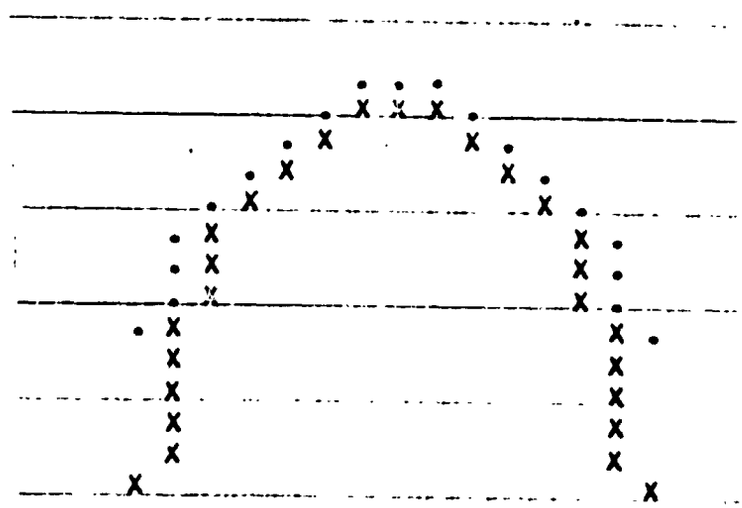

$\beta, \theta = const.$

$\beta, \theta = f(b)$

Fig. 65. Comparison between fixed and variable scan

EDGE ENHANCEMENT BASED ON FOUR DIRECTIONAL RATIO (N=2)

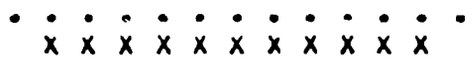

EDGE ENHANCEMENT BASED ON NORMALIZED HAMILTONIAN

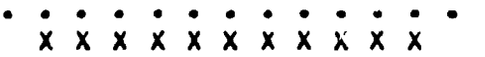

Fig. 66. The Edge detection scheme applied to a crater

C.2.b. Parameter Estimation for Terrain Modeling from Gradient Data -
K. R. D'Angelo
Faculty Advisor: Prof. C. N. Shen

Objective. The objective undertaken in the area of terrain modeling was to develop a method for representing sections of the Martin terrain by analytic curved surfaces, using range data obtained from two successive laser scan rows. The model was also checked to determine the effect of instrumental errors on the model's accuracy.

Progress Summary. A two step modeling procedure was developed. Height, location and gradient were computed from sixteen raw data points. The model formed from this data is a third degree, two dimensional polynomial.

There were two reasons for using a two step process rather than a process using only height data to form the polynomial. Since the gradient of the modeled surface is an important factor in determining whether the surface is passable or impassable by the vehicle, the model should give accurate gradient information. Moreover, the largest measurement inaccuracy, due to the roll and pitch angles of the vehicle, affects the height measurement greatly. However, it has only a small effect on gradient.

A complete error analysis has been obtained which gives the standard deviations of height and gradient for simulated models. Finally a computer program has been developed which simulates the scanning process, takes rangefinder readings, forms polynomial models, carries out the error analysis, and compares the modeled results with the actual surface shape and gradient.

Discussion

a) Modeling Procedure - Step 1

The first step in the modeling procedure is to model stochastically a plane from four data points, Ref. 15. This plane is formed in the (h",a",b") coordinate system attached to the vehicle and then transformed to the (h,a,b) coordinate system which is aligned with the local vertical, Fig. 69. Four planes are modeled in this way. Each plane yields the height, location, cross-path slope, $\partial h/\partial a$ and in-path slope, $\partial h/\partial b$, at the center point, p,n, Fig. 68.

b) Modeling Procedure - Step 2

Once four planes have been modeled, a new coordinate system is formed, by shifting the axis so that the point P' is located at (0,0) in the a b system, Fig. 68. This shift improves the model's accuracy and simplifies calculations.

To represent the terrain, two dimensional third degree polynomial

$$h = f(a^{\mp}, b^{\mp}) = C_{00}^{\mp} + C_{10}^{\mp} a^{\mp} + C_{01}^{\mp} b^{\mp} + C_{20}^{\mp} a^{\mp 2}/2 + C_{11}^{\mp} a^{\mp} b^{\mp} + C_{02}^{\mp} b^{\mp 2}/2 + C_{30}^{\mp} a^{\mp 3}/6 + C_{21}^{\mp} a^{\mp 2}/2\, b^{\mp} + C_{12}^{\mp} a^{\mp} b^{\mp 2}/2 + C_{03}^{\mp} b^{\mp 3}/6 \quad (1)$$

C-2

was chosen where the C_{ij}'s are unknown parameters which must be determined in order to represent the surface. Expressions for $\partial h/\partial a^{\mp}$ and $\partial h/\partial b^{\mp}$ can easily be found. Because of the coordinate shift, three parameters are found immediately

$$h_1 = C_{00}^{\mp}, \quad (\partial h/\partial a^{\mp}) = C_{10}^{\mp}, \quad (\partial h/\partial b^{\mp}) = C_{01}^{\mp} \tag{2}$$

Since there are four P^n points and at each P^n point the height, $\partial h/\partial a^{\mp}$ and $\partial h/\partial b^{\mp}$ are known, 12 equations can be written. If we eliminate the three above equations, Eq. (2), then a matrix equation

$$\underline{h}^{\mp} = \underline{A}^{\mp} \underline{C}^{\mp} \tag{3}$$

can be written where $\underline{h}^{\mp}$ is a 9 element vector containing

h_i $(\frac{\partial h}{\partial a^{\mp}})_i$, $(\frac{\partial h}{\partial b^{\mp}})_i$ and $C_{00}^{\mp}$, $C_{10}^{\mp}$, $C_{01}^{\mp}$, where i = 2,3,4. $\underline{A}$ is the coefficient matrix, and $C^{\mp}$ is the vector containing the 7 remaining unknown parameters.

This system of equations is overdetermined and must be solved stochastically. This is done by least square approximation which results in

$$\underline{C}^{\mp} = (A^{\mp} TA^{\mp})^{-1} A^{\mp} Th^{\mp} \tag{4}$$

Once $C^{\mp}$ has been found by Equation 4 then the surface polynomial, Equation 1, can be written. The gradient of this surface can then be determined immediately as:

$$S = \text{Gradient} = \left[(\partial h/\partial a^{\mp})^2 + (\partial h/\partial b^{\mp})^2 \right]^{\frac{1}{2}} \tag{5}$$

c) Error Analysis - Step 1. - Error covariance matrix for the data points. This and the following sections outline the procedure for finding the standard deviation of the gradient for the modeled surface.

The first step is to find the covariance matrix for the coordinates, a", b", h", at eachof the sixteen raw data points. This is found as a function of the standard deviation of the measured quantities, R, β and θ.

d) Error Analysis - Step 2 - Error covariance matrix for modeled planes. The covariance matrix for the slopes of the modeled planes are found next. These four matrices are a function of those found in Step 1.

e) Error Analysis - Step 3 - Error covariance matrix for the center points. This step involves finding the covariance matrices for the center points, p^n. To do this we must find find the covariance matrix of the variables at the center point ($a_p''^n$, $b_p''^n$, $h_p''^n$, $\partial h/\partial a''^n$, $\partial h/\partial b''^n$) in the (h",a",b") coordinate system.

Next we must transform this matrix into the (h,a,b) coordinate system. This

is done by use of a transformation involving a matrix D, which is a function of the angles φ and ξ, Fig. 67.

f) Error Analysis - Step 4 - Error covariance matrix the model parameters. This step involves finding the covariance matrix for the C_{ij} parameters found in Equation 1. This involves use of all four covariance matrices found in Step 3.

g) Error Analysis - Step 5 - Error covariance matrix for the gradient. This step yields the covariance of the gradient. To do this, first the covariance matrix of the slopes, $\partial h/\partial a$ and $\partial h/\partial b$, must be found. This matrix is a function of the matrix found in Step 4.

Finally, the covariance matrix of the gradient is found using the above covariance matrix. The standard deviation of the gradient is a function of the point under consideration and varies accordingly.

Example

This example will illustrate the modeling process and the error analysis procedure. It will also show how the effect of roll and pitch on the model's accuracy. This example was simulated using the computer program developed.

The vehicle and terrain are shown in scale in Fig. 69. The vehicle is situated on level ground traveling toward the center of a mound located 23 meters away from the front of the vehicle. The mound is a Gaussian hill larger in width than in depth, with a maximum height of two meters. The equation of the height of the hill is

$$h = 2\, e^{\left[-\ .08(b-23)^2 - \ .05\ a^2\right]} \qquad (6)$$

Where h,a,b refer to the inertial coordinate system.

This example will show only one polynomial model since only sixteen data points are found. The raw data points were found by scanning two "W" shaped rows. Although there is roll and pitch of the vehicle between each row, here the points in a row are assumed to be taken so fast that the vehicle essentially does not roll or pitch between points.

The actual scan was carried out by using constant $\Delta\beta$ and $\Delta\theta$ increments. The $\Delta\beta$ angle between successive points in a scan row was 0.03261 rad., while the $\Delta\theta$ angle between corresponding points in the two scan rows was 0.06523 rad. The $\Delta\theta$ spacing between successive points in both rows was 0.016305 rad. The actual data for the sixteen data points are shown in Table III. Here the data point number refers to the row number(first column) and the number of the data point left to right (second column). For each measured point, the vehicle transmits the laser beam at a certain elevation and azimuth angle and receives the range measurement. It also measures its roll and pitch angle corresponding to that point.

The first step in the modeling process was to form planes from sets of four data points and determine the location, height, cross-path and in-path slope of the center points. The numerical results are shown in Table IV, where HP refers to the height of the center point, AP and BP are the a and b coordinates

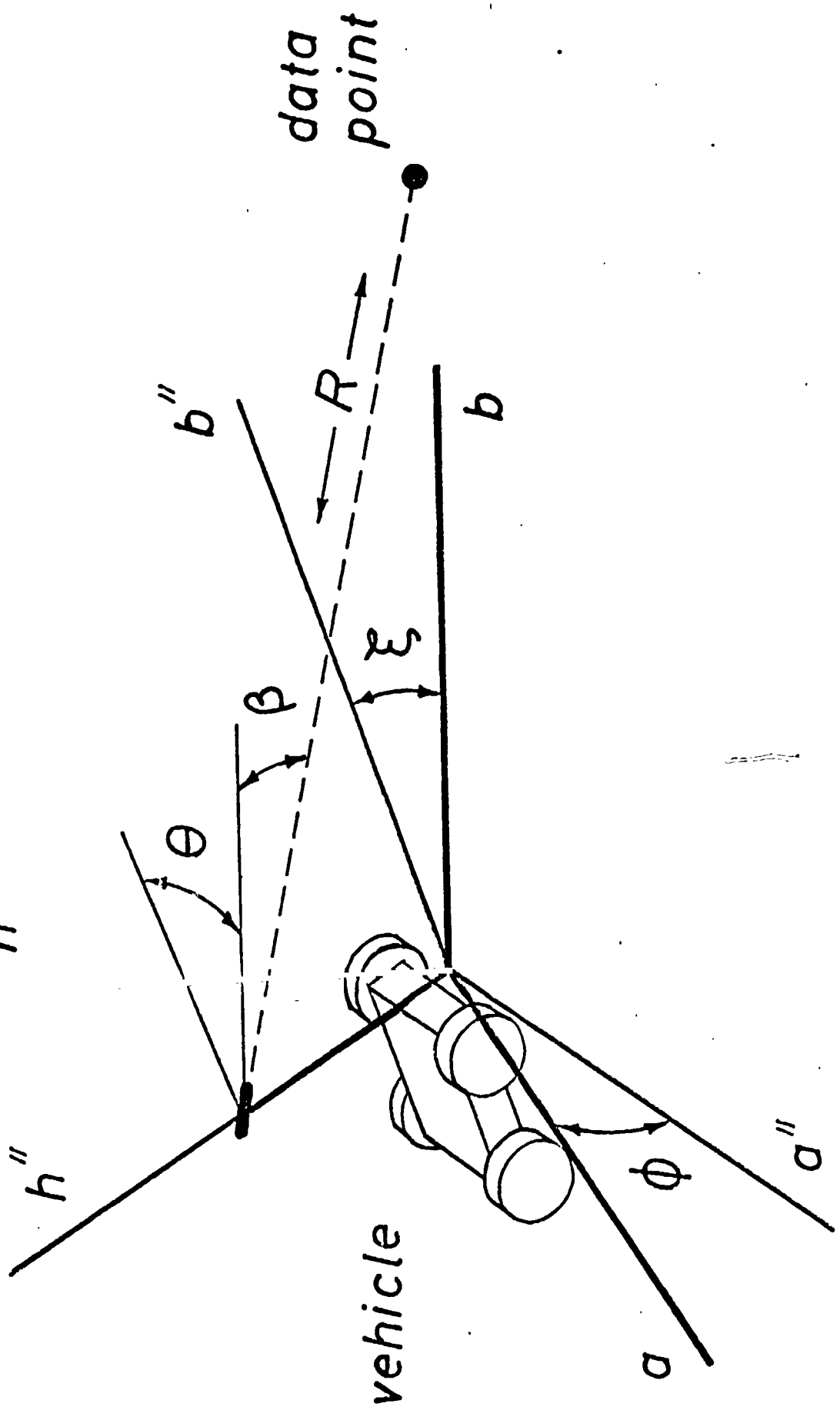

Fig. 67. The three measured quantities, R, β and θ, in the two coordinate systems, and the transformation angles ϕ and ξ.

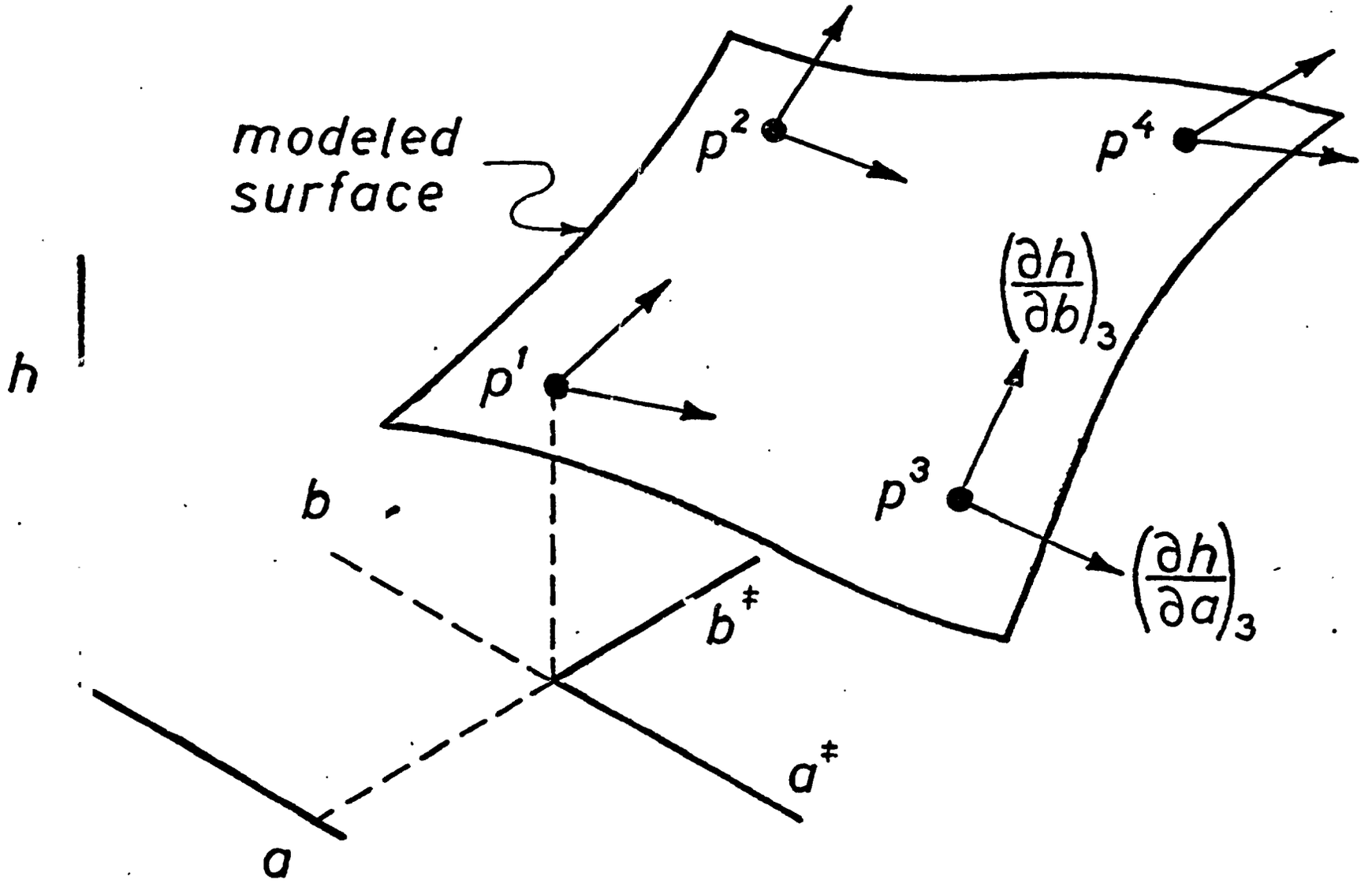

Fig. 68. The location, height and two directional derivatives for each center point and the position of the $a^{\neq}$, $b^{\neq}$-coordinate system.

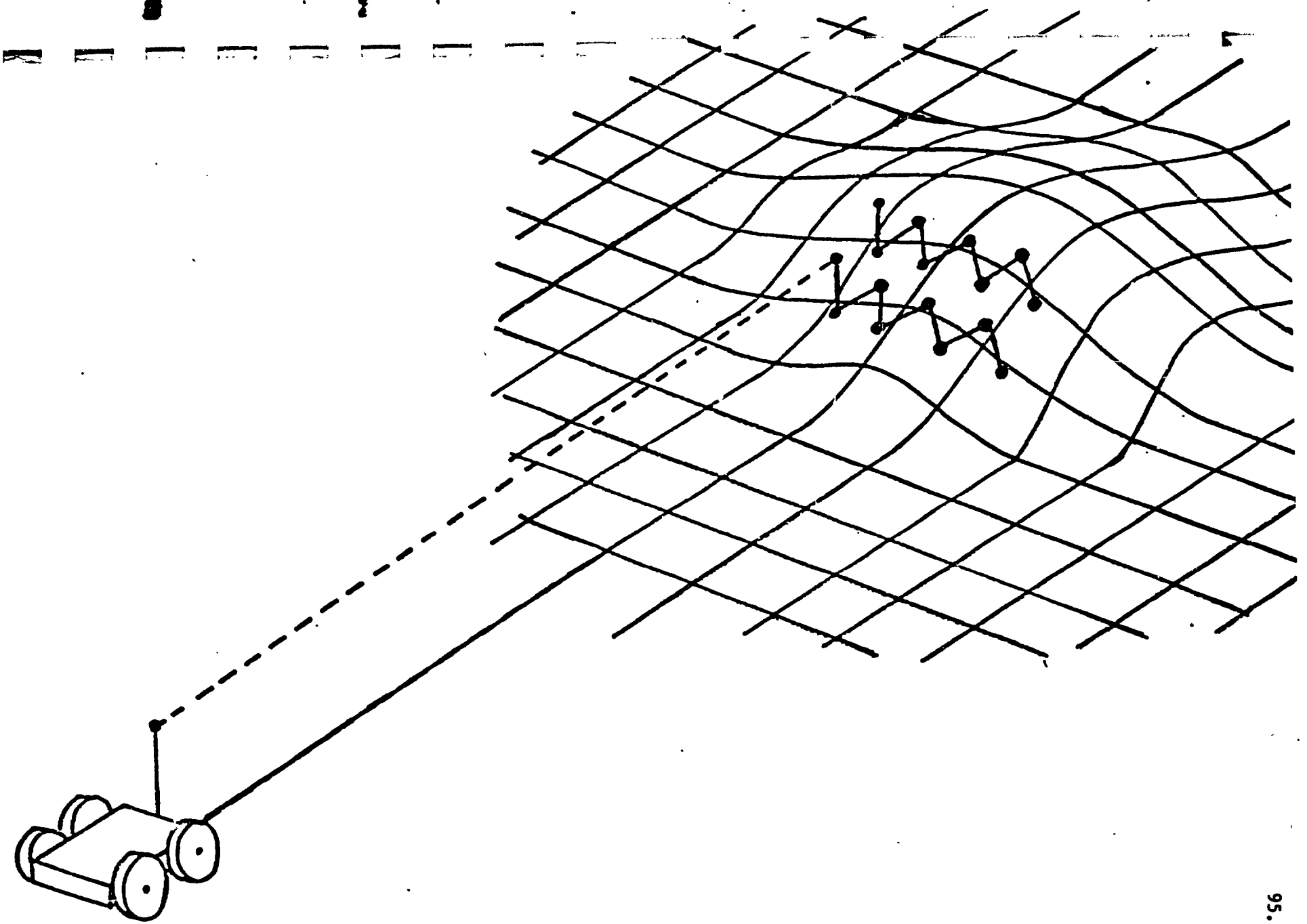

Fig. 69. Vehicle approaching a 2 meter high exponential hill with the center of the hill 23 meters away from the vehicle.

TABLE III

POINT	ELEVATION	AZIMUTH	RANGE	ROLL	PITCH	HEIGHT	A	B
1, 1	0.05268	-0.05000	22.42480	0.0	0.0	1.81928	-1.11917	22.36472
1, 2	0.08529	-0.03369	20.69824	0.0	0.0	1.23689	-0.69473	20.61031
1, 3	0.05268	-0.01739	22.05371	0.0	0.0	1.83882	-0.38295	22.01880
1, 4	0.08529	-0.00108	20.63574	0.0	0.0	1.24222	-0.02231	20.55974
1, 5	0.05268	0.01522	22.04395	0.0	0.0	1.83923	0.33505	22.01176
1, 6	0.08529	0.03153	20.69043	0.0	0.0	1.23756	0.64976	20.60399
1, 7	0.05268	0.04783	22.38184	0.0	0.0	1.82155	1.06858	22.32423
1, 8	0.08529	0.06413	20.87207	0.0	0.0	1.22192	1.33291	20.75439
2, 1	0.11791	-0.05000	19.60449	0.0	0.0	0.64393	-0.97296	19.44305
2, 2	0.15052	-0.03369	18.22363	0.0	0.0	0.26720	-0.60702	18.00830
2, 3	0.11791	-0.01739	19.53223	0.0	0.0	0.70220	-0.33731	19.39462
2, 4	0.15052	-0.00108	18.20410	0.0	0.0	0.27013	-0.01953	17.99922
2, 5	0.11791	0.01522	19.53027	0.0	0.0	0.70266	0.29516	19.39143
2, 6	0.15052	0.03153	18.22168	0.0	0.0	0.26779	0.56782	18.00572
2, 7	0.11791	0.04783	19.59863	0.0	0.0	0.69438	0.93058	19.44125
2, 8	0.15052	0.06413	18.27637	0.0	0.0	0.25958	1.15804	18.03160

TABLE III. Table of the numerical values of the parameters which locate each of the 16 raw data points.

of the center point and XP1 and XP2 are the cross path and in path slopes respectively.

The next step was to form the surface equation polynomial. Here the C_{ij} parameters were compute' using the center point information. The actual values computed are shown in Table V.

Since the parameters were determined, the height and gradient for any point could be found. The height along a cross section of the mound is shown in Fig. 70. The cross section is approximately along the vehicle's path. Fig.70 shows that the model approximates the actual surface shape very well with a maximum deviation from the actual height of only 5 cm.

A plot of the modeled gradient versus the actual gradient, Fig. 71, shows again that the model approximates the actual surface very well. Here for the range of interest, the model shows a maximum deviation from the true gradient by only 2.4°. However, since the maximum gradient which the vehicle can climb is 25°, the actual surface indicates an impassable obstacle while the model indicates it is passable. Therefore the maximum threshold must be lowered to compensate for modeling error.

For the error analysis, the standard deviation for elevation and azimuth angles was set at one arc minute while the standard deviation of range was set at 5 cm. The standard deviation of roll (σ_{roll}) and pitch (σ_{pitch}) angles was set at 0.0°, 0.25°, 0.5° and 1.0°. The covariance matrices of the parameters are shown in Table VI for the four values of $\sigma_R(\sigma_{roll} = \sigma_{pitch} = \sigma_R)$. Here the covariance matrix of the parameters is defined by

$$E\left\{ \underline{C}\ \underline{C}^T \right\} \tag{7}$$

where $\underline{C}$ is the parameter vector.

The standard deviation for height (σ_H) was found for the same cross section as before. The plot of σ_H as a function of dis'ance is illustrated in Fig. 72, which shows that in order to keep σ_H below 15 cm requires a σ_R of 0.5° or less.

Fig. 73 shows the standard deviation of gradient (σ_G), again for the same cross section. In order that σ_G be less than 5° for the region of interest requires that σ_R be less than 0.5° and for σ_G to be less than 3° requires σ_R to be less than 0.25°.

Conclusion. The modeling method described above provides a means for modeling the terrain, which makes efficient use of the data points. This is important since there is a limit to the number of data points which may be used. The data point spacing may be varied to change the amount of detail.

This procedure also requires a relatively small amount of calculations. Since time is an important factor in the path selection system and the number of data points are high, calculations must be performed quickly.

From the simulation results this method of terrain modeling seems to have the potential for usefully portraying the actual terrain contour and gradient

CENTER POINT INFORMATION

CENTER POINT NUMBER 1	
HP=	1.53408
AP =	-0.55481
BP =	21.38936
XP1 =	0.12824
XP2 =	0.39474

CENTER POINT NUMBER 2	
HP=	1.53014
AP =	0.84657
BP =	21.42360
XP1 =	-0.14778
XP2 =	0.37392

CENTER POINT NUMBER 3	
HP=	0.48339
AP =	-0.48420
BP =	18.71082
XP1 =	0.02486
XP2 =	0.30909

CENTER POINT NUMBER 4	
HP=	0.48101
AP =	0.73792
BP =	18.71799
XP1 =	-0.03171
XP2 =	0.30584

TABLE IV

Numerical values for the four center points which are found in the first modeling step.

C00=	1.534870
C10=	0.128256
C01=	0.394753
C20=	-0.212926
C11=	0.029409
C02=	-0.066491
C30=	0.023077
C21=	-0.056413
C12=	-0.005039
C03=	-0.075679

TABLE V

Values of the C_{ij} parameters used in Eq. 1 to specify the polynomial.

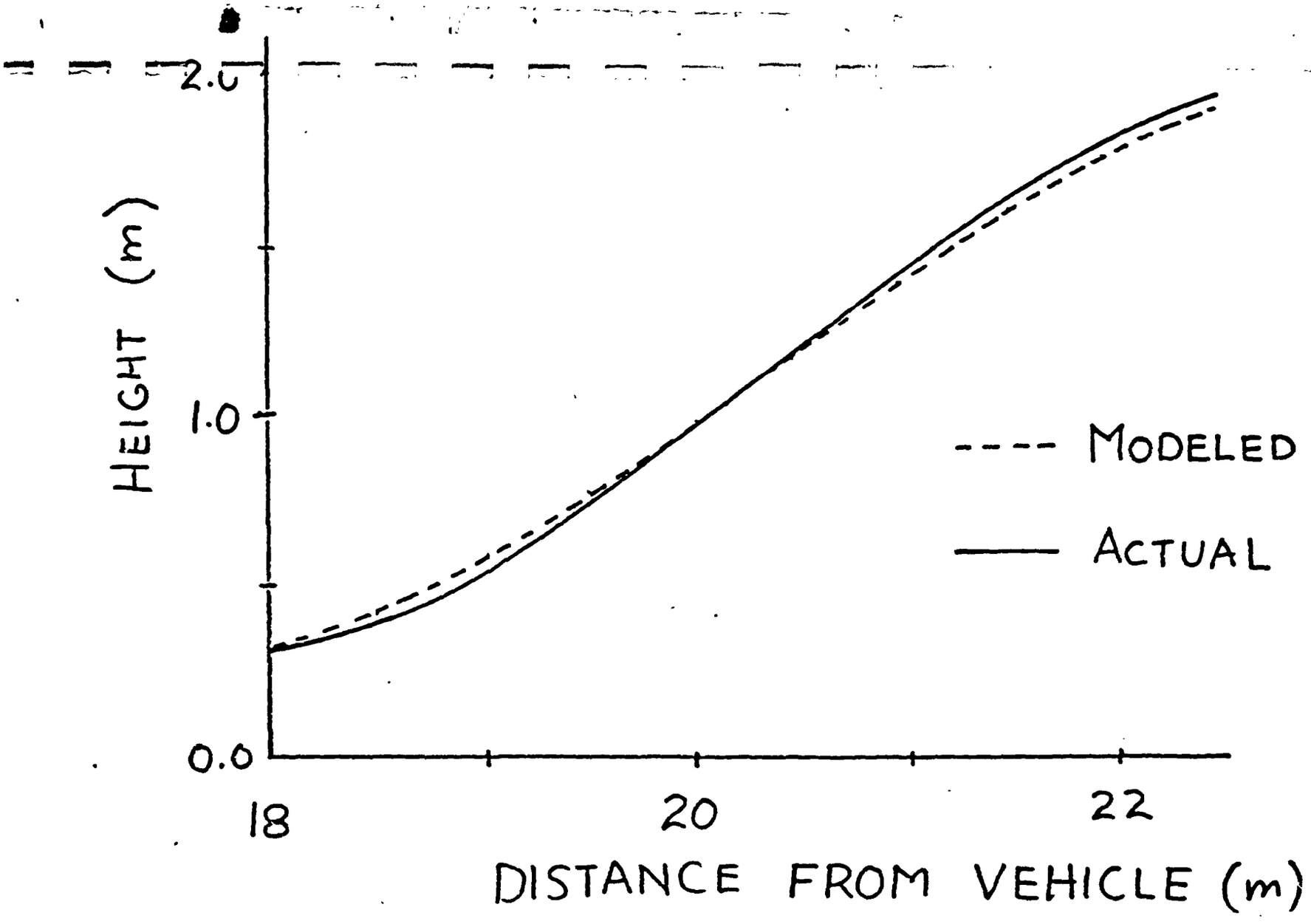

Fig. 70. Plot comparing the modeled height with the actual height along a cross section of the mound (a = const =-0.03m)

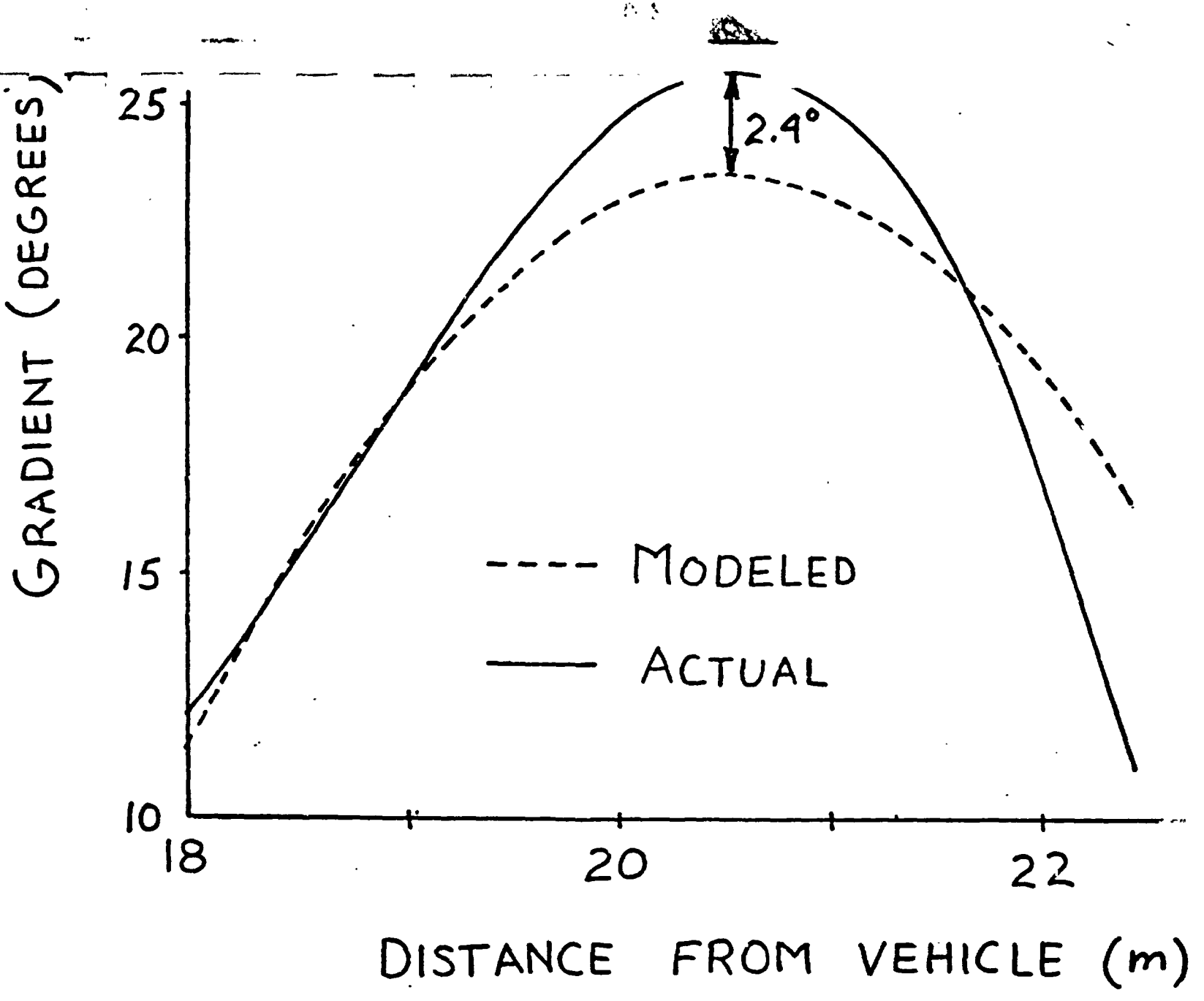

Fig. 71. Plot comparing the modeled gradient with the actual gradient along a cross section of the mound (a = const = -0.03m)

TABLE VI.

Error covariance matrices of the C_{ij} parameters for the four different values of σ_R

COVARIENCE MATRIX OF THE PARAMETERS FOR SIGMA ROLL= 0.0 DEG SIGMA PITCH= 0.0 DEG

0.00001	-0.00000	-0.00001	-0.00007	0.00000	-0.00002	0.00010	-0.00000	0.00000	-0.00002
-0.00000	0.00134	0.00039	-0.00349	0.00012	0.00052	0.00351	-0.00041	-0.00018	0.00021
-0.00001	0.00039	0.00033	-0.00106	-0.00008	0.00042	0.00106	-0.00012	-0.00014	0.00018
-0.00007	-0.00349	-0.00106	0.01263	-0.00020	-0.00152	-0.01527	0.00080	0.00033	-0.00066
0.00000	0.00012	-0.00008	-0.00020	0.00026	-0.00008	0.00010	-0.00019	0.00006	-0.00004
-0.00002	0.00052	0.00042	-0.00152	-0.00008	0.00076	0.00153	-0.00012	-0.00014	0.00045
0.00010	0.00351	0.00106	-0.01527	0.00010	0.00152	0.02032	-0.00050	-0.00024	0.00078
-0.00000	-0.00041	-0.00012	0.00080	-0.00019	-0.00012	-0.00050	0.00042	0.00009	-0.00002
0.00000	-0.00018	-0.00014	0.00033	0.00006	-0.00014	-0.00024	0.00009	0.00012	-0.00003
-0.00002	0.00021	0.00018	-0.00066	-0.00004	0.00045	0.00078	-0.00002	-0.00003	0.00032

COVARIENCE MATRIX OF THE PARAMETERS FOR SIGMA ROLL= 0.250 DEG SIGMA PITCH= 0.250 DEG

0.00873	0.00001	0.00046	-0.02218	-0.00046	-0.00463	0.03106	-0.00039	0.00026	-0.00335
0.00001	0.00136	0.00040	-0.00356	0.00013	0.00051	0.00360	-0.00042	-0.00018	0.00020
0.00046	0.00040	0.00036	-0.00225	-0.00011	0.00017	0.00274	-0.00014	-0.00012	0.00000
-0.02218	-0.00356	-0.00225	0.13557	0.00220	0.00321	-0.18771	0.00246	-0.00065	0.00203
-0.00046	0.00013	-0.00011	0.00220	0.00034	0.00001	-0.00323	-0.00015	0.00004	-0.00000
-0.00463	0.00051	0.00017	0.00321	0.00001	0.00659	-0.00469	0.00003	-0.00029	0.00483
0.03106	0.00360	0.00274	-0.18771	-0.00323	-0.00469	0.26448	-0.00278	0.00112	-0.00281
-0.00039	-0.00042	-0.00014	0.00246	-0.00015	0.00003	-0.00278	0.00046	0.00007	-0.00008
0.00026	-0.00018	-0.00012	-0.00065	0.00004	-0.00029	0.00112	-0.00007	0.00013	-0.00013
-0.00335	0.00020	0.00000	0.00203	-0.00000	0.00483	-0.00281	0.00008	-0.00013	0.00362

COVARIENCE MATRIX OF THE PARAMETERS FOR SIGMA ROLL= 0.500 DEG SIGMA PITCH= 0.500 DEG

0.03498	0.00004	0.00187	-0.08850	-0.00183	-0.01844	0.12395	-0.00154	0.00103	-0.01335
0.00004	0.00142	0.00040	-0.00378	0.00014	0.00050	0.00385	-0.00043	-0.00019	0.00019
0.00187	0.00040	0.00043	-0.00584	-0.00018	-0.00058	0.00776	-0.00021	-0.00008	-0.00054
-0.08850	-0.00378	-0.00584	0.50036	0.00941	0.01710	-0.70504	0.00746	-0.00358	0.01011
-0.00183	0.00014	-0.00018	0.00941	0.00057	0.00028	-0.01320	0.00000	-0.00004	0.00012
-0.01846	0.00050	-0.00058	0.01710	0.00028	0.02407	-0.02332	0.00049	-0.00073	0.01796
0.12395	0.00385	0.00776	-0.70504	-0.01320	-0.02332	0.99694	-0.00963	0.00518	-0.01357
-0.00154	-0.00043	-0.00021	0.00746	0.00000	0.00049	-0.00963	0.00059	0.00001	0.00037
0.00103	-0.00019	-0.00008	-0.00358	-0.00004	-0.00073	0.00518	0.00001	0.00017	-0.00043
-0.01335	0.00019	-0.00054	0.01011	0.00012	0.01796	-0.01357	0.00037	-0.00043	0.01353

COVARIENCE MATRIX OF THE PARAMETERS FOR SIGMA ROLL= 1.000 DEG SIGMA PITCH= 1.000 DEG

0.13947	0.00016	0.00752	-0.35381	-0.00735	-0.07376	0.49551	-0.00617	0.00411	-0.05335
0.00016	0.00165	0.00043	-0.00462	0.00017	0.00045	0.00486	-0.00049	-0.00020	0.00014
0.00752	0.00043	0.00074	-0.02020	-0.00047	-0.00356	0.02785	-0.00046	0.00008	-0.00270
-0.35381	-0.00462	-0.02020	1.26354	0.03825	0.07267	-2.77433	0.02743	-0.01532	0.04242
-0.00735	0.00017	-0.00047	0.03825	0.00152	0.00138	-0.05308	0.00060	-0.00037	0.00060
-0.07376	0.00045	-0.00356	0.07267	0.00138	0.05401	-0.05785	0.00233	-0.00248	0.07051
0.49551	0.00486	0.02785	-2.77433	-0.05308	-0.09785	3.92680	0.03704	0.02143	-0.05663
-0.00617	-0.00049	-0.00046	0.02743	0.00060	0.00233	-0.03704	0.00112	-0.00024	0.00153
0.00411	-0.00020	0.00008	-0.01532	-0.00037	-0.00248	0.02143	-0.00024	0.00031	-0.00164
-0.05335	0.00014	-0.00270	0.04242	0.00060	0.07051	-0.05663	0.00153	-0.00164	0.05314

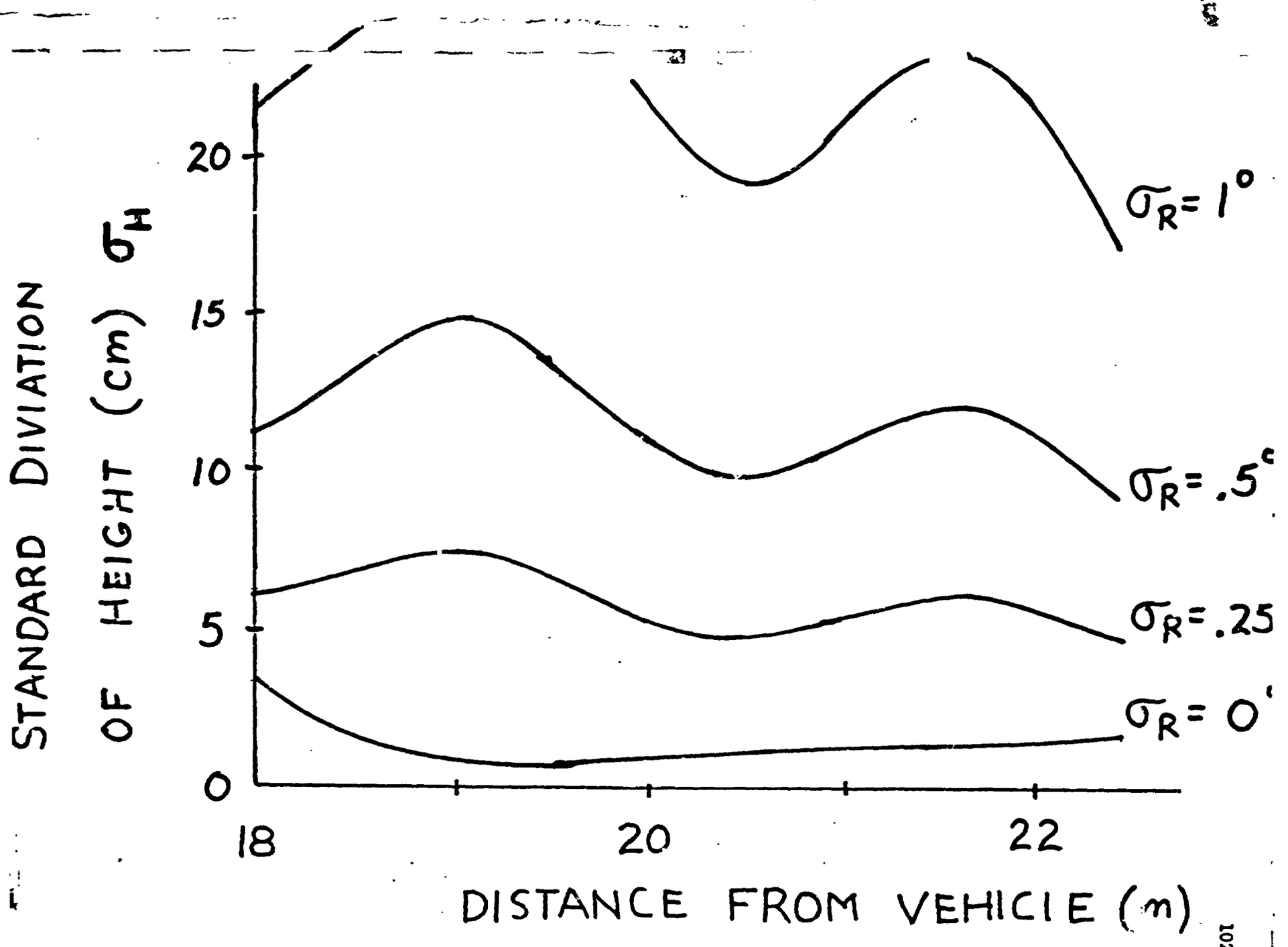

Fig. 72 Plot showing the standard deviation of height for four different values of σ_R along the cross section a = const = -0.03m

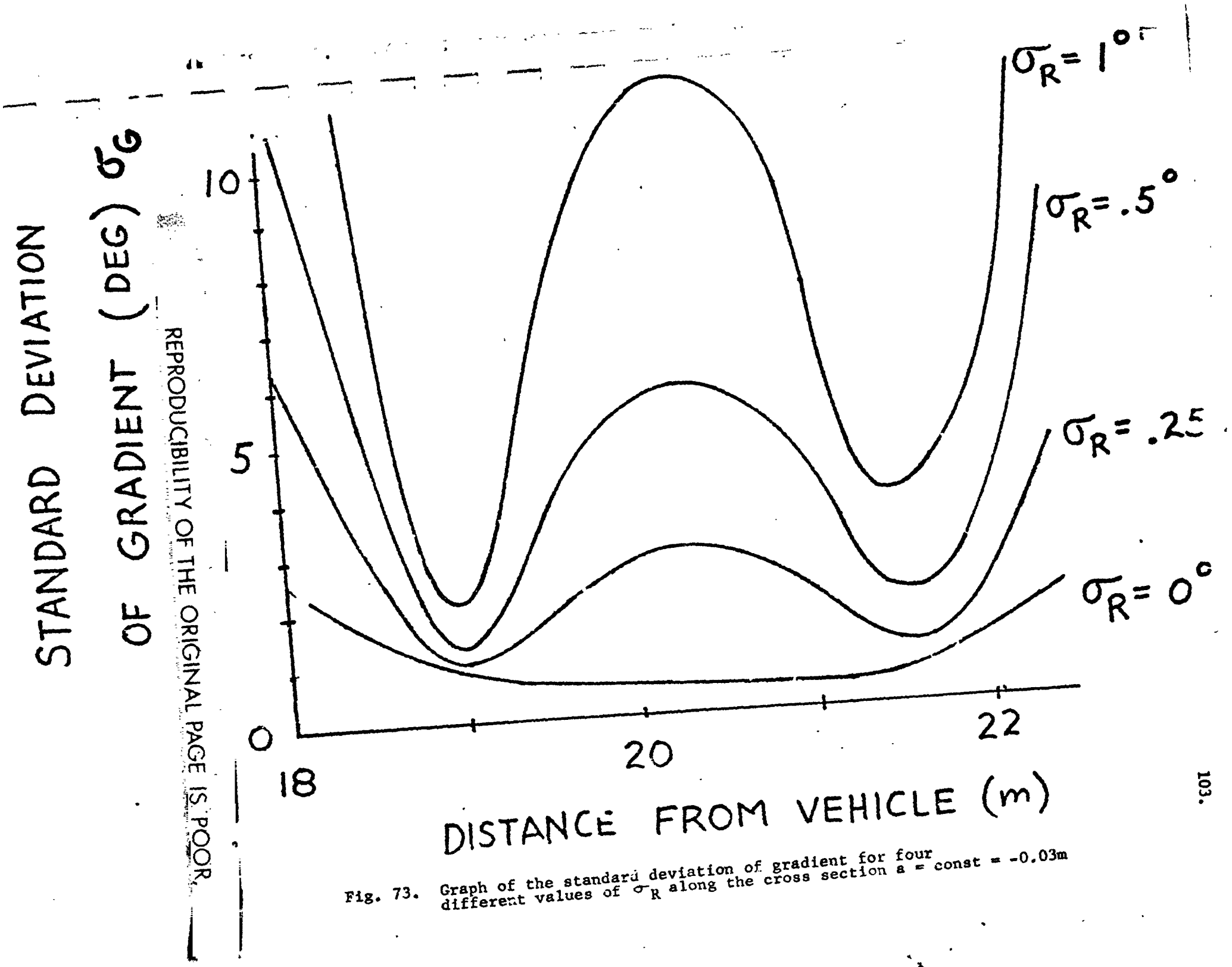

Fig. 73. Graph of the standard deviation of gradient for four different values of σ_R along the cross section a = const = -0.03m

although much development work is still needed to refine the modeling method.

The use of two scan rows for the terrain model may not prove practical unless the standard deviation of the roll and pitch measurement are reduced to about 0.25^{o}. If this is not practical this modeling method may still be used if a scanning scheme can be developed to obtain the needed data points within a sufficiently short time space.

C.2.c. Obstacle and Terrain Classification - D. Scanlon
Faculty Advisor: Prof. C. N. Shen

Objective. The primary objective of the task at this time is to logically categorize all terrain features and qualities that could be potential obstacles to the Martian vehicle. If done effectively, this could provide a basis for a more systematic and comprehensive approach to obstacle detection, pattern recognition, and vehicle design problems.

Progress Summary. A classification of landforms by basic size and shape was done on the assumption that nothing was known about the size of capabilities of the actual vehicle, and suggestions are made for refining the classification. This will lead into consideration of the vehicle's relationship to the terrain in respect to the orientation of the obstacle with respect to the vehicle and the vehicle's inability to see the rar side of hills. Another factor considered that is important to the determination of whether a slope is an obstacle are the shear strength and flotation properties of the top soil.

Discussion. The first step was to list all possible types of terrain and land forms found on earth and studied under geomorphology. Once this listing was compiled, some basic classes could be recognized into which all terrain features would fit. The first obvious division was between so-called positive and negative obstacles. Positive obstacles are those such that the central portion of the obstacle is at a greater height than the margins. Examples are mountains, hills, boulders, or ridges. Negative obstacles are those with the central portion lower than the edges, and includes such forms as craters, holes, valleys, and cracks. Two relatively familiar landforms that are encountered on earth do not readily fall into either of these categories. A cliff represents a very distinct obstacle, but whether or not it should be considered positive or negative depends on where the vehicle is when it detects it. For simplicity a cliff will arbitrarily be called positive, and the canyon, a "vertical-walled valley", should be a just representation of a cliff as seen by a vehicle on top. Also, caves are not readily apparent as either positive or negative, but for our purpose can be considered as a severe concavity in an otherwise positive landform. An extreme of this case would be an "aperture", or a hole all the way through an otherwise solid wall.

The next basic characterization accounts for the elongation of both the positive and negative obstacles. Fig. 74 shows the plan view of either a positive or negative obstacle. The ratio D/W is indicative of the elongation and decreases with elongation. D and W are the two sides of the smallest possible rectangle fully enclosing the obstacle, D being the smaller dimension. Both the positive and negative categories are subdivided into "elongated"

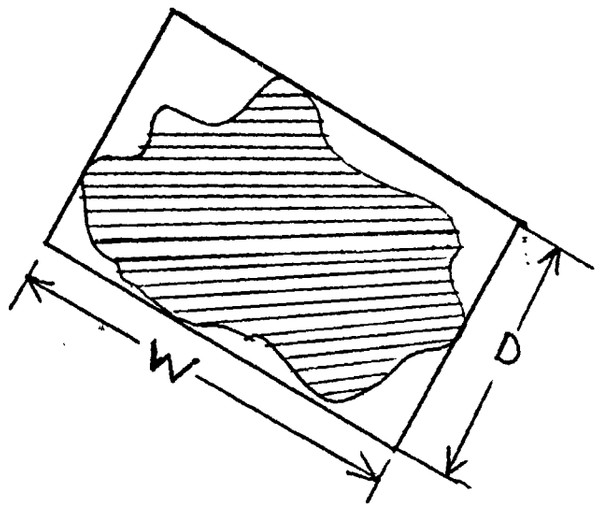

Fig. 74. Plan view of obstacle showing dimensions for determining D/W.

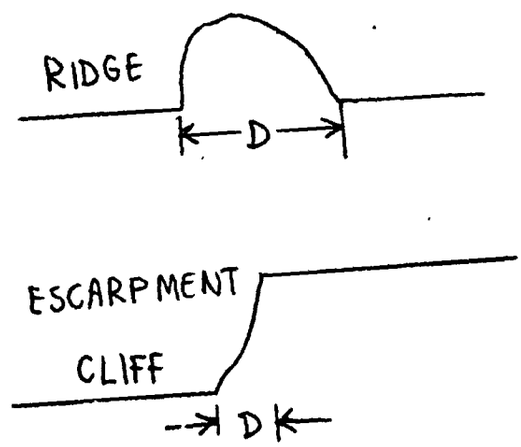

Fig. 75. Categorization of General Landforms

and "not-elongated" classes, the cutoff being D/W is equal to one-tenth for positive obstacles and D/W is equal to one-third for negative obstacles. For the special case of the cliff the D dimension is considered to be the projection of the distance between the top edge and bottom edge. See Fig. 75 and 76.

Another ratio indicative of obstacle shape is H/W, where H is the maximum height or depth of the obstacle and W is the width found before. This parameter is used for further refining the cross-sectional shape of crater-like negative obstacles into three divisions as seen in Fig. 76. The elongated negative obstacles are roughly divided into two categories, canyon and valley, depending on the steepness of their slopes (valleys with slopes greater than about 60 degrees can be considered canyons). These categories can be further broken down by size and shape with knowledge of H and the ratio H/D.

The elongated positive obstacles can generally be divided into the two types of terrain depicted in Fig. 72. Other positive obstacles generally fit into two categories distinguished by the overall relief of the terrain as either gentle and smoothly changing, or steep and abrupt. The smoothly changing category would include rolling terrain, rises, and hills, and can be typified by a concave-convex gradient change and comparatively low absolute gradients, Fig. 77. The abrupt category would be typified by a steep concavity, convexity, or linearity to the sides. Categorizing this group into more specific groups by a few parameters is a difficult task due to the infinite variety of irregular three-dimensional shapes and sizes possible. One conceivable method might involve finding the area of the intersection of the obstacle with a plane parallel to the surface of the ground at predetermined fractions of the total height, and noting the increase or decrease of this area. For example, if areas are measured at heights of 0,(1/3)H, and (2/3)H the following classification might be made:

INCREASING	DECREASING	DEC-INC	INC-DEC	CONSTANT
boulder	pyramid	hoodoo	boulder	column
stock	tower	boulder		plateau
block	mountain			block
	spike			stock
	boulder			boulder

Although it is difficult to compute these areas in reality, an indication could be derived by multiplying the width of the obstacle for each height by the respective depths as shown in Fig. 78.

Another possible classification could depend on width ratios for characterization of the basic shape of the obstacle. Also necessary for accuracy would be a more basic indication such as the H/W ratio, and a term to identify any severe off-setting of the measured widths with respect to one another, and would be used in conjunction with the width ratios for a fairly close outline of the obstacle. Given H/W (maximum height divided by maximum width), it would then be possible to choose a more appropriate width ratio scheme that could reveal more information with less data. A third dimension could be approximated by anindication of the convexity, concavity, or linearity of the surface, Fig. 79.

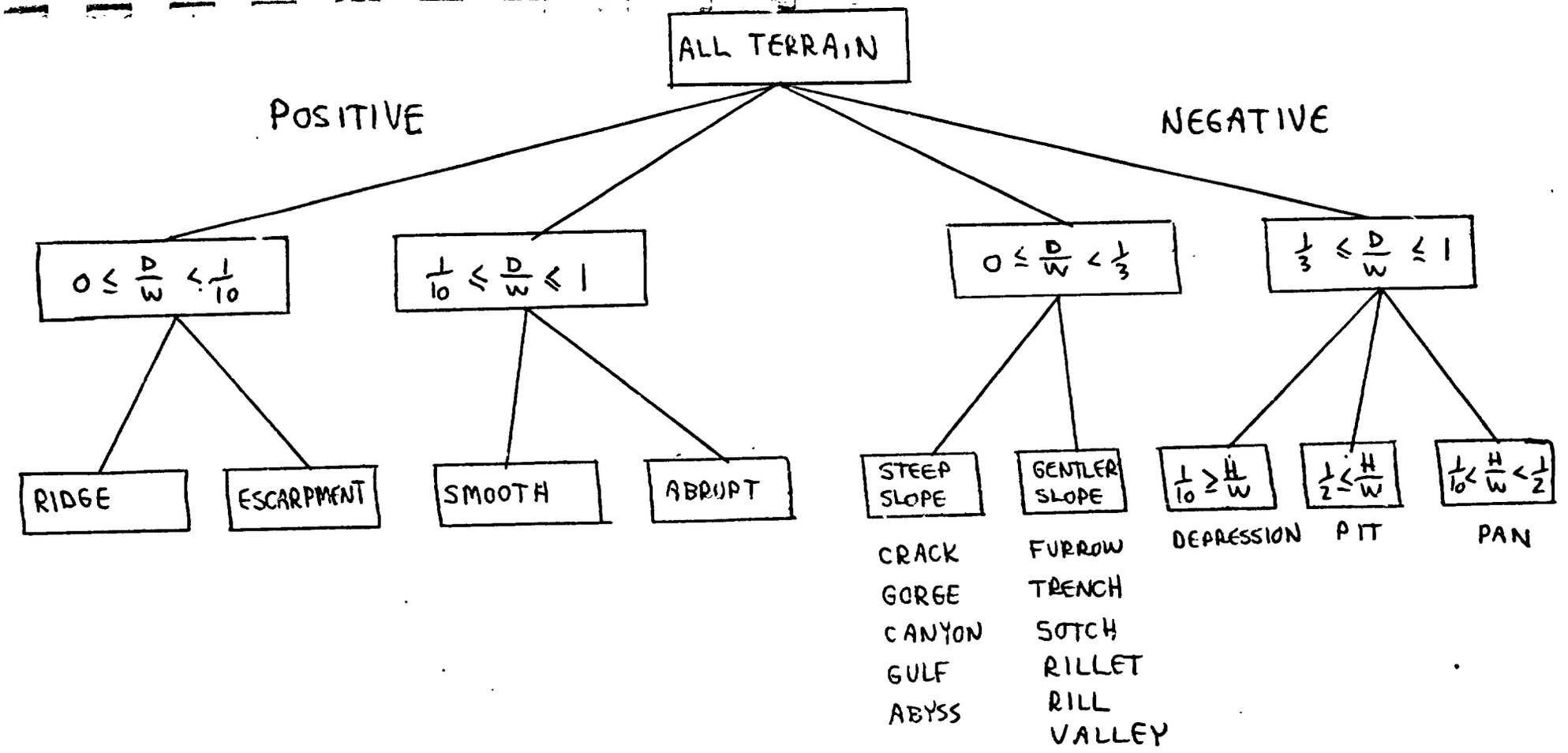

Fig. 76. Side view showing difference between ridge and cliff. Dimension W is into the paper

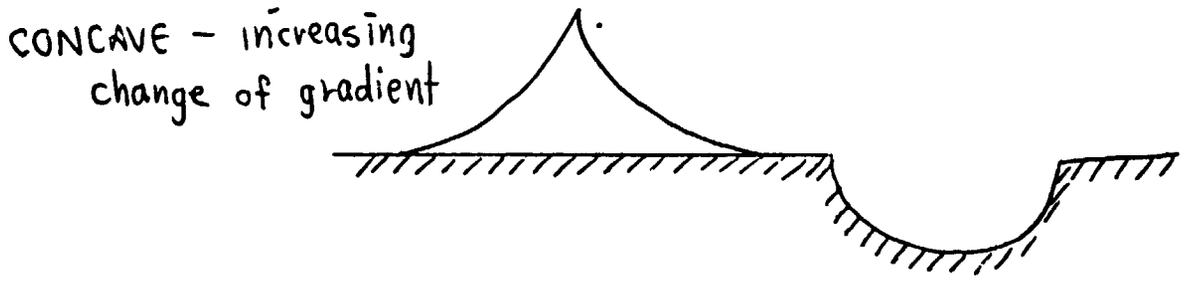

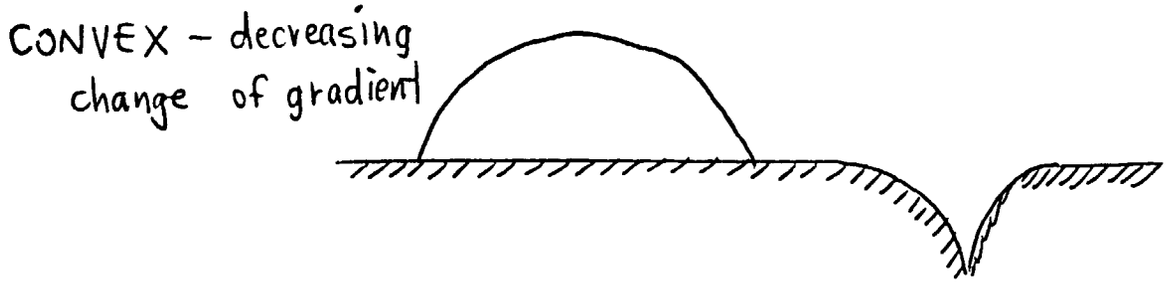

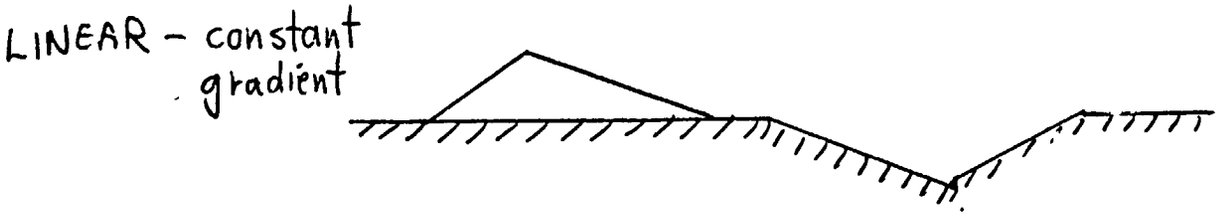

"SMOOTH TRANSITION"

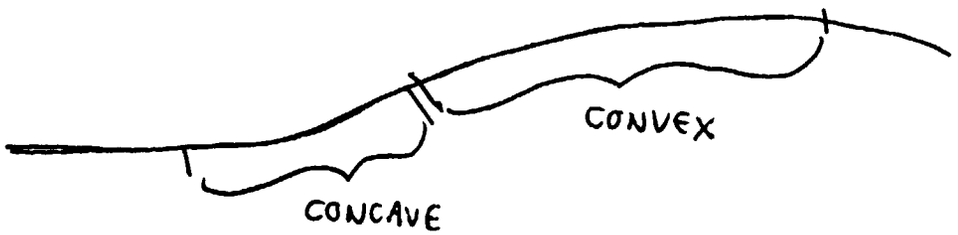

Fig. 77. Definitions of concave, convex, and linear

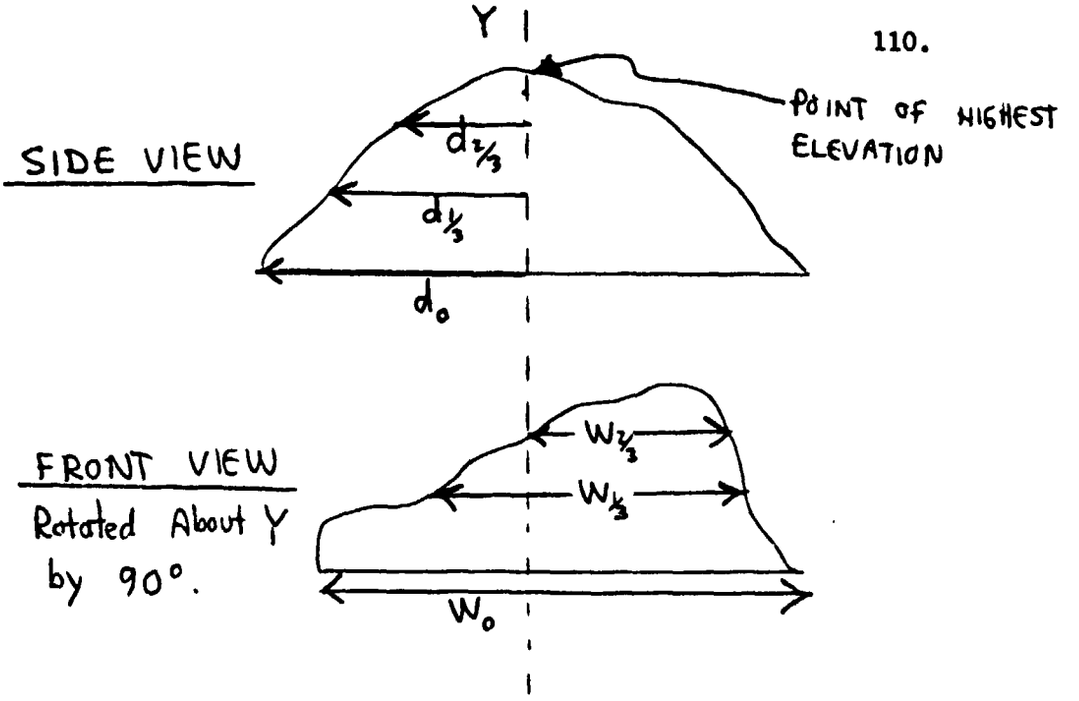

Fig. 78. Indication of area at specific heights by multiplying d by W

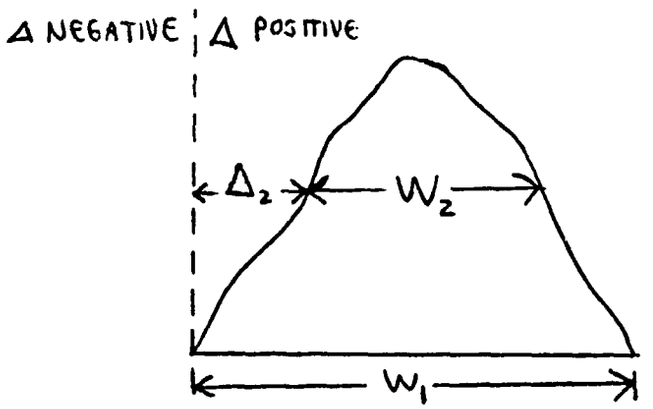

Fig. 79. Shape indication by W_2/W_1 and Δ_2/W_1

A third possible system could involve dividing the immediate area of an obstacle into a grid (either two-dimensional or three-dimensional) and different combinations of grids "occupied" and "unoccupied" by the obstacle would be a rough classification of the obstacle shape, Fig. 80a and 80b. The fineness of the grid will determine the accuracy of the representation. Grid size could be made a function of height, especially in the more advanced situation when the height and other parameters of the vehicle are considered.

The above general classifications are an introduction to this task, and should provide a basis for continued and more detailed work.

Soil qualities were also considered as to their effect on vehicle navigation, Ref. 16 and 17. Soil can be and has been classified by particle size, and a typical classification is the following which is known as the "M.I.T. Classification":

CLAY	0-0.002mm	MEDIUM SAND	0.2-0.6mm
SILT	0.002-0.06mm	COARSE SAND	0.6-2mm
FINE SAND	0.06-0.2mm	GRAVEL	2-30mm

Meaningful classification in relation to the Martian vehicle divides soil into two types dependent on its shear characteristics. Cohesive soil is soil that can sustain a shear force due to the soil's inherent ability to hold together. The cohesive strengthof soil is independent of any normal force being applied at the same time as the shearing. Fine-grained soils such as clay and silt are typically cohesive (cohesion increases with decreasing particle size and increasing moisture), and will sustain shearing forces on the magnitude of (1 psi)(AREA of wheel-soil interface) lbs. Frictional soil has a shearing strength that increases directly proportional to the normal force being exerted on the soil, and is independent of the area of contact. Gravel and sand exhibit frictional characteristics, and typically for these types of soils the shear force developed will approach the normal force in magnitude. Most normal soil, however, will display a combination of friction and cohesion, and is described by Coulomb's equation for shear failure of soils:

$$H = Ac + W\tan\phi$$

H soil thrust

A area of wheel or track transmitting the force

W weight per wheel or track

c empirical constant descriptive of a soil's cohesion (0. to 1)

ϕ empirical constant descriptive of a soil's friction (0. to 45)

Although the shearing strenth of the soil on a slope can be an important factor in determining the negotiability of that slope, in practice it would be very difficult to measure the soil thrust of distant slopes. One could, however, test the soil in one location and assume the surrounding terrain was covered with similar soil. Perhaps the most straightforward method of

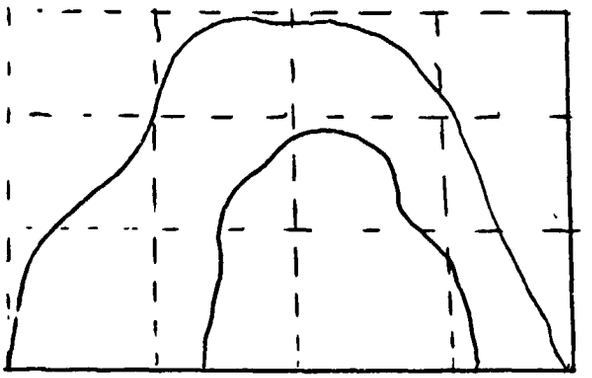

Fig. 80a. Possible grid with arch as obstacle

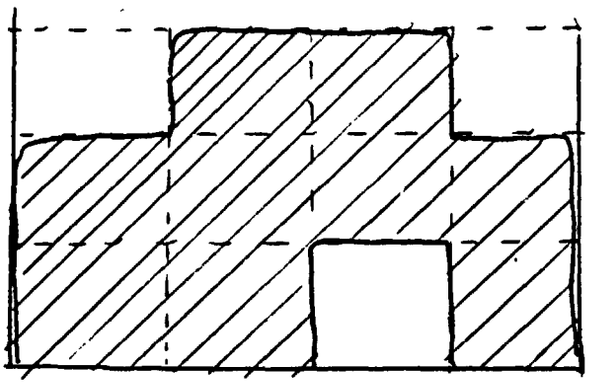

Fig. 80b. Reproduction of obstacle from information in (a).

doing this would be to use a studded plate of equal area to the contact surface of the Rover's wheels, apply a known normal force to it, then measure what shear force is necessary to move it. One repetition of this procedure with a different normal force should be sufficient to determine the shear coefficients of the soil, c and ϕ. Then if the following inequality holds, and the vehicle still has sufficient power to turn the wheels, the slope may be negotiable.

$$(Ac + W\cos\theta\tan\phi) \geq (W\sin\theta + \text{External Motion Resistance})$$

θ = slope angle

External Motion Resistance is from sinkage in soil, wind, etc.

Term on the left is the "soil thrust" or force at which the soil will shear.

Also of possible importance to the Martian vehicle are the flotation characteristics of the soil. Although flotation does not affect the soil thrust, the more the vehicle sinks, the greater the resistance to movement. Flotation depends on the area of the wheel or track through which the force is transmitted and also the width. It has been shown both analytically and experimentally that a wider wheel improves flotation as long as the sinkage is negligible, but once the vehicle starts sinking due to either extremely deformable soil or high vehicle weight, a thinner wheel will improve the sub-surface flotation. This fairly unexpected characteristic implies that it might be to the Rover's advantage to have wheels capable of changing width in transit.

Task C.3 Path Selection System Development and Evaluation - R. Campbell, D. Matthews, D. Sharp, R. Simonds
Faculty Advisor: Prof. D. K. Frederick

The objectives of this task are to evaluate the potential performance of proposed path selection systems and to develop new path selection system concepts. To aid in the accomplishment of these objectives a comprehensive digital computer simulation program has been developed and refined during the past three years. A detailed development of this simulation program may be found in Ref. 18.

The progress attained during the past year consists of the following:

a) Development of standard test terrains and simulation procedures.

b) Evaluation of a proposed mid-range sensor system.

c) Initial development and evaluation of a short range sensor system having a maximum range of only 3 meters.

d) Incorporation of non-zero vehicle dimensions into the simulation.

e) Formulation of plans for improved program documentation and the implementation of an existing monitor program.

First the specific accomplishments noted above will be described, then the goals which have been set for the coming year will be presented. A more detailed discussion of the first three items then will be presented here and may be found in Ref. 19.

A. Development of Standard Test Terrains

To facilitate the use of the computer simulation package as an evaluation tool, the development of a standard testing procedure has been undertaken. This testing procedure consists of investigating the obstacle avoidance behavior of a path selection system by simulating the system's performance on a sequence of test terrains of increasing difficulty in the presence of random effects.

In developing this testing sequence, an effort was made to determine general rules for the structuring of test terrains, the use of random effects, and the examination of system characteristics that would provide the most information from each simulation. The developed testing sequence not only provides the program user with a set of terrains and techniques to meet his analysis needs but also a set of guidelines for incorporating additional test situations into the sequence as the need arises.

1. The Use of Random Effects

The simulation package has the capability of adding uniformly distributed white noise to a variety of variables in a given simulation. The simulation procedure calls for the use of three types of noise:

1) attitude
2) range measurement
3) slope measurement

Attitude noise represents the random effects encountered during a range measurement due to the pitching and rolling motion of the vehicle as it passes over small terrain irregularities. To create this effect, filtered whie noise is added to the vehicle's in-path and cross-path slopes, thereby randomly tilting the vehicle and perturbing the sensor orientation accordingly. Knowedge of the natural frequencies and damping ratios of the rover's dominant pitch and roll modes is used to specify the filter's characteristics.

To simulate the effects of noise-corrupted range measurements on system performance, unfiltered white noise is added to each measurement during every scanning operation.

Slope measurement noise is the addition of unfiltered white noise to the measured in-path and cross-path slopes of the vehicle. This simulates the information that would be available from on-board accelerometer measurements of the vehicle's pitch and roll orientations.

The procedure used in the test sequences is, first to examine the functioning of the system in the absence of

noise and, if the performance is satisfactory, to repeat the sequence with the addition of noise effects. Noisy performance is examined using all noise effects simultaneously after appropriate noise levels for each effect have been determined by simulation.

2. Obstacles

The principal types of obstacles available in the simulation are spherical or drum-shaped boulders and spherical craters. The boulders selected for use in the test terrains have height-to-diameter ratios of unity. Boulders with heights of 2/3 and 2 meters were used for analysis purposes. The craters selected for use have depth-to-diameter ratios of 1/3 and are used in diameters of 1, 3, and 9 meters.

3. Standard Testing Procedure

The testing begins with relatively simple avoidance problems involving a single boulder or crater as in Fig. 81, and proceeds to more complicated situations. Each avoidance problem is repeated on several different base terrains in order to determine the effects of in-path and cross-path slopes on the system's functioning. The testing procedure is as follows:

1) Single obstacle encounter on flat base terrain

2) Single obstacle encounter on rolling base terrain

   a) gently rolling terrain
   b) rolling incline

3) Special cases

   a) key hole problem
   b) box canyon

4) Boulder-crater field

Heavy emphasis is placed on obtaining information from single-obstacle encounter situations. The simplicity of a single-obstacle encounter makes the effect of changing a system parameter easier to determine. The system's avoidance performance is observed on the basis of both the clearance that is maintained as the vehicle travels past the ostacle and the distance from the obstacle at which avoidance behavior is first exhibited.

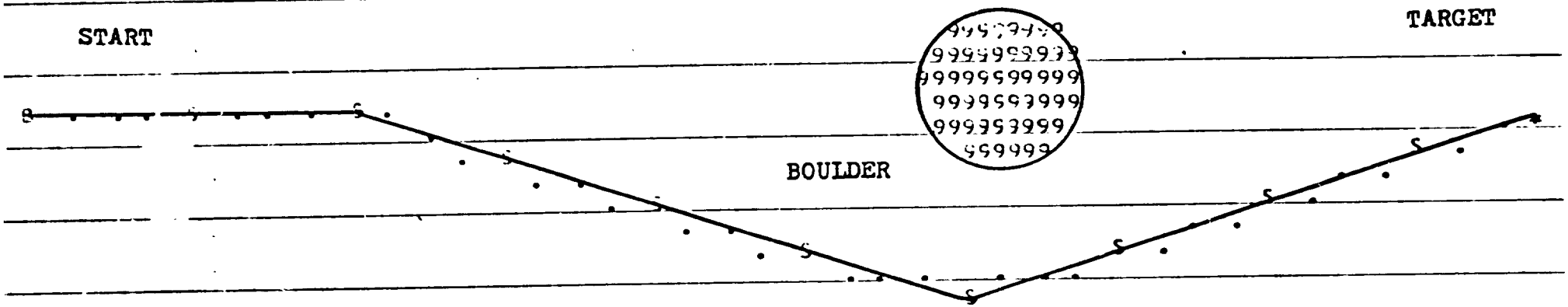

Fig. 81. Single boulder encounter (flat base terrain)

4. Conclusions and Recommendations

The test terrains that have been developed to date place emphasis on single-obstacle encounters in a variety of slope settings and in the presence and absence of random effects. Satisfactory system performance on these basic terrains is required before performance on more complicated multi-obstacle terrains is examined. It is recommended that future efforts concentrate on the development of additional multi-obstacle terrains.

B. Evaluation of a Mid-Range Sensor System

The mid-range sensor system evaluated was proposed by the navigational computer group at Cornell University in 1972. A brief description of the system is presented below. The development of this system is discussed in greater detail in Ref. 20.

1. System Description

The proposed path selection system, as represented in the simulation package, is divided into three distinct operations: the sensor, the terrain modeler, and the path selection algorithm. A description of each operation follows:

(i) Sensor - A sensor which projects a single beam is mounted on a vertical mast fixed to the front of the vehicle. The beam moves in a plane perpendicular to the mast and provides range measurements at discrete angles. The scan time is assumed to be instantaneous and the time between scans is uniform. A scan consists of 29 range measurements which are made in a uniform sweep of the area in front of the vehicle, as indicated in Fig. 82.

(ii) Terrain Modeling Process - This process operates on the range measurements received from the sensor simulator. The result is a go/no-go map generated along the fifteen forward paths P1, Pa,...,P15 in Fig. 82 by comparing the range measurements with the minimum ranges required for a clear path. The vehicle width and specified buffer zone are incorporated in the calculations of the minimum range values.

(iii) Path Selection Algorithm - In normal operation the path selection algorithm chooses the most direct "safe" path to target. If all of the paths are blocked the emergency mode is called and the following steps are taken:

1) the vehicle is backed up in a straight line,
2) a new sensor scan is taken,

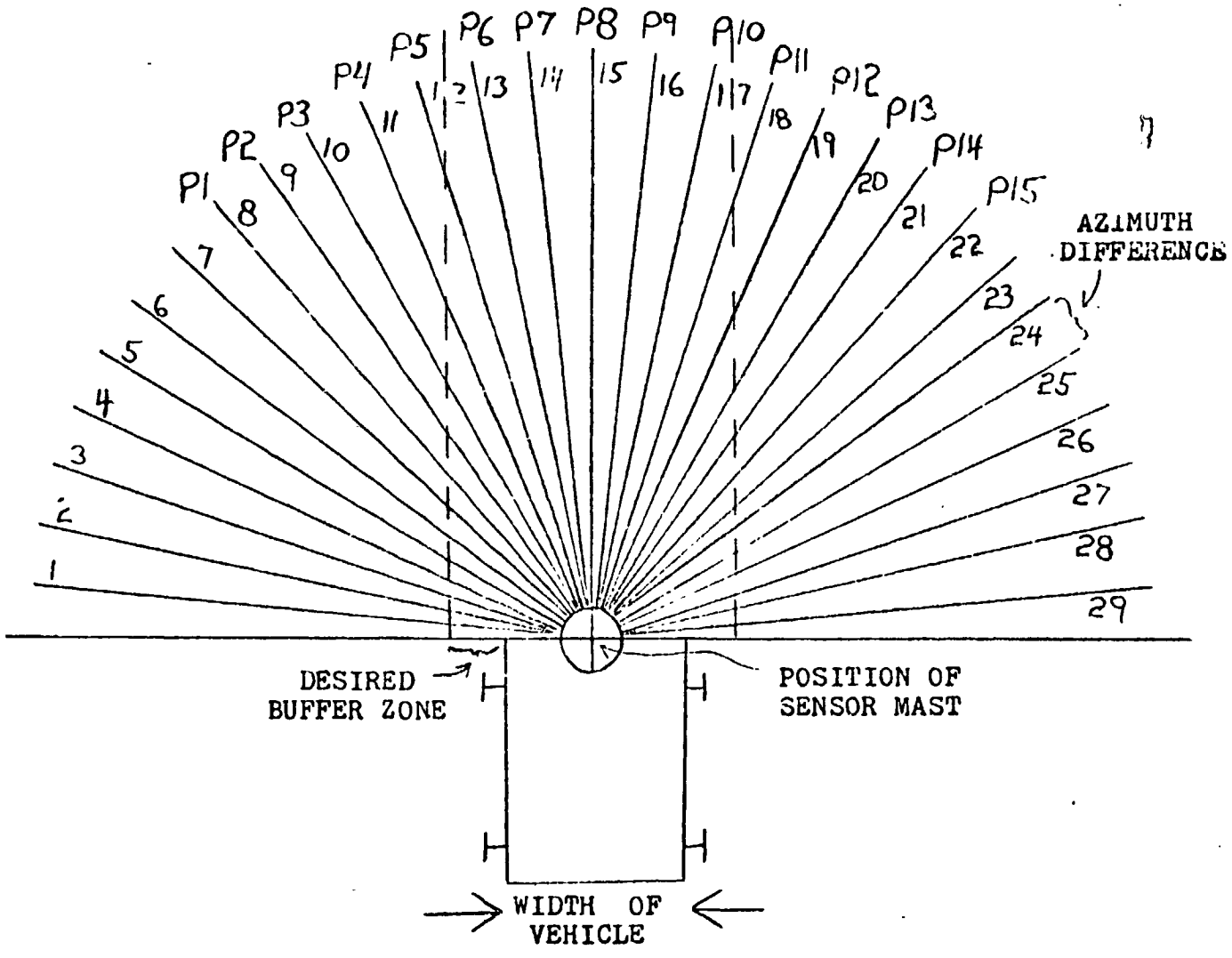

Fig. 82. Sensor scan (top view)

3) the seven forward paths, P5 through P11, are blocked, and
4) the closest "safe" path to target is again selected.

2. Simulation Procedure

The simulation and evaluation of the mid-range system was performed in a systematic fashion, corresponding to the guidelines of the standard test procedures described in Section A.

In the single boulder encounters and rolling incline cases, three system parameters were varied; namely, the sensor mast height, the specified buffer zone, and the azimuth difference between adjacent beams (see Fig. 82).

3. Results and Conclusions

The analysis of this system to date has shown that good performance is achieved on most simple and clearly defined obstacle encounters, but performance is substantially degraded on realistic terrains and in the presence of random effects.

The size of the obstacles which are detectable by this system is a function of the mast height. With small mast heights, noise disturbances frequently trigger the emergency mode, when no emergency really exists. Larger mast heights result in a failure to detect smaller obstacles. A mast height between 1 and 2 meters appears to be about the best compromise.

The additional obstacle clearance obtained as the desired buffer zone isincreased beyond 1 meter is small, with a ½ to 1-meter buffer recommended. This specification should produce an actual obstacle clearance of 0.4 to 0.85 meters.

Fig. 83 illustrates the performance of the vehicle over a realistic terrain consisting of 10 boulders, 4 craters, and a small rise. For this simulation a 1-meter mast height and ½-meter buffer zone were specified. In addition, attitude noise with a 10-degree maximum deviation was used. Although the vehicle successfully reached its destination, overall performance was not very efficient, as the vehicle misinterpreted the small rise as an unnegotiable obstacle and called for emergency help 13 times.

4. Recommendations

To increase the system's capability to negotiate realistic terrains the following path selection system modifications

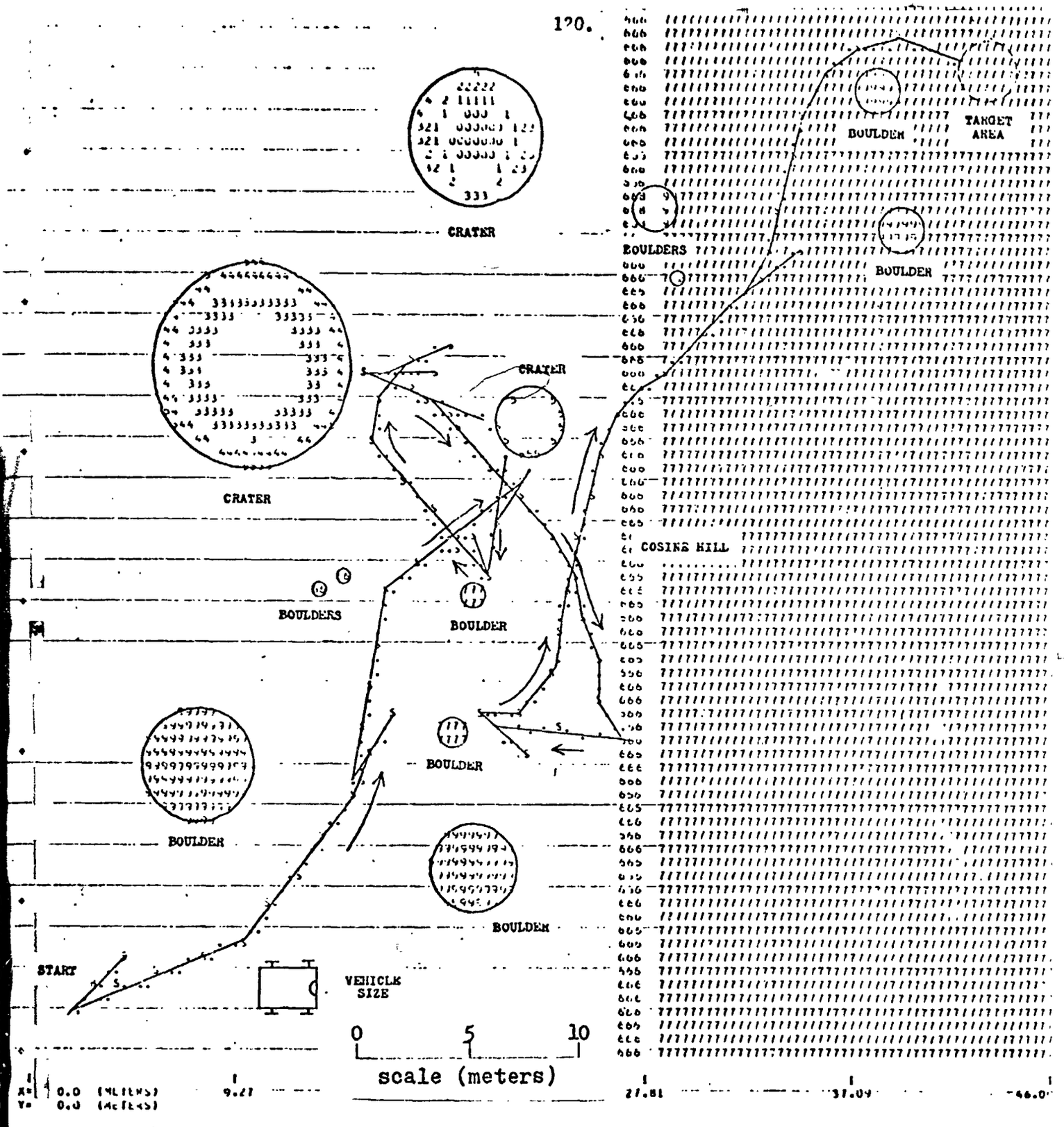

Fig. 83. Boulder-crater field (mid-range system)

are recommended as items for future study:

(i) The addition of a dual or multi-beam sensor scheme incorporating different elevation angles or sensor heights.

(ii) The use of nonuniform azimuth differences in a scan, the greatest density of range measurements being taken directly in front of the vehicle.

(iii) The incorporation of an emergency mode which has the ability to remember where a trouble area exists until the vehicle has safely passed the problem.

C. Performance of a Short Range Sensor System

The following discussion describes the initial development and evaluation of a short range path selection system. By the term "short range" it is to be understood that the system's sensors are constrained to have a maximum range of three meters, and can only make measurements with reasonable accuracy up to this distance. The sensor model and mounting configuration that were simulated in this analysis should properly be thought of as a conceptual method of gathering terrain modeling information at a distance of one to two meters in front of the vehicle and not as a specific hardware design.

1. System Description

(i) Sensors and Sensing Configuration -- The sensors used are ideal beam-type rangefinders that make instantaneous measurements. Fig. 84 shows the sensing configuration. Two of the beam type sensors are mounted at the end of an arm attached to the vehicle. The beam which points directly down, referred to as the "down beam", makes range measurements that are used for terrain modeling purposes whereas the forward beam measurements are used only to protect the arm from colliding with a terrain feature.

During each scanning operation the arm is rotated through a 180-degree traverse and every 6-degrees measurements are made with both beams. It is assumed that the arm can be retracted to a length of one meter if necessary to avoid contact with an obstacle. To compensate for random tilts of the vehicle resulting in inadvertent retractions of the arm, the forward beam is gimballed as a function of the change in the down-beam range measurement.

(ii) Terrain Modeling Process - The terrain modeler simulates an on-board processor. Down-beam information is processed by a slope modeler that converts each measurement

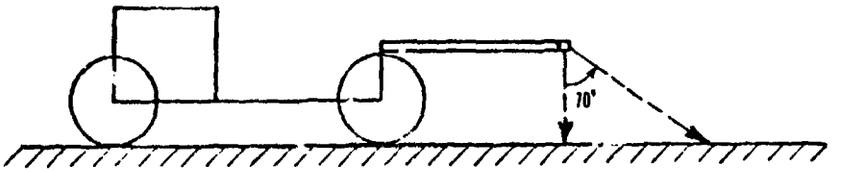

(A) Side View

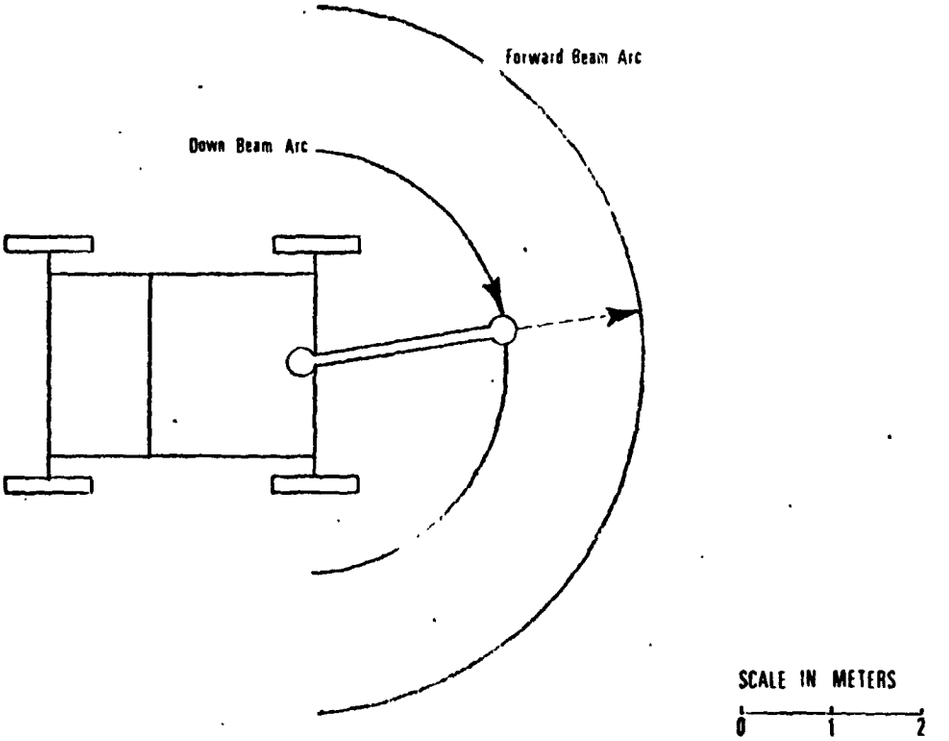

(B) Top View

Fig. 84. Sensing configuration

to a slope by assuming a linear slope from the vehicle's position to the beam's impingement point. The modeler converts the resultant slopes to a go/no-go array by comparing the absolute value of each of the slopes to a 20-degree threshold.

Forward-beam information is processed into a go/no-go array by comparing each measurement to a 1.5-meter threshold. A measurement of less than 1.5 meters is assigned a no-go condition. Both go/no-go arrays are then passed to the path selection algorithm for processing.

(iii) Path Selection Algorithm - Both forward - and down-beam go/no-go arrays are scanned to determine if a no-go condition exists. If the area in front of the vehicle is clear the azimuth from the vehicle's current position to the target is assigned as the next steering command. If a no-go condition exists the algorithm goes into its avoidance mode and the vehicle is backed up two meters on a straight line to obtain room to maneuver. The algorithm then computes a path around the right-most or left-most no-go condition by assigning two intermediate targets on a four-meter radial arc centered on the no-go condition. The choice of moving to the right or left is made so as to yield the shorter avoidance path.

2. Simulation Procedure

The analysis of the short range system generally followed the standard testing procedure guidelines outlined in Section A. The system's deterministic performance was examined as well as its performance in the presence of attitude, range, and slope measurement noise. Maximum deviations of 10 degrees, 0.1 meters, and 5 degrees, respectively, were chosen to simulate these effects.

3. Results and Conclusions

The evaluation indicates that the short range sensor system performs reasonably well in the presence of moderate amounts of noise on relatively flat base terrains. However, performance begins to degrade in the presence of non-zero local slopes and noise. Frequently these effects cause the system to confuse a clear terrain for an impassable feature. Simulation results for these cases seem to indicate that improper gimballing due to range and slope measurement noise is the principle cause of confusion.

As a final examination of the short range sensor system's performance the system was tested on the boulder-crater field shown in Fig. 85. The vehicle path map shows that the system performed reasonably well and successfully reached the target. An interesting aspect of the system's behavior is exhibited

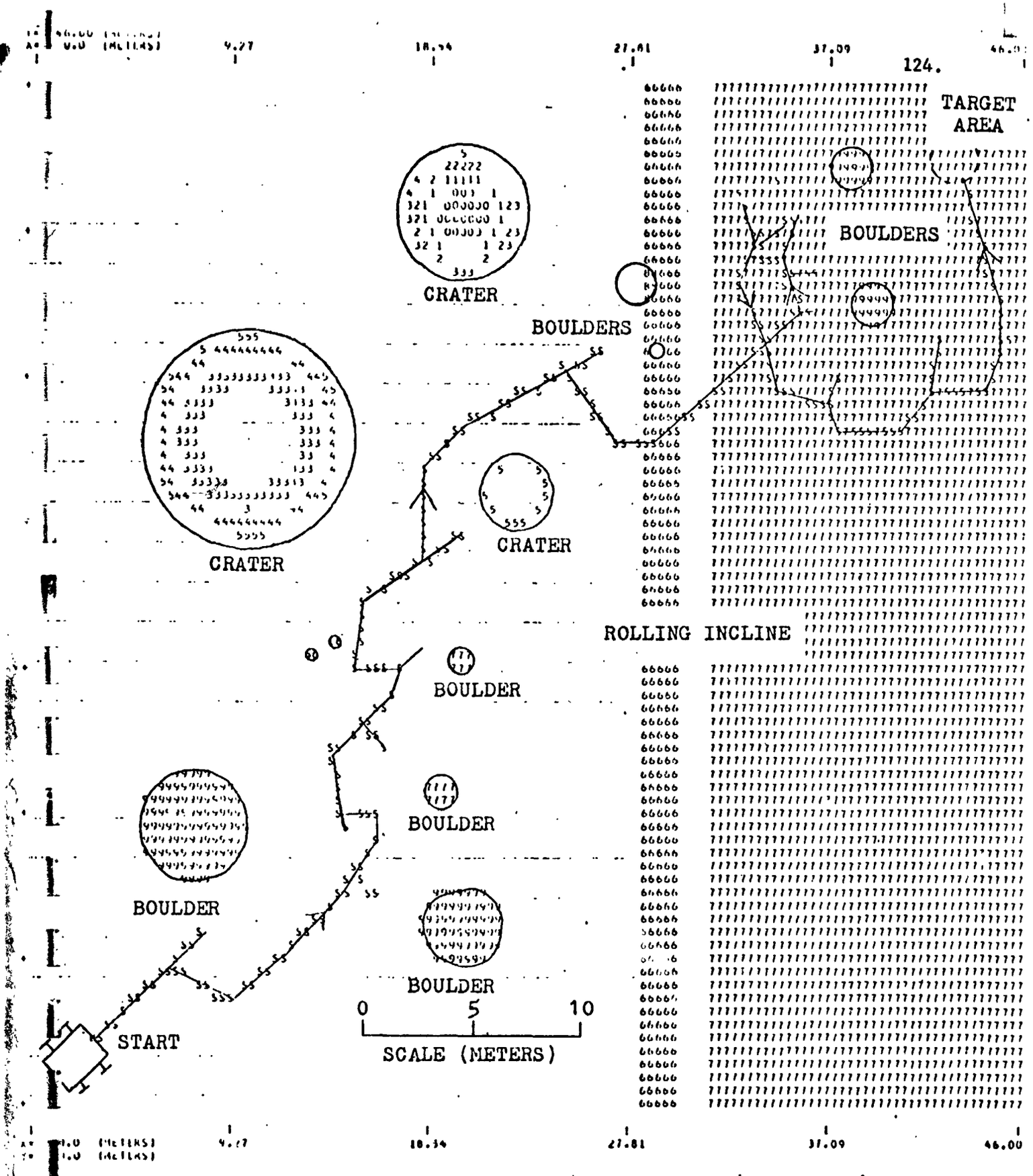

Fig. 85. Boulder-crater field (short range system)

as the vehicle approaches the two boulders near the target position. The vehicle path oscillates between the boulders because the system has no memory capability to keep it from repeating the same mistakes.

4. Recommendations

All of the simulations indicate that a memory capability and more extensive path selection algorithm would enhance the system's performance. The system should be modified so as to not only estimate the size, type, and location of detected obstacles but to store this information for future reference. In addition, keeping a record of the current average in-path slope would lend itself to estimating the type of terrain that is being traversed. This information could be used to control the vehicle's speed and the sensors' orientations in order to obtain better performance near the crest of a hill or on a rolling incline. Finally, the simulation should be expanded to include a scanning operation that would require a finite amount of time and take into account the vehicle's motion during scan periods.

D. Addition of Finite Vehicle Width

An on-going task is the enhancement of the realism of the vehicle's systems and dynamics. Another improvement in this realism was made by the inclusion of the finite width of the vehicle. Previously, the vehicle was modeled as a point mass positioned at the center of the front edge of the vehicle. As a result, without a sensing and obstacle avoidance system, the vehicle would collide only with obstacles directly in the front of it, and could pass between two obstacles which were closer together than the assumed vehicle width.

The method used to implement the width of the vehicle involves the calculation of terrain heights at points along the entire front edge of the vehicle and at points "STEP" meters in front of the vehicle, where "STEP" is the distance traveled by the vehicle in each path increment (presently assumed to be 1/2 meter). The terrain heights are then used to compute in-path slopes which are compared to threshold values set by the user. If any calculated slope exceeds the threshold value, the simulation assumes an obstacle has been encountered, the vehicle backs up, and a new path is selected.

A test simulation was developed to determine the validity of the new vehicle model. Conditions for the simulation were such that the sensor would fail to detect a boulder placed off-center between the vehicle and its target. Without the program changes, the vehicle would have passed through the boulder and arrived at the target. The test verified the expected operation of the vehicle; the vehicle collided with the boulder and avoidance procedures were undertaken.

E. Program Maintenance

The growth in size and sophistication of the path selection simulation program has created problems in several areas of

of program maintenance. Two of these areas have been given serious consideration, and corrective measures are being implemented.

1. Construction of a Disk-Oriented Program Package

Handling a large volume of computer cards is always awkward and increases the probability that the program will be impaired during handling. To alleviate this problem, the source and object code for the path selection simulation program has been placed on disk files, and is now accessible through an assembly language monitor/text-editor for updating, compilation, link-editing, and execution. Copies of the necessary files will be maintained on cards and/or magnetic tape to guard against permanent loss.

2. Organization of a System for Program Documentation

A programmer's first concern is usually to make his code interface with the computer as cleanly and clearly as possible, because he needs results. However, if the program is to be used repeatedly by persons other than the original programmer, an interface must be generated for humans, namely, good program documentation. To satisfy the needs of all anticipated users as adequately as possible, a three-segment system was conceived having each segment directed at a specific level of understanding. The first section will give instructions for using the program, e.g., data formats and keywords. The second section will be a programmer's guide with a block diagram, flow charts, and a commented listing of each routine. The final section will be a program logic manual which specifies the models, formulae, and assumptions used in constructing the various elements of the simulation program. In addition, styles for program coding have been adopted which will be adhered to by all future programmers.

F. Future Work

The activities of the coming year will be devoted to the tasks listed below, along with their target dates:

1. Evaluation and specification of a multiple beam, mid-range sensor system with memory capability (November 1974).

2. Continued development and evaluation of a very short range sensor system (February 1975).

3. Preliminary evaluation of obstacle identification by edge detection (March 1975).

4. Continued development of alternative sensor and path selection concepts (May 1975).

5. Continued improvement and documentation of simulation program (May 1975).

Task D. Chemical Analysis of Specimens

One important phase of the initial missions to Mars is the search for organic matter and living organisms on the martian surface. The present concept for attaining this objective consists of subjecting samples of the atmosphere and surface material to certain chemical and biochemical reactions and thereafter analyzing the products produced, probably in a combination gas chromatograph/mass spectrometer (GC/MS). The gas chromatograph is proposed for separating complex mixtures evolved from the experiments into small groups of similar chemical species. Chemical analysis of these groups would be accomplished in the mass spectrometer. It is the objective of this task to provide engineering techniques and criteria for designing such a system.

Most of the previous effort has involved the systems analysis of the gas chromatograph using simulation, Ref. 21 and 22. This technique uses mathematical models, which incorporate fundamental parameters evaluated from reported experiments, to explore various concepts and to direct further experimental research. Application of prior work to multicomponent chemical systems and improvement of the mathematical model were considered during the past year.

Task problems were attacked by a three-member team, each of whom pursued a specific assignment:

1. Chromatograph system characteristics
2. Chromatograph simulation development
    a. Multicomponent chromatography
    b. Chromatograph model improvement

D.1. Chromatograph System Characteristics - A. N. Stovall
Faculty Advisor: Prof. P. K. Lashmet

It is the objective of this subtask to develop techniques for designing chromatograph systems using simulation models currently under study, Ref. 23. As the purpose of the chromatograph is to separate chemical species, the initial effort involved a quantitative definition of resolution or degree of separation obtained in a specific design under particular operating conditions. A large value of resolution should imply a chromatogram having distinct peaks, whereas a low value should suggest poor separation or overlapping peaks. Resolution should be a function of the physical parameters of the chromatograph.

Resolution R has been defined in the literature, Ref. 24, as

$$R = \frac{T_2 - T_1}{(W_1 + W_2)/2}$$

where

T_1, T_2 = peak times for first and second component, respectively

W_1, W_2 = base widths for first and second component peaks, respectively

For almost symmetrical peaks, resolution of unity corresponds to peak bases immediately adjacent to one another with no overlapping. Overlapping peaks give resolution of less than unity. The above parameters may be approximated by the moments, Ref. 24 and 25:

$$T \sim \mu(1)$$

$$W \sim 4\sqrt{\bar{\mu}(2)}$$

where

$\mu(1)$ = the peak mean or first time-moment about the origin.

$\bar{\mu}(2)$ = the variance or second time-moment about the mean.

Resolution now becomes

$$R = \frac{0.5\left[\mu(1)_2 - \mu(1)_1\right]}{\sqrt{\bar{\mu}(2)_2} + \sqrt{\bar{\mu}(2)_1}}$$

These moments may be calculated from the model equations and are functions of the system parameters, Ref. 25.

Further investigation showed this definition to be independent of sample size or composition. Fig. 86 shows that the chromatograms of the same chemical but of different sample sizes are different although they have the same moments. Because of this characteristic, resolution as defined above inadequately represented separation in mixtures of similar components having widely different sampl. sizes. Fig. 87 shows such a system where the leading edge of the large chromatogram largely obscured the chromatogram of the trace component. Thus another definition of resolution or separation, sensitive to sample size, was required.

In a chromatogram, the output signal is the sum of composition contributions of all components. Based on this concept, chromatograph performance, designated by the term separation (S) to distinuish it from the previously used resolution (R) was defined as

$$S_i = A_i/A$$

where

S_i = separation of component i for the peak where the component predominates.

A_i = contribution of component i to the area under the peak where the component predominates

A = total area under the peak of interest.

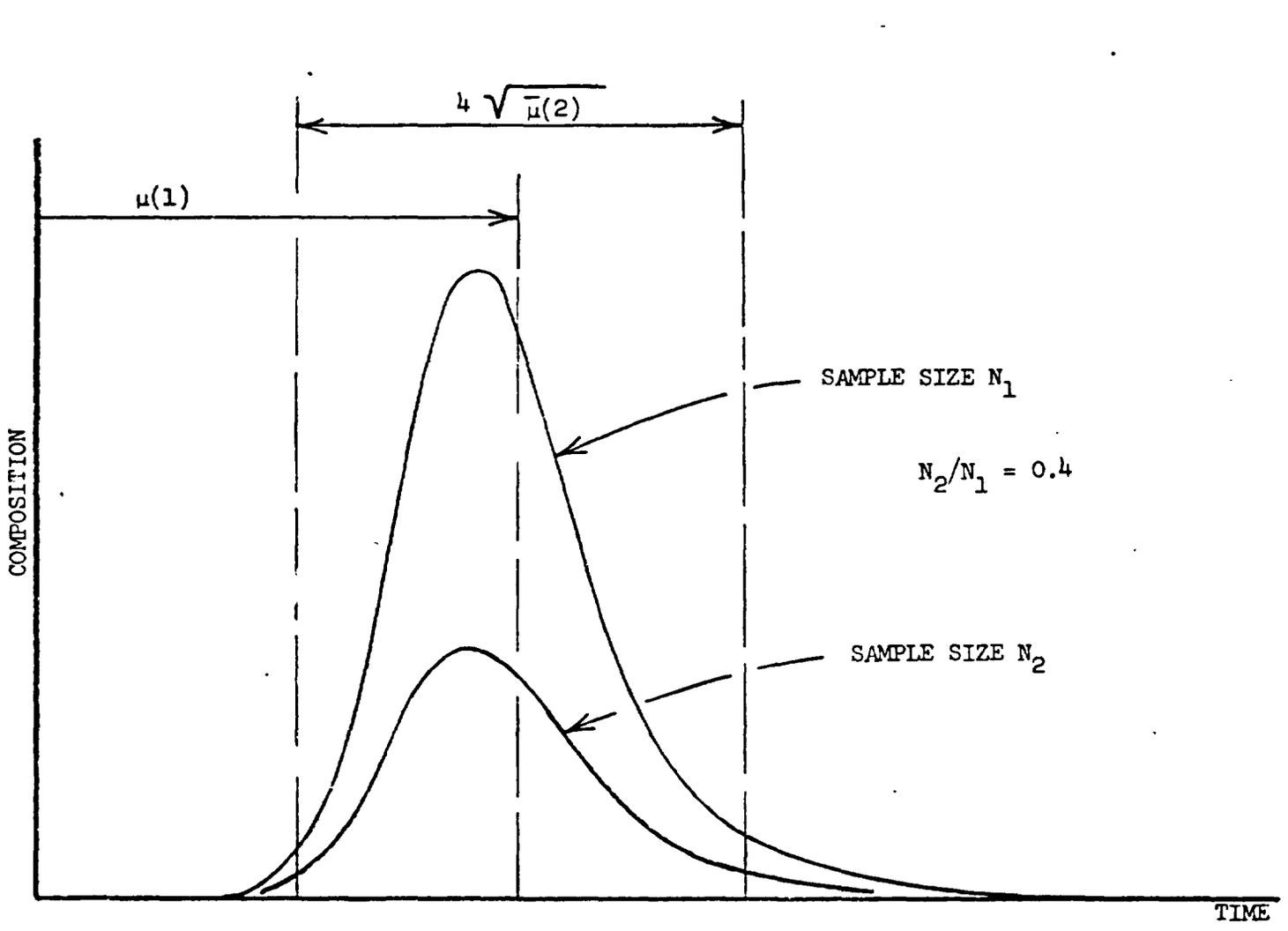

Fig. 86. EFFECT OF SAMPLE SIZE ON CHROMATOGRAM

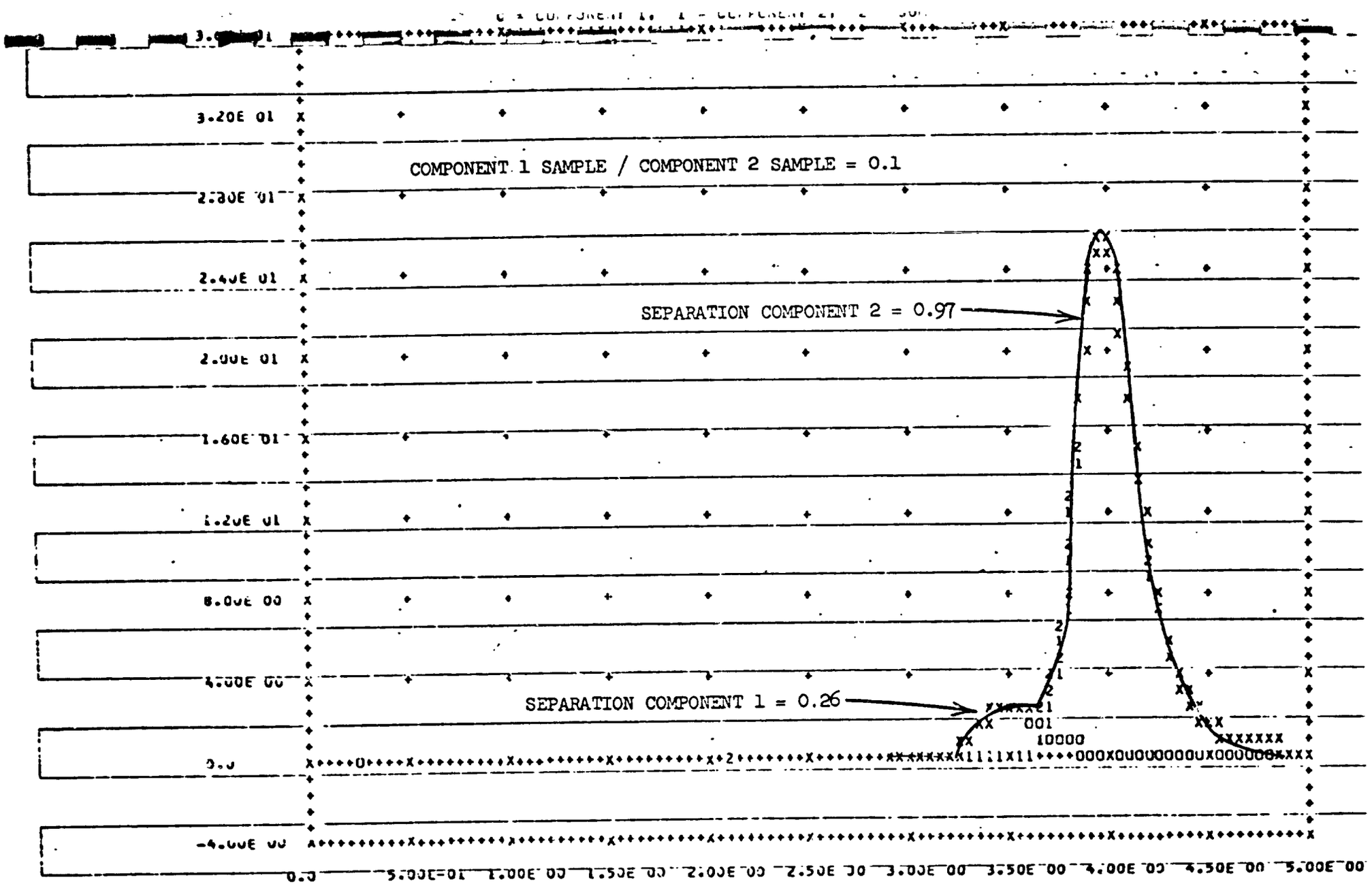

Fig. 8. PERFORMANCE OF 100 CM COLUMN

In these studies, the areas were computed over the finite peak W as given approximately by the second moment or variance, Fig. 86. Prior studies have shown that at least 94% of the chromatogram area lies within this region. S_i is the effective composition of component i in the peak where component i should appear. It ranges from unity for complete separation to zero for essentially no separation; i.e., the sample is small compared to amounts of other interfering chemicals. Thus each component is assigned a value of S indicative of its separation from the other components. For excellent separation, a high value of S, perhaps 0.85 or higher, is expected.

To evaluate this concept of separation, a computer procedure was developed to simulate the chromatograph. Simulation was accomplished by numerically convolving a previously developed mathematical model with typical sample injection pulses represented by data. These studies were limited to a simple binary system, to system characteristics similar to those of the experimental test facility, and to the simple equilibrium adsorption model, Ref. 25. Effects of the following design parameters upon chromatograph performance were determined: column and packing dimensions, injection pulse characteristics, relative sample amounts, carrier gas velocity, and chemical characteristics of the system (the thermodynamic parameter mR_0). Output information included plots of the input pulse, the resulting chromatogram, and output curves corresponding to the two components if injected separately. Separation as defined above was also determined. Representative simulations appear in the next four figures.

Fig. 87 described earlier shows component 2 is well separated (S=0.97) whereas the component having a small sample size is obscured (S=0.26). Tripling the column length as shown by the simulation of Fig. 88 yields complete separation. Other simulations showed the importance of sample injection in obtaining good separation. Fig. 89 shows essentially no separation between two similar species when the sample was injected as a broad pulse. Decrease of the sample injection time (actually obtained experimentally by modifying the injection block of the test facilty) significantly improved the separation, Fig. 90.

Comparison of the moment-defined resolution R and the area-defined separation S in Fig. 91 shows the two methods for representing chromtograph performance are equivalent for widely separated peaks ($R > 1.8$). For peaks which are close, sample size becomes important and the area-defined separation is a better index of performance.

Analysis of many simulations showed that the qualitative trends of parameter effects which have been reported in the literature can easily be predicted quantitatively through simulation, and that the separation index S realistically represented chromatograph performance. In the future, this activity will be continued and extended as follows:

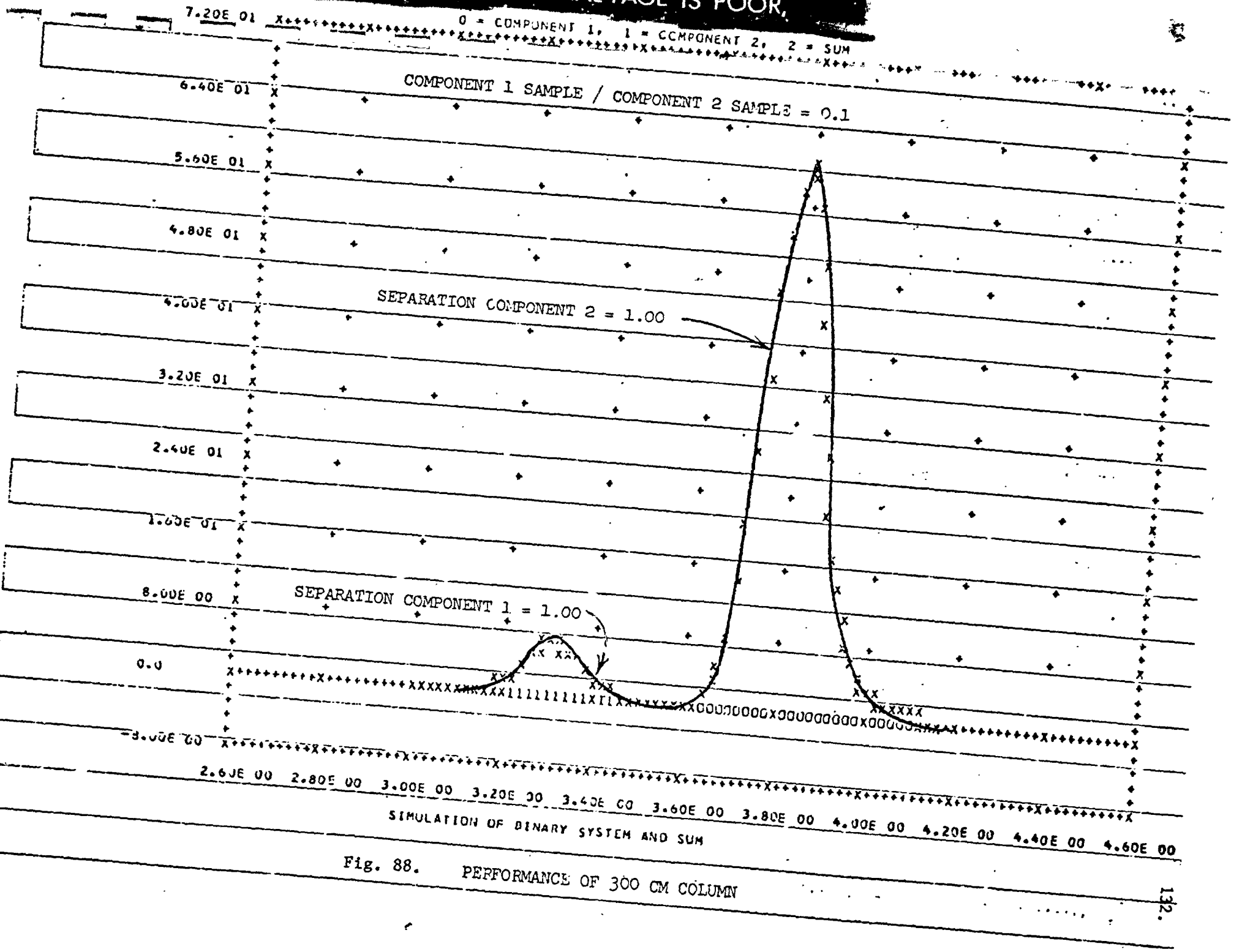

Fig. 88. PERFORMANCE OF 300 CM COLUMN

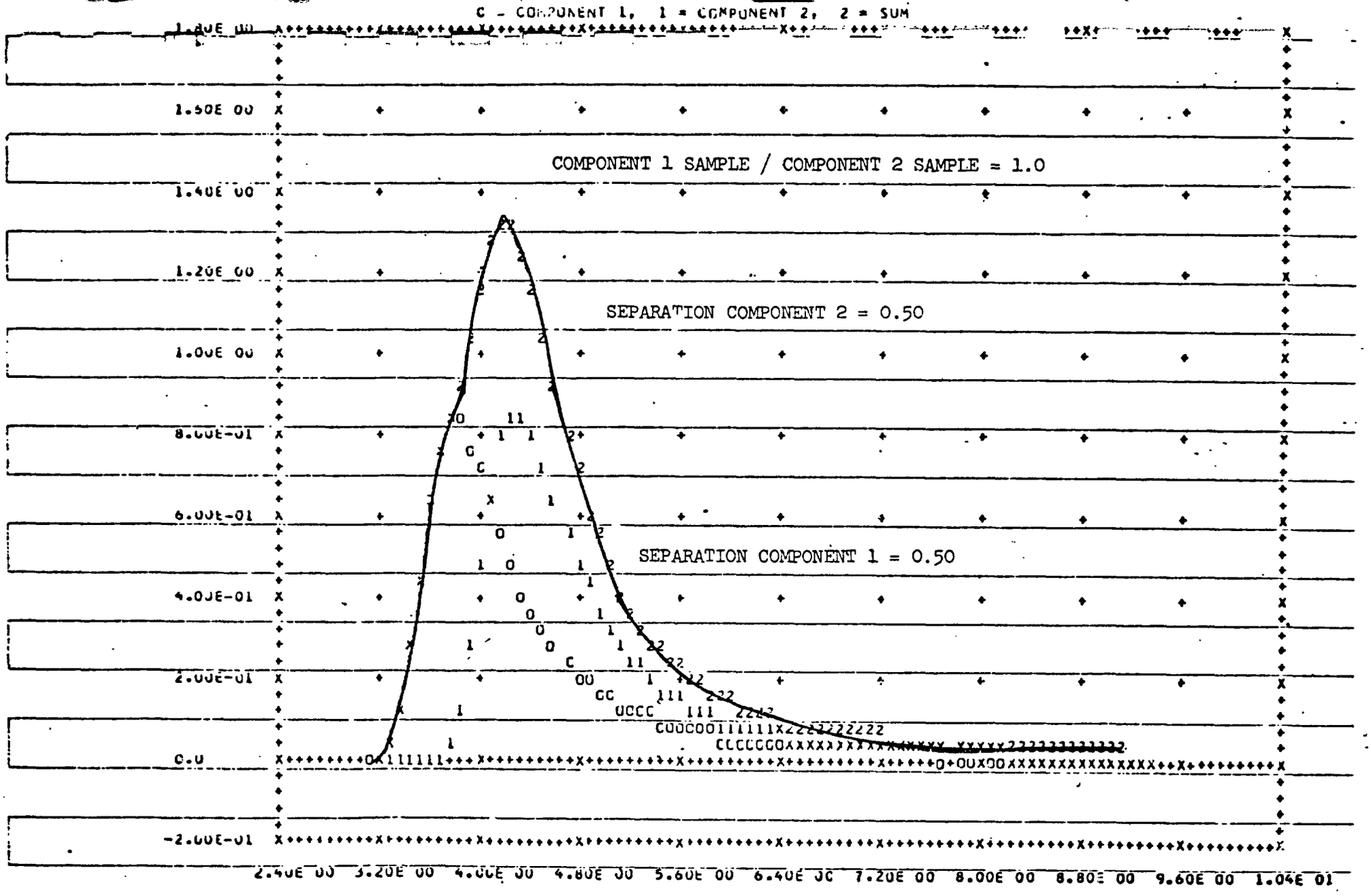

Fig. 89. PERFORMANCE OF 300 CM COLUMN WITH BROAD INPUT

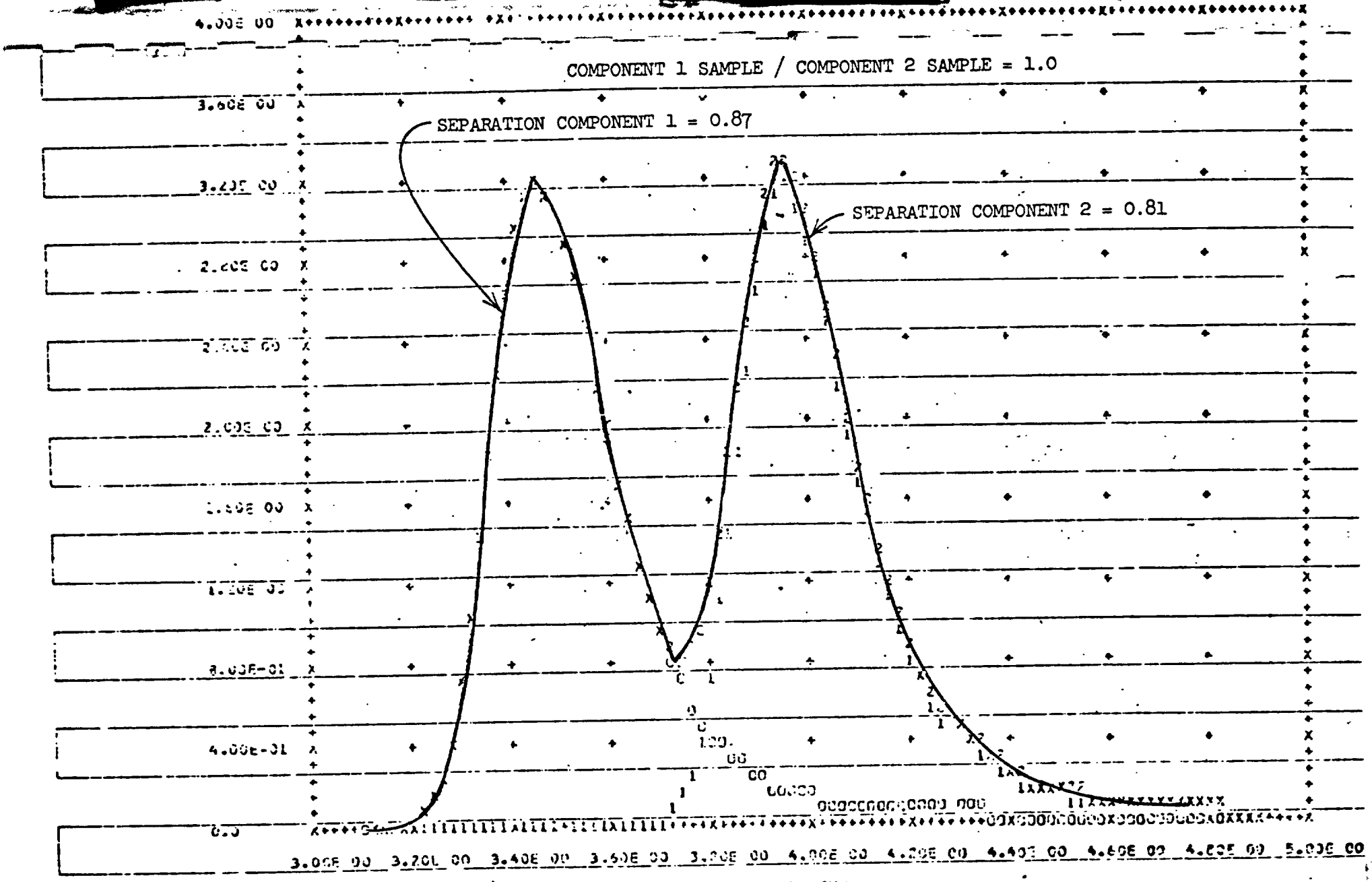

Fig. 9C. PERFORMANCE OF 300 CM COLUMN WITH NARROW INPUT

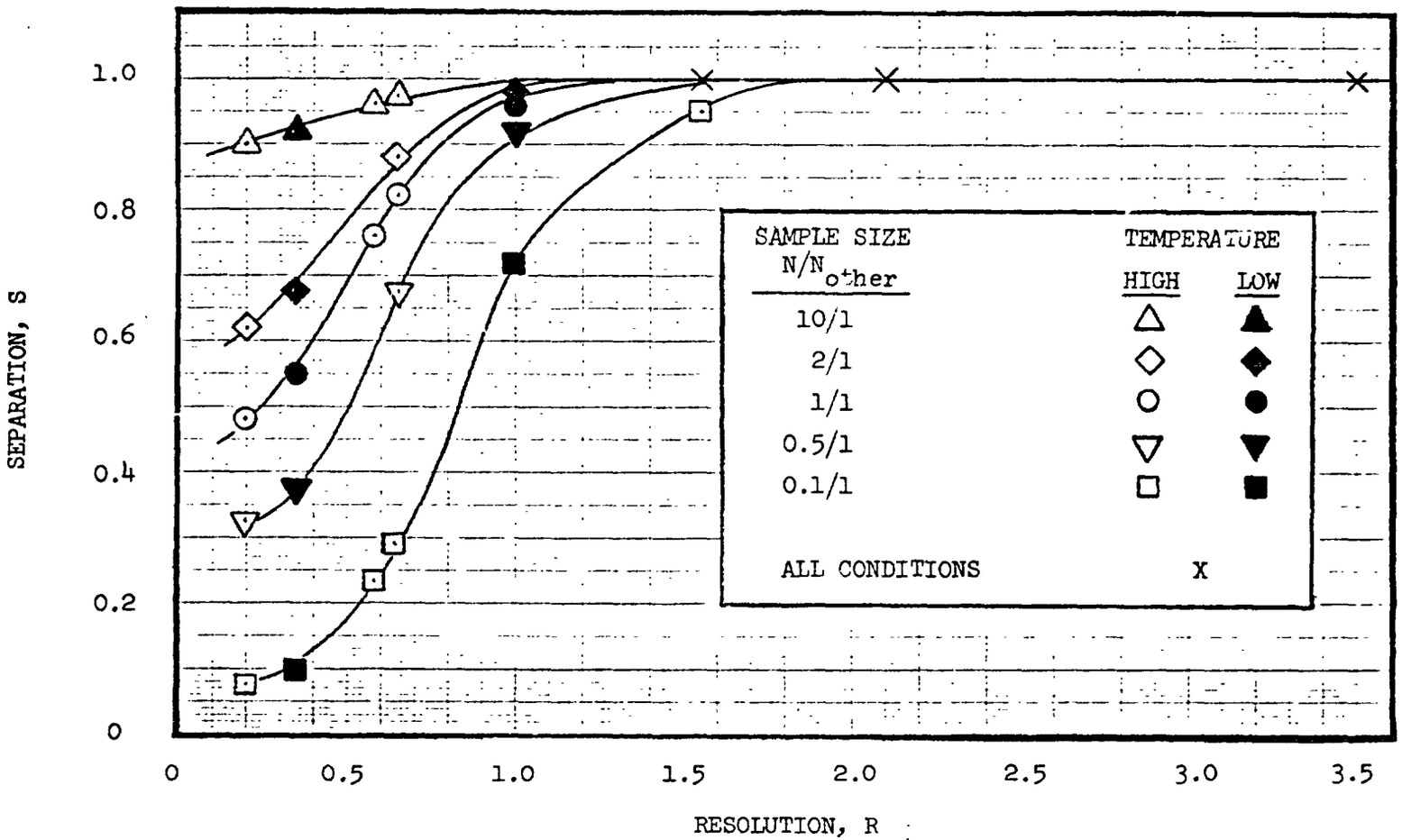

Fig. 91. COMPARISON OF SEPARATION WITH MOMENT-DEFINED RESOLUTION

1. The simulation procedure will be generalized.

2. Quantitative characteristics of input pulses will be determined.

3. A systematic study of the design parameters upon the separation index S will be made.

D.2. Chromatograph Simulation Development

D.2.a. Multicomponent Chromatography - R. C. Lavoie
Faculty Advisor: Prof. P. K. Lashmet

Prior efforts have shown that representation of binary chromatograms by superposition of pure component data was a first-order approximation and in certain cases led to large discrepancies, Ref. 22 and 27. This subtask had as its objective the generation of additional binary data and analysis of the observed nonlinear effects. A technical report describing the progress in detail has been issued, Ref. 26.

Toward the goal of producing more accurate and useful data, modification of the chromatograph equipment was first undertaken. The equipment consists of a gas chromatograph column with thermistor probes which produced electrical signals proportional to the input and output compositions of the test samples, Ref. 28. The signals were detected in a DC bridge before being recorded by an oscillograph. Recording accuracy was improved by replacing a discrete, multiposition voltage divided in the bridge with a potentiometer to allow continuous attenuation of the thermistor signal. The signals could then be adjusted to give full scale recordings on the oscillograph. Relative error in reading the graphical output was reduced in some cases by a factor of 3 or 4.

It was noted that injection of liquid samples produced a dispersed pulse at the column inlet. For maximum resolution, the sample input to the column should be a sharp, narrow pulse as noted in Fig. 89 and 90. Modifications were made to the sample injection block which was a cylindrical chamber containing an electrical heater. A cylindrical sleeve, designed to reduce dead volume, was fitted into the chamber and power to the block heater was increased to hasten sample vaporization. As seen in Fig. 92, the input pulze was markedly improved by the changes.

In the experimental program, new data were collected to supplement previous data and to explain deviations from predicted results. Major deviations were encountered in using the Carle minivalve to inject gas samples such as ethylene, and in running binary samples on the Chromosorb-102 column. In the ethylene system, a sharp, narrow input produced a low, flat output pulse with excessive tailing, whereas the model predicted a relatively sharp, high output peak, Ref. 22. It was noted that the porous Chromosorb-102 column, Table VII, might be poorly represented by the model which assumed

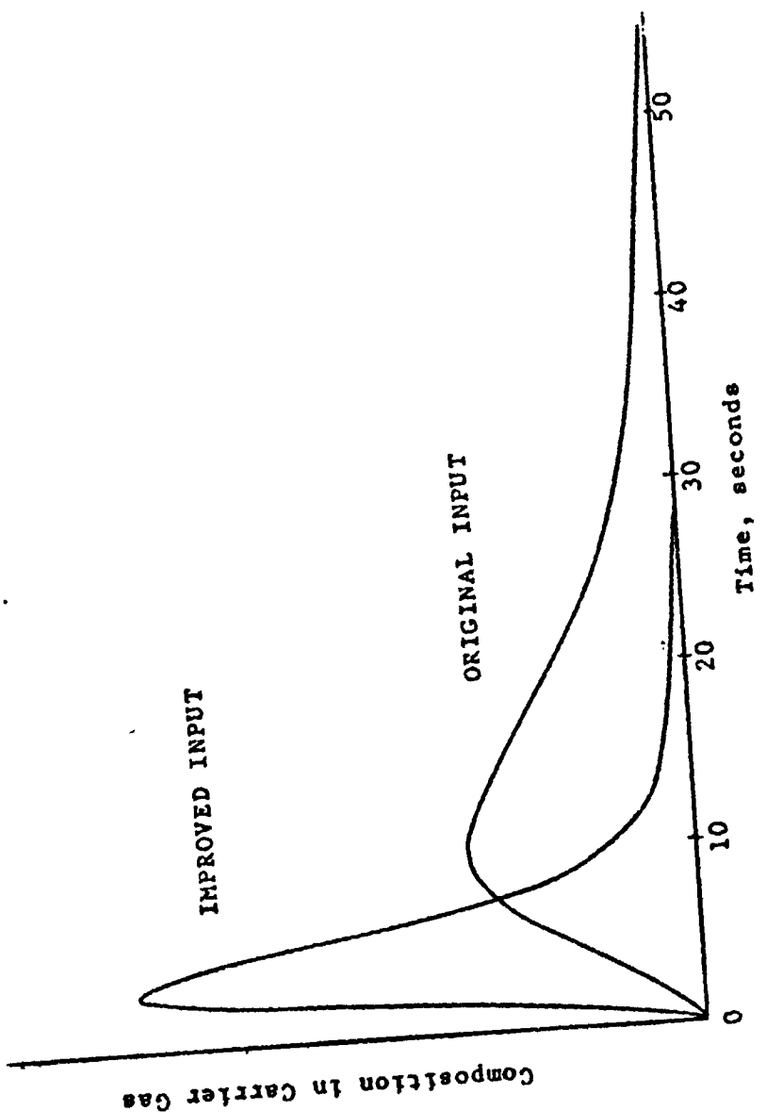

Figure 92. Input Pulse to Column for Liquid Samples

TABLE VII

COLUMN CHARACTERISTICS

	CHROMOSORB 102	CARBOWAX 1500	DES
Length	100 cm	100 cm	100 cm
Outside Diameter	.318 cm	.318 cm	.635 cm
Inside Diameter	.22 cm	.22 cm	.555 cm
Mesh	60/80	60/80	60/80
Particle Size	.025/.0177 cm	.025/.0177 cm	.025/.0177 cm
Composition	Microporous Styrene-divinyl Benzene Polymers	Polyethylene Glycol 20% by Weight on Chromosorb P (diatomaceous earth)	Di-2-ethylhexyl sebacate 20% by Weight on Chromosorb P
Temperature Range	Room-250° C	Room-225° C	Room-125° C
Application	Separation of low molecular weight very polar substances	Separation of high boiling polar compounds	. paration of hydrocarbons from C_4 and up

no porosity. However, similar behavior resulted when using a Carbowax-1500 column, Table VII, which was believed to be nonporous. At the column entrance (input), the maximum composition of ethylene was computed as 0.2 mole fraction. As the mathematical models assumed dilute mixtures, a composition effect was suspect. Reducing the maximum concentration at the column inlet to about 0.07 mole fraction by increasing the mean time of the injection peak from 0.1 second to 12.5 seconds provided the column with a more dilute mixture, and the system was well simulated, Fig. 93.

Model predictions of binary sample separation were based on linear superposition of pure component data. Pentane-heptane samples on porous Chromosorb-102 deviated markedly from this model, and the thermodynamic parameter mR_0 was shown to vary with the amount of the component in the injected sample, Ref. 26. Attempts to separate these components on the non-porous Carbowax-1500 column to determine if porosity was a factor were not successful. A new, non-porous column composed of di-2-ethyl-hexyl sebacate (DES) on an inert substrate, Table VII was purchased and tested.

Data from this column were especially well-modeled by the simple equilibrium adsorption model, Ref. 25. Pure pentane and heptane samples were run at temperatures of 50 to 125° C, and adsorption activation energies of 4.0 and 6.6 kcal/mole respectively were derived from temperature behavior of the thermodynamic parameter mR_0. Sample sizes ranging from 0.2 to 3.0 microliters gave no significant differences in values of mR_0. Binary samples were run, and linear superposition of pure component data predicted the binary results well. Comparison of the simulation with experimental data, shown typically in Fig. 94, indicated a slight non-linear effect in the heptane data. However, considering the error in determining the parameter mR_0 from pure component data, the simulation and experimental results were essentially the same.

The composition-dependent effect noted for the pure ethylene system and the pentane-heptane binary on Chromosorb 102 suggested an investigation of sample-size behavior of pure pentane and heptane systems. Experiments using pure heptane samples ranging from 0.2 to 3.0 microliters showed the parameter mR_0 to be sample-size dependent for the pure component, Fig. 95. Fig. 95 also shows the variation of the heptane mR_0 values in the binary systems with the amount of heptane present in the originally injected mixture. As the two sets of data were the same within experimental error, it was concluded that interactions between pentane and heptane had a negligible effect upon mR_0 and that any composition dependence was primarily due to the actual composition of the component in the carrier gas stream. This further suggested that the linear isotherm used in deriving the simulation model be replaced by a nonlinear isotherm which would exhibit the observed nonlinear effects.

Preliminary studies using the nonlinear Langmuir isotherm, which is simple, has a theoretical basis, reduces to the linear isotherm for very dilute mixtures, and can be extended directly to multicomponent systems, have shown that large samples elute sooner than small samples and exhibit more tailing. As these characteristics were observed in

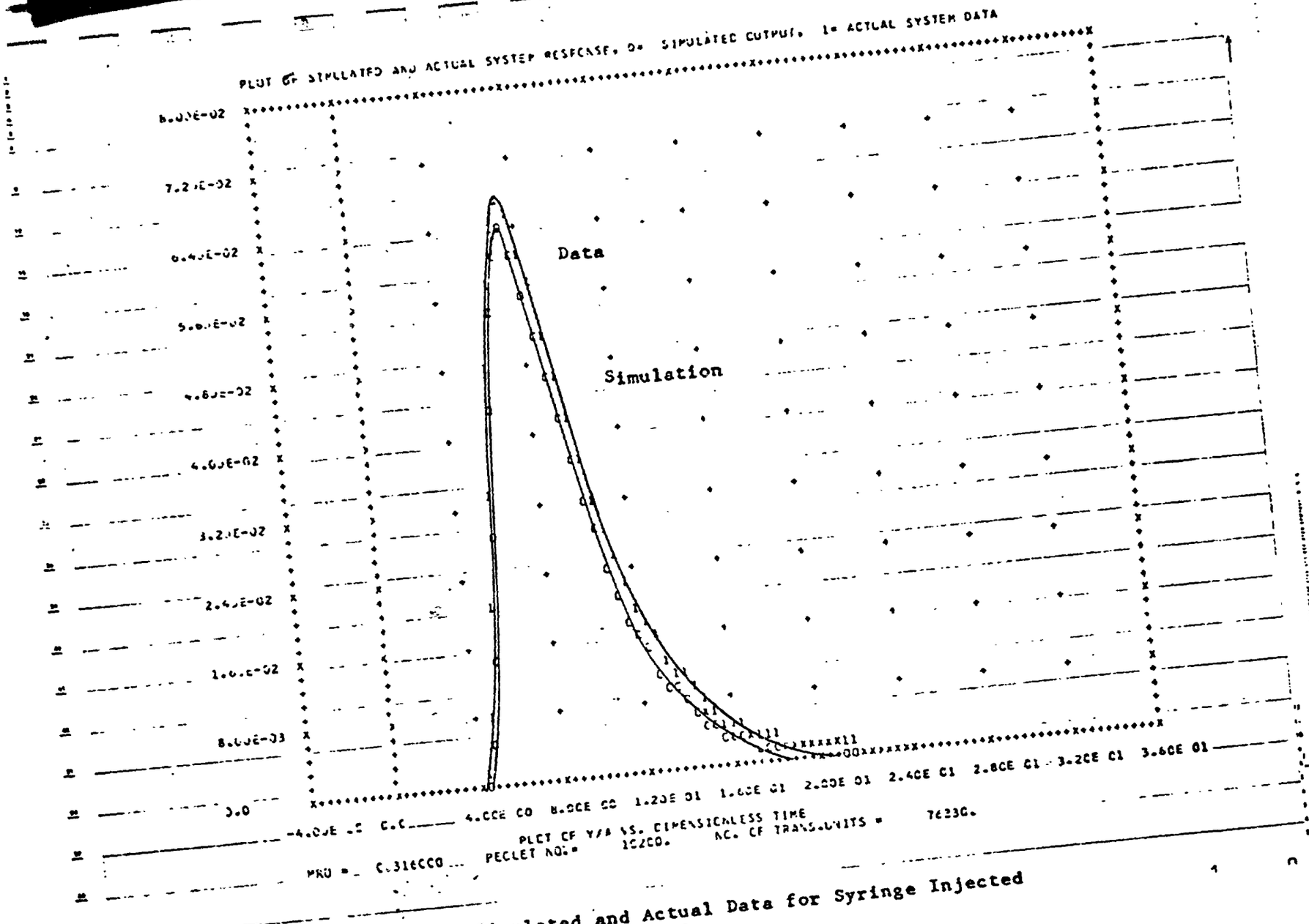

Figure 93. Simulated and Actual Data for Syringe Injected Ethylene on C-1500

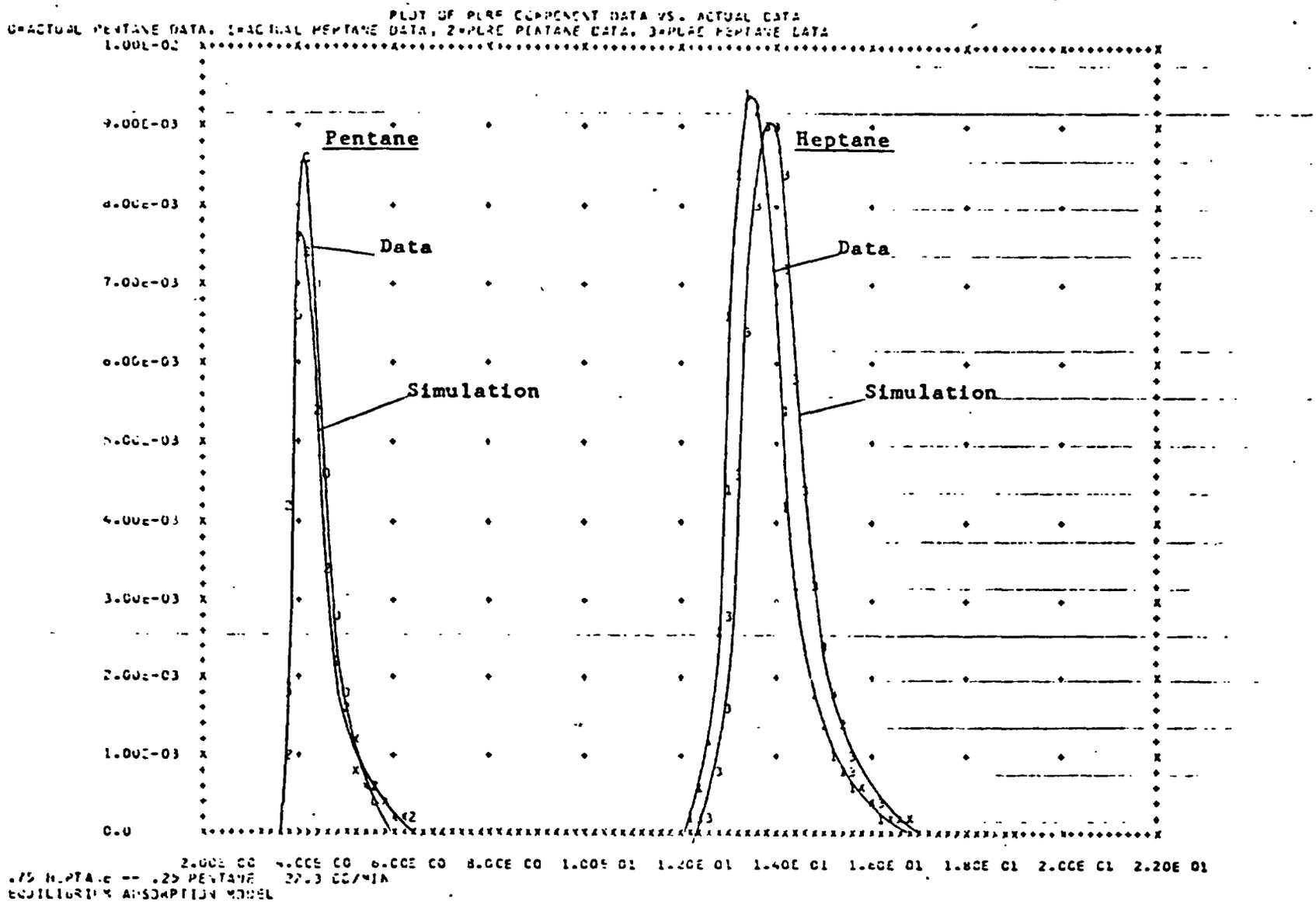

Figure 94. Simulated and Actual Binary Data for Pentane - Heptane on DES at 100° C.

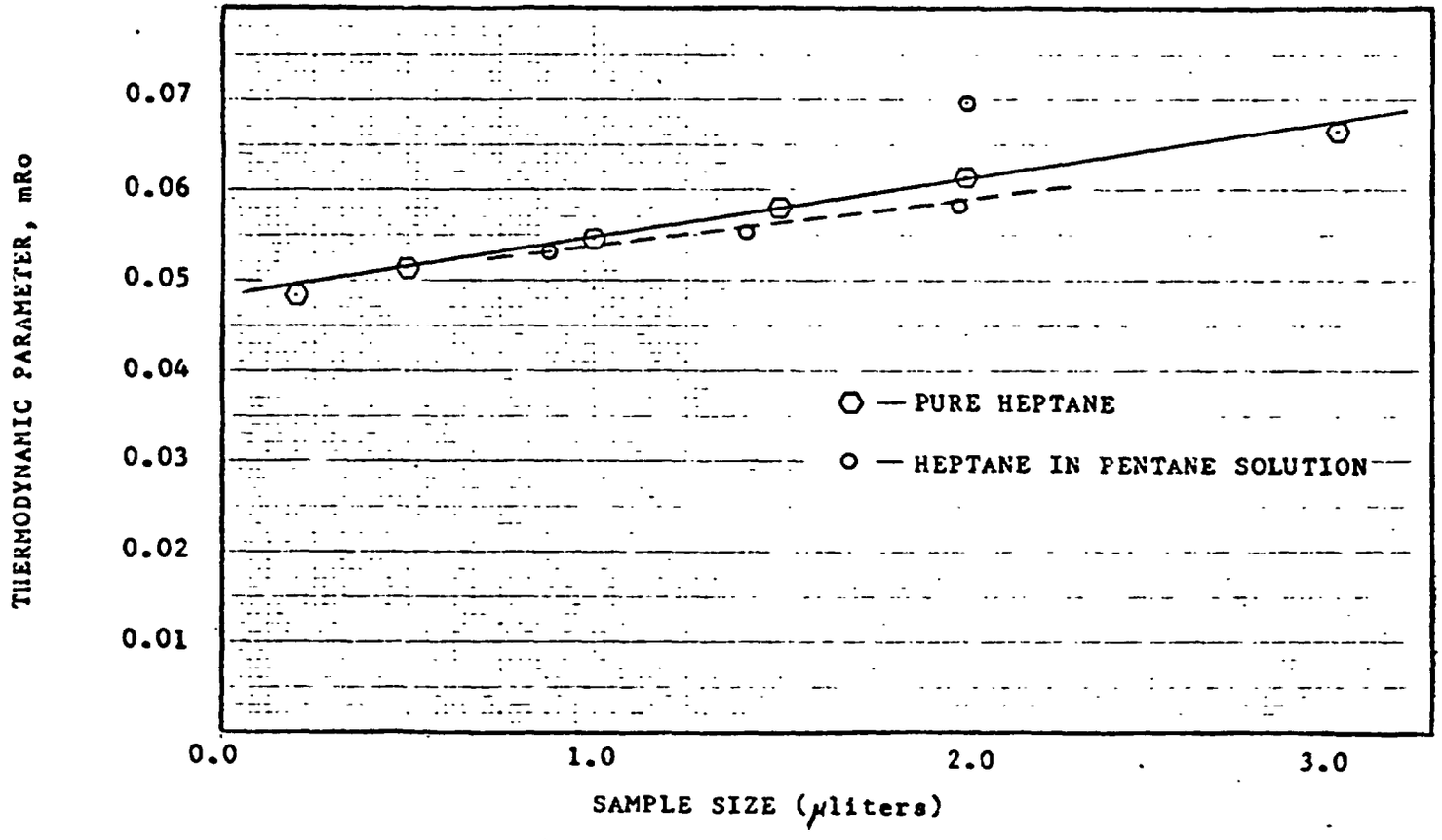

Fig. 95. Effect of Sample Size On mRo For Heptane On Chromosorb 102

the data, future work will involve examination of the resulting nonlinear system model.

D.2.b. Chromatograph Model Improvement - P. T. Woodrow
Faculty Advisor: Prof. P. K. Lashmet

The objective of this task was the development and verification of a mathematical model that adequately predicts the component behavior of a sample injected into a gas chromatograph. A comprehensive model, in the form of a set of coupled, partial differential equations, was developed and studied using the techniques of moment analysis. These studies are described in detail in two technical reports which have been issued, Ref. 29 and 30. This model included the following transport mechanisms: axial diffusion, axial convection, mass transfer between the interparticle and intraparticle regions, intraparticle diffusion, and a finite rate of adsorption within the particle. Moment analysis of this model has shown it to be more capable of predicting characteristics of actual data than the simpler models previously studied, Ref. 22. Details on model development, appropriate boundary and initial conditions, and moment analysis have been documented (Ref. 29).

Because of the complexity of the model, analytical techniques were not feasible and a study of applicable numerical techniques was made. The technique of orthogonal collocation, Ref. 31, was studied and applied to several systems of equations to determine if it could be used routinely for numerical solutions and hence verification of the complicated chromatograph model. Three models of increasing complexity, shown in Fig. 96, were considered: 1) a simple, diffusion-convection model; 2) a rate-of-adsorption limited, inter-intraparticle model; and 3) an inter-intraparticle model with negligible mass transfer resistance.

The study of this sequence of systems was motivated by the knowledge that systems 1 and 2 have known, exact, analytical solutions, and simulations using orthogonal collocation could be evaluated directly. In addition, this sequence provided an opportunity to appraise the technique of orthogonal collocation in its ability to solve systems of one, two, and three coupled, partial differential equations. The orthogonal collocation treatment reduced the models to sets of ordinary differential equations which were integrated using the Bulirsch-Stoer extrapolation technique, Ref. 32. Shifted Legendre polynomials were used as the collocation functions.

The simple model, system 1 of Fig. 96, was studied using unit rectangular pulses and actual data as forcing functions for high and low values of the Peclet number Pe. Fig. 97 shows a third order collocation solution using actual data as a forcing function. Fig. 98 shows a fifteenth order simulation which agreed almost exactly with the analytical solution except for small oscillations where the response should have been essentially zero. This behavior was inherent in the method. Increasing the order of the collocation approximation reduced the magnitude of the oscillations so that they became unimportant when compared to the magnitude of the simulated response.

1. Simple, diffusion-convection model:

$$\left(\frac{1}{Pe\ z_0^2}\right) \cdot \frac{\partial^2 y}{\partial z^2} - \left(\frac{1}{z_0}\right) \cdot \frac{\partial y}{\partial z} = \frac{\partial y}{\partial \theta}$$

2. Inter-intraparticle model without diffusion

$$\left(\frac{1}{Pe\ z_0^2}\right) \cdot \frac{\partial^2 y}{\partial z^2} - \left(\frac{1}{z_0}\right) \cdot \frac{\partial y}{\partial z} - N_{RU}\ (y-y^*) = \frac{\partial y}{\partial \theta}$$

$$\left(\frac{1}{R_I}\right) \cdot \frac{\partial x}{\partial \theta} = N_{RU}\ (y-y^*)$$

$$y^* = m\ x$$

3. Inter-intraparticle model with diffusion

$$\left(\frac{1}{Pe\ z_0^2}\right) \cdot \frac{\partial^2 y}{\partial z^2} - \left(\frac{1}{z_0}\right) \frac{\partial y}{\partial z} - \frac{3(1-\epsilon)\beta}{\epsilon} \left(\frac{L}{R}\right)^2 \left(\frac{1}{Pe_A}\right) \left.\frac{\partial y_i}{\partial r}\right|_{r=1} = \frac{\partial y}{\partial \theta}$$

$$\left(\frac{L}{R}\right)^2 \left(\frac{1}{Pe_A}\right) \left[\frac{\partial^2 y_i}{\partial r^2} + \left(\frac{2}{r}\right) \frac{\partial y_i}{\partial r}\right] - N_{RU}\ (y_i - y_i^*) = \frac{\partial y_i}{\partial \theta}$$

$$\left(\frac{1}{R_I}\right) \frac{\partial x}{\partial \theta} = N_{RU}\ (y_i - y_i^*)$$

$$y_i^* = m\ x$$

Fig. 96. Equations Being Studied by Orthogonal Collocation

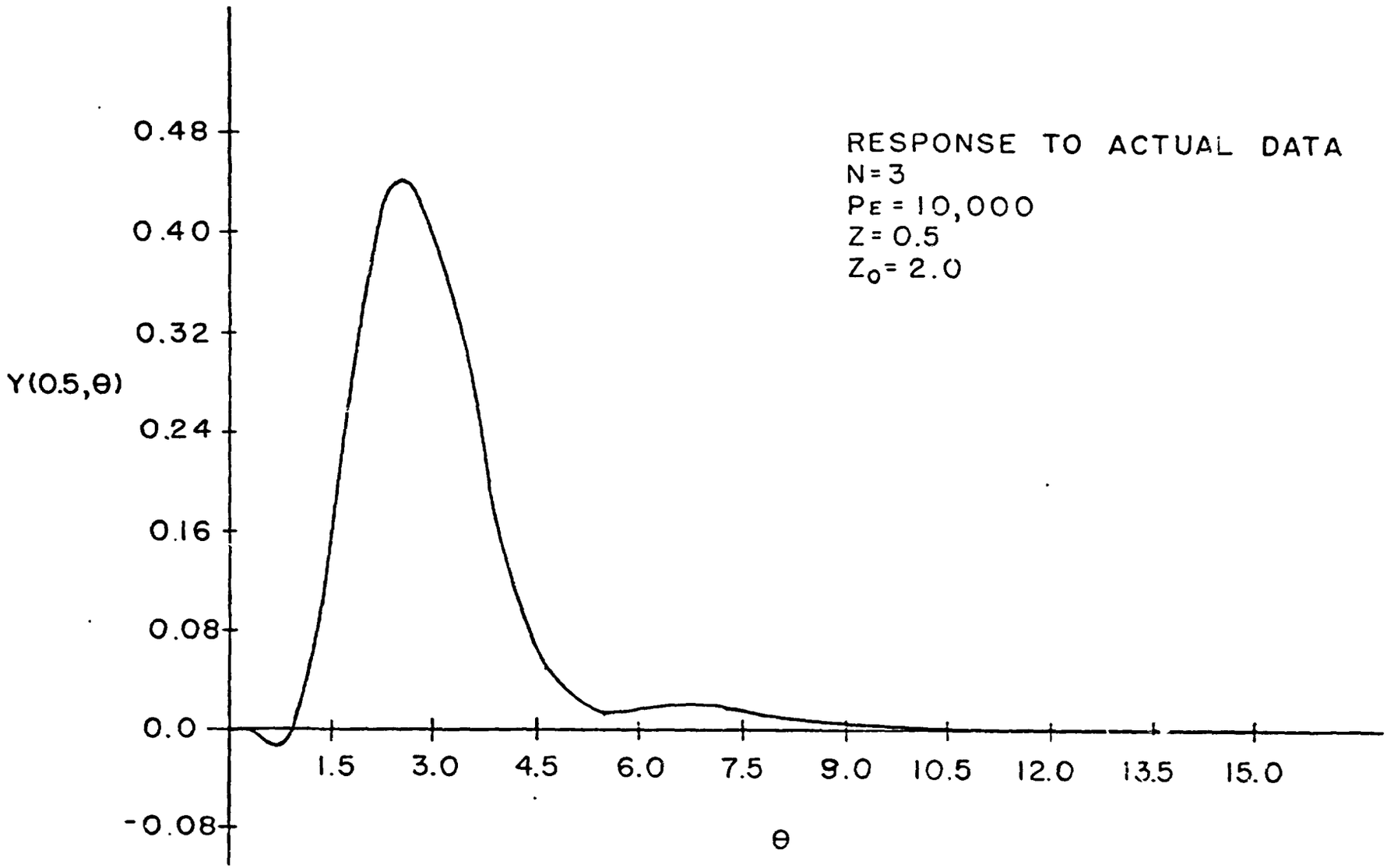

Fig. 97. Simulation of Simple Model Using 3 Collocation Points

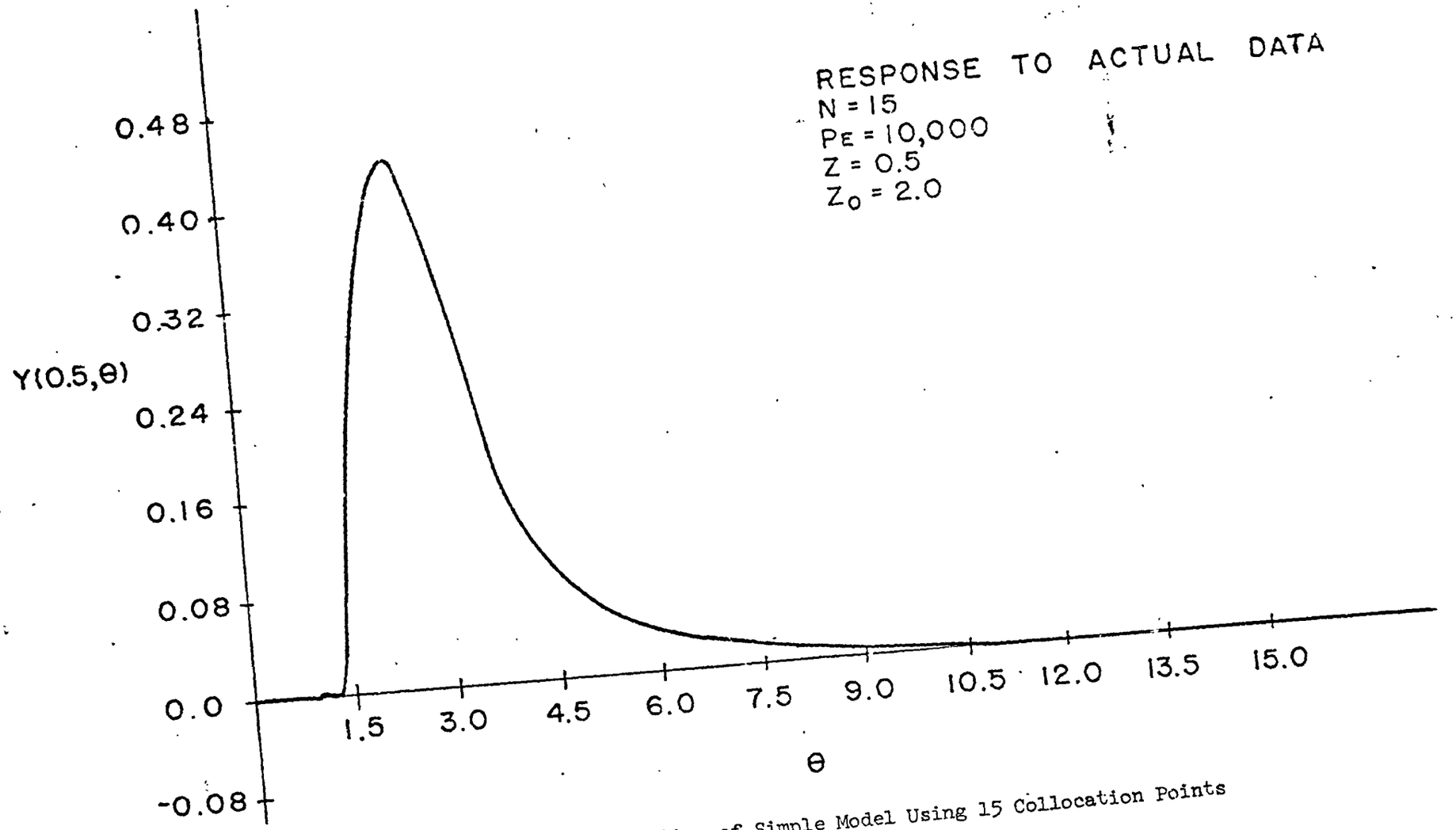

Fig. 98. Simulation of Simple Model Using 15 Collocation Points

Fig. 99 and 100 show the simulation of the simple inter-intraparticle model, system 2 of Fig. 96, using 15 and 21 collocation points respectively. Again, oscillations were present, and high order collocation was required to satisfactorily approximate the analytical solution. This problem was more complex than the previous problem in that two coupled partial differential equations were treated. As shown in Table VIII, computation time became large.

The current investigation was terminated with the application of orthogonal collocation to the inter-intraparticle-diffusion model (system 3 of Fig. 96) which had no known analytic solution. Unlike the previous two problems where only one spatial domain was discretized, this problem required orthogonal collocation discretizations for both the interparticle and intraparticle regions and the order of the numerical problem became high. Several cases were studied for short computer run times, and the results were extrapolated to give estimates of computer requirements necessary to complete the analysis. As shown in Table VIII, the computation times suggested a thorough analysis was not feasible using orthogonal collocation as it was formulated in this study.

In summary, it was found that simulation of the complicated model using orthogonal collocation, while being more efficient than traditional numerical schemes, was too time-consuming to be practical. A review of the prior-studied systems which were not well-represented by the simple, equilibrium adsorption model and additional experimental work showed the chromatographic data were sample-size dependent (Task D.2.a. above): i.e., peak times and spreading depended upon the amount or composition of the sample. Furthermore, chromatograms resulting from reduced sample sizes were well-represented by the simple simulation model, and discrepancies in simulating binary systems using superposition were qualitatively explained.

Based upon these observations, it is proposed that research on the complicated inter-intraparticle model be terminated and that a composition-dependent effect such as the nonlinear Langmuir adsorption isotherm be incorporated in the sample, equilibrium adsorption model. The resulting partial differential equation is nonlinear so a numerical procedure must be used for simulation. As a relatively simple mathematical system is involved, finite difference schemes or orthogonal collocation may be practical for numerical computations.

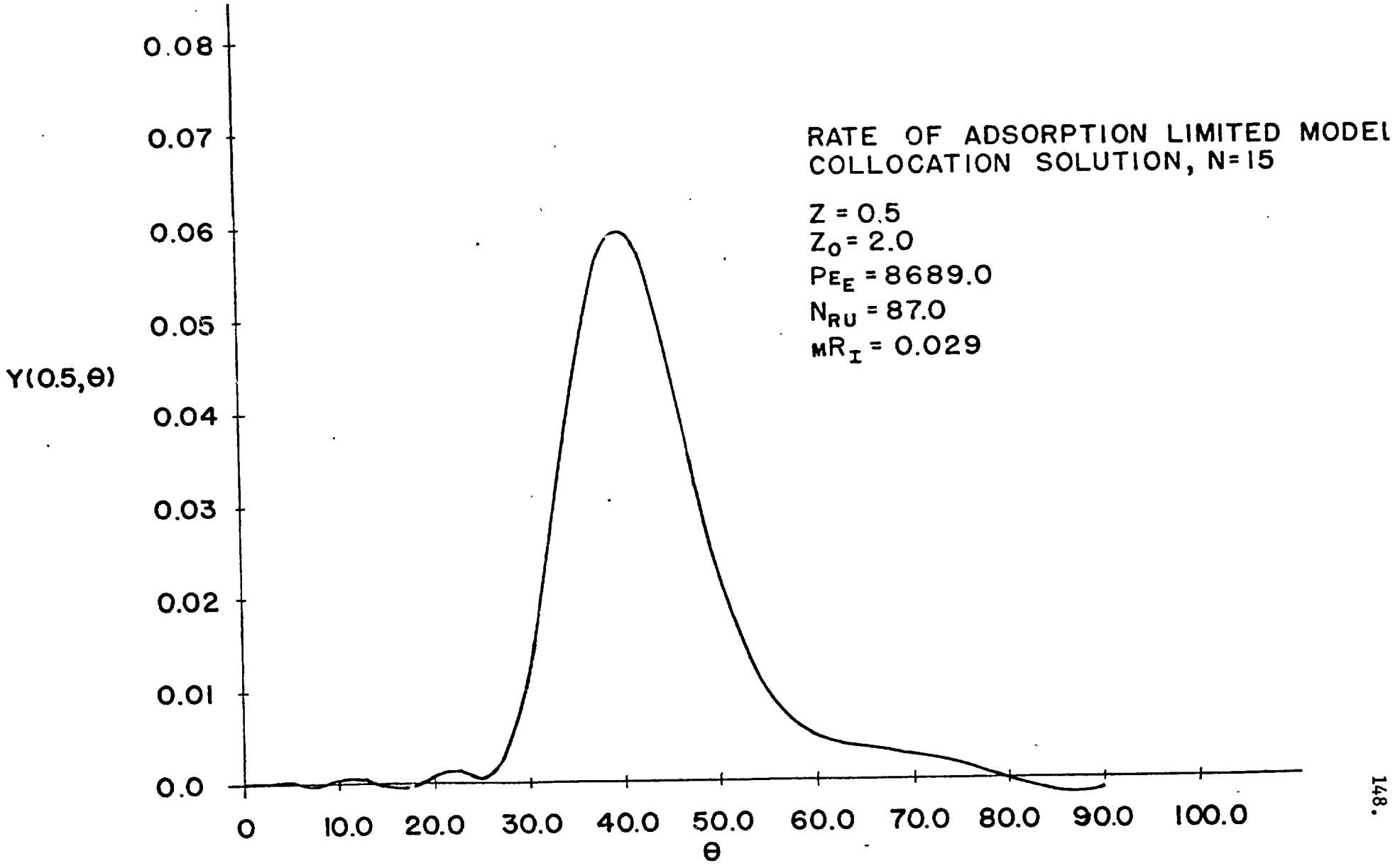

Fig. 99. Simulation of Simple Inter-Intraparticle Model Using 15 Collocation Points

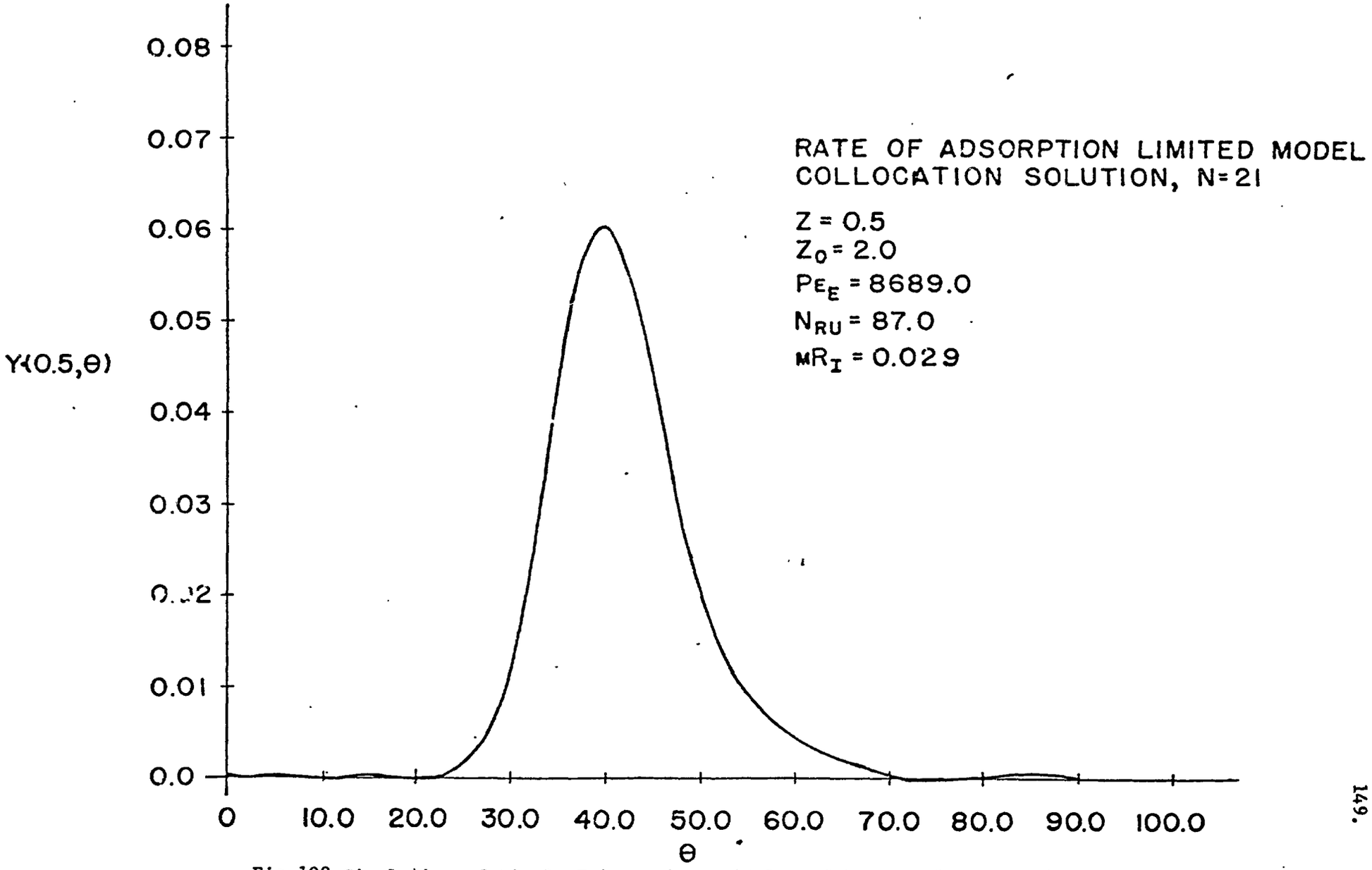

Fig.100. Simulation of Simple Inter-Intraparticle Model Using 21 Collocation Points

TABLE VIII

Summary of Orthogonal Collocation Simulation Times

Rate-of-Adsorption Limited, Inter-Intraparticle Model

	Number of Collocation Points			
Computer	3	7	15	21
IBM 360/50	6.49 min.	23.5 min.	100 min. (estimated)	350 min. (estimated)
CDC 7600	------	0.316 min.	----------	2.87 min.

All execution times are for single precision integration up to 90 units of dimensionless time.

Inter-Intraparticle-Diffusion Model

Collocation Points			
Axial	Radial	System Order	Estimated Execution Time (min.)*
3	1	9	630
3	3	21	22500
7	1	21	1442
7	3	49	90000
15	1	45	3750

* IBM 360/50 single precision integration up to 90 units of dimensionless time.

REFERENCES

1. Sandor, G. N., "Seven Dangers of Designer Overspecialization and How to Avoid Them Through Designer Education", Design Engineering Conference and Show, Chicago, Ill., March 1-4, 1974. Selected for publication as a feature article in Mechanical Engineering.

2. Sandor, G.N., Hassel, D.R. and Marino, P.F., "Modern Mechanisms Make Manless Martian Mission Mobile -- Spin-off Spells Stairclimbing Self-Sufficiency for Earthbound Handicapped," accepted for presentation at the Ninth Aerospace Mechanisms Symposium sponsored by the NASA-Kennedy Space Center, Cal. Inst. Tech. and Lockheed Missiles and Space Corp., Kennedy Space Center, Florida, Oct. 17-18, 1974.

3. Ryder, Alan, G., "Dynamic Evaluation of RPI's 0.4 Scale Unmanned Martian Roving Vehicle Model," RPI Technical Report, MP-38, Rensselaer Polytechnic Institute, Troy, New York, December 1973.

4. Pavarini, Carl, "System Design Optimization for a Mars-Roving Vehicle and Perturbed Optimal Solutions in Non-Programming, RPI Technical Report MP-43, Rensselaer Polytechnic Institute, Troy, New York, June 1974.

5. Torrance, K.E. and Sparrow, E.M., "Theory for Off-Specular Reflection from Roughened Surfaces," Journal of the Optical Society of American, Vol. 57, No. 9, Sept. 1967, pp. 1105-1114.

6. Christie, F.A. and DeVriendt, A.B., "Bidirectional Reflectance from Surfaces Formed by the Ruling of Orthogonal Parallel V-grooves," 10th Aerospace Sciences Meeting, American Institute of Aeronautics and Astronautics, San Diego, Cal., Jan. 17-19, 1972.

7. Zuraski, G.J., "Laser Range Measurement for a Satellite Navigation Scheme and Mid-Range Path Selection and Obstacle Avoidance," Master of Engineering Project, Rensselaer Polytechnic Institute, May 1975.

8. Motorola Application Note No. AN-440.

9. Environmental Products Application Notes UN 319 and UN 328.

10. An Exploration Investigation of a 1979 Mars Roving Vehicle Mission," December 1, 1970, JPL, C.I.T., Pasadena, Calif.

11. Shen, C.N. and Berger, D., "Stochastic Estimates of Gradient from Laser Measurements for an Autonomous Martian Roving Vehicle," Proceedings of the 3rd IFAC Symposium, The Hague/Delft, The Netherlands, June 1973.

12. Shen, C.N. and D'Angelo, K.R., "Parameter Estimation for Martian Terrain Modeling from Gradient Data," Seventh Hawaii International Conference on System Sciences, Honolulu, Ha., January 1974.

13. Neuberger, A., "Characterization of Pictures by Essential Contours," M.S. Thesis, M.I.T., 1966.

14. Reed, Martin, Probal Sanyal and Shen, C.N., "A Practical Obstacle Detection System for the Mars Rover," Second Annual Milwaukee Symposium on Automatic Control, Milwaukee, Wisconsin, March 1974.

15. Shen, C.N. and Burger, P., "Stochastic Estimates of Gradient from Laser Measurements for an Autonomous Martian Roving Vehicle," Rensselaer Polytechnic Institute, Troy, N.Y., Proceedings of the 3rd IFAC Symposium, The Hague/Delft, The Netherlands, June 12-15, 1973.

16. Bekker, M.C., Off-the-Road Locomotion, University of Michigan Press, 1960.

17. Capper, P.L., Cassie, W.F., The Mechanics of Engineering Soils, McGraw-Hill Book Co., 1953.

18. Boheim, S.L. and Purdon, W.C., "Path Selection System Simulation and Evaluation for a Martian Roving Vehicle," RPI Technical Report MP-29, Rensselaer Polytechnic Institute, Troy, New York, December 1972.

19. Campbell, R.S. and Simons, R.R., "Path Selection System Development and Evaluation for a Martian Roving Vehicle," RPI Technical Report MP-42, Rensselaer Polytechnic Institute, Troy, New York, May 1974.

20. McGrath, C., Oey, K., and Patten, R., "A Navigational Computer for an Unmanned Mars Roving Vehicle," MRV 72-5, Cornell University, Ithaca, New York, June 1972.

21. Benoit, G.L., "Reduction of Chromatographic Data and Evaluation of a GC Model," RPI Technical Report MP-22, Rensselaer Polytechnic Institute, Troy, New York June 1971.

22. Keba, P.S., and Woodrow, P.T., "A Comparison of Two Gas Chromatograph Models and Analysis of Binary Data," RPI Technical Report MP-27, Rensselaer Polytechnic Institute, Troy, New York July 1972.

23. Stovall, A.N., "Chromatographic Systems Analysis: Design Parameter Evaluation," M. Eng. Project Report, Rensselaer Polytechnic Institute, Troy, New York, 1974.

24. McNair, H.M., and Cooke, W.M., "Use of Statistical Moments in Chromatography," Amer. Lab., 5 (2), 12-18 (1973).

25. Voytus, W.A., "Chromatographic Systems Analysis: Moment Analysis of the Equilibrium Adsorption Model," RPI Technical Report MP-9, Rensselaer Polytechnic Institute, Troy, New York, August 1969.

26. Lavoie, R.C., "Composition Dependent Effects in Gas Chromatograpy," RPI Technical Report MP-41, Rensselaer Polytechnic Institute, Troy, New York, May 1974.

27. Meisch, A.J., "Binary Chromatographic Data and Estimation of Adsorbent Porosities," RPI Technical Report MP-31, Rensselaer Polytechnic Institute, Troy, New York, July 1973.

28. Baer, S.R., and Benoit, G.L., "Chromatographic Test Facilty, RPI Technical Report MP-19, Rensselaer Polytechnic Institute, Troy, New York, March 1971.

29. Woodrow, P.T., "Preliminary Numerical Analysis of Improved Gas Chromatograph Model," RPI Technical Report MP-36, Rensselaer Polytechnic Institute, Troy, New York, September 1973.

30. Woodrow, P.T., "Analysis of Chromatographic Systems using Orthogonal Collocation," RPI Technical Report MP-40, Rensselaer Polytechnic Institute, Troy, New York, May 1974.

31. Finlayson, B.A., "The Method of Weighted Residuals and Variational Principles," Academic Press, New York, 1972.

32. Bulirsch, R., and Stoer, J., "Numerical Treatment of Ordinary Differential Equations by Extrapolation Methods, Numerische Mathematik, 8, 1-13 (1966).